Doctoral Dissertation
Doctoral Program in Electrical, Electronics and Communications Engineering
(33rd Cycle)

Methodologies for Frequency Stability Assessment in Low Inertia Power Systems

Carmelo Mosca
* * * * * *

Supervisors
Prof. Ettore Bompard, Supervisor
Prof. Gianfranco Chicco, Co-supervisor

Politecnico di Torino
2020

I hereby declare that the contents and organisation of this dissertation constitute my own original work and does not compromise in any way the rights of third parties, including those relating to the security of personal data.

…….....

Carmelo Mosca

Turin, 2020

Summary

The energy transition is a needed and undeferrable pathway for a sustainable future towards the transformation of the global energy sector from an extensive use of fossil fuels to a massive implementation of zero-carbon assets. Renewable energy sources (RESs) exploitation is crucial in this framework, to decarbonise the energy sector and reduce CO_2 emissions to limit the climate change.

The electrical sector is playing an important role in the energy transition, being subjected to major changes in its historical paradigms. Nevertheless, the shift from conventional generators, synchronous and centralized, to non-conventional RESs, non-synchronous and decentralised, is challenging the way Transmission System Operators (TSOs) manage and plan their networks.

RESs have different features which affect the security of traditional power systems, designed to work with conventional generation. First, they are dispersed, mostly connected to the lower voltage systems, and variable, with uncertainty in different time scales, rising needs for new sources of flexibility to maintain constantly the balance between generation and demand and to ensure an efficient electricity system. Furthermore, RESs are mainly connected through power electronics devices, which provide lower short-circuit levels, imply reduced control capabilities, reduced inertia, and reduced system strength, impacting the system security and stability.

This thesis has the primary objective to contribute and provide a methodological framework to assess the frequency stability of modern power systems by exploring, applying, adapting, and combining the main methods, tools, and solutions in low inertia contexts.

A review of the scientific literature is performed to identify limitations and weaknesses of different approaches, particularly when dealing with real case studies and practical applications of system operators. The technical organization of the existing frequency control structure in Continental Europe is investigated in deep and the state-of-the-art in technologies, control schemes and services that can support frequency stability is presented and analysed, highlighting benefits and drawbacks of each solution. The main examined technologies are Battery Energy Storage Systems (BESSs), High Voltage Direct Current (HVDC) and

Synchronous Compensators (SyCs). A set of tools to estimate and calculate the inertia and parameters to quantify the frequency performance in both current and future power systems is defined and implemented, together with possible trajectories to investigate the distributional impact of inertia.

A dynamic aggregate model is developed and validated using MATLAB/Simulink to study the frequency performance of real power systems in case of contingencies and during normal operation. The aggregate model is demonstrated to be reliable and fast enough for security contingency studies and to carry out extensive parametric analysis in the planning phase when the primary objective is the overall frequency stability. The model can be used also to estimate the generation-load imbalance which determine a specific frequency deviation during normal operation. The explored contingencies are the reference incident and system separations, presenting novel approaches to identify and quantify the consequences of large power system splits in subsystems. The impact of SyCs, HVDC and BESSs during contingencies shows their capabilities to improve the frequency response. Emphasis is placed on assessing the BESSs contribution in primary and inertial control and ensuring its accurate dimensioning, imitating the behaviour of synchronous generators using an Equivalent Saturation Logic. It is shown that only the implementation of inertial control is not enough, and a primary response is needed to balance the system. At the same time, inertial and primary controls are not able to significantly improve frequency deviations in normal operations, where the slow dynamics make the secondary control apparently more valuable. Frequency stability and inertia constraints are investigated and evaluated in the power plant unit commitment in a technical economic view, analyzing costs and dynamic performance. A Multiple-Criteria Decision Analysis is outlined to select the best compromise solution and it can be easily managed by a decision maker to create a preliminary background and to deliver technical, financial, and environmental insights for the definition of energy plans.

The proposed methodological framework is applied to several real case studies, from smaller (Sardinia) to larger power systems (Continental Europe), from current to future cases taken by the most relevant scenarios developed by the European system operators. All the case studies provide numerical evidence to results and offers a background to assist system operators, researchers, and decision-makers in managing and planning future power systems.

Preface

This thesis summarizes the work carried out during the Ph.D. program in Electrical, Electronics and Communications Engineering at different institutions and locations: the Department of Energy, Politecnico di Torino, Turin, Italy, the Planning and Dispatching Department, Terna, Torino/Rome, Italy and the System Development Committee, ENTSO-E, Brussels, Belgium.

This Ph.D. project was funded by the Planning and Dispatching Department, Terna. It started in November 2017 and it was concluded in December 2020.

During this period, the Ph.D. candidate contributed to several research and development activities, collaborating with many National and European institutions (ESL, ENEA, JRC and SRM among others). The main achievements are proved by international and national publications, presentations at international conferences and several reports and analysis.

Politecnico di Torino is one of the most prestigious public institutions in Italy and at international level in the education, research, technological transfer, and services in all the sector of Architecture and Engineering. It is based in Turin, Italy.

The *Terna* group is the owner of the Italian national transmission grid for high and extra-high voltage power and is the largest independent electricity transmission system operator (TSO) in Europe. The main premises are in Rome, Italy.

ENTSO-E is the European Network of Transmission System Operators for Electricity, which represents 42 electricity transmission system operators (TSOs) from 35 countries across Europe. It is based in Brussels, Belgium.

Acknowledgment

My Ph.D. path has been a unique and life-changing experience that would not have been possible to pursue without the support and guidance I received from many people.

I would like to first express my deep gratitude to my supervisor, Prof. Ettore Francesco Bompard, who wisely and patiently guided me throughout this hard and amazing journey. Without his experience and vision this Ph.D. would not have been achievable. I would also like to thank my co-supervisor, Prof. Gianfranco Chicco, for his valuable and constructive suggestions, encouragement, and constant support.

I wish to extend my special thanks to my company's supervisors, Eng. Paolo Cuccia and Eng. Chiara Vergine, for having advised, taught, and endured me over these long years and for the countless opportunities they have given me. They constantly offered insightful comments, guidelines, and lessons, introducing me to the everyday working life.

I am grateful to Jean-Baptiste Paquel, Dante Powell, Maria-Chiara Cavaretta, Simone Biondi and João Moreira, who provided the opportunity to join their team welcoming me in an amazing work environment at ENTSO-E. They have always believed in my abilities, knowledge, and skills, giving me trust and responsibility. A big thank you goes also to all the colleagues from SD, DTPS, DTCBA and friends that made my stays in Brussels special (Omar, Monica, Maria, Mira, Simón, Marcos, Thanh, Nils, Sergio, Vincent among many others I do not have space to list).

A big thank you goes also to my colleagues and friends at DENERG and Terna. Thanks to Francesco, for his enthusiasm, initial boost, and sincere friendship. Thanks to Antonio and Stefano, who contributed to my survival during these years. Always available, they gave me a lot on a professional and human level. Thanks to Cristiano, Benedetto and Michela for their valuable and constructive suggestions during the planning and development of many works.

A unique thank you goes to my parents, my grandfather, my siblings for the biggest support and trust, for their unconditional love and for always being a reference point.

Thanks to Claudia, for the trust placed in me, loving cares and endless patience.

Contents

List of Figures

List of Tables

Nomenclature

AAC	Already Allocated Capacity
AC	Alternating Current
ACE	Area Control Error
ADLP	Average Daily Load Profile
AEMO	Australian Energy Market Operator
AHP	Analytical Hierarchy Process
ATC	Available Transfer Capacity
BAU	Business As Usual
BE	Best Estimate
BESS	Battery Energy Storage Systems
CAISO	California Independent System Operator
CBA	Cost-Benefit Analysis
CCGT	Combined Cycle Gas Turbines
CE	Continental Europe
CEP	Clean Energy Package
CO	Carbon Dioxide
COI	Centre of Inertia
COP	Conference of the Parties
COVID	COronaVIrus Disease 19
DAM	Day-Ahead Market
DC	Direct Current
DEC	Decentralized
DER	Distributed Energy Source
DG	Distributed Generation
DSO	Distribution System Operator
EB	Evening Base
EC	European Commission
EIA	U.S. Energy Information Administration
EMS	Energy Management System
ENEA	Agenzia nazionale per le nuove tecnologie, l'energia and lo sviluppo economico sostenibile
ENTSO-E	European Networks of Transmission System Operators for Electricity
ENTSO-G	European Networks of Transmission System Operators for Gas
EP	Evening Peak
EPRI	Electric Power Research Institute
ER	Evening Ramp
ESL	Equivalent Saturation Logic
ESS	Energy Storage Systems
ETS	Emissions Trading System
EU	European Union

EUCO	European Commission scenario
FACTS	Flexible Alternating Current Transmission System
FCP	Frequency Containment Process
FCR	Frequency Containment Reserve
FCS	Frequency Control Schemes
FFR	Fast Frequency Response
FRCE	Frequency Restoration Control Error
FRP	Frequency Restoration Process
FRR	Frequency Restoration Reserve
FSM	Frequency Sensitivity Mode
GB	Great Britain
GCA	Global Climate Action
GDP	Gross Domestic Product
GHG	Greenhouse Gas
GME	Gestore dei Mercati Energetici
HD	Holiday
HV	High Voltage
HVAC	High Voltage Alternating Current
HVDC	High Voltage Direct Current
ICT	Information and Communication Technologies
IE	Ireland
IEA	International Energy Agency
IEEE	Institute of Electrical and Electronics Engineers
ILF	Integratore Locale di Frequenza
IoSN	Identification of System Needs
IPCC	International Panel on Climate Change
IRENA	International Renewable Energy Agency
LCC	Line Commutated Converter
LFC	Load-Frequency Control
LFDD	Low Frequency Demand Disconnection
LFSM	Limited Frequency Sensitive Mode
LV	Low Voltage
MB	Morning Base
MCDA	Multiple-Criteria Decision Analysis
Med-TSO	Mediterranean Transmission System Operators
MGP	Mercato del Giorno Prima (Italy)
MI	Mercato Infragiornaliero (Italy)
MP	Morning Peak
MR	Morning Ramp
MSD	Dispatching Service Market
MTDC	Multi-Terminal Direct Current
MV	Medium Voltage
NECP	National Energy and Climate Plan
NI	Northern Ireland
NTC	Net Transfer Capacity

OCGT	Open Cycle Gas Turbine
PCI	Project of Common Interest
PEIG	Power Electronic Interfaced Generation
PMU	Phasor Measurement Unit
PNIEC	Integrated National Energy and Climate Plan
PUN	Prezzo Unico Nazionale (Italy)
PV	Photovoltaic
RES	Renewable Energy Source
ROCOF	Rate Of Change Of Frequency
RR	Replacement Reserve
RRP	Replacement Reserve Process
SA	Synchronous Area
SACOI	Sardinia Corsica Italy HVDC
SAPEI	Sardinia-Italian Peninsula HVDC
SARCO	Sardinia-Corsica HVAC
SCADA	Supervisory Control and Data Acquisition
SEW	Socio-Economic Welfare
SNAM	Società Nazionale Metanodotti (Italian TSO for gas)
SNSP	System Non-Synchronous Penetration
SoC	State of Charge
SSI	System Split Indicator
ST	Sustainable Transition
STATCOM	Static Synchronous Compensator
SVC	Static VAR Compensator
Terna	Italian Transmission System Operator
TOPSIS	Technique for Order Performance by Similarity to Ideal Solution
TRM	Transmission Reliability Margin
TSO	Transmission System Operator
TYNDP	Ten-Year Network Development Plan
UCTE	Union for the Coordination of Transmission of Electricity
USA	United States of America
UTC	Coordinated Universal Time
VSC	Voltage Source Converter
WD	Working Day
WHO	World Health Organisation

Chapter 1

1 Introduction

1.1 Background and motivation

Energy plays a crucial role as a productivity enhancing factor in the economic development and human well-being. The United Nations put energy at the foreground of the Sustainable Development Goals, with the Goal 7 to "ensure access to affordable, reliable, sustainable and modern energy for all" by 2030. At the same time, addressing the climate change is acknowledged as an imperative by almost all countries. Energy provision is recognized as a key element in a sustainable development policy framework that needs to be met jointly with specific climate change policy objectives [1]. In the last few years, the European Union has adopted several policies to facilitate the clean energy transition by setting ambitious energy and climate targets for 2030 and to achieve net-zero emissions by 2050. The 2020 objectives of achieving a 20% greenhouse gas emissions reduction, 20% in renewable energy and 20% in energy efficiency are being reached, moving further ahead for 2030, setting greenhouse gas emissions reduction of at least 40%, energy efficiency at 32,5% and 32% of renewables, and for 2050, with the long-term vision of more than 80% of electricity coming from renewables.

In the power sector, these efforts facilitated the vast growth of Renewable Energy Sources (RESs) and particularly of wind and photovoltaic. A fundamental difference between traditional and most RES generation is the type of connection, non-synchronous through power electronic-based devices. Such generation will be referred to as Power Electronic Interfaced Generation (PEIG). Furthermore, the priority dispatch status of PEIG and the increasing levels of installed High Voltage Direct Current (HVDC) interconnections between synchronous systems, are changing the unit commitment and the economic dispatch order, bringing to the gradual shutdown of large conventional units.

As depicted in Figure 1.1, the energy transition involves thus the major challenge of replacing conventional generators, synchronous and centralized, and

their well-known dynamics and controllers with PEIG whose regulation and interaction with the rest of the system is yet to be fully recognized [2]. Drastic changes will be needed in power system operation, control and planning to keep the current levels of security and stability.

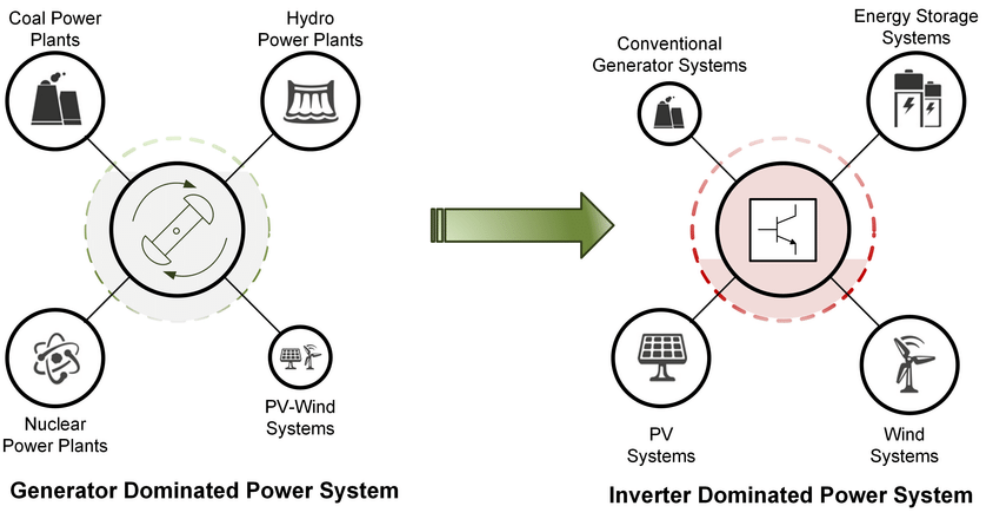

Figure 1.1: Evolution of modern power systems [3].

Among others, the progressive shutdown of large conventional plants and the high penetration of PEIG jeopardizes the frequency regulation and stability, linked to the instantaneous load-generation balance and to the system inertia. Until now, conventional power plants have been the traditional providers of services that ensure frequency stability (mechanical inertia and governor response). These power plants are being displaced by marginally zero-cost non-synchronous generation, without intrinsic inertial response.

Therefore, the first research question is:

1. What is the impact of the massive penetration of PEIG on the frequency stability and how can it be modelled, analysed and evaluated?

By exploring current literature and looking at the developed models, it is evident that a standardized and clear framework to assess the frequency stability still lacks, particularly looking at the definition and harmonization with current grid codes and frequency control schemes, validations and applications on real power systems. The aim is to cover the main gaps between academia and industry and to address the current needs of Transmission System Operators (TSOs) in both operation and planning, developing and implementing methodologies and tools to be practically used by the power system utilities.

Several technologies, control schemes and services have been investigated to support the frequency stability. Consequently, the second research question is:

2. Which are the main solutions to support frequency stability and how can their benefit and drawbacks be measured?

These two questions lead this thesis to contribute and provide a methodological framework to assess the frequency stability of modern power systems by exploring, applying, adapting, and combining the main methods, tools and solutions in low inertia contexts.

1.2 Research contribution

This thesis focuses on the frequency stability in terms of real-time operation and long-term planning and analyses primarily the issue of the reduced inertia in current and future power systems.

The main contributions can be identified as follows:

- A generalization and harmonization of fundamentals describing the frequency control schemes in Europe is given. The consequences of the increasing penetration of PEIG are detailed, with focus on the frequency stability.
- An aggregate model to study the frequency stability is developed, validated and applied to study the frequency performance of real power systems in case of contingencies and during normal operation
- Battery Energy Storage Systems (BESSs), High Voltage Direct Current (HVDC) and Synchronous Compensators (SyCs) are investigated and analysed to support frequency stability. Emphasis is placed on assessing the HVDC and BESSs contribution in primary and inertial control and ensuring its accurate dimensioning, using an Equivalent Saturation Logic.
- A methodology for Cost-Benefit Analysis evaluation of network enhancement projects which affect frequency stability is developed. The methodology is being currently implemented for the TYNDP at ENTSO-E.
- A methodology to identify and quantify the consequences of large power system splits in subsystems is presented and it is being currently implemented by ENTSO-E.
- Frequency control and inertia constraints on the market unit commitment are investigated, proposing a methodology to compare the outputs in terms of overall system costs and frequency security performance and to find the best compromise in a technical-economic view, using a multiple criteria decision analysis methodology.
- A methodology to analyse the impact of pandemic on the electricity system is presented. The effects are evaluated in terms of direct impact on demand and load profiles, and indirect impact on operation and markets.

The proposed methodological framework is applied to several real case studies, from smaller insulas (Sardinia) to larger power systems (Continental

Europe), from current to future cases taken by the most relevant scenarios developed by the European system operators. All the case studies provide numerical evidence to results and offers a background to assist system operators, researchers, and decision-makers in managing and planning future power systems.

1.3 Structure of the thesis

This Ph.D. thesis is structured into 6 chapters aiming at answering the identified relevant research questions.

Chapter 1 (Introduction) and Chapter 2 (The Energy Transition in the European framework) are dedicated to set out the research background and context related to the energy transition. Key data are gathered and showed by using the most recent outcomes from public and private institutions. Future scenarios coming from the European TSOs are detailed and translated to the Italian context. The main challenges and threats of the PEIG integration are explained together with guidelines towards a massive penetration in future power systems.

Chapter 3 (Frequency dynamics characterization and instability mitigation strategies) gives an overview on the frequency dynamics characterization, starting from the fundamental regulation and control in modern power system to the current implications due to a massive penetration of PEIG. The scope of this chapter is to help the reader in understanding the development and implementation of the methodologies described in Chapter 4.

The methodological framework to assess frequency stability is proposed and designed in Chapter 4. The actual international state of the art is reviewed step by step. This screening is fundamental to identify the limits in current research and to set the theoretical basis on which the whole thesis relies.

The different methodologies are combined and applied to several case studies in Chapter 5, derived from National scenarios by Terna, the Italian TSO, to European scenarios by ENTSO-E.

Considering the current health, social, and economic crisis due to the COVID-19 pandemic, which greatly influenced my last and most important Ph.D. year, with missed (many) and provided opportunities, it was considered appropriate to report in Chapter 6 some analysis on the lockdown's impact on the national and European power systems, as an experiment of high renewables penetration and low inertia.

Chapter 7 (Conclusions) draws conclusions and provides the key takeaways and an outlook on the associated future research.

1.4 List of publications

The following papers have been published during the Ph.D. activities, most of them relevant for this thesis.

Journal Papers

- Mosca C., Arrigo F., Mazza A., Bompard E., Carpaneto E, Chicco G., Cuccia P., "Mitigation of frequency stability issues in low inertia power systems using synchronous compensators and battery energy storage systems", *IET Generation, Transmission and Distribution*, 13(17), pp. 3951-3959, Jul. 2019.
- Mosca C., Bompard E., Chicco G., Aluisio B., Migliori M., Vergine C., Cuccia P., "Technical and Economic Impact of the Inertia Constraints on Power Plant Unit Commitment", *IEEE Open Access Journal of Power and Energy*, vol. 7, pp. 441-452, Oct. 2020.
- Mosca C., Bompard E., P. Colella, G. Antonopoulos, G. Fulli, M. Masera, M. Poncela-Blanco, S.Vitiello, "The Immediate Impacts of COVID-19 on European Electricity Systems: A First Assessment and Lessons Learnt", *Energies*, 14(1), 96, Jan. 2021.
- Mosca C., Bompard E., Chicco G., Moreira J., Sermanson V., Powell D., "Frequency Stability of the European Interconnected Power System under Grid Splitting in Market Zones", *Energy Systems Research*, 3(4), 37-47, Dec. 2020.

Conference Papers

- Mosca C., Bompard E., Aluisio B., Migliori M., Vergine C., Cuccia P., "HVDC for frequency stability under RES penetration: the Sardinia island case", *AEIT HVDC International Conference 2019*, Firenze, Italy, May 2019.
- Mosca C., Marin E., Huang T., Bompard E., Cuccia P., Campisano L., Neri S., "A new real time approach for the load forecasting in the operation of sub-transmission systems", *AEIT International Annual Conference 2019*, Firenze, Italy, Sep. 2019.
- Arrigo F., Mosca C., Bompard E., Cuccia P., "Frequency Models and Control in Normal Operation: the Sardinia case study", *2020 55th International Universities Power Engineering Conference (UPEC)*, Sep. 2020.
- Mosca C., Colella P., Bompard E., Yan Z., "Techno-economic Impacts of COVID-19 Pandemic on the Italian Electricity System", *AEIT International Annual Conference 2020*, Sep. 2020.

Book's Chapters

- Mosca C., Bompard E., Profumo F., Arco E., "Electricity based corridors connecting North and South shores of the Mediterranean", *ENEMED Med & Italian Energy Report*, Jun. 2020.

Italian Journal Papers

- Mosca C., Marin E., Huang T., Bompard E., Cuccia P., Campisano L., Neri S., "Approcci innovativi per la stima di carichi in tempo reale nelle reti elettriche di sub-trasmissione", *L'Energia Elettrica*, Sep. 2019.
- Gracceva F., Bompard E., Baldissara B., Corgnati S., Mosca C., Zini A., "Prime stime degli effetti dell'emergenza COVID-19 sul sistema energetico italiano", *Analisi trimestrale del sistema energetico italiano*, ENEA, Apr. 2020.
- Gracceva F., Bompard E., Baldissara B., Corgnati S., Mosca C., Zini A., "COVID-19 e sistema energetico italiano: una prima valutazione", *Energia*, Editore Ricciardi & Associati S.r.l., Jun. 2020.
- Bompard E., Mosca C., Profumo F., "Crescente penetrazione della generazione da fonti rinnovabili e sicurezza del sistema elettrico nazionale", *Analisi trimestrale del sistema energetico italiano*, ENEA, Aug. 2020.

Parts of this thesis were also published in some of the above-mentioned papers. These will be referenced in the introductory section of the respective chapters.

Chapter 2

2 The Energy Transition in the European framework

2.1 Introduction

The environmental concerns due to the global warming are leading the economies to deep changes in recent years, from being largely powered by fossil fuels to a massive implementation of zero-carbon sources. RESs exploitation is crucial in this framework, to decarbonise the energy sector and reduce greenhouse gas (GHG) emissions to limit the climate change.

This Chapter presents and describes current and future scenarios focusing on the role of electricity in the European context and the adopted policies, setting out the research background and context related to the energy transition. Key data are gathered and showed by using the most recent outcomes from public and private institutions. Future scenarios coming from the European TSOs are detailed and translated to the Italian context. The main challenges and threats of the PEIG integration are explained together with guidelines towards their massive penetration in future power systems.

2.2 Energy transition: perspectives and overview

The first major international **climate agreement** was the United Nation's Framework Convention on Climate Change, held in Rio de Janeiro in 1992. The goals aspired only to identify thresholds levels of atmospheric emissions of GHG, stating the need to control them to prevent dangerous anthropogenic interference with the climate system [4]. It soon became clear that more specific targets were needed, and the response was the Kyoto Protocol in 1997 where 37 industrialized countries and the European Community have committed to reduce their emissions by an average of 5 percent against 1990 levels over the five-year period 2008-

2012, under the principle of "common but differentiated responsibilities" [5]. Most recently, in December 2015, the Paris climate agreement (COP 21) was adopted, to limit global warming to well below 2°C by the end of the century compared to pre-industrial levels while pursuing efforts to limit the increase to 1.5°C [6]. The energy sector was always referred to as crucial to fight the climate change.

World **final energy consumption** increased from 8766 Mtoe in 1990 to 14279 Mtoe in 2018. This trend has been mainly towed by the development countries, while industrialized nations kept a flat or even decreased energy profile [7]. Energy intensity per unit of Gross Domestic Product (GDP) is decreasing over time, from 7.7 MJ/$ in 1990 to 5 MJ/$ in 2018, which both reflect a development toward economic sectors with lower energy intensity, and energy efficiency improvements. At the global scale, carbon dioxide (CO_2) is the primary source of GHG [8]. The CO_2 emissions per unit of GDP had the same trend, passing from 0.5 kg/$ to 0.3 kg/$. Nevertheless, the total CO_2 emissions increased by 63% in the same period, passing from 20.6 Gt to 33.5 Gt and looking at the global renewable share in the final energy consumption, no significant increase can be seen, passing from 16.5% in 1990 to 17.3%. Still great efforts are needed at the global level to contrast the climate change. In 2018, the top carbon dioxide (CO_2) emitters were China (9.6 Gt), the United States (4.9 Gt), the EU-28 (3.2 Gt), India (2.3 Gt), the Russian Federation (1.6 Gt), and Japan (1.1 Gt).

The **electricity sector** is responsible for one third of total CO_2 emissions, with an increasing share in the total final consumption from 12% in 1990 to 19% in 2018. Electricity consumption increased from 10897 TWh in 1990 to 24738 TWh in 2018 and it is expected to further accelerate. The electrification is seen as a concrete opportunity to decarbonize economies, for different reasons: ① electricity is clean at the end use and in total if generated by RES ② electricity is efficient in all stages of production, transmission and consumption and easy to transport given a solid infrastructure ③ all RES can be converted into electricity with existing technologies ④ electricity can be used for a huge variety of efficient and low carbon technologies at the end use (e.g. electric vehicles, heat pumps) and for new services (e.g. demand response), giving more power and value to the final consumer. However, electricity has also weak points which will be discussed later (storage, substantial investments needed).

China is today the largest energy user and CO_2 emitter, responsible for the 28.7% of the total global emissions. In 2019, China covered more than 60% of its electricity generation using coal [9], but the Chinese government committed to move towards a more climate-friendly economy within 2050 [10], also subscribing the Paris agreement in 2015. By 2050 electricity is expected to represent around 50% of the final demand and mainly generated by clean energy sources.

The **United States of America** are responsible for the 14.6% of the total CO_2 emissions. In 2019, the share of RESs in total electricity generation was just 17% [11]. In the "Reference Energy Scenario towards 2050", the EIA foresees an increase in the electricity generation from natural gas (from 34% in 2018 to 39% in 2050) and renewables (from 18% to 31%.), while both coal (from 28% to 17%) and nuclear (from 19% to 12%) are expected to decline [12].

For the past 25 years the **European Union** (EU) has been a global leader for policies to address the climate change, reaching a reduction of emissions by 23% between 1990 and 2018, while the economy grew by 61% over the same period [13], with a clear decoupling from the greenhouse emissions. In the period between 2004 and 2008, RESs have grown much faster in the electricity sector (on average 1.2%/year) compared to the heat sector (0.7% /year) and transport (0.5%/year) [14]. The European energy policies comes from over seven decades of cooperation and efforts [15]. An initial phase started in 1951, with the European Community of Coal and Steel and expanded to Euratom in 1957 to ensure the cooperation on the nuclear energy and provide a solution for the declining coal reserves as well as the increasing dependency on oil. This starting point was followed by three decades of national energy policy primacy, where environmental externalities were not considered. The Maastricht Treaty in 1992 established the EU and started the liberalization process for energy, evolving in the Lisbon Treaty, where energy was mentioned as a community domain. Recently, the EU has adopted new policies to facilitate the clean energy transition by setting ambitious energy and climate targets for 2030 and to achieve net-zero emissions by 2050.

The 2020 objectives of achieving a 20% greenhouse gas emissions reduction, 20% in renewable energy and 20% in energy efficiency were set in 2007 by the 2020 climate & energy package and are currently being reached.

In 2016, the European Commission (EC) launched the **Clean Energy Package** (CEP) with the aim of making regulations more effective in achieving the climate objectives for 2030. The three key targets for 2030 are: cut at least 40% in greenhouse gas emissions (from 1990 levels), have at least 32% share for renewable energy and have at least a 32.5% improvement in energy efficiency [16]. These initiatives were taken even further in December 2019 by the **European Green Deal**, which increased the EU's climate ambition with a reduction of GHG emission to at least 50% for 2030 to achieve the climate neutrality by 2050, with the long-term vision of more than 80% of electricity coming from RES [17].

Despite it is well known that the global challenge of climate change requires a global action (EU is responsible for less than 10% of GHG emissions), EU is demonstrating that a pathway toward a sustainable future is possible. However, EU cannot solve climate change without others also acting.

Among others, several initiatives and instruments were taken to ensure these goals. It worth to mention the idea of introducing, for the first time in the world, a European GHG **Emissions Trading System** (ETS) from 2005 [18], to limit emissions from heavy energy-using installations and airlines working on a "cap and trade" system. Furthermore, the **Innovation Fund**, for financial support to the development of low carbon technologies, carbon capture and utilization, energy storage, which can be combined with funding from other support programmes (e.g., Horizon 2020 programme for funding research & innovation), and energy efficiency measures through the Energy efficiency Plan and Directives.

Considering the EU **electricity mix**, on a total production of 2941 TWh, the highest share of electricity in 2018 was produced using RES (32.9 %), followed by nuclear (25.9 %), coal (20.2 %) and gas (17.8 %). Lower shares were noticed for oil (1.9 %) and non-renewable wastes (0.7 %) [19]. There have been significant changes in the contribution of the different RES to electricity production over the last two decades. In 2000, 87.0% of renewable electricity was produced from hydro, a share which dropped to 38.3% in 2018. Other renewable energy sources with large shares in electricity production in 2018 were wind (33.1 %), solar photo-voltaic (11.4 %), primary solid biofuels (7.8 %) and biogases (5.7 %). The trend of gross electricity production by fuel for the EU-27 in the period 2000-2018 is shown in Figure 2.1. In 2012, RES generation overcome for the first-time fossil fuel generation, and the bifurcation is expected to grow further.

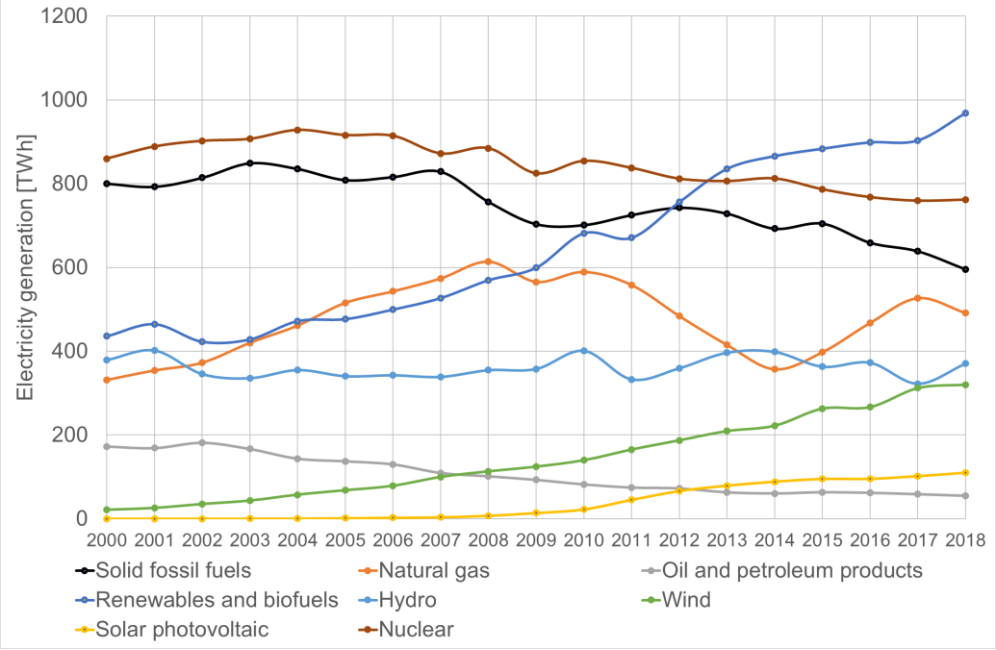

Figure 2.1: Gross electricity production by fuel for the EU-27 (elaboration on Eurostat data [19]).

The installed electrical capacity increased by 51.6 % in the period from 2000 to 2018. Its structure changed significantly over this period. In 2000, the highest

share of installed capacity was accounted for combustible fuels (55.5 %), followed by hydro (22.0 %), nuclear (20.4 %) and wind (2.0 %), with all others at less than 2.0 %. In 2018, the share of installed capacity of combustible fuels decreased to 43.5 %, the share of hydro to 16.2 % and the share of nuclear to 12.0 %. On the other hand, the share of wind increased to 16.9 % and the share of solar to 11.2 %, while geothermal and tide, wave and ocean remained negligible.

Focusing on the **Italian context**, while in 2005 the 15% of the electricity generation was covered by RES with prevalence of hydro, in 2019 the share has more than doubled, passing to 40% of the national generation (113 TWh over a total of 284 TWh). Enlarging the analysis to the total electricity demand, in 2019 the RES share was around the 35%, which also considers the foreign power exchanges. The thermal generation reduced from 236 TWh in 2005 to 169 TWh in 2019 (around -30%). Looking at the installed thermal capacity, until 2012 there was a modernizing and development phase guided by the increasing demand and electricity prices, reaching around 77 GW. In the subsequent years, the trend has started to decline, reducing to a value lower than 60 GW in 2019.

The growth of RES installed capacity between 2008 and 2018 has been mainly influenced by wind and photovoltaic (PV), reaching 10.7 GW for installed wind capacity (more than 90% in the South) and around 20.9 GW for the photovoltaic (PV) capacity starting from a total of only 4 GW in 2008. In 2019, the installed hydro capacity is around 23 GW, mainly in the Northern regions, with a constant trend since 2000. The installed wind capacity interested mainly the HV transmission grid, while PV (over 90%) has been installed in the MV and LV grids. Historically, Italy is an electricity importer, with main exchanges with Switzerland and France (more than 90% in 2019) and where the interconnection capacity is higher. The import is influenced by the electricity price differential among Italy and the bordering bidding zones and the interconnection capacity. In particular, the bordering countries have in general lower prices, as France produces mainly by nuclear, Austria from hydro and Switzerland is a bridge with Germany, characterized by high share of coal, nuclear and wind.

In sum, in the last decades, RESs have reached high degrees of technological maturity and are becoming cost-competitive with conventional generation in a broader range of market conditions. This trend is leading to a large share of variable RESs capacity installed in Europe, mostly wind (both onshore and offshore) and solar PV. Moving forward, the challenge will be to operate power systems dominated by these cheap but also challenging sources, as it will be explained in detail in the next Sections. A diversified portfolio of flexibility options, including not only flexible generating units, but also demand response, storage, interconnectors, flexible operational practices, market designs and business models, will be the key to keep an increasing share of variable RES in a cost-effective way.

2.3 The European scenarios

It is central to understand future and multiple consequences of any action to decision making and particularly for the energy sector. This role is undertaken by energy scenarios, to map, analyse and compare possible future developments. The scenario building process implies a coherent set of assumptions on the current trends or possible different future constraints, as environmental awareness, policy intervention, socio-economic and technological trends. Scenarios are not a prediction of the future and a proper use of them need to consider a wide range of scenarios with different sets of assumptions as well as different methodological approaches. The scenario building process is initiated by the formulation of one or several high-level purposes, followed by different steps: definition of scope and granularity, definition of methodology and assumptions, implementation and analysis [20]. These steps constitute the scenario "storyline". It is possible to distinguish two methodological approach for the scenario building process: top-down, which formulates high-level values, targets and development and breaks those down to a level of granularity, and bottom-up, defines low-level fundamental characteristics and calculate the resulting system development. Nowadays, almost all scenario-building activities are supported by computational tools which reflect socio-economic dispatch and investment decisions in a comprehensive and consistent analytical framework (market modelling tools).

Several actors as European and National Institutions, Parliamentary Commissions, intergovernmental organisations, system operators, businesses, consultancies, and research institutes build a veritable forest of scenarios to explore the energy transition. The International Energy Agency (IEA) publish every year the World Energy Outlook, which provides critical analysis and insights on trends in energy demand and supply, and what they mean for energy security, environmental protection and economic development using a scenario-based approach [21]. The most recent scenarios are the Stated Policies Scenario, provides a detailed sense of the direction in which today's policy ambitions would take the energy sector, and the Sustainable Development Scenario to meet energy goals across all parts of the energy system aligned with the Paris Agreement. Among others, scenarios are released by the International Renewable Energy Agency (IRENA), with the Renewable Energy Roadmap (RE-map), the International Panel on Climate Change (IPCC), the basis of the United Nation Framework on Climate Change, the European Commission and the European Networks for Electricity and Gas Transmission System (ENTSOs).

To estimate the potential impact of the EU's climate and energy targets, the EC has developed a set of scenarios called the EUCO scenarios, derived from the EU Reference Scenarios. The EU Reference Scenario is updated regularly, and it projects the impact of current EU policies on energy, transport and climate [22]. In 2016, two policy scenarios were built, the EUCO27 and the EUCO30, which

foresee a GHG emission reduction target of 40%, a RES share of 27% and an energy efficiency target of 27% and 30%, respectively [23]. Different EUCO scenarios were formulated to consider different sensitivities and explore more ambitious targets (EUCO+33, EUCO+35 and EUCO3030). The most recent scenario is called the EUCO3232.5 and implement an energy efficiency target of 32.5% and a renewable energy target of 32%, as agreed in the CEP. This scenario was used to support the assessment of the draft National Energy and Climate Plans (NECPs).

The ENTSOs release every two years a common set of European energy scenarios primarily designed to assist infrastructure investment decisions in the framework of the **Ten-Year Network Development Plan** (TYNDP), which is described in detail below.

2.3.1 Ten-Year Network Development Plan

The joint planning of the European electricity grid is a legal mandate for ENTSO-E based on the needs described in Art. 30 of Reg. 943/2019 [24]. TSOs published their first common TYNDP ever in 2010. The 2010 TYNDP was largely a systematic collection of existing planned transmission infrastructure projects by all TSOs with some consistency checking among the different development plans. Future TYNDPs evolved strongly towards a joint determination of the needed infrastructure for economic and reliability reasons, complemented by consistent Cost-Benefit Analysis (CBA) of all known projects with a multi-criteria analysis. Recently, both ENTSO-E and ENTSOG focused on joint scenario building using an interlinked electricity and gas model.

The TYNDP is published by ENTSO-E every two year, to present how the grid is developing in the next 10 to 20 years and how it can effectively contribute to achieving the competing goals set by the European energy transition [25]. The main role of the TYNDP is to identify where investment in the electricity system would help to deliver the Energy Union and benefit all Europeans.

The starting point is the development of future scenarios which is complemented by a system need analysis and a call for transmission and storage projects (under different stages of development) across Europe. The Identification of System Needs (IoSN) shows where action is needed to ensure continuous access to electricity in terms of cross-border transmission capacity increase, internal reinforcements and how to address them in the most cost-efficient way., The IoSN is conducted for each scenario using market and network simulations. The market simulations outputs represent the input for the network simulation, to analyse possible bottlenecks and identify projects which would benefit the system in a feasible and cost-efficient manner. The new projects are assessed in terms of their performance under the different scenarios using the CBA methodology.

The scenarios' storylines are agreed with the European stakeholders and are built using a mix of top-down, bottom-up and external references approach. The EC uses the CBA based on these scenarios to select the Project of Common Interest (PCI) among the gas and electricity interconnection and storage projects.

The latest TYNDP 2018 and 2020 scenarios describe possible European energy futures up to 2050, made jointly by the ENTSOs. The scenarios which were developed for TYNDP 2018 used the following storyline names [26]:

- **Sustainable Transition, ST** (2030, 2040), which seeks a quick and economically sustainable CO_2 reduction by replacing coal by gas in the power sector. It foresees a share of demand covered for 20% from wind and 8% from PV in 2030 which rise respectively to 29% and 12% in 2040. Gas also displaces some oil usage in heavy transport and shipping. The electrification of heat and transport develops at a slower pace than other scenarios. In this scenario, reaching the EU goal requires rapid development during the 2040s to be achieved through increased technological adoption or evolution.
- **Distributed Generation, DG** (2030, 2040), which represents a more decentralised development with focus on end user technologies (smart technology, hybrid heat pumps, electric vehicles have the highest penetration with PV and batteries widespread in buildings). It foresees a share of demand covered for 19% from wind and 15% from PV in 2030 which rise respectively to 27% and 25% in 2040. These developments lead to high levels of demand side response available.
- **Global Climate Action, GCA** (2040), which represents a global effort towards full speed decarbonisation (more than 80% of CO_2 reduction compared to 1990). The emphasis is on large-scale renewables and nuclear in the power sector. Residential and commercial heat become more electrified, leading to a decline of gas demand. Decarbonisation of transportation is achieved through both electric and gas vehicle growth. It foresees a share of demand covered for 36% from wind and 21% from PV. Power-to-gas production see the strongest development within this scenario (3% share of demand).

The highest levels of electricity demand are in the Distributed Generation scenario in both the 2030 and 2040 timeframes (between 4250 and 4500 TWh). Sustainable Transition has the lowest demand in both the 2030 and 2040 scenario (around 4000 TWh). The TYNDP 2018 scenarios also include 2020 and 2025 scenarios, labelled as **Best Estimate** scenarios, due to a lower level of uncertainty. In the 2020, 2025 scenario the amount of RES contributing to demand is 45%±2%. In the 2030 scenarios this is 53%±5%. In the 2040 scenarios the variation between the scenarios can be seen at a much higher scale, from 65% to 81%.

Based on the "lessons learned" and the continuously evolving energy landscape, the joint scenario evolved in three storylines for the TYNDP 2020 [27]:

- **National Trends** (2030, 2040), the central bottom-up policy scenario which reflect the EU member state National Energy and Climate Plans (NECP) in line with the requirement to meet current European 2030 energy targets (32 % RES, 32.5 % energy efficiency, 80-90% CO_2 reduction). Electricity demand is between 3237 TWh in 2030 to 3554 in 2040.
- **Distributed Energy** (2030, 2040, 2050), compliant with the 1.5°C target of the Paris agreement, based on a decentralized approach and an active role of the end users. It foresees a share of demand covered for 29% from wind and 14% from PV in 2030 which rise respectively to 42% and 18% in 2040 and 54% and 19% in 2050. Electricity demand sees the highest values between 3422 TWh in 2030 to 4269 in 2050.
- **Global Ambition** (2030, 2040, 2050), compliant with the 1.5°C target of the Paris agreement, based on a centralised generation and emerging technologies such as offshore wind and Power-to-X. It foresees a share of demand covered for 32% from wind and 10% from PV in 2030 which rise respectively to 45% and 13% in 2040 and 50% and 15% in 2050. Electricity demand is foreseen between 3213 TWh in 2030 to 3478 TWh in 2050.

The common trends in all European scenarios are the decrease in the CO_2 emissions, the stable or slightly declining electricity demand due to major efficiency despite the electrification of the heating and transport sectors, and the increase of RES except for hydro, due to the already reached high level of maturity. On the generation side, wind and solar sources are the key driver that differentiates the main scenarios. Wind power will be the largest source pushed by the offshore deployment supported by the construction of HVDC super-grids. Other RES technologies, such as geothermal, marine, and small biofuel remains stable in all scenarios. Gas sources are expected to take over the coal and they are still needed even in 2050 for flexibility and back-up capacity although they will operate with a much lower capacity factor. However, the decarbonisation of gas will play a significant part and it will be necessary, employing technologies such as bio-methane, Power-to-Gas, and Carbon Capture and Storage, which tend to appear at significant scale from 2040 or 2050. In the longer-term, hydrogen could become an equally important energy carrier towards full decarbonisation in 2050.

A well-integrated energy market is considered a fundamental prerequisite to achieve the EU energy and climate objectives in a cost-effective way. Interconnectors are a vital physical component of Europe's energy transition and offer capacity for energy trade. The socio-economic value of electricity

interconnectors comes from their ability to increase the efficiency of the electricity systems by reducing the costs of meeting electricity demand and in parallel improving security of supply and facilitating the cost-effective integration of the growing share of renewable energy sources. Another crucial aspect in the framework of electricity as main energy commodity will be the shift from open sea and captive corridors based on fossil fuels to captive electricity-based ones.

In the last years, TSOs stated the need to systematically assess the long-term changes in various operational parameters such as inertia and short-circuit current levels, and requirements such as flexibility, and availability of ancillary services such as reactive power support, frequency response, and contribution to short-circuit current [28]. TYNDP recently started exploring real-time system operation needs (voltage and frequency control) in response to new challenges expected to grow in the future because of the changing energy generation mix and increasingly responsive energy demand [29], [30].

2.3.2 A Mediterranean perspective

Inside the European energy framework, the Mediterranean region has a crucial role for relations and cooperation with the neighbour African and Asian countries. Recently, the association of the Mediterranean Transmission System Operators (Med-TSO) for electricity, share the necessity to enhance the coordination of the development plans including north and south shores of the Mediterranean. While the northern shore is engaged in ambitious decarbonisation targets and market integration within a general stagnation of the electricity demand, the southern shore is characterized by large potentiality of RES and by a fairly high rate of growth of the demand, with a market is still in evolution [31]. This is arising the vision for future interconnected electricity grids throughout the Mediterranean Sea. The Mediterranean transmission system consists of around 400,000 km of high voltage lines as per the end of 2016 and it is made by three different synchronous zones: ① ENTSO-E synchronous **Continental Europe** zone, which includes the European countries and Turkey; ② **South Western Mediterranean block**, which is synchronous with the ENTSO-E Continental Europe, and it includes the Maghreb region; ③ **South Eastern Mediterranean block**, which included Libya, Israel, and some of the Mashreq countries (Egypt, Jordan, Syria, Lebanon, Palestinian Territories).

There is currently 4 GW of interconnector capacity in operation through the Mediterranean Sea, while around 25 GW is under construction or planned [32]. Mostly of the interconnections uses the HVDC technology, even if a few HVAC links are present. The interconnections can be distinguished in three geographical clusters, considering Western corridors (corresponding to the Iberian Peninsula and western Maghreb), Central corridors (corresponding to the Italian Peninsula, central Maghreb and Libya) and Eastern corridors (corresponding to the southern

Balkans, Anatolia and Egypt). In Figure 2.2 an illustration of existing and future interconnectors across the Mediterranean Sea and their features is represented.

The major outcome of the interconnection between the northern and southern sides of the Mediterranean Sea is the sustainable electricity flow and the market integration.

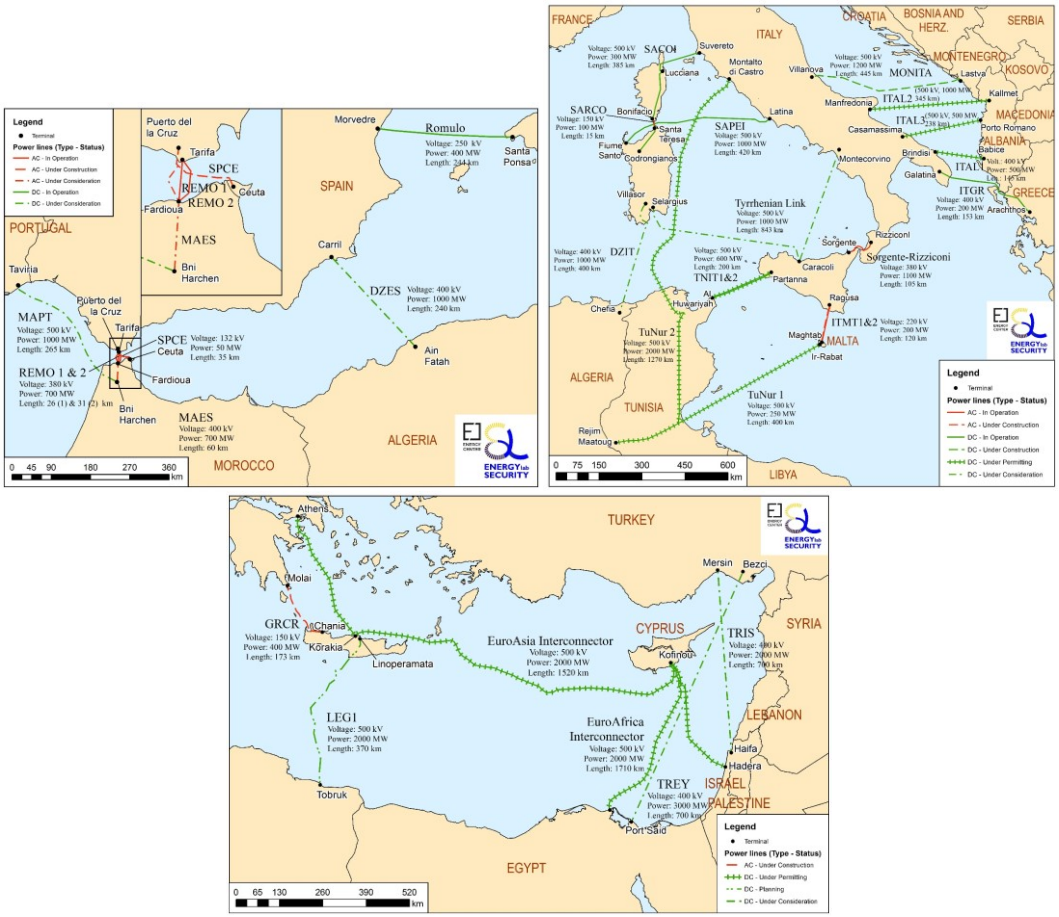

Figure 2.2: Main electricity interconnectors across the Mediterranean Sea [32].

Different actions were made in the past to promote the coherent development of interconnections between the power systems of the Mediterranean Sea.

The Maghreb regional interconnection, which includes Morocco, Algeria, and Tunisia was initiated in the 1950s. In the late 1990s, Morocco was connected to Spain via an AC interconnection, and thus Algeria and Tunisia are now all synchronized with the ENTSO-E Continental Europe network.

The interconnection between Tunisia and Libya has been built since 2002, but it is currently not operational. Closure of the interconnection lines between Tunisia and Libya would have created a synchronous AC system from Spain to Syria, between Tunisia, Algeria, Morocco and Libya, Egypt, Jordan, and Syria system. Two more cut-sets therefore remain open: Tunisia-Libya and Syria-Turkey. If synchronisation with the Tunisian grid is successful, it will mean that interconnection is achieved between the West and East Southern Mediterranean through the Egyptian electrical system, which is already interconnected with

Libya and the Mashreq. Syria and Turkey are physically connected, but for islanded mode and they are not synchronized [33]. Libya and Egypt are interconnected with Jordan, Syria and Lebanon of the South Western Mediterranean block. However only Libya, Egypt, Jordan and Syria are operated synchronously [34], while Lebanon and Israel could be currently described as an energy island.

In the east, Turkey is synchronized with the ENTSO-E grid, through three lines to Greece and Bulgaria. The interconnection was achieved in September 2010 and the interconnection has been turned into a permanent connection in April 2014. Turkey operates asynchronously with other countries: Georgia, Armenia, Azerbaijan, Iran, Iraq and Syria.

The Italian power system have a central role as a potential hub in the Mediterranean area, due to its position and experience in the electricity sector. Nevertheless, further and larger investments will be needed to interconnect Africa and Asia to Europe and to reinforce the local networks to be able to accept the inter-zonal flows, without security issues. Interconnecting North Africa and Europe arises the need of also integrating regulation, to avoid possible reliability problems. Mediterranean could be an ideal region where to develop a modern, secure, affordable and clean electricity system. European countries can export know how and technologies, enabling the creation of new industries in Africa, and at the same time exploit clean energy.

2.4 The Italian scenarios

The Italian electricity system is currently characterized by a prevalence of conventional generation with a decreasing trend. In 2018, the non-conventional installed capacity rose to just over 30 GW compared to around 4 GW in 2008, with a simultaneous decrease in the installed capacity of conventional thermal generation to 61 GW, after the all-time peak of 77 GW in 2012. The RES installed capacity was around 54 GW, including 22.5 GW of hydro, 20.1 GW of PV and 10.2 GW of wind. The electricity demand was 321.4 TWh, with a net national production of 279.8 TWh; production from renewable sources (bioenergy, hydro, wind, photovoltaic and geothermal) is worth 114.4 TWh, 34.5% of internal consumption. The maximum power required by the national electricity system was around 58 GW.

The possible evolutions of the National energy system are defined coherently with the European process undertaken by the EC and the ENTSOs in the TYNDP. The different temporal alignment between the elaboration processes, and a greater level of detail in national analysis resulted in scenarios being similar but not the same to their corresponding European scenarios.

In 2019, the Italian government, with national academies and research institutions, elaborated the "**Integrated National Energy and Climate Plan**" (PNIEC), which is valid for the period 2021-2030 and represents the Italy's contribution to the reaching of the European target in 2030 [35]. The main targets of PNIEC 2030 are the 33% reduction of GHG emissions compared to 2005 levels, 43% reduction of primary energy consumption, 30% of RES penetration on the final electricity consumption. The PNIEC target and measures are declined by the Italian TSO for electricity (Terna) and for gas (SNAM) in their **PNIEC scenario** for 2025 and 2030. considered as the policy scenario. It is characterized by high diffusion of heat pumps and electric vehicles, with noticeable energy efficiency measures, the total phase-out of coal plants within the 2025 horizon, the minimization of grid congestions and overgeneration, the increase of resilience and flexibility, the development of storage systems. The electricity demand lightly grows to 325 TWh in 2025 and 330 TWh in 2030.

The total coal-phase out is one of the main challenges for the Italian power system, posing non-negligible impacts and problems for the future safe management of the network [36]. The Italian coal plants interested by the phase-out are depicted in Figure 2.3, with a total of 8 GW of dismissed capacity.

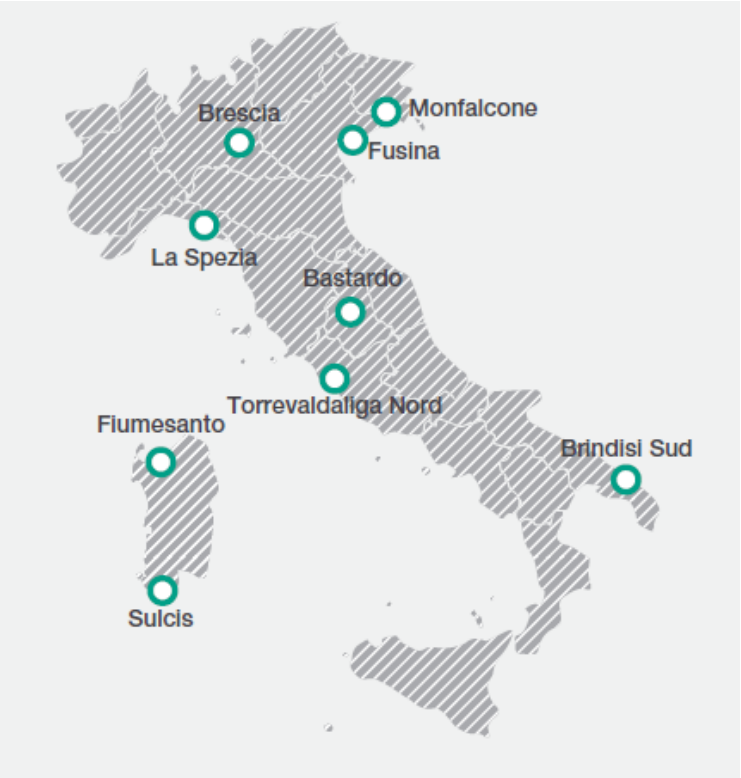

Figure 2.3: Italian coal power plants interested by the coal-phase out [36].

The Sardinian power system, characterized by limited thermal generation, highly dependent on coal generation, will require specific mitigating measures and infrastructural interventions for the phase-out. The main measures to enable the decarbonization in Sardinia are the realization of a new interconnector

between Sicily and the peninsula, the installation of new gas generation, storage and synchronous compensators.

The Italian TSOs finalised other two different scenarios up to 2040 [37]:

- **Business as usual** (BAU), scenario based on current policies, in which the system is left free to evolve without imposing targets and technological development is based only on economic merit. The coal phase-out is reached not for policies but for economic reasons only later than 2030. The electricity demand slightly increases, reaching 340 TWh in 2030 and 371 TWh in 2040, as in this scenario limited energy efficiency measures are considered. The RES installed capacity reaches 70.7 GW in 2030 (14 GW of wind and 31 GW of PV) and 92.7 in 2040 (18 GW of wind and 47 GW of PV).
- **Decentralized** (DEC), in which technology's diffusion and system evolution are foreseen according to the achievement of the European targets for decarbonisation, energy efficiency and share of RES. It is characterized by high electrification of end uses (heat pumps, electric vehicles), the total coal phase-out at 2025, high penetration of DER and storage. This scenario is characterized by the highest electricity demand (356 TWh in 2030 and 391 TWh in 2040). The RES installed capacity reaches 94.3 GW in 2030 (19 GW of wind and 49 GW of PV) and 123.1 in 2040 (25 GW of wind and 70 GW of PV).

Table 2.1 reports a characterization of the main future Italian scenarios compared to the current situation.

Table 2.1: Characterization of current and future Italian scenarios.

Scenario		CO_2 emissions reduction vs 1990 [%]	RES on gross final consumption [%]	Electricity demand [TWh]	Peak load [GW]	RES [GW]	Thermal capacity [GW]
2018		17.4	18.1	321	58	57	64
BAU	2030	28,4	20	340	56	70.7	50
	2040	31	22.7	371	62	92.7	50
DEC	2030	41.4	31.3	356	62	94.3	50
	2040	63.7	50.5	391	72	123.1	50
PNIEC	2025	N/A	22.5	325	54	66.1	49
	2030	40	30	330	62	93.3	50

The Italian TSO foresees several development interventions for the power system, based on the scenario described above and on the identification of system needs. The main interventions of the Network Development Plan 2019 are reported in Figure 2.4.

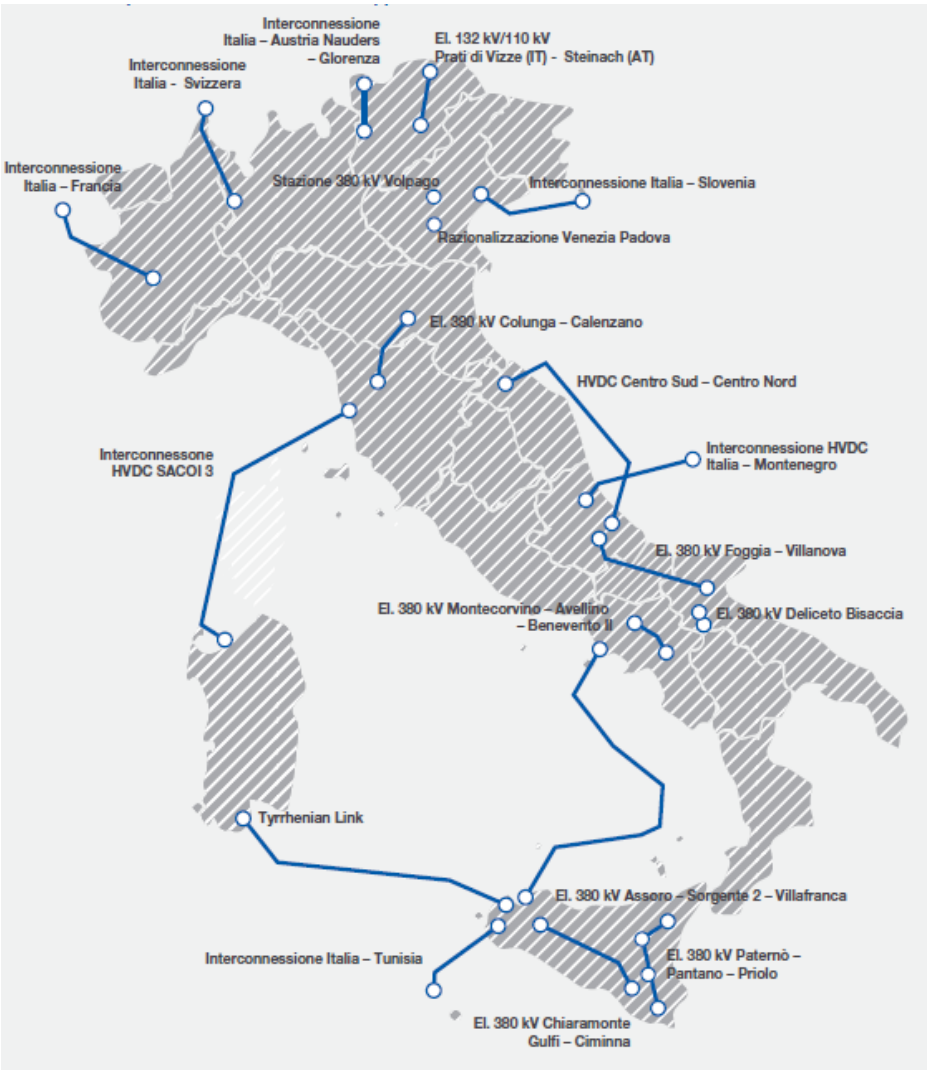

Figure 2.4: Main interventions from the Network Development Plan of Terna, 2019 [36].

2.5 Challenges for PEIG integration in future power systems

Power generation comprises different types of plants (thermal, nuclear, hydro, PV, wind, geothermal, biomass, etc.) which can be classified considering three main aspects: ① sustainability ② connection to the grid ③ variability.

RESs with larger diffusion (solar PV and wind) are mainly dispersed, mostly connected to the distribution systems, and variable (not programmable). Their production depends on meteorological conditions not predictable with large advance and precision (unless in the short timeframe), except for hydro with reservoirs, which can regulate water for flood control, dispatchable electrical power, and the provision of fresh water for agriculture. The variability of RES is evident from Figure 2.5, where a daily wind plant profile (a) is compared with a coal thermal plant profile (b). The thermal plant generation is almost constant and changes during the operation with ramps according to the generation schedules.

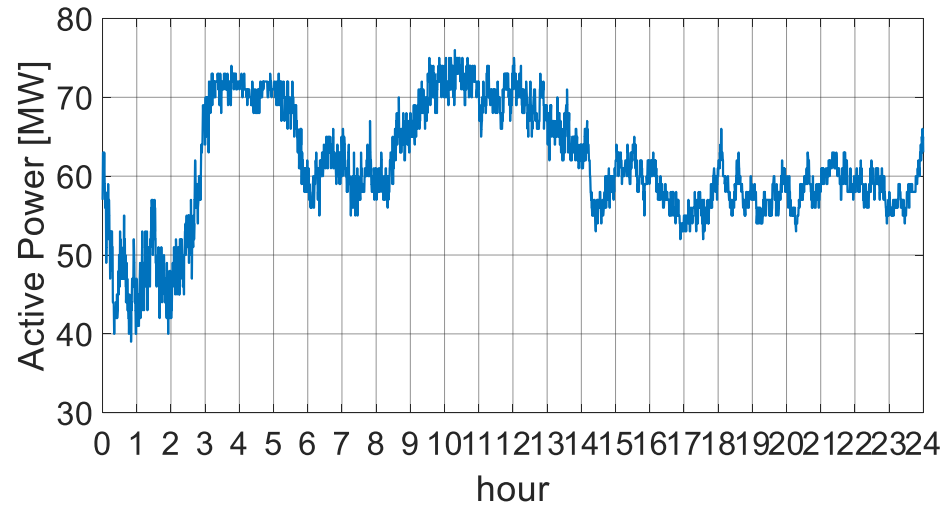

a.

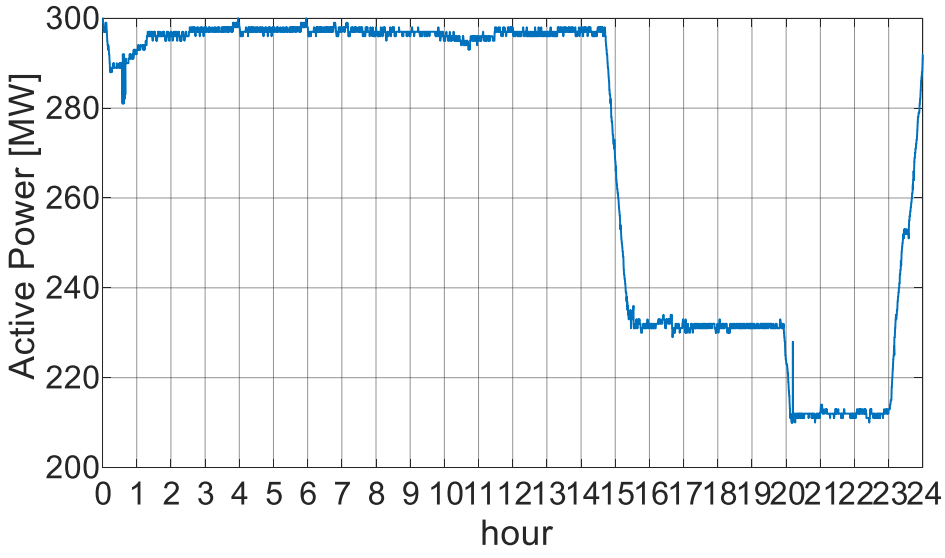

b.

Figure 2.5. Daily generation profiles for a wind (a) and a thermal (b) power plant.

Traditionally, converters are operated according to a Maximum Power Point strategy, trying to exploit the RES at its maximum. This kind of control may not be feasible in the future if the penetration of PEIG in the electric grid reaches higher levels. In fact, converters will be required to provide ancillary services that are traditionally in charge of synchronous generators. The major share of RESs is connected through power electronics devices, which provide lower short-circuit levels, imply reduced control capabilities, reduced inertia, and reduced system strength.

Considering the connection to the grid, it is possible to distinguish between **conventional** power plants, which are synchronous and centralized, and **non-conventional** power plants, non-synchronous and decentralised. Conventional generation has physical inertia, it can store and exchange kinetic energy, being directly linked to the network and it can be significantly overloaded for a short

time. Figure 2.6 shows the classification of main power generation sources considering whether they are synchronous, sustainable and/or predictable.

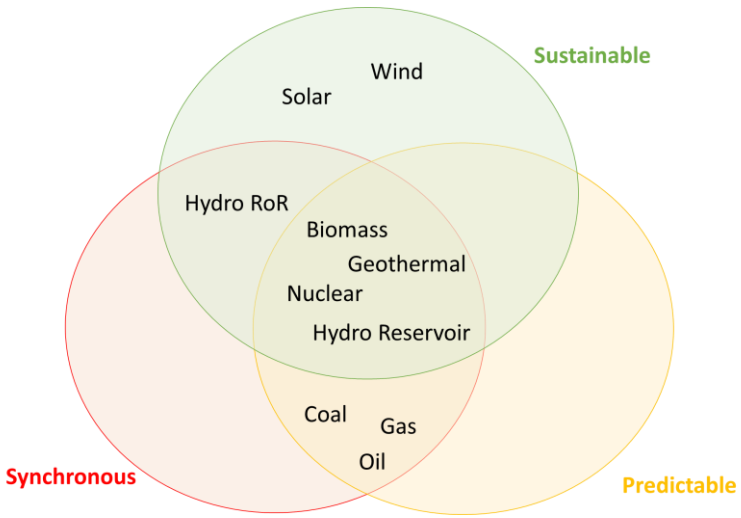

Figure 2.6. Classification of main power generation sources.

A power system consists of many components which form a large, complex and dynamic system having the purpose of generating, transmitting and distributing electricity over a large geographical area. The interconnection of such elements pones the basis for a large variety of possible dynamic interactions, characterized different cause, consequence, time frame, and physical character [38]. The concept of dynamics is directly linked with its stability after moving from a steady-state point and possible control actions to avoid unstable conditions. A power system is generally considered **stable** if it has the "ability for a given initial operating condition, to regain a state of operating equilibrium after being subjected to a physical disturbance, with most system variables bounded so that practically the entire system remains intact" [39].

When subjected to a disturbance, the resulting stability condition depends on the nature of the disturbance (location, type, duration) and the initial operating condition (power flow profile and topology of the system). Traditionally, power system stability is categorized according to the classification shown in Figure 2.7.

Three main classifications of stability are defined by giving priority to angles, frequency, and voltages: rotor angle stability, frequency stability, and voltage stability. The three types are divided into small-disturbance and large-disturbance and into short-term and long-term (except for angles). These concepts can be described and analysed by linearized and nonlinear models and concepts of Lyapunov stability theory, partial stability and bifurcation theory, and the classification works given the timescale separation for angles, frequency, and voltage issues [2]. However, the whole view of stability was focused on a system based on synchronous generator dynamics, quite different from the current grid development and power electronic dynamics were not explicitly considered. The higher penetration of PEIG may affect the classifications, as the dynamic time

scales and variables of interest change, and their inherent characteristics and capabilities can jeopardize the established types of stability.

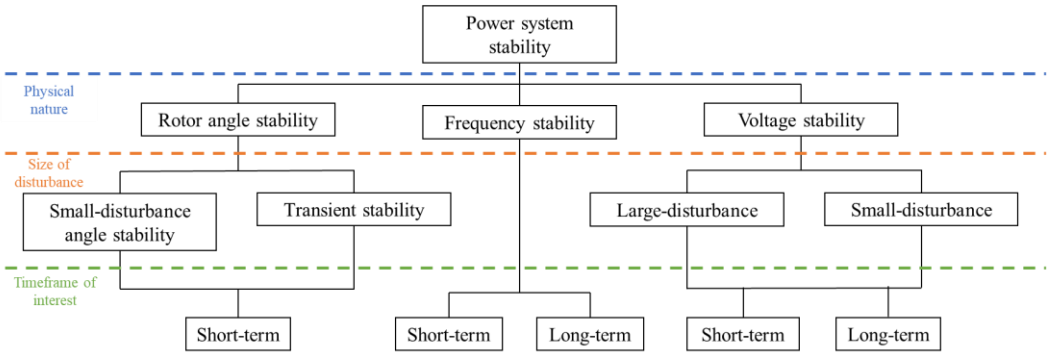

Figure 2.7: Classification of power system stability [40].

By 2030 several areas of the European transmission system will be operated with extremely high penetration of RES. To quantify such a trend, Figure 2.8 presents the anticipated share of PEIG on the total installed capacity in the European system based on the TYNDP 2018 scenario, which can reach up to 60% of total installed capacity in some synchronous areas (SAs).

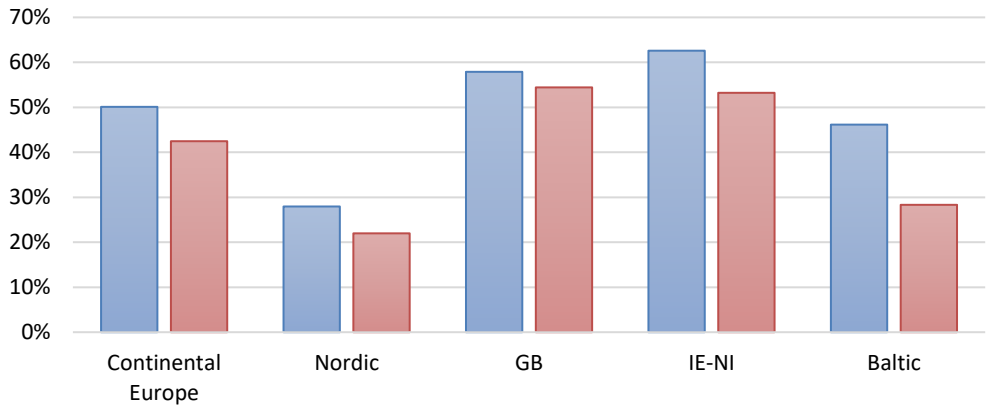

Figure 2.8. Share of PEIG installed capacity by 2030 (DG in blue, ST in red).

Even in those scenarios, it is necessary to guarantee the system adequacy and security, which require the availability of ancillary services. The large-scale integration of power electronic based systems poses new challenges to the stability and power quality of modern power grids.

A list of issues due to high penetration of PEIG is presented below.

The reduced inertia and the missing or incorrect participation of PEIG in terms of spinning and primary reserve impact the **frequency stability**. Higher reserve demand due to the uncertainty and intermittency of RES and decrease of reserve margins due to lower conventional generation can happen. These aspects will be discussed in detail in the next Chapter.

The inertia reduction significantly affects the **rotor angle stability**, associated with the capability of conventional synchronous generation units to remain in synchronism after being subjected to disturbances and classified into transient and small signal stability. The main impact is in the reduction of the critical clearing times of conventional generators [41], which affects the system protection settings, in terms of the time that fault need to be cleared before the generator's trip. The small signal stability and interarea electromechanical oscillations present through large power system might worse with the shift towards generators without power system stabilizers. To face this issue, power oscillation damping controllers need to be provided to PEIG [42].

Voltage stability is associated with the reactive power flow in the grid and the ability to maintain stable voltage profiles during steady state and grid fault conditions. While conventional synchronous generators can control the voltages through their automatic voltage regulators, high penetration of PEIG determines insufficient reactive margin and reactive power deficiency, with need to provide reactive support, high voltages in the sub-transmission system, with need to absorb reactive power. Moreover, synchronous generators provide high levels of **short-circuit currents** during faults, compared to PEIG which have low overloading and can typically inject a fault-current of only 1 or 1.2 times their rated current. The short circuit power reduction can lead to a wider propagation of voltage dips during grid faults, effecting the medium and low voltage levels and leading to potential disconnection of distributed generation. This trend is related to frequency stability, with the voltage dip induced frequency dip phenomena, and to the adequate setting of fault-ride-through capabilities and protections to prevent this impact. The loss of normal short-circuit current from conventional generators, can lead to **misfunctioning of the existing protections**, as classical overcurrent and distance protection could not be able to detect and clear grid fault in a fast and effective way if fault currents are very similar to the normal ones. This requires changes in the models and strategies for protection and control.

PEIG operation need a **stable grid voltage** or a minimum short circuit level provided by conventional synchronous generators. The control is currently based on the detection of sinusoidal voltage waveforms and it is called "grid following".

With a very low number of available synchronous generators, the missing stiff voltage sinusoidal waveform can lead to unstable situations [43]. "Grid forming" control might prevent this situation, as they use a different control strategy which allows the converter to operate and form a grid without the need for synchronous machines. In the last years new stricter rules have been demanded to avoid the disconnection of PEIG in the case of contingency or in the presence of low voltages, which can worse the stability (Low Voltage Ride Through Capability).

The wide timescale and frequency-coupling dynamics of converters tend to bring **harmonic instability** in the form of resonances or abnormal harmonics in a wide frequency range [44]. Some incidents have been reported with the integration of PEIG [45], where the undesired harmonics, inter-harmonics, or resonances caused disruption to the power supply. These interactions may lead to power oscillations (observable in voltage, current and power outputs) increasing the stresses to the equipment. Moreover, such oscillation can trigger malfunction in the device protections, and they may affect the power system reliability due to the increased probability of inadvertent equipment tripping.

The PEIG characteristic can cause **control interactions** with the grid resonance, visible as sub-synchronous, near synchronous or higher order harmonics up to 9 kHz [43]. Better filtering, procedures and new devices are needed to avoid such interaction phenomena.

Inter-area oscillations are exacerbated by the weakness of the system (long distances or weakly meshed) and high-power flows. These oscillations need to be damped as they can lead to significant power flow oscillations in the transmission lines and to physical damage to generating units.

PEIG exhibits **high volatility** which requires the need for advanced forecasting algorithms. Furthermore, the reduction of controllable sources able to provide ancillary services to the grid, for voltage and frequency regulation can result in risks for security and increasing costs to keep the system secure.

RESs variability affects the residual load, defined as the difference between the total demand and the variable RES. It shows how much capacity is left for conventional power plants to operate. The **Residual Load Ramp** is an indicator used to highlight the response (in MW/hour) that must be provided by controllable generating units, to maintain the balance between generation and demand. Figure 2.9 depicts the Residual Load Ramp duration curves for Italy in different scenarios coming from the TYNDP 2018. The ramps increase passing from 2025 to 2030.

The shape of the residual load evolved in the last years from the shape of the total load to a “duck curve” [46], with high variation during the day and a steep evening ramp due to the contemporary increase of demand and the sudden decrease of PV generation. It is necessary to ensure a fast ramp of programmable generation to avoid the associated risk of imbalances.

Interconnecting very large power systems with a huge number of RES can smooth the output variability and increase flexibility, sharing services and reserves. This is the goal of the super-grids, which can connect areas rich of RES with demand centre, or areas with excess of generation (in the night) with areas at their peak in demand (day) using HVDC high-capacity power transmission lines.

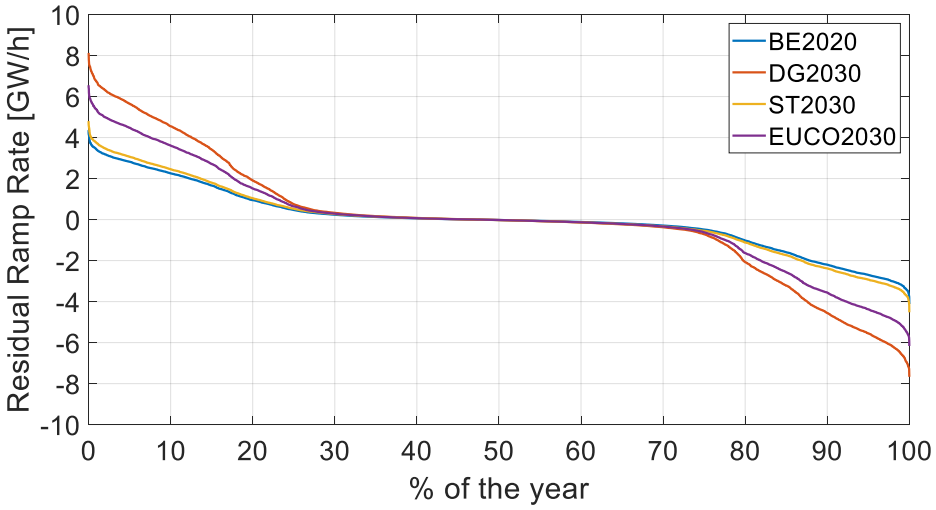

Figure 2.9: Residual Load Ramp duration curves for Italy in different scenarios taken from TYNDP 2018.

RES variability can be overcome using storage facilities (like pump hydro plants or innovative battery energy storage systems). The possibility of Power-to-X technologies (Power-to-Gas, Hydrogen, Heat) could be exploited to give more flexibility to the electric grid, but it will need a strict coordination between the electrical, natural gas and district heating infrastructure. Extensive use of **Energy Storage Systems** (ESSs) will provide new flexibility margins and solutions both from the generation and demand perspective.

The massive number of resources installed in the distribution network generate several **distribution-side operational effects**, as the risk of creating unintentional electrical islands during faults [47]. Another issue is the occurrence of **reverse power flow** from distribution to transmission grids, in the case the distributed generation overcome the local load under the same HV-MV substation. **Congestions** can happen locally in the case of reverse power flow from MV grids, but also in specific HV grid sections characterized by high RES generation compared to the load and lower meshing degree. This impact the markets increasing system charges but also RES curtailment to reduce the overgeneration. The generation needs to be able to both act as a voltage source and provide adequate power to start electrical equipment with high in-rush currents (**black-start**). Synchronous generators can do both tasks when the load is properly sized to their capabilities. PEIG need to be able to provide such capability as well. It is necessary to consider that a power system with very few (or no) synchronous machines will behave very differently, with much faster dynamics and different control schemes. The same meaning of frequency will change, as it will be not a physical variable and its variation will be immaterial for the determination of the power imbalance. Also, the familiar performance indicators (ROCOF, frequency nadir, or damping ratio) or the total (virtual or rotational) system inertia will not necessarily represent the system dynamics [48].

Another challenge come from the **sector integration** (electricity, gas, heat, transport, and industry) in terms of networks and the conversion of one commodity into another. Different options for coupling are available: power to heat, power to transport, power to "high value energy", as power to gas or power to X. The main difficulties are related to market design (to recognize each commodity value in different sectors), regulations and new technologies which could impact future power system, as interdependency and more exchange of information are needed, arising at the same time opportunities in terms of new flexibility sources and ancillary services.

2.6 Guidelines towards massive penetration of PEIG

This Section presents directions that would enable the stable and robust operation of power systems with high levels in PEIG, based on the five main pillars described in [43]. The main directions to follow are:

- The **improvement of system stability** includes expanded control capabilities of PEIG, such as: synthetic inertia, grid forming controls, supported system restoration, active and reactive power control, power oscillation damping and active harmonic filtering, among others. Using flexible protection schemes, the system can operate under different operational conditions with high PEIG penetration and a more variable short-circuit power levels. Flexible Alternating Current Transmission systems (FACTS) can improve power system stability and ensure cost-effective grid operation of systems with high level of PEIG, optimising system controllability and operation, controlling active and reactive power flows.
- The **improvement of system observability**, to assess dynamic stability margins and criteria to define the acceptable stability limits. Real-time monitoring tools (as Wide Area Monitoring Systems based on Phasor Measurement Units PMUs) give information about the dynamic behaviour of the grid and consequently increasing awareness for system dynamics. PMUs combined with communication technology bring the possibility to monitor system dynamics in real-time, allowing the development of remedial actions, automatic control schemes, restoration strategies. New generation of EMS/SCADA allows dynamic security assessment, short-circuit power levels and system inertia evaluation, to provide decision support to control room operators.
- The **improvement of system flexibility**, to manage the RES variability in different timeframes. RESs mean higher flexibility demanded to traditional power generation, because of the need for frequent and quick ramps to stop and start. There are a few options that system operators can decide to

perform, from evaluating to increasing flexibility. The types of intervention range from physical (e.g., storage, transmission), operational (e.g., cycling thermal fleets, forecast integration), or institutional (e.g., new market designs, integration of demand response) [49]. Higher flexibility could be achieved using modern Combined Cycle Gas Turbine plants, more interconnection between countries to share reserves, and the possibility for the consumers to vary their load profile thanks to the use of ICT technologies coordinated by resource aggregators (demand Side Response). Modulation of the demand made possible by the digitalisation of the electricity system (smart grids) contributes to the integration of variable renewables in the system.

- The **improvement of coordination** as the integration of distributed generation forecasts into the power system planning and operation is required to effectively tackle the challenges of large-scale integration of PE. The presence of significant generation capacity embedded in the distribution level creates possibilities for their participation in providing the capabilities and ancillary services which are needed to maintain a secure transmission system, e.g., active participation in frequency control. Cooperation between the different actors of the power system at the pan-European scale is needed to develop common tools and common grid models that will enhance the power system stability in the future. Especially, the reinforcement of cooperation between TSOs and DSOs also needs fast pace developments. The role of DSOs in the participation of system flexibility provision is expected to increase significantly. In this context, the amount of information exchanged among players is expected to expand rapidly, because improves the awareness, controllability of the system and, consequently, network security. TSO-DSO cooperation and coordination, due to the large integration of small scale and distributed energy resources, in terms of generation, storage and the increasing share of electromobility. This is changing the customers in prosumers, leading to possibility of delivering services to the power system, and raising different kind of challenges (congestion management, voltage control actions, demand side response). An appropriate aggregation of DER can deliver more advanced services such as balancing services and congestion management (mainly aFRR, mFRR, RR). Solving these kind of situations will require special coordination on regional or European level, but also better coordination between local and national level, between TSOs and DSOs. Virtual power plants.

To integrate up to 100 % renewable sources in the grid, no single and easy pathway is available. Several changes in technical, commercial and policy regulations must be introduced to lower the costs of having more RESs into the system.

Chapter 3

3 Frequency Dynamics Characterization and Instability Mitigation Strategies

3.1 Introduction

Frequency stability is defined as the ability of a power system to maintain steady frequency after a severe contingency, resulting in a considerable imbalance between generation and demand. To maintain the frequency within an admissible range it is necessary that the total generated active power be equal to the total consumed active power at every instant of time. The balance between generation and load is permanently perturbed, e.g., by load variations, by the inaccuracy of real time generation control or by the unscheduled/scheduled disconnection of a generator or a transmission line. The frequency variations need to be corrected by a rapid process which requires high performances for generators and different hierarchical control levels [50].

In this Chapter, an overview on the frequency dynamics characterization is given, starting from the fundamental regulation and control in modern power system to the current implications due to a massive penetration of PEIG. The classical control structure for frequency control is shifted to the current European Load-Frequency scheme, which will be the basis to develop the models described in Chapters 4 and 5. The major contingencies happened in recent years are reported, to highlight the arising challenges in power systems. Possible options to mitigate the issues are also investigated, reviewing the framework of the current trend in the literature.

3.2 Frequency control fundamentals

The equation of central importance in power system stability analysis are the rotational inertia equations describing the effect of an imbalance between the electrical and the mechanical torque of individual machines.

The mechanical dynamic of a synchronous machine is governed by the torque equation, coming from the Newton's second law of motion:

$$J\frac{d\omega_m}{dt} = T_m - T_e \tag{3.1}$$

with

$$\omega_m = \frac{d\theta}{dt} \tag{3.2}$$

where J is the combined moment of inertia of generator and turbine $[kg \cdot m^2]$, whose value depends on rotor physical structure and materials; θ_m is the mechanical angle of the rotor in $[rad]$ while ω_m is the mechanical rotational speed, T_m is the mechanical torque given by the turbine to the electrical machine and T_e is the electrical torque. It is possible to introduce the mechanical starting time T_a defined as the time required for the rated torque to accelerate the rotor from standstill to the rated speed ω_n. The mechanical starting time is variable depending on the nominal power (size) of the generator S_n and the type of prime mover and it is defined as:

$$T_a = \frac{J\,\omega_{m,n}^2}{S_n} \tag{3.3}$$

However, in the literature the inertia constant H is commonly used, defined as the kinetic energy $E_{k,n}$ in $[W \cdot s]$ at the rated speed divided by the nominal power:

$$H = \frac{\frac{1}{2}J\omega_{m,n}^2}{S_n} = \frac{E_{k,n}}{S_n} \tag{3.4}$$

Therefore

$$T_a = 2H \tag{3.5}$$

The inertia in power systems is referred to the motion of rotating component and their resistance to motion changes is expressed by the inertia constant. It can be interpreted as the time for which the energy stored in rotating parts of a turbine-generator is able to supply a load equal to the rated apparent power of the turbine-generator. The inertia of a rotating machine is defined as:

$$H = \frac{J\,\omega_n^2}{2\,S_n} \tag{3.6}$$

Equation (3.1) can be now normalized using (3.4), and considering that $\omega_m = \omega_e/p$, where ω_e is the electrical speed and p the number of poles of the machine, and $\theta_e = \omega_e t - \omega_0 t + \theta_0$, where ω_0 is the synchronous speed and θ_0 the initial angular position of the rotor, obtaining:

$$\frac{2H}{\omega_0}\frac{d^2\theta_e(t)}{dt^2} = T_m - T_e \tag{3.7}$$

The inertia of a single machine expresses thus the resistance to the change in rotational speed. Equation (3.7) is commonly referred to as the swing equation because it represents swings in rotor angle during disturbances.

In the description of the power system dynamics, it is possible to assume only small deviations from the synchronous speed $\omega_m \approx \omega_0 \approx \omega_{m,n}$. With this assumption, torques and powers differ for a fixed value ω_0, and considering the frequencies, yields:

$$\frac{2HS_n}{f_0}\frac{df}{dt} = P_m - P_e \tag{3.8}$$

where P_m represents the mechanical input power to the shaft and P_e the electrical output power. The parameters in Equation (3.8) can be concentrated using the inertia factor M:

$$M = \frac{2HS_n}{f_0} \tag{3.9}$$

The electrical power can be considered as the sum of a load variation ΔP_L and the correspondent load-frequency dependence ΔP_C:

$$\Delta P_e = \Delta P_L + \Delta P_C = \Delta P_L + E_C \Delta f \tag{3.10}$$

where E_C is the load regulating energy, which takes into account the rotating-load variation due to the frequency variation.

When moving to a power system with n generators, all units can be assumed to be assumed to be connected to the same bus, representing the Centre of Inertia (COI) of the system, under the hypothesis of well damped oscillations. In this case, it is possible to sum the swing equations for each machine i, obtaining:

$$2\frac{\sum_{i=1}^{n} H_i S_{n,i}}{f_0}\frac{df_{COI}}{dt} = \sum_{i=1}^{n}(P_{m,i} - P_{e,i}) \tag{3.11}$$

The following quantities can be defined:

COI frequency
$$f = \frac{\sum_{i=1}^{n} H_i f_i}{\sum_{i=1}^{n} H_i} \tag{3.12}$$

Total power
$$S_n = \sum_{i=1}^{n} S_{n,i} \tag{3.13}$$

Total inertia constant
$$H = \frac{\sum_{i=1}^{n} H_i S_{n,i}}{\sum_{i=1}^{n} S_{n,i}} \tag{3.14}$$

Total kinetic energy
$$E_k = \sum_{i=1}^{n} H_i S_{n,i} \tag{3.15}$$

Total mechanical power
$$P_m = \sum_{i=1}^{n} P_{m,i} \tag{3.16}$$

Total electrical power
$$P_e = \sum_{i=1}^{n} P_{e,i} \tag{3.17}$$

It is possible to describe the main system frequency dynamics using:

$$\frac{df}{dt} = \frac{f_0}{2HS_n}(P_m - P_e) \tag{3.18}$$

When an imbalance between the electrical power requested by the load and the mechanical power provided by the generator happens, each generator oscillates with small variations over the average frequency value of the COI.

3.3 Frequency regulation and control in modern power system

A power system must work at a frequency as much as possible constant (and normally equal to the nominal value) to ensure the correct operation of the end users. To this end, active power needs to be generated at the same time as it is consumed in a power system. Frequency is linked to the rotational speed of the electrical machines, which is constant when the driving and load torques are in equilibrium. However, during the operation of a power system, such equilibrium is continuously disturbed due to the volatility of the load (for connection and disconnection of end users or demand variation) or for generators trip following failures. Consequently, a mismatch between power demand and generation causes an imbalance between driving and load torque and the rotating masses in the system accelerate or decelerate, with a deviation of the system frequency from the set-point value. This immediate answer is noted as the inertial response. It is essential then to intervene to contain, control and restore the frequency value inside the admissible ranges. At this purpose, frequency regulation schemes have been implemented in the power system industry, based on three hierarchical levels of control. The automatic control system comprises the primary and secondary control, while the tertiary control is manually activated. A fourth level is the time control, which is usually not considered as a separate level, as it is implemented by adjusting the secondary control set point. Time control is used if producers or network users rely on electrical time, i.e., an average frequency of 50 Hz.

In the first sub-section, the theoretical background on the frequency control mechanism in power systems is described, while in the second one it is shown how the theory is applied practically and currently in the European power system.

3.3.1 Classical control structure for frequency control

The classical frequency control structure foresees three main levels of regulation: primary, secondary, and tertiary regulation.

Primary regulation is the result of local speed governors, based on setpoints for frequency and power. The objective is to react rapidly to the load variation and bring the frequency back to acceptable values. The primary regulation has the

following characteristics: ① fast ② speed regulation ③ analogic ④ local (based on the generator's speed measurement).

This service is provided by large synchronous generators, which change their power reference set-point according to their droop σ_P, defined as the ratio between the frequency variation Δf and the corresponding active power variation ΔP_e, measured in steady state and referred to the nominal power:

$$\sigma_P = -\frac{\Delta f / f_0}{\Delta P_e / P_n} \tag{3.19}$$

Generally, droop values are in the range between 2% and 7%. Primary intervention has also a dead-band, to avoid over-stress on the governor, set-point and measurements errors. The permanent regulating energy E_P is correlated to the droop. The regulating energy of a unit is the ratio between the active power variation and the frequency variation that caused the regulator intervention. The units participating in the primary control make available a power reserve, which is commonly referred to as spinning reserve. The total system spinning reserve is the difference between the sum of the power ratings of all the operating units and their actual load. The allocation of spinning reserve is an important factor in power system operation, as locating the spinning reserve in one region may be dangerous for security reasons (the missing power would come from another region and some transmission lines might get overloaded).

The primary regulation leaves an unavoidable frequency error because the control law is purely proportional, and it acts regardless the location of the disturbance. Nevertheless, it is not possible to insert a pole at origin in the speed regulator, for unavoidable measurement and setpoint errors. Therefore, the secondary regulation is needful: to counter the frequency error inserting a pole at origin, to restore the primary reserve and the changes in the power exchanges according the scheduled to other areas. **Secondary regulation** relies on a unique central regulator, which acts on the local speed governors of the generators through appropriate signals and acts only for disturbances within its own control zone [51]. The secondary regulation has the main following characteristics: ① slow, compared to the primary ② frequency regulation ③ digital ④ centralized (area).

In the case of a synchronous isolated power system, the automatic secondary control is implemented as a decentralized control function by adding an integral control loop to the governor.

In an interconnected power system with different control areas, the secondary control is centralized, as the information of where the power imbalance occurs is needed to avoid the intervention of regulation in all the other areas. Centralized control is also used to avoid undesirable changes in the tie-lines flows with consequent violation of the contracts between the cooperating systems. In interconnected power systems, each area, or subsystem, has its own central regulator.

In general, the primary contribution is extended to the as high as possible number of generators in the grid, while the secondary regulation relies on a reduced number of generators, which receive the central regulator's signal.

Figure 3.1 shows the post-contingency frequency behaviour of a traditional power system in terms of activated power reserves. It can be seen the importance of the inertial response, which is the immediate action of the synchronous generators to counterbalance the contingency. In longer timescales, the primary ΔP_p and secondary ΔP_s contribution are activated, to control and restore frequency. ΔP_m represent the sum of primary and secondary contributions.

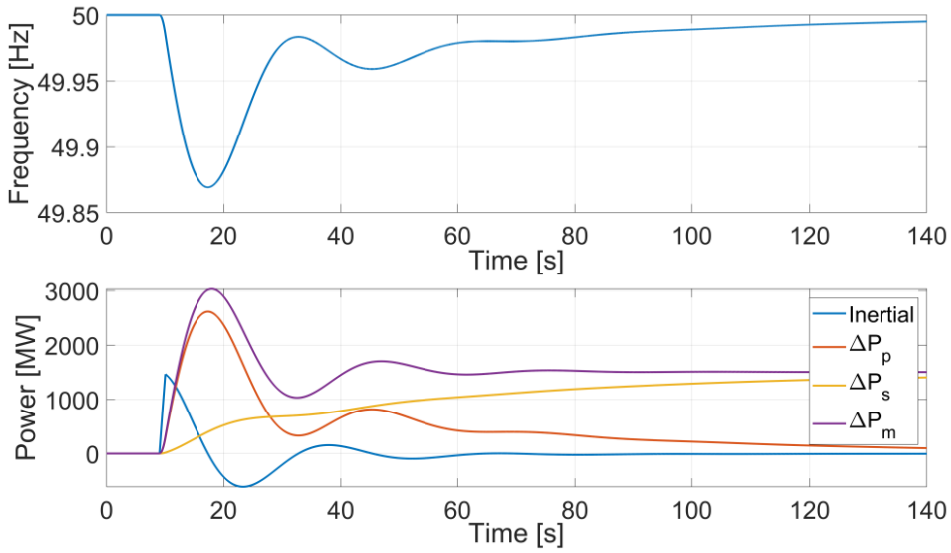

Figure 3.1: Post-contingency behaviour of a traditional power system in terms of frequency and activated reserves.

The **tertiary regulation** is additional to, and slower than, primary and secondary frequency control. The task of tertiary control depends on the organizational structure of a given power system and the role that power plants play in this structure [38]. Tertiary is manually activated and has one specific goal, which is the secondary reserve restoration, and a general goal, which is the balancing of the generation and load in compliance with the operational constraints (currents, voltage, N-1 security). The plants used for this service are the least costly ones. Possible causes of automatic regulation intervention are load and renewable generation forecasting errors, systemic hourly deviations of scheduled production programs and generators/load failures. In the aggregate models the tertiary power intervention can be represented as a power ramp.

Primary and secondary control are continuously active also in normal operation of the grid to compensate the small fluctuations. Conversely, the deployment of tertiary reserves occurs less often. However, not all the random load oscillations are followed by the primary and secondary regulation. In large part, the load oscillations compensate each other, particularly with many

generators and loads, for the inherent statistical behaviour. The oscillations with high frequency are balanced by the inertial power.

A superior level of control is related to the adjustment of the frequency signal in regular interval according to the long-term cumulated frequency deviation to sustain a constant average nominal frequency. This process is the **time control** or time error correction, as the difference between the nominal time and the electrical time, this last being computed as the integration of the second-by-second frequency. Time control is meant to correct deviations between electrical time and Universal Coordinated Time [52] and is essential for customers and equipment relying on the frequency for timekeeping (old electrical meters to distinguish different tariff periods, electric clocks, energy systems control, power quality devices).

3.3.2 European Load-Frequency Control and Reserves

The European frequency control structure, with definitions, services and processes have been harmonized by ENTSO-E through the implementations of network codes, starting from the "Load-Frequency Control and Reserves" code which become regulation in 2017 with [53]. This Regulation applies to all transmission systems, distribution systems and interconnections in the EU and regional security coordinators, which are operated synchronously with Continental Europe (CE), Great Britain (GB), Nordic, Ireland and Northern Ireland (IE/NI) or Baltic synchronous area[1]. Each synchronous area (SA) is reported in Figure 3.2 with the belonging countries.

Part IV of Regulation [53] is the fundamental basis for the **Load-Frequency Control** (LFC) **and Reserves** and it is composed by 11 Titles. Each Title comprises frequency quality criteria, the LFC structure and operation, reserves dimensioning, exchanges and sharing within and among synchronous areas as well as suggestions for the cooperation with DSOs and transparency.

A SA consists of one or more **control area** (LFC block), which is physically demarcated by points of measurement at interconnectors, operated by one or more TSOs fulfilling the obligations of load-frequency control. A control area consists of one or more LFC area, which in turns includes one or more TSO's **monitoring areas**. Each element of the structure fulfils different obligations (control processes, quality targets, reserve dimensioning). The SA CE consist of the LFC blocks, LFC areas and monitoring area which are set in [54]. Each LFC block has a **K-factor**, which is an estimation in [MW/Hz] for the change of active power output resulting from a frequency deviation and represent its contribution to the LFC.

[1] Other isolated synchronous areas are Sardinia-Corsica, Cyprus, and Crete.

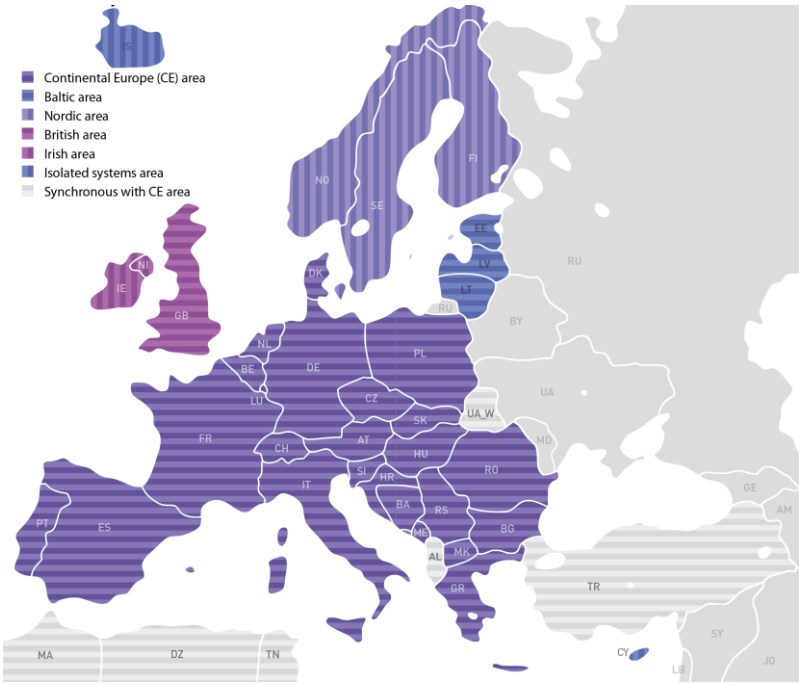

Figure 3.2. ENTSO-E synchronous areas.

In 2017 for instance these three components led to a total K-Factor of 27000 MW/Hz for the CE. ENTSO-E determines once per year the K-factor for each LFC area using the methodology reported in [55].

European TSOs use different processes and products to balance the system and restore the frequency, based on historic developments and different balancing philosophies. Balancing energy in Europe is organised in different steps, which are described below.

3.3.2.1 Frequency Containment Process

The **Frequency Containment Process** stabilises the frequency after a disturbance at a steady-state value within the permissible maximum steady-state frequency deviation using the **Frequency Containment Reserve** (FCR). All TSOs determine the reserve capacity for FCR required for the SA and each initial FCR obligation. The basic criterion used for **FCR dimensioning** is to withstand the reference incident in the SA by containing the system frequency within the maximum frequency deviation (±800 mHz for CE) and stabilizing the system frequency within the maximum steady-state frequency deviation (±200 mHz for CE). This expected instantaneous power deviation includes the losses of the largest power generation modules or loads, loss of a line sector or a bus bar, or loss of a HVDC interconnector. The **reference incident** is defined as the maximum expected instantaneous power deviation between generation and demand in the SA for which the dynamic behaviour of the system is designed.

The Regulation also introduces a **probabilistic** dimensioning approach for CE and Nordic, considering the tripping rates of the generation plants, pattern of load, generation and inertia, including synthetic inertia with the aim of reducing the

probability of insufficient FCR to below or equal to once in 20 years. The probabilistic approach depends then on aspects which are difficult to estimate and have a strong influence on the results. On the other hand, in the recent past, the FCR capacity dimensioned in Continental Europe (equal to the reference incident 3 GW in both directions) has proven to be enough to ensure the conditions for maintaining the frequency quality level and respecting the operational security requirements. For all these exposed above, the FCR dimensioning capacity in Continental Europe shall be equal to the reference incident for positive and negative directions [56]. Nonetheless more severe disturbances exceeding this reference incident cannot be excluded and may occur if an interconnected system splits into separate parts each with a high load imbalance due to a high-power exchange between these parts before the disturbance.

For the GB, IE/NI, and Nordic SAs, the reference incident is the largest imbalance (maximum instantaneous loss of active power) as the trip of a single power generating module, single demand facility or single HVDC interconnector. The reference incident is determined separately for positive and negative direction. Recently, ENTSO-E published an **incident classification scale**, which consist of 4 scales with levels of severity, from 0 (anomaly), 1 (noteworthy incident), 2 (Extensive incident) to 3 (wide area incident or major incident) based on frequency degradation effects for each SA, without giving a precise value for the reference incident [57]. For GB the reference incident was indicated in the range between 1320 MW (normal infeed loss) to 1800 MW (infrequent infeed loss) [58]. During the studies conducted for the Dynamic Security Assessment, the Irish TSOs set a value among 500 and 600 MW for the reference incident in IE/NI, while the Nordic TSOs used a value of 1450 MW [59]. The Nordic TSOs distinguish between the FCR-D for large disturbances and the FCR-N for normal operation [60]. The objective of FCR-N is to ensure continuous frequency stability within the standard frequency range (± 100 mHz). FCR-N is a specific Nordic product that is active between 49.9 Hz and 50.1 Hz and responds within 3 minutes. The FCR-N shall be at least 600 MW. The FCR-D is dimensioned to cover the reference incident, deducted by 200 MW due to the estimated load frequency dependency. In [61], the authors consider a reference incident of 1450 MW.

The shares of the reserve capacity on FCR required for each TSO as **initial FCR obligation** shall be based on the sum of the net generation and consumption of its control area divided by the sum of net generation and consumption of the SA over a period of 1 year. The shares of the reserve capacity on FCR required for each TSO Pi as initial FCR obligation for a considered calendar year t shall be based on the following expression [62]:

$$P_{i,t} = FCR_{dim} \cdot \left(\frac{G_{i,t-2} + L_{i,t-2}}{G_{u,t-2} + L_{u,t-2}} \right) \tag{3.20}$$

where

- $P_{i,t}$ is the initial FCR obligation for TSO i for the calendar year t.

- FCR_{dim} is the FCR dimensioning value calculated for SA CE.
- $G_{i,t-2}$ is the electricity generated in the control area i (including the electricity production for exchange of reserves and scheduled electricity production from jointly operated units or groups) during the second last calendar year with respect to the considered year t.
- $L_{i,t-2}$ is the electricity consumption in the control area i during the second last calendar year with respect to the considered year t.
- $G_{u,t-2}$ is the sum of electricity production in all control areas of the SA CE during the second last calendar year with respect to the considered year t.
- $L_{u,t-2}$ is the total consumption in all control areas of the SA CE during the second last calendar year with respect to the considered year t.

Every year each TSO of the SA CE shall provide to each other the data regarding the generation and consumption in its control area in the previous calendar year [62].

FCR activation time depends on level of frequency deviation and on the size of the system. For CE, in case of a frequency deviation equal to or larger than 200 mHz, at least 50% of the full FCR shall be delivered at the latest after 15 s and the 100% at the latest after 30 s. Each TSO monitor its contribution to the FCR obligations, including the **FCR providing units**, based among others the on self-regulation of the load, the frequency response by HVDC and the exchange of FCR. Each FCR provider shall be able to fully activate FCR continuously for at least 15 minutes. In Italy, FCR is a mandatory service for all generating units (except the non-programmable ones) with a power higher than 10 MW and it was decided recently to remunerate it. The power generating units that participate to the FCP must guarantee an active power reserve greater than ±1,5% of the efficient power for the continent and ±10% for Sardinia and Sicily (in insular condition). For hydro units, the droop must be set to 4%, while for thermal units to 5% [63].

The TSOs of the SAs connected via an HVDC interconnector can implement a frequency coupling process to enable FCR exchange and/or sharing between SAs. For CE, the exchange of FCR shall be limited to 100 MW of reserve capacity.

3.3.2.2 Frequency Restoration Process (Automatic and Manual)

The **Frequency Restoration Process** aims at restoring frequency to the nominal frequency and, for SAs consisting of more than one LFC area, at restoring the power balance to the scheduled value, by activation of the Frequency Restoration Reserve (FRR) which replaces the activated FCR. The FRR comprises the **automatic** (aFRR) and **manual** (mFRR) reserves. The aFRR includes all the active power reserves that can be activated within a delay less than 30 s, while the mFRR with activation time less than the time to restore frequency,

i.e., the maximum expected time after the occurrence of an instantaneous power imbalance smaller than or equal to the reference incident in which the system frequency returns to the admissible range.

The European Regulation introduces the **Frequency Restoration Control Error** (FRCE), which indicates the control error for the FRP, equal to the ACE of a LFC area or equal to the frequency deviation where the LFC area geographically corresponds to the SA. The FRP is designed to control the FRCE towards zero by activation of manual and automated FRR within the time to restore frequency. The ACE is the sum of the power control error (ΔP_S), that is the real-time difference between the measured actual real time power interchange value (P) and the control program (P_0) of a specific LFC block and the frequency control error ($K \cdot \Delta f$), that is the product of the K-factor and the frequency deviation of that specific LFC block, where the area control error equals $\Delta P_S + K \cdot \Delta f$. All TSOs specify the values of the level 1 and level 2 that the ACE shall not exceed for respectively the 30% and 5% of the time intervals of the year [64].

The minimum requirement for the **FRR dimensioning** is defined based on a combination of a deterministic and probabilistic approach and coherent with the quality requirements. The suitable dimensioning approach differs from control area to other control area due the physical sources and patterns of its imbalances. The **deterministic** approach requires that the FRR capacity shall not be smaller than the reference incident (separate for positive and negative direction). The **probabilistic** assessment defines a minimum value for the sum of FRR and RR capacity, which is defined by the 99% quantile of the control area imbalances (separated for positive and negative direction). This approach was recommended in the former Union for the Coordination of Transmission of Electricity (UCTE) and it may also be considered leading to recommended minimum amount of aFRR with respect to the maximum anticipated consumer load in the LFC area [55]. All TSOs of a LFC block determine the ratio of automatic FRR, manual FRR, the automatic FRR full activation time (time period between the setting of a new setpoint value by the frequency restoration controller and the corresponding activation or deactivation of automatic FRR) and manual FRR full activation time (time period between the setpoint change and the corresponding activation or deactivation of manual FRR) to respect the FRCE target parameters, defined in Article 128 of [65].

The aFRR controller has a **proportional-integral** behaviour and its parameters reflect the dynamic properties of the aFRR. The typical values for the controller parameters are:

- 0% to 50% for the proportional term;
- 50 s to 200 s for the integral term;
- 1 s to 5 s for the controller cycle time.

TSO computes the frequency from a specific stable node and monitors all the tie-lines of the grid, then gathers all these signals, computes the level L and communicates it to the regulating generators every few seconds (for ex. in Italy, 4 seconds). A **FRR providing unit** for aFRR shall have an automatic activation

delay not exceeding 30 seconds and shall be capable of activating its complete automatic reserve capacity on FRR within the automatic FRR full activation time and its complete manual reserve capacity on FRR within the manual FRR full activation time. The FRR full activation time is determined by all TSOs of a LFC block. Currently, the FRR full activation time requirements of CE cover a wide range from 2 to 15 minutes and reflect the local generation structures and requirements. The requested FRR must be available at least for 2 hours. In Italy, the FRR providing units must provide a FRR equal at least to the major between ±10 MW and the 6% for thermal or the 15% for hydro of the maximum power within 200 s [63]. The Italian Grid Code contemplates the implementation of the "Integratore Locale di Frequenza" (ILF), an additional speed controller loop, activated on request in case of grid separation and with frequency deviations higher than 0.3 Hz. Table 3.1 shows the values for the LFC parameters in the different European SAs.

Table 3.1: Main LFC parameters for different European synchronous systems [53].

	CE	**GB**	**IE/NI**	**Nordic**	**Cyprus**	**Baltic**[2]
Reference incident	3 GW	Largest imbalance (1.32 to 1.8 GW)	Largest imbalance (600 MW)	Largest imbalance (1450 MW)	Largest imbalance (130 MW)	1.2 GW
Standard frequency range	± 50 mHz	± 200 mHz	± 200 mHz	± 100 mHz	± 200 mHz	±50 mHz normal range ±200 mHz permissible range
Maximum instantaneous frequency deviation	800 mHz	800 mHz	1000 mHz	1000 mHz	1200 mHz	800 mHz
Maximum steady-state frequency deviation	200 mHz	500 mHz	500 mHz	500 mHz	500 mHz	200 mHz
Time to restore frequency	15 min	15 min	15 min	15 min	20 min	15 min
Dead band of governors	10 mHz	15 mHz	15 mHz	10 mHz	150-200 mHz	20 mHz
FCR full activation time	30 s	10 s	15 s	30 s	No requirements	30 s
FCR full activation frequency deviation.	± 200 mHz	± 500 mHz	± 500 mHz	± 500 mHz	± 200 mHz	± 200 mHz

[2] The strategic goal and big challenge of the Baltic States is to disconnect their power systems from the Integrated Power System/Unified Power System (IPS/UPS) of Russia (of which is currently technically part) and join the Continental European power grid and frequency area foreseen by the end of 2025 [273].

3.3.2.3 Replacement Reserve Process

The **Replacement Reserve Process (RRP)** means the process to replace the activated FRR and/or complements the FRR activation through the Replacement Reserve (RR). The RRP is operated through manual activation. The RR dimensioning rules comprise sufficient positive/negative reserve capacity to restore the required amount of positive/negative FRR. The European Electricity Balancing Guideline [66] foresees the implementation of common European platforms to harmonise the balancing market processes for the exchange of balancing energy: PICASSO for aFRR process, MARI for mFRR and TERRE for RR process.

3.3.2.4 Time Control Process

The target of the time control process is to control the average value of the system frequency to the nominal frequency to eliminate an existing time deviation between the **synchronous time** (which is the fictive time based on the system frequency in the SA) and the **Coordinated Universal Time** (UTC). This time deviation is a performance indicator for the long-term period. The difference between the actual and the nominal value of the system frequency to correct the synchronous time is denoted as **frequency offset**. Where applicable, all TSOs of a SA define the methodology to correct the electrical time deviation, which include: the time ranges within which TSOs shall endeavour to maintain the electrical time deviation; the frequency setpoint adjustments to return the time deviation to zero; the actions to increase or decrease the average system frequency by means of active power reserves. The SA monitors the electrical time deviation, calculate the frequency setpoint adjustments and coordinate the actions of the time control process. The actual **frequency set-point** value for time control is used in the frequency restoration controller for the calculation of the frequency deviation [67]. A discrepancy between synchronous time and UTC is tolerated within the range of ±20 s (without need for time control actions).

The electrical time control is both a final frequency control process as long-term frequency stability and a service given by the TSOs of a SA to its users which have internal processes based on electrical time. In this last category are devices which dependent on electrical time: meters of electrical energy which calculate different tariff periods in a precise time measurement based on frequency as input value; power plants control energy; power quality devices; old industries processes; customers in textile industries, synchronous motors.

Figure 3.3 gives an overall overview of the hierarchical frequency control in Europe, based on [68]. In this thesis, the terms primary/FCP, secondary/automatic FRP and tertiary/RRP will be interchangeable.

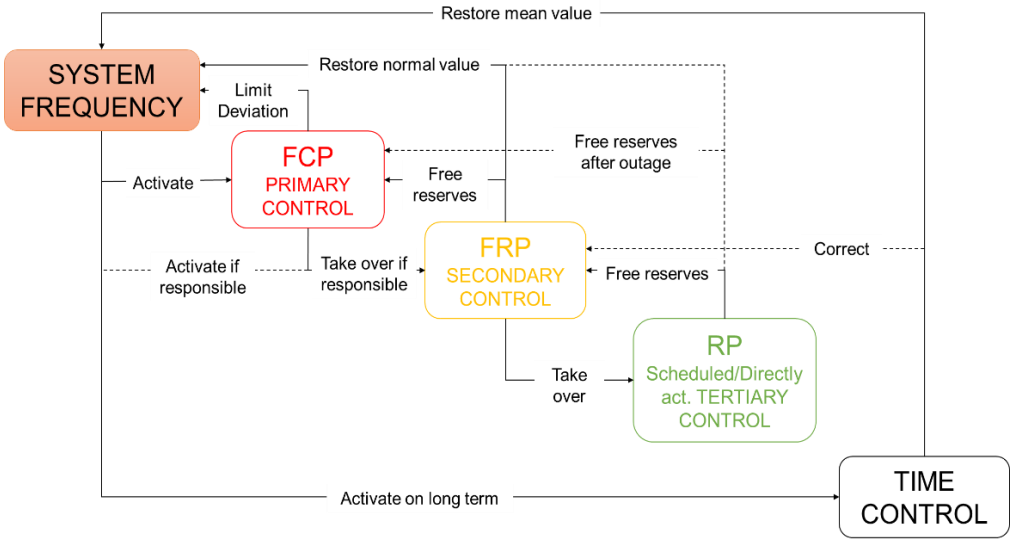

Figure 3.3. Overview of the hierarchical frequency control in Europe [69].

3.3.2.5 Requirements for Generators and Emergency

The requirements for grid connection of generators are harmonized in [70]. This Regulation introduces the concepts of **Frequency Sensitivity Mode** (FSM), **Limited Frequency Sensitive Mode** in **Over** and **Under-frequency** (LFSM-O, LFSM-U) meaning a power-generating module or HVDC system which result in active power output reduction/increase in response to a change in system frequency above/below a certain value.

LFSM-O and LFSM-U need to be activated when the system is in an emergency state of over/under-frequency and all FCR in negative/positive direction have already been deployed [71]. Response to frequency variations requires a coordinated response, moving from an early response to small frequency deviation (Frequency Sensitivity Mode FSM), a response to larger frequency variation (LFSM, active and reactive power control) and finally a last response to avoid network collapse (Low Frequency Demand Disconnection, LFDD). By principle, LFSM-O service can be provided by every power generating module in operation above its minimum regulating level. In contrast, the provision of LFSM-U service may be subject to further preconditions. An active power increase is possible only for generators running below their maximum capacity. Typically, RES generation however is dispatched according to their maximum available primary energy, unless there are network constraints. The economic generation dispatch hence shall not be limited by LFSM-U performance.

The power-generating modules are divided in **synchronous** or a **power park** module. A power park module means a unit or ensemble of units generating electricity, which is either non-synchronously connected to the network or connected through power electronics, and that also has a single connection point to a transmission or distribution system. Power-generating modules are

distinguished in different types according to control capabilities, connection point voltage and maximum capacity, each subject to stricter levels of requirements going from A to D. The general requirements for the power-generating modules are described in chapter 1 (Articles 13-16) for the different types, while the specific for synchronous and power park modules in chapter 2 and 3.

All the power-generating modules are requested to be capable of remaining connected to the network and operate within the frequency ranges and time periods specified in Table 3.2 for CE.

Table 3.2: Minimum time periods for which a power generating module must be capable of operating on different frequencies without disconnecting from the network

SA	Frequency range	Time period for operation
CE	47.5 – 48.5 Hz	To be specified by each TSO, but not less than 30 minutes
	48.5 – 49.0 Hz	To be specified by each TSO, but not less than the period for 47.5 – 48.5 Hz
	49.0 – 51.0 Hz	Unlimited
	51.0 – 51.5 Hz	30 minutes

Type A are required only to provide LFSM-O, while LFSM-U start from type C. Type C and D shall be capable of providing active power frequency response at a frequency threshold and droop settings specified by the TSO, within the ranges shown in Table 3.2. The droop settings shall be between 2% and 12%. An adjustable droop is technically feasible not a significant cost issue for plant design. However, a very low droop setting with more frequency sensitive responses could lead to increased maintenance costs.

The FSM implies the delivering of the FCR. In case of more severe disturbances than the reference incident, LFSM is activated.

From the system transient behaviour and for successful LFSM-O/-U performance it is essential to define the response time of LFSM-O/-U activation. The response time depends on the power generating module technology. Synchronous power generating modules can provide inertia, but on the other hand are typically not able to adapt power output very fast. Power park modules have no or just very little inherent inertial response but are typically able to swiftly adapt their power output. Taking these characteristics into consideration it is recommended to distinguish between these types of power generating modules.

The five different critical system states are identified and defined in [53]: ① Normal ② Alert ③ Emergency ④ Blackout ⑤ Restoration. The emergency and restoration principles and guidelines are established in [73]. A power system is in the emergency state when the FCR is not sufficient to cover the power imbalance (as in the case of system splits) and the frequency is not within the standard frequency range and larger than the maximum steady state frequency deviation. The automatic under and over-frequency control schemes are among the measures of the system defence plan. They include scheme for the automatic low frequency

demand disconnection and the settings of the LFSM-U/O in the LFC area. The frequency thresholds and schemes are established by each TSO in its system defence plan. They include scheme for the automatic low frequency demand disconnection and the settings of the LFSM-U/O in the LFC area. As the activation of this scheme implies the loss of load in entire regions, it must only be activated if necessary, in order to save the system. In the ENTSO-E Continental Europe system, the first load shedding stage is activated at a frequency of 49 Hz, causing the shedding of about 15 % of the overall load. The frequency thresholds and schemes are established by each TSO in its system defence plan. A general overview of the automatic low frequency demand disconnection characteristics is reported in Figure 3.4.

The emergency control actions are divided in **automatic** actions (load shedding with relays sensible to frequency and its derivative, generation shedding for over-frequency) and **manual** actions (hydro units power variation by-passing governors, interruptible loads, pumps shedding).

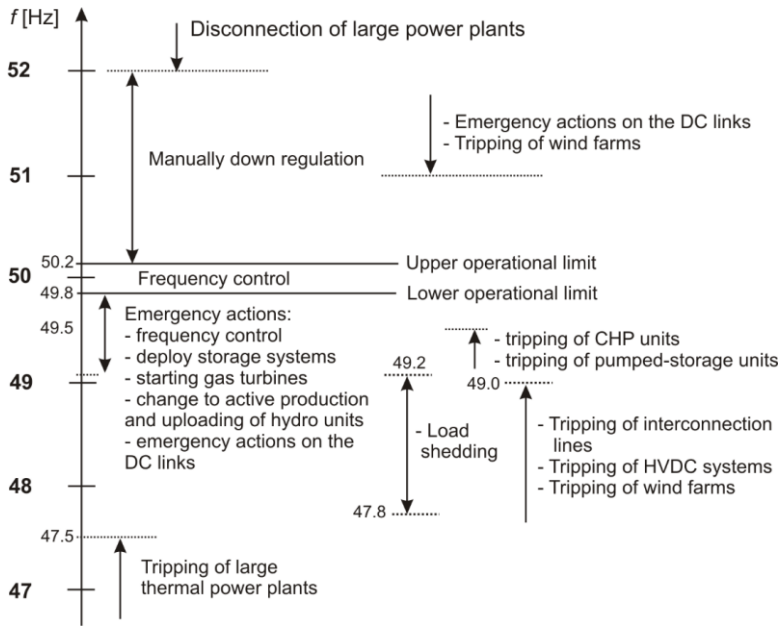

Figure 3.4. Tripping thresholds to frequency variations [73].

3.3.3 Major recent contingencies in power systems

Power systems are continuously subjected to different kind of disturbances which can have several origins. The main causes can be considered [74]:

1. Disturbance or trip of a power generating module, HVDC interconnector or load,
2. Continuous load and generation oscillations,

3. Forecast errors, due to the uncertainty of load and RES generation, e.g., related to the weather conditions,
4. Deterministic imbalances, due to the deviation between load and step-shaped schedules causing the deterministic frequency deviations,
5. System split, which consist to the separation of an interconnected power system in two or more portions, with imbalances generally out of the security dimensioning and most likely leading to emergency situations.

It seems important to review some of the major outages in power system, to understand the main causes, consequences and get them in the future context.

In the last few years, various blackouts occurred in different parts of the world [75]. Although in each case the blackout was initiated by specific technical reasons, many observers argued that systemic reasons underlie for such many disturbances in this limited timeframe [38]. The liberalization of the electricity sector, different marginal prices and unpredictable RES mostly far away from load centres gave birth to significant increase in cross-border exchanges, affecting interconnected systems for purposes they were not designed for. In meshed grids this can originate loop flows[3], which may endanger and generate unpredicted overloading.

The major system disturbances in CE occurred on September 28th, 2003, with the **Italian** system separation [76] and on November 4th, 2006 [77]. The Italian blackout was initiated by line flashovers to trees and overloading on the Swiss border and ended with the separation of the entire Italian system from the UCTE grid. Italy suffered an under-frequency transient and a complete blackout affecting around 45 million people [78]. The automatic load shedding was not sufficient to avoid the blackout, with a net imbalance around 1900 MW.

A significant change in actual wind generation was one of the contributing factors to a widespread disturbance leading to the shedding of 17 GW of load in the **UCTE** network in November 2006. The tripping of several high-voltage lines, which started in Northern Germany, split the UCTE grid into three separate areas (West, North-East and South-East) with significant power imbalances and frequency deviations in each area [77].

The major disturbances in 2003 and 2006 revealed the need to enhance cooperation and coordination of defence and restoration plan at a Pan-European level.

A third serious event in the CE system was a blackout occurred in **Turkey** on March 31st, 2015 [79]. The trip of an overloaded line initiated the loss of synchronism between the Eastern and the Western subsystems of Turkey, with the consequential tripping of many parallel lines. This caused first the separation of

[3] Loop flows (or parallel flows) are flows which do not travel along an agreed contract path between a seller and a buyer, but over many parallel routes in a meshed grid.

the two subsystems from each other and later the separation of the Western subsystem from CE. The Turkish subsystems collapsed, without major impact on the CE system.

It worth to mention other two events happened inside Europe between 2003 and 2004. On September 23rd, 2003 the **Nordic** power system experienced a 1200 MW unit trip, followed by cascading failures which led to the blackout of southern Sweden and eastern Denmark [80]. On July 12, 2004, the south part of the **Hellenic** Interconnected Transmission System (including Athens) was split from the rest of the system and collapsed, initiated by the opening of a north south HV transmission line [81].

However, several other critical events happened throughout Europe in 2019. A long-lasting steady-state frequency deviation with average -30 mHz began on Wednesday, 9 January 2019 at 13:25 and persisted until 11 January 2019 at 09:37. On 10 January, this frequency deviation coincided with a deterministic frequency deviation (evening peak-load at the hourly schedule transition) which quickly caused the frequency to decrease to a value of 49.81 Hz [82].

On June 2019, 12nd, a wrong RES generation forecast in **Germany** determined a power deficit of around 6.5 GW and the frequency dropped at 49.9 Hz for 20 minutes, with high risk of load shedding in all Europe.

On August 2019, 9th a lightning strike occurred on a transmission circuit causing a generation loss of around 2 GW [83]. The generation loss included embedded generation and offshore windfarm. The frequency fell very quickly to 48.8 Hz, triggering the Low Frequency Demand Disconnection scheme. This resulted in approximately 1.1 million customers being without power for a period between 15 and 45 minutes [84].

A nuclear power plant trip originated a sequence of events resulted in a power deficit of 3.5 GW in **France** in October 2019, 7th. The frequency dropped at 49.8 Hz, with interruptible load shedding of 1.4 GW in France.

Looking outside Europe, two major blackouts occurred in **Brazil** on November 10th, 2009 and on February 4th, 2011, involving respectively the disconnection of a HV transmission line and a HV substation. In both cases, cascading failures following the main events led first to regions islanding and later to the system collapse [85].

The North-East **United States** and Ontario, **Canada** experienced a blackout on August 14, 2003. About 50 million people were affected and 63 GW of load was interrupted. The major reason was found to be insufficient reactive power, which led to voltage instability [86].

On July 30th, 2012, the **Indian** power system suffered a severe disturbance which led to blackout, initiated by the overloading of an inter-regional tie line and followed by cascading failures and separation of the interconnected regions [87].

The **South-Australia** blackout on September 28th, 2016 was the first known due to very high renewable penetration [88]. A severe storm damaged several transmission towers, and subsequently the South Australia grid lost more than half of its wind generation within a few minutes. This deficit caused an increased

power flow and the trip of the interconnectors with Victoria. The result was the separation of South Australian and its collapse. Australia was affected by another severe disturbance on August 25th, 2018. **Queensland** region was separated by the rest of the system, due to severe weather conditions, with subsequent separation of South Australia and under-frequency load shedding around 1 GW [89].

All the events previously described had similar characteristics such as high corridor loading, underfrequency load shedding, non-conform power plant behavior with respect to abnormal frequency deviations and in the last years high share of variable RES. Power blackouts have large technical, economic, and social consequences and as power systems evolve with innovative technologies and regulations, their continuous analysis will be crucial to identify and update new prevention measures to keep the lights on.

If there is a system split, the TSOs affected by it switch to an emergency state. According to the [72], a TSO is entitled to suspend market activities during emergency state or black-out. Additionally, the TSO is entitled to suspend the operation of its processes impacted by such separation. The suspended market activities may include, inter alia, the schedule energy and cross-border capacity.

3.4 PEIG impact on frequency stability

Modern power systems have been designed and relies on the dynamics of synchronous machines and their control, which are very different compared to the PEIG. The increasing penetration of PEIG is arising major challenges on the system dynamics and operation, mainly related to frequency regulation, reactive support, and harmonic distortion.

The present Section reports a brief overview of these challenges which could impact the frequency dynamics and need to be monitored to assess the possible impacts and investigate solutions when necessary [30].

Traditionally, PEIG are typically operated at their maximum power output and are not expected to respond dynamically to frequency changes. The reserve and thus the ability to provide primary frequency control is limited. The stochastic nature of PEIG makes the problem to persist even if operated with a given reserve below the maximum power point, due to the stochastic nature of PEIG. On the other side, power converters are generally fast and can provide a primary frequency control faster than conventional power plants. However, since power converters do not respond inherently to power imbalances, their response might not be effective in the first seconds or hundreds of milliseconds after a contingency [2].

PEIG lack the natural coupling with the grid and its interaction is based on the chosen control approach. Two approaches are usually distinguished: grid-following and grid-forming control. In the grid following approach, the PEIG

control the output of real and reactive power by injecting current at a given phase angle simply following the imposed voltage and frequency by the grid. In the grid-forming mode the PEIG regulates the voltage magnitude at its terminal and the frequency to specific setpoints, as a synchronous machine. During contingencies, the grid-forming sources will increase or decrease their output power instantaneously to balance loads and maintain local voltage and frequency, while the grid-following shut down [90]. These actions are much faster than the grid-following sources. As the penetration of PEIG increases, there will be few synchronous generators forming voltage and frequency for grid-forming sources and it will be necessary to have grid-forming PEIG, which should offer all capabilities that are offered primarily by synchronous machines.

The total system inertia reflects the amount of kinetic energy stored in the rotating shafts of the conventional synchronous generators and motors. The increasing penetration of non-synchronous generation decreases the available inertia of the grid, which mainly influences the frequency stability. The direct consequence of reduced inertia for the frequency stability is an increased Rate Of Change Of Frequency (ROCOF) and more extreme frequency oscillations, with reductions in the lowest values (nadir) and increases in the highest value (zenith) of the oscillations following a system disturbance. Figure 3.5 shows an example of frequency response after a generation loss equal to 0.1 p.u. of the system's size in case of different inertia.

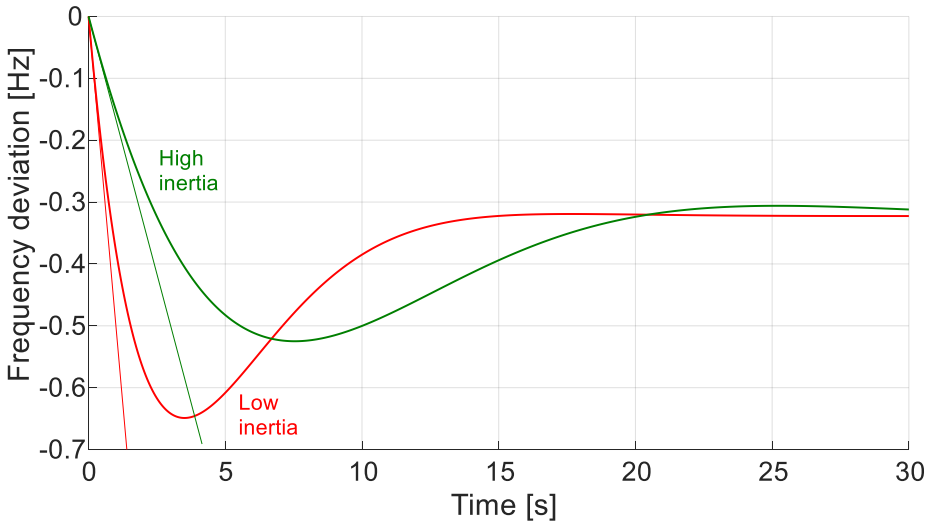

Figure 3.5: Frequency response after a generation loss equal to 0.1 p.u. of the system's size in case of high and low inertia (ratio 3:1).

This trend can be problematic if exceeding the withstand capability of synchronous generators, PEIG and HVDC. Such worsened parameters might cause several issues [91], particularly for the stress on the synchronous machines: ① torque swings, as the torque values increase with higher ROCOF values up to 160% for 1 Hz/s; ② pole slip, as the machine can lose the synchronism; ③ accidental reverse power flow, as the oscillations of the rotor angle can make the

generator to absorb power (motor). All these events can determine the intervention of generator's protection devices, which could lead to cascading failures, and consequently load shedding, system separations or blackout [92]. Further effects could be inter-area oscillations, due to synchronous generators oscillating against each other, and plant-side impact, as torsional torques, flame and combustion control, hydraulic transients in hydro power plants, impacts on auxiliaries' components [93]. During severe frequency gradients conventional protection devices might experience conditions where a reliable operation is difficult [94]. The distributed energy resources (DER) are equipped with loss-of-mains protection, which can be activated by high ROCOF without any real islanding event, worsening a situation where DER could support the system [95]. The higher the initial ROCOF following an event, the greater the risk of the system frequency dropping below load-shedding thresholds of protection systems and heading towards system collapse.

A minimum level of inertia depends on the ROCOF withstand capability of the system, to ensure a proper functioning of the protection system, generator operation and converter unit controllers. The maximum threshold for ROCOF depends on the size of the SA and the fault ride-through of the generating units. It is difficult to harmonize a clear threshold. The current technical debate oscillates between 0.5 Hz/s and 2 Hz/s over 500 ms [96], [97]. The Australian Energy Market Operator (AEMO) set a limit of ±3 Hz/s ROCOF with a filter and averaging period of approximately 100 ms after fault clearance is applied for any credible contingency event [98]. Parametric studies have been conducted for CE by the ENTSO-E System Protection & Dynamics Subgroup [94], [99], which consider values between 0.5 and 3 Hz/s. ROCOF in a range between 100 mHz/s up to 1 Hz/s have been recorded within the last 15 years in CE. Based on scheduled grid expansion and planning measures, corresponding market simulations and dynamic system studies, ENTSO-E is proposing a capability for grid users to handle a ROCOF of at least 2 Hz/s for CE [100]. However, some studies outlined that ROCOF protection can be very ineffective with 1 Hz/s over 500 ms, particularly in smaller power systems [101]. A value of 0.035 Hz/s is defined as the starting time of a frequency disturbance in the Nordic [93]. In GB, the ROCOF requirements following a power outage is 0.125 Hz/s, with an admissible maximum of 0.5 Hz/s [102].

It is possible to calculate theoretically the minimum kinetic energy from Equation (3.18) necessary to face the relevant incident, using:

$$E_{k,min} = \frac{f_0 \, \Delta P_{L_{max}}}{2 \left(\frac{df}{dt}\right)_{max}} \tag{3.21}$$

where $(df/dt)_{max}$ is the initial ROCOF withstand capability and $\Delta P_{L_{max}}$ is the imbalance defining the reference incident.

Figure 3.6 depicts the minimum kinetic energy needed for different values of imbalances and initial ROCOF. Selecting a threshold of 0.5 Hz/s, a minimum kinetic energy of 150 GWs is needed to contain an imbalance of 3 GW.

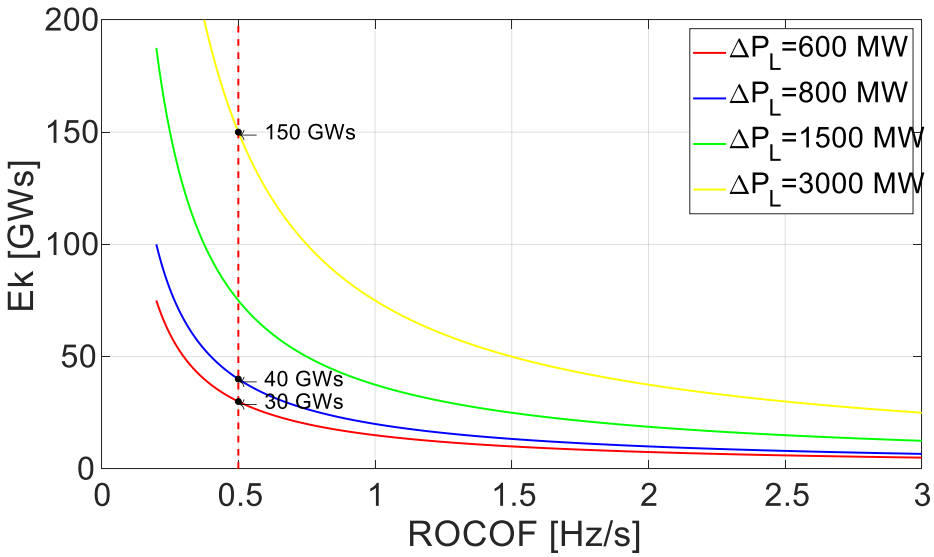

Figure 3.6. Minimum kinetic energy trend for different imbalances and initial ROCOF values.

3.4.1 Hints on the inertia allocation and distribution

The placement and size of distributed RES become an important issue in the last decades for operating safe and reliable power systems. Generally, RESs are far away from load centres and this implies overloading on the lines, congestions, and uneven distribution of regulating generators. RES can be strategically located and operated to reduce system losses, to reinforce grids, and to improve voltage profiles, system reliability and efficiency [103], [104], [105]. These criteria are based on steady state studies, optimizing the economic dispatch, or using steady-state indicators for voltage stability [106], [107]. With different PEIG distribution also the inertia is varying, not only temporally but also spatially. Although the aggregate model enables many important conclusions concerning the overall electromechanical dynamics and stability of a multi-machine system, new concerns are arising also on the local impact. For a given contingency, the resulting impact is not only a function of the overall system inertia but also of the spatial distribution of inertia across the grid [2], particularly on the local dynamics and operation also in a large synchronous power system. Moreover, another question arises: where is it optimum to introduce solutions to mitigate the reduced inertia impact?

In a grid with a non-uniform inertia distribution, the frequency in a node with low inertia can differ significantly from the COI frequency after a contingency. The main effects of non-uniform inertia distribution are on **local ROCOF**, as generators electrically closest to a disturbance and in zones with relatively low inertia see higher ROCOF than the system one [108], **inter-area oscillations**, as reduced local inertia significantly increases the local oscillations during incidents close to these areas, system modes oscillate faster and their damping ratio tends to negative values, leading to an unstable system condition, and smaller **Critical Clearing Time** [109]. Higher local ROCOF increases the probability of protection's intervention and relays, as they measure and operate based on local

frequencies and ROCOF values. The incident impact is distributed among the various machines according to the share of their individual synchronizing power in the entire synchronizing power of the system [110].

Robust inertia allocation problems are proposed in [111], [112] to find the optimal placement of virtual inertia, grid-following and grid-forming devices, while in [113] the optimal sizing of storage and tuning of virtual inertia is proposed to balance a predefined active power loss. The impact of high regional RES generation, electrical distance and grid configuration on initial ROCOF values in the four-area power system, based on the Croatian power system, are examined in [114]. Indicators to study the inertia distribution estimation are proposed in [115] which have the potential to investigate questions as the placement of PMUs or ESSs. An index of inertia distribution is defined in [116] to optimally locate distributed sources and to estimate the distance of a bus from the COI location. A matrix perturbation theory approach is used to optimize the geographical distribution of inertia and primary control in [117].

All these studies have the common understanding that, beside the total system inertia, its geographical location in the grid is very significant for the dynamic performance. The optimal placement should be aligned with the probability, entity and location of the grid disturbance and also on different timescales. Several open problems are related to the regional inertia unit commitment, considering economic aspects and minimum admissible levels to provide useful information, both for planning and operation.

3.5 Options to mitigate frequency stability issues

Various technologies and services can be used to physically increase the inertia or to improve the system frequency response. This Section provides a brief description of various technologies and services, dealing with synchronous compensators, energy storage systems, and new control schemes, which can provide the required fast response to mitigate an extreme frequency deviation in presence of low inertia.

3.5.1 Synchronous compensators (SyCs)

The first and easy way to address such challenge is introducing more physical inertia, e.g., using **synchronous compensators** (SyCs) or phasing-out thermal power plants as synchronous compensators.

A SyC, also known as a synchronous condenser, is a synchronous generator operating without a prime mover. It has the potential to support voltage, by providing reactive power compensation and additional short circuit power, and frequency, by increasing the inertia [118], [119]. SyCs are being planned and

implemented by several TSOs to solve ROCOF issues, regional stability, voltage dips and management, and HVDC commutation failures [36], [120], [121]. SyCs can be retrofitted by thermal plants scheduled for decommissioning, saving on the implementation costs. However, the cost of such frequency control ancillary services may be imposed [122]. The required capacity of SyCs and their optimal location in the grid can be investigated using mixed-integer nonlinear optimization techniques minimizing installations costs [123].

The impact of SyCs on the frequency stability has been investigated in [119] for a system with high level of RES, using several scenarios of wind and disturbances. This study has been extended in [124] proposing and analysing different strategies using SyCs, synthetic inertia and their combination to enhance the frequency stability under various scenarios and wind conditions. A simplified Western Danish power system is simulated in real time digital simulator to demonstrate the effectiveness of the strategies.

A comparison between SyCs and Static Synchronous Compensators (STATCOM) in terms of inertia frequency response is shown in [125] using a test system with two areas and four machines implemented in MATLAB/Simulink. The authors in [118] review the frequency stability challenges and potential solutions in the GB power system and present a case study to evaluate the impact of synchronous compensators using one present scenario on an in-house developed GB transmission model. Synchronous compensators are also studied as additional frequency control strategy in [122], in a network which loosely represents the South Australia power system. Five simulation scenarios are investigated in presence of high wind generation and low load condition. The number of SyCs is varied from 1 to 11 and the minimum number needed to keep ROCOF within its acceptable limit (<1 Hz/s) and to reduce the amount of LFDD is analysed.

Applications of SyCs on a real case study will be presented in Chapter 5.

3.5.2 Energy Storage Systems (ESS)

Energy storage comprises a wide portfolio of technologies for storing electricity, such as flywheels, electrochemical Battery Energy Storage Systems (BESSs), super capacitors, compressed air, thermal storage (heat storage) and pumped-hydro storage. Today only pumped hydro is mature and largely installed. It is used for peak levelling or energy arbitrage, but the installations of new plants are limited by the presence of suitable physical sites. ESSs can be used to store excessive RES production, avoid congestions and curtailments, improving RES integration and optimizing thermal power plant operation. Synchronous storage technologies increase system inertia and provide short circuit power and voltage regulation, whereas non-synchronous can provide synthetic inertia or fast frequency regulation. ESSs can act as a dynamic reactive power source and they can provide black start capability. BESS or hybrid power plants which combine

both electrical storage with super-capacitors could be used to provide grid forming capabilities [126]. Storage can be classified depending on the typology of energy transformation (usually divided into electrical, electrochemical, mechanical, thermal storage). For the grid applications, it is useful to consider the power and energy typical ranges of the different ESS, looking at the Ragone plot in Figure 3.7.

Battery energy storage systems (BESSs) represent a promising solution to maintain power system stability and to provide ancillary services. National Grid in UK developed the "enhanced frequency response" service to address the issue of the reduced inertia [127]. At the same time, BESSs are used in the Australian [128] and Central Europe [129] frequency control market where they were able to successfully deliver a fast control and at the same time lower the TSOs costs related to the reserve provision.

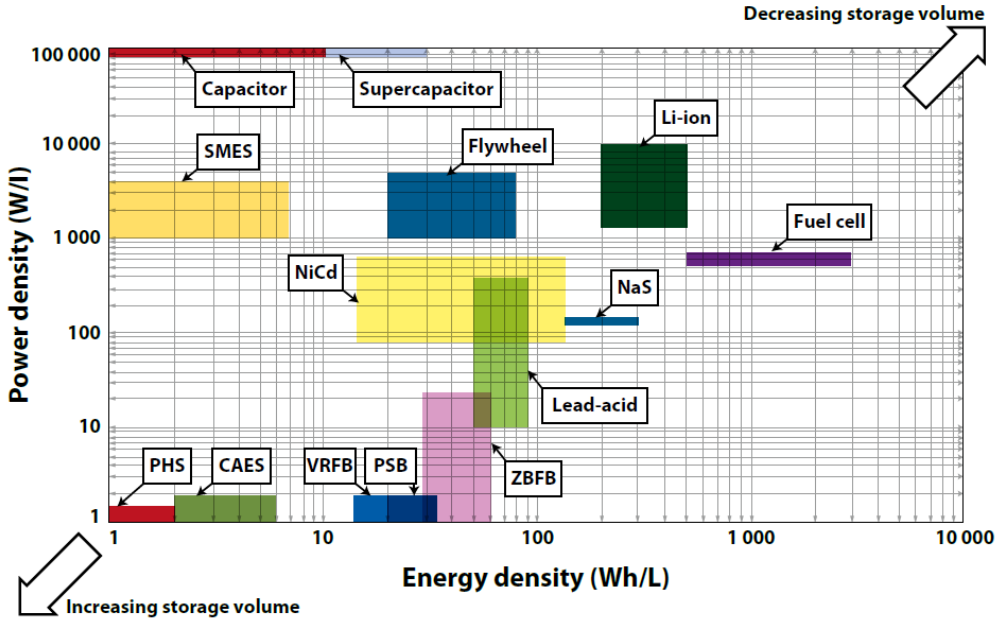

Source: Luo *et al.*, 2015.
Note: SMES = superconducting magnetic energy storage; NiCd = nickel cadmium; NaS = sodium sulphur; PHS = pumped hydro storage; CAES = compressed air energy storage; VRFB = vanadium redox flow battery; PSB= polysulfide bromine flow battery; ZBFB = zinc bromine flow battery.

Figure 3.7. Power and energy typical ranges for different ESS [130].

In literature, a large group of studies focus on the impact of BESSs after a contingency: a variety of probabilistic approaches and optimization techniques can be used to precisely quantify and improve the BESS performance [131], [132]. Another group concentrates on multiple hours/day simulations. In this case, the main difficulty is to reproduce a realistic frequency oscillation which is essential to measure the BESSs potential. In general, frequency dynamics are formed by stochastic frequency deviations due to load and renewables fast power changes and deterministic frequency deviations caused by the long-term mismatch between synchronous generators and the net load due to the market structure [133]. In work like [134] [135] real data of wind power swings or stochastic noises such as the Ornstein-Uhlenbeck are used without considering the presence of deterministic frequency deviations. In [136], the impact of a BESS is evaluated considering different storage capacities and variable droop strategies. To

reproduce the frequency, a procedure based on the Fourier transform is used where frequency oscillations have similar harmonic content with respect to real data inside a 6-hour window. Simulated frequency is different from real data, but it has the same dynamic behaviour inside this time window. In [137] a procedure to reproduce real data frequency signal is implemented but the frequency reserves intervention cannot be precisely simulated, making difficult to assess the performance of new resources.

Storage technologies have higher ramping capability than conventional generators, and they can be used to achieve better dynamic performance. The state of art and modelling of ESS will be extensively given in the next Chapter.

3.5.3 High Voltage Direct Current (HVDC)

Interconnecting existing grids has been traditionally seen as a mean to improve network stability and security. More recently, with the introduction of competition in electricity markets, the interconnection has been a way to widen the size of the markets and increase the overall market efficiency. The interconnectors can be based on **High Voltage Direct Current** (HVDC) or High Voltage Alternate Current (HVAC). HVDC links allow connection of asynchronous AC grids and they can be used for market purposes and ancillary services, due to the advanced use of inherent controllability to mitigate congestions, optimise line loading, to keep adequate voltage profiles and to regulate frequency. Furthermore, longer distances beyond a break-even and undersea path make HVDC more efficient and economic than AC [32].

Figure 3.8 presents the planned installed capacity of HVDC systems in Europe by 2030 based on TYNDP 2018, including the share of embedded links and DC connected wind farms. The level of novel HVDC links is anticipated to drastically increase by 2030, reaching a capacity around 70 GW.

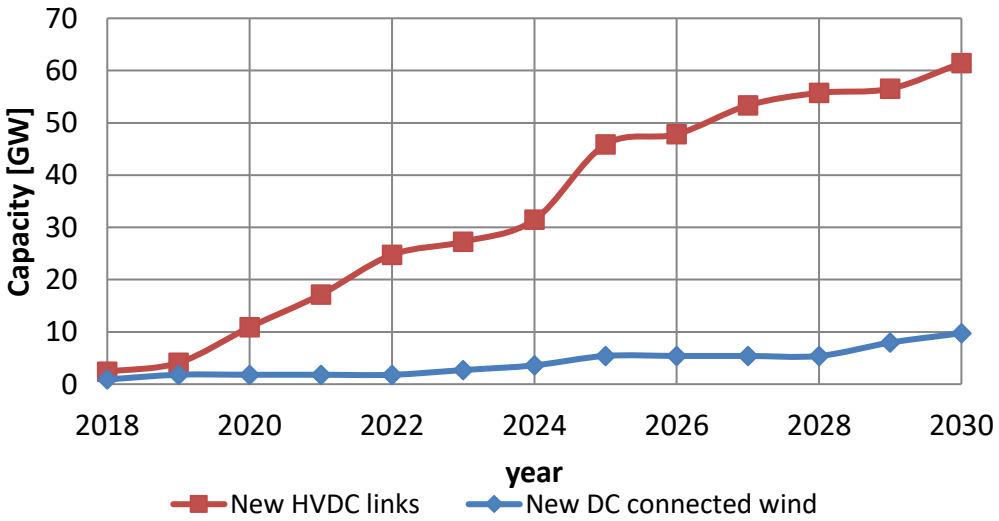

Figure 3.8. Total installed HVDC transmission capacity in Europe [43].

Currently HVDC links are used not only for connecting asynchronously two synchronous systems (**non-embedded**) but also for submarine power transmission, long distance power transmission, embedded links, ancillary services and for connecting offshore wind farms to the main synchronous grid.

The term **embedded HVDC systems** refers to the HVDC which are located within a SA under normal system operating conditions. The frequency at all terminals of an embedded HVDC system is the same under normal system operating conditions.

Modern HVDC transmission systems exhibit high degree of controllability: they are capable to independently and regulate their active and reactive power infeed in very short period, to facilitate dynamic voltage control, provide black start functionality and enhance the power system stability when integrated with advanced wide area control schemes. However, HVDC have very limited overloading capability and short circuit current contribution. Furthermore, advantages like the active power control, can be realized mainly if the HVDC is operating far away from the operational limits. The European Regulation [138] requires that the HVDC systems shall be capable of regulating by means of automatic control their active power as a function of the deviation of frequency from its nominal value measured at its connection point when operating in FSM. The interpretation of the FSM requirement is obvious for power generating modules that have only one connection point to which the active power frequency response in case of a frequency deviation shall apply. However, in case of HVDC system the interpretation may be not so clear: the capability to provide active power frequency response is a relevant feature for HVDC systems connecting different SAs and therefore do not share the same frequency. In this situation, the HVDC system can provide support to one SA, which suffers a frequency deviation, by increasing/decreasing the active power infeed/offtake. This active power regulation of the HVDC system providing support to one SA has an immediate impact on the frequency of the other SA, which then needs to be compensated by active power frequency response of generators in that area.

The two HVDC available technologies are the Line Commutated Converter (LCC) technology, based online commutated thyristor valve converter, which needs a highly stable AC grid, and it is still the preferred technology especially for its maturity and the lower cost, and the Voltage Source Converter (VSC) technology, relatively recent for high rated power. Today, VSC-HVDC with voltages above ±500 kV and 2 GW are feasible, but with very limited operating experience so far (INELFE VSC-HVDC system between France and Spain with a voltage of ±320 kV and a rated power of 2x1 GW is currently the VSC system with the highest transmission capability).

LCC-HVDC employs line commutated thyristor valve converters, which highly depend on a stable AC voltage for a reliable commutation. VSC-HVDC employs Insulated Gate Bipolar Transistors, which enable to generate a voltage on

the AC side with a specific amplitude and phase angle and can operate in weaker and even in passive AC systems.

In addition, in VSC converters a fast power flow reversal is feasible: this is very useful in helping the system stability after a fault and makes it possible to change up to two times the power of its rated value [139]. On the contrary, in the LCC converters the power reversal is carried out by inverting the DC voltage polarity at both stations [140], and the operation switch from inverter to rectifier (and vice versa) cannot be done with continuity, but it implies the converter turn off for some minutes. HVDC transmission systems can have two different configurations: monopolar (with a single conductor line and the return is made by the earth/sea) and bipolar (the most common configuration with two independent poles). Depending on the number and locations of the converters, the configuration can be point-to-point (with only two converters, in back-to-back if there is only a short direct current line) or multi-terminal (with more than two sets of converters operating independently and each converter can operate as a rectifier or an inverter). Several advanced operational functions can be provided by the HVDC links in supporting power system stability. The main functionalities are associated to the typology and the technology, e.g., frequency control can be provided by non-embedded LCC/VSC, AC line emulation by embedded LCC/VSC, while synthetic inertia and voltage support only by VSC embedded/non-embedded. In some cases, the Multi-Terminal Direct Current (MTDC) systems may be more attractive to fully exploit the economic and technical advantages of HVDC technology, although there are a few MTDC links in operation around the world today. There are still barriers to the development of meshed MTDC grids, especially due to protection issues. The main drivers are the large-scale integration of remote renewable energy resources into the existing alternative current (AC) grids and the development of international energy markets through the so-called super grids [141]. The first MTDC system designed for continuous operation is the Sardinia-Corsica-Italy scheme, as an expansion of the Sardinia-Italy two-terminal DC system, built in 1967 with a third terminal at Corsica added in 1991. Non-embedded HVDC links can support asynchronous AC grids by means of providing balancing power when needed. An offshore wind farm or a storage connected to the AC by an HVDC system can support as well.

A focus on the HVDC modelling is provided in the next Chapter.

3.5.4 Other options

Decreasing the magnitude and probability of the reference contingency could be a viable path to avoid frequency instability, by limiting the worst-case failure or system splits based on the available inertia. In future scenarios, many more but likely smaller contingencies from loss of generation are expected, but even larger faults caused by HVDC lines. An accurate operation and dispatching can contain

the magnitude of the reference incident, avoiding very large frequency deviations. Also adapting the current equipment, grid codes and protection to cope with higher ROCOF and larger frequency swings could be examined, without jeopardizing stability or damaging the turbines and auxiliary equipment in conventional power plants [142]. Another short-term solution employs a market for inertia, short circuit power and ancillary services provided by conventional generators operated at their minimum power generation.

The **inertia estimation** will play a vital role in the planning of stable operation of power systems. Without an accurate measurement of inertia, TSOs cannot operate the grid in an economic and reliable way [143]. There are currently three ways of estimating inertia:

a. Summing inertia constants from online synchronous generators. This approach requires an accurate knowledge of the grid-connected plants, in terms of parameters and real-time connection, and assumptions are needed to provide a view of the inertia from distribution and demand.
b. Deriving the inertia during large contingencies in the grid. Inertia can be calculated from the recorded power loss and the resultant ROCOF using the swing equation. This method considers the demand side inertia but is gives a 'snapshot' of what total inertia is on the power system at a given time.
c. Calculating inertia based on small perturbations during the day, with an estimation similar to the previous method.

The last two methods are based on the probability of occurrence of some events, which sometimes are not easy predictable, both in timing and magnitude. In general, synchronized measurements from Phasor Measurement Units (PMUs) and measurement of power within the SCADA system are used [144], [145].
Using apposite devices evolved from PMUs, the eXtensible Multi-function Units, a direct and continuous inertia measurement method have been implemented and tested in several small power systems by Reactive Technologies [146]. This approach uses a small power change in the network (<10 MW) to alter the frequency, which are used to measure continuously and directly the inertia from both the generation and demand side. Different operational benefits can be experienced when performing inertia estimation and measurements, as increased capability to integrate RES while maintaining security of supply and reducing RES curtailment, decreased need of ancillary services procurement, mitigation of the number, risk and duration of islanding events and blackouts, reducing the costs for society in terms of loss of load. By monitoring the actual inertia level of a grid, TSOs can make better-informed decisions to take action to avoid dangerous situations.

As already discussed, conventional power plants deliver an inertial response by releasing part of the kinetic energy stored in their rotating mass. The mechanical inertia is an inseparable part of the synchronous generator. It is

possible to provide an equivalent response by PEIG, referred to as synthetic or virtual inertia provision. The term **synthetic inertial response** corresponds to the controlled response from a generating unit to emulate the exchange of rotational energy from a synchronous machine with the power system. The contribution is proportional to the ROCOF. Any other form of fast controlled response can be termed as **Fast Frequency Response (FFR)**, which contains different responses based on frequency deviations [147]. TSOs have recognized the need to plan sufficient levels of frequency support capabilities implementing new services. Already in 2013 ERCOT discussed the need for a new Fast Responding Regulation Service [148]. Enhanced frequency response was introduced in recent years in Great Britain [149], where further reform is now in progress [150]. Similarly, the AEMO and the Italian TSO (Terna) recently discussed and implemented market and pilots for the FFR as an option to overcome the low inertia issues [151], [152].

However, PEIG requires an energy source and an energy storage to properly resemble the synchronous machine. The capacitor on the DC side is designed and sized for reducing the DC voltage ripple. Thus, the energy stored in the DC capacitor is negligible with respect to that stored by the inertia of synchronous machines. However, only a small part of the total stored energy in the synchronous machines is released as inertial response. Some studies reveal that the DC capacitor can still provide the same amount of energy released by conventional plants during the frequency drop if some relaxations in the DC link voltage are allowed [142]. To make the analogy viable and practically useful, it is necessary to connect a large energy storage system (ESS) to the DC side of the converter. The needed energy could be stored either in the rotor of a wind turbine or in another dedicated energy storage device, such as a battery for Solar-PV units. FACT devices such as Static VAR Compensator (SVC) or STATCOM, which are used for reactive power compensation, could also support frequency stability, as they typically include a VSC and a DC link capacitor [125].

Recently, several strategies have been proposed to emulate synchronous machine models to provide synthetic inertia. **Virtual Synchronous Compensator** (VSC) have been integrated into the inverter control scheme to provide grid services, such as virtual inertia, harmonic compensation and reactive grid support during faults [153]. The VSC is designed to provide only grid services, working therefore always at a low power level. However, most strategies are based on measurements coming from the system which imply time delays for acquisition and processing, while the inherent physics of a synchronous machine provide natural means of synchronization and inertia without any delays [154]. This makes the virtual inertia control ineffective. Furthermore, while a synchronous machine can be heavily overloaded (up to 2-3 times the rated current for 10 seconds) and can provide short-circuit current during a fault, converters have stricter limits and cannot respond as a synchronous machine if not over-dimensioned.

Grid forming converters can facilitate the frequency containment through their instantaneous control, free from measurement and control delays associated with the current grid-following control strategy of converters. Grid forming control could remove the dependency of PEIG and HVDC on the short-circuit power levels in the network, and could provide local frequency support capability, ensure high ROCOF withstand capability and an inherent response to power imbalances. It is important to highlight that grid forming control is not necessarily linked to synthetic inertia and fast active power response which could be also provided with the technology already used today.

Generally, demand has been considered essentially uncontrollable. However, self-regulating loads, including thermostatically controlled loads such as refrigerators, air-conditioners or electric vehicles, can be used to track the frequency and switch on the appliance accordingly [155]. Using distributed loads to support system stability will require large-scale aggregators [156] and the smart management of home appliances [157], to align the different objectives of users and aggregators in terms of costs and benefits. **Virtual Power Plants** can aggregate different types of distributed sources to make them visible to the system operator as a single controlled unit [158].

Chapter 4

4 Methods and Models for Frequency Stability Assessment under high PEIG penetration

4.1 Introduction

After the description of the frequency dynamic characteristics and regulation in modern power systems, frequency control methodologies and models are proposed and designed in this Chapter.

For this purpose, an aggregate model of a power system including the essential dynamics, the generator's controller design with primary and secondary control and the frequency dependency of the load is derived. Possible applications of the aggregate model will be discussed, ranging from different types of contingencies, including the reference incident and system split, to normal operation disturbances. The model is also used to study the frequency performance of possible inertia constraints in the power plant unit commitment. In the sequel, analysis and studies on the effects of the inertia allocation and distribution are introduced. Finally, possible models of options to mitigate the impact of the PEIG are investigated and described[4].

4.2 Frequency performance indicators

Given the trend toward more PEIG, the same level of imbalance between generation and demand can create a faster and greater change in the system frequency. Therefore, it is important to quantify this trend analysing the frequency

[4] Parts of this chapter were also published in [175], [239], [241], [69], [208].

sensitivity during the normal operation or with respect to large generation/demand imbalances.

The performance of the frequency response in the case of large generation/demand imbalances can be assessed using the indicators depicted in Figure 4.1 [159]:

- Initial **Rate of Change of Frequency** $ROCOF$, which is the derivative of frequency at the time in which the disturbance happens.
- **Maximum transient frequency deviation** Δf_{MAX} given by the difference in absolute value between the frequency at the time in which the disturbance happens and the minimum reached frequency f_{nadir} for under-frequency or the maximum reached frequency f_{zenith} for over-frequency phenomena. It represents the maximum frequency excursion before frequency starts to recover.
- **Time** of **nadir** or **zenith** frequency (T_{nadir}, T_{zenith}).
- **Steady-state frequency deviation** f_{reg}, the frequency to which the primary control is stabilized.
- **Time of steady-state frequency deviation**, evaluated as the time where the frequency is within a band of freg±0.005 Hz, i.e., one half of the dead band of the generators.

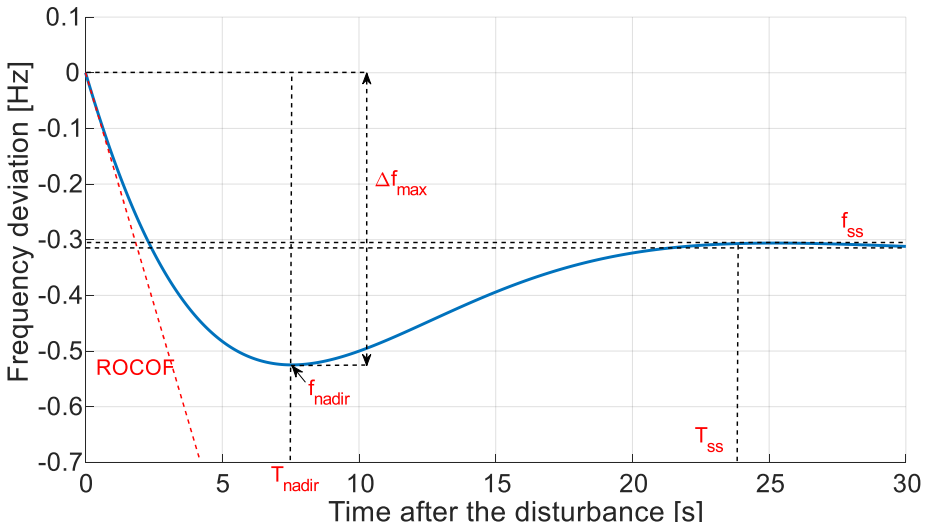

Figure 4.1: Typical frequency performance indicators in the case of an under-frequency event.

The reduced inertia has operational security implications and impacts the main performance indicators. The thresholds for the beforementioned indicators have been discussed in Chapter 3.

For most of the time, the system is in transient conditions and, hence, the frequency is not the same everywhere. During the normal operation, other criteria can be used to evaluate the frequency quality. In Art. 131 of [53], the main system

frequency variables and targets that define the principles of frequency quality are defined together with the frequency quality evaluation criteria, which comprise:

- the mean frequency value f_m,
- the standard frequency deviation sd_f,
- the 1-,5-,10-,90-,95- and 99-percentile,
- the total time in which the absolute value of the instantaneous frequency deviation is larger than the allowed maximum value, distinguishing between negative and positive instantaneous frequency deviations,
- the number of events in which the absolute value of the instantaneous frequency deviation exceeded 200% of the standard frequency deviation.

To assess the impact of a network enhancement project improving the frequency stability it is possible to compare the frequency deviation with and without a new network enhancement project, through a set of further indices with an hourly granularity, over one year:

- **Average variation of maximum frequency deviation** $\overline{\Delta f}$, defined as average difference of the maximum frequency deviation Δf_i, on a yearly basis, for each hour i of the year with f_{N_+} and without f_{N_0} a network enhancement project:

$$\overline{\Delta f} = \frac{\sum_{i=1}^{N} \Delta f_{N_i}}{N} \tag{4.1}$$

  where $\Delta f_{N_i} = f_{N_+} - f_{N_0}$ and N is the total number of hours of the year.

- **Average ROCOF variation** $\overline{\Delta R}$, defined as the yearly average difference of the ROCOF ΔR_i for each hour i of the year with R_+ and without R_0 a network enhancement project. N the total number of hours of the year.

$$\overline{\Delta R} = \frac{\sum_{i=1}^{N} \Delta R_i}{N} \tag{4.2}$$

  where $\Delta R_i = |R_+ - R_0|$ and N is the total number of hours of the year.

- **Maximum variation of the maximum frequency deviation** Δf_{MAX}, defined as the yearly maximum value of the difference of the maximum frequency deviation for each hour of the year with and without a network enhancement project.

- **Maximum ROCOF variation** ΔR_{MAX}, defined as the yearly maximum value of the difference of the ROCOF for each hour of the year with and without a network enhancement project.
- **Percentage hour maximum frequency deviation variation** $\%\Delta f$, defined as the value of the difference of the frequency nadir with and without a network enhancement project, seen at least for the 50% percentage of hours in the year.
- **Percentage Hour ROCOF variation** $\%\Delta R$, defined as the value of the difference of the ROCOF with and without a network enhancement project, seen at least for the 50% percentage of hours in the year.

4.3 Frequency Aggregate Dynamic Model

Given the large size and complexity of modern power systems, analysis programs do not usually model the complete system in detail. The main reasons are: practical limitations on the size of computer memory; the excessive computing time required particularly for dynamic and stability simulations; far parts of the system from a disturbance which have little impacts without need of full modelling; full models require a large dataset, which is difficult and expensive to keep precise and updated. Even with increased penetration of PEIG is considered, it is expected that power systems will still mostly depend on synchronous machines. Current operating and control principles are therefore still applicable and the use of well-established tools and study methods to assess the impact of inertia on system stability is still feasible.

The basic concept of the aggregated model is based on the idea of retaining the uniform or average frequency, denoted in Chapter 3 as the COI frequency (see Equation (3.12)), where the oscillations of each generator are filtered out [160]. An example of oscillations is illustrated in Figure 4.2**,** considering a test system of four generators with different inertia constants. The COI frequency is obtained averaging the individual machine responses with Equation (3.12) and it is represented by the black line.

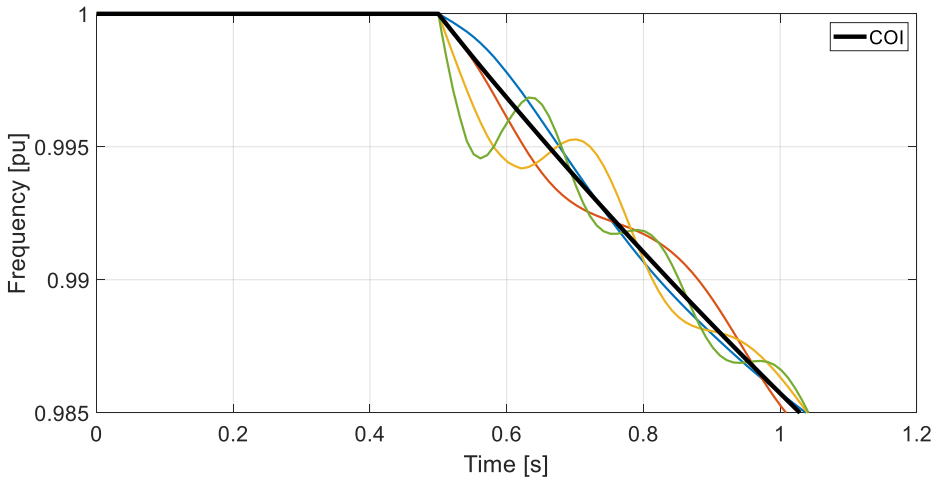

Figure 4.2: Simulated unit frequencies and COI frequency after a power imbalance.

In the studies for the primary regulation, it is generally considered that the electrical speed, and frequency, is equal for all the machines, also during transients. The phenomena linked to the swings between the machines are much more rapid and affect less the frequency regulation [161]. The slow components of the speed transients are more relevant for the frequency regulation and they can be evaluated with good approximation. This holds under the assumption that generators maintain their rotor angle stability with respect to each other (grid synchronism), which has been well observed in actual power systems [162].

The approach used to develop the aggregate model in this thesis is similar to [163], where a basic low order system frequency response model averages the machine dynamic behaviour in a large system into an equivalent single machine. The separate machines are replaced by a single large machine, and the model is validated using an actual system disturbance. The model is obtained assuming the time constants for the reheat and inertia dominating the response in the first few seconds. The average frequency behaviour of a multi-machine system after a major generation loss or load change is modelled in [164]. The model appears to be well suited to answer questions concerning the maximum frequency deviation, the time the maximum deviation occurs and load or RES shedding. It is simple and fast enough to be implemented "on-line" on a central control computer for security contingency studies or to do extensive parametric studies for system planning purposes. In [165] the proposed aggregated model can accurately represent the multi-machine model and the COI frequency response of large systems. Two independent concepts are proposed, which can transform the closed-loop high-dimensional nonlinear model into an approximate open-loop low-dimensional linear model (delay and canonical model). The canonical model expresses the turbine reheat response as a linear combination of a set of basic functions and provides a basis for combining many machines into a simplified low-dimensional model. The model can support the studies related to power

system dynamics as a fast calculation tool. Other authors [166], [167] and [168] , have shown the accuracy and fast performance of aggregate models, when using new technologies which can support the frequency response.

However, it should be noticed that there are some intrinsic limitations in the reviewed model, first because the turbine governor nonlinearity is neglected, which ignores the frequency dead band and maximal turbine governor response. Secondly, the models mainly aim to the first instants after a contingency and they generally lack protection schemes. The aggregate model developed in this thesis takes the main characteristics from the previous cited, it keeps multi-machines for each generator type, it includes non-linearity and protection schemes, and it allows to simulate slower frequency services, when the FRR and RR loops are activated. Table 4.1 summarises the characteristics of the aggregate dynamic model developed in this thesis with respect to the examined literature.

Table 4.1 Peculiarities of the aggregate dynamic model developed in this thesis with respect to the examined literature.

	Single/Multi machine	**Nonlinearities**	**Frequency control**	**Protections**
This thesis	Aggregated multi-machine per type	Governor nonlinearity considered	Inertial, FCR, FRR, RR	Protection schemes
[163]	Aggregated single machine	Governor nonlinearity neglected	Inertial, FCR	No protection schemes
[164]	Aggregated single machine	Governor nonlinearity neglected	Inertial, FCR	No protection schemes
[165]	Aggregated single machine	Governor nonlinearity neglected	Inertial, FCR	No protection schemes
[166]	Aggregated multi-machine per type	Governor nonlinearity considered	Inertial, FCR	No protection schemes
[167]	Aggregated single machine	Governor nonlinearity considered	Inertial, FCR	No protection schemes
[168]	Aggregated single machine	Governor nonlinearity neglected	Inertial, FCR	No protection schemes

Starting from Equation (3.11), it is possible to derive a linearized power system model, where an equivalent power plant is adopted to represent all the synchronous generators of the same type present in the system. An automatic speed regulator is needed to keep the frequency constant and to adjust the mechanical power to the load, and it can be represented using a zero-pole

dynamic, with a fixed droop and the power band coming from the grid code requirements.

The mechanical response of the generators can thus be simplified using the zero-pole dynamic transfer function $G_f(s)$:

$$G_f(s) = E_P \frac{1 + sT_z}{1 + sT_p} \tag{4.3}$$

where T_z is the zero-time constant, T_p the pole-time constant and E_P the permanent regulating energy, associated to the permanent droop σ_P, defined as:

$$\sigma_P = \frac{S_n}{E_P f_0} \tag{4.4}$$

The transient regulating energy E_T and the correspondent transient droop σ_T are defined as:

$$E_T = \lim_{s\to\infty} G_f(s) = \frac{T_p}{T_z} E_P = \frac{S_n}{\sigma_T f_0} \tag{4.5}$$

A load variation ΔP_L in the electrical power P_e is first balanced by the inertial power $P_w = -M\frac{df}{dt}$, the speed of the machines and consequently the frequency is reduced. A damping coefficient is adopted for the load, which represents the load behaviour and tends to increase or decrease its consumption in opposition to the frequency error. In general, the frequency dependency of the aggregated load is clearly observable, with a stabilizing effect on the frequency. Loads have a component depending directly on frequency and an additional contribution depending on the derivative of frequency (e.g., kinetic energy stored in industrial motor loads) [51]. Tests conducted on actual systems indicate that the generation response characteristic is much more frequency dependent than the demand response characteristic. Typically, the load droop σ_L is between 0.3 to 2, while the total generators droop σ_T is between 0.02 to 0.12 [38]. The stiffness of a power system is defined as $K_f = \frac{1}{\sigma_T} + \frac{1}{\sigma_L}$. The regulating energy of the load is given by:

$$E_C = D_L P_L \tag{4.6}$$

The total load droop is defined as

$$\sigma_L = \frac{\Delta f / f_0}{\Delta P_L / P_L} = \frac{P_L}{E_C f_0} \tag{4.7}$$

Putting Equation (4.6) and (4.7) together yields to:

$$D_L = \frac{1}{\sigma_L f_0} = 0.01 \div 0.06 \tag{4.8}$$

In this work, only the load frequency dependency component depending directly on frequency with E_C is modelled. This is made for two reasons: ① in general smaller power systems does not supply large rotating motor loads, due to

the absence of widespread large industrial customers; ② in the future, the contribution of loads to inertia will be much lower, due to the massive penetration of electronic converters to control rotating motor loads.

ΔP_L includes the eventual presence of a contingency ΔP_c, for example the trip of a generator and/or the power fluctuations caused by stochastic ΔP_{sto} and deterministic ΔP_{det} frequency deviations due to the unit commitment scheduling:

$$\Delta P_L = \Delta P_{sto} + \Delta P_{det} + \Delta P_{cont} \tag{4.9}$$

The power variation ΔP_m by the regulating resources in the system can be considered as the sum of the primary ΔP_{PRI}, secondary ΔP_{SEC} and tertiary ΔP_{TER} contributions.

In an interconnected power system with different control areas, the secondary control is centralized. The secondary regulation is made using a signal, the Regulating Level l, sent by the Grid Regulator, an automatic centralized device for each area. The Grid Regulator is sensible to the Area Control Error (ACE), calculated using the frequency deviation and the exchanged power error ΔP_S between the programmed power exchange among areas and the actual power exchange due to the activation of primary reserves or other not scheduled events:

$$ACE = k_{rs}\Delta f + \Delta P_S \tag{4.10}$$

where k_{rs} is the participation factor of the control area. In case of only one control area, $k_{rs} = 1$ and $\Delta P_S = 0$. The choice of the participation factor plays an important role in the non-intervention rule, i.e., each subsystem should cover its own power imbalance and try to maintain planned power interchanges. The ACE is 0 for all areas, except for the one in which the disturbance occurs. The Grid Regulator is a proportional-integral controller, and it calculates the Regulating Level to be send to the units that participate to the secondary control:

$$l = -\frac{100}{FRR_{tot}}\left(k_p\, ACE + \frac{1}{k_T}\int ACE\, dt\right) + 50 \tag{4.11}$$

where k_p and k_T are imposed by the TSO and FRR_{tot} is the total secondary reserve. The level l is a value between 0 (corresponding to the minimum of the secondary band) and 100 (corresponding to the maximum of the secondary band). A value $l = 50$ means the unit to keep its scheduled value for generation. The regulator output signal l is then multiplied by the participation factors ρ_{SEC} which define the contribution of the individual generating units to the total generation control. The obtained control signals are then transmitted to the regulating generators every few seconds and delivered to the reference set points of the governors. The activation time depends on the nature of the generator used: gas, water and coal power plants have different rate constraints and ramp mechanisms.

The tertiary regulation is implemented assuming that reserves are ready, and it can be called by the TSO when requested. The tertiary reserve is assumed to be called when the secondary reserve reaches almost its maximum or minimum acceptable level l, which is equal respectively to TER_{up} and TER_{dw} as defined

by the user. After the tertiary reserve is activated, it starts as a ramp and it is stopped when the secondary reserve is restored decreasing the regulating level. The ramp is formulated as follows:

$$\Delta P_{TER}(t) = FRR_{TOT}\frac{t - t_0}{TER_{time} - t_0} \tag{4.12}$$

where $\Delta P_{TER}(t)$ is the RR requested at time t, FRR_{TOT} is the total FRR and TER_{time} is the timeframe in which the RR needs to be fully activated and t_0 is the starting activation time. The RRP is stopped when the level is $48 < l < 53$.

When using the generation-load imbalance ΔP_L as input, the frequency behaviour can be derived using the aggregate model in a "forward" mode. The forward model for a synchronous isolated power system can be seen in Figure 4.3 and it is formed by:

- The total system inertia obtained by using Equation (3.14).
- The load damping considered as Equation (4.6).
- The equivalent power plant transfer function with a pole and a zero for each type of resource as Equation (4.3).
- Primary, secondary, and tertiary control models.
- Dead bands, saturations and ramp rate limiters added to generators and controllers' blocks when needed.

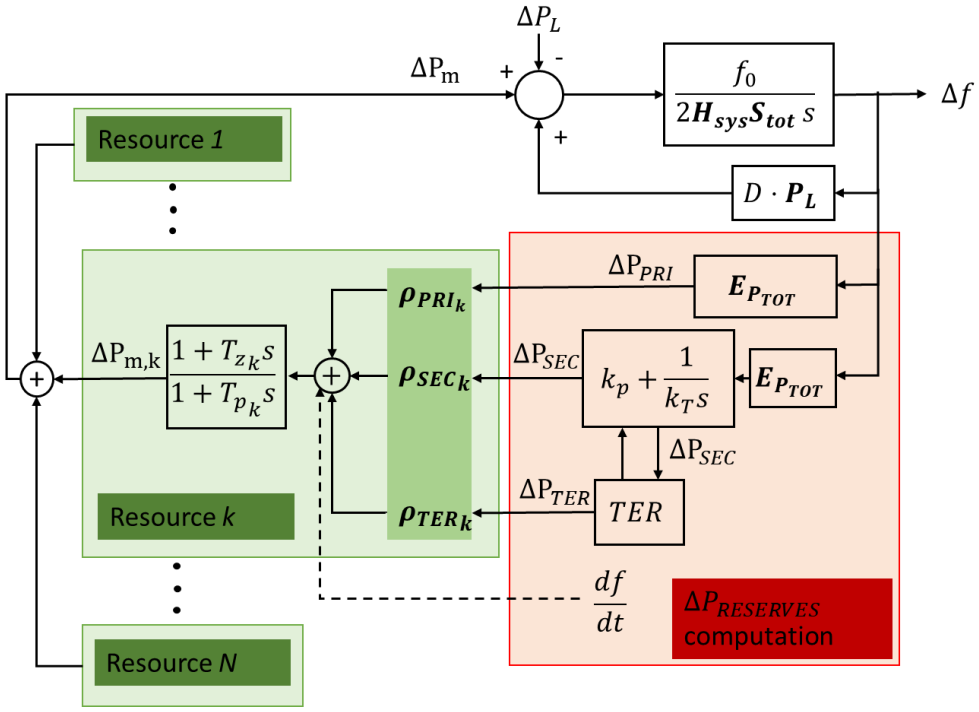

Figure 4.3: Schematic view of the aggregate dynamic model for a synchronous isolated power system [69].

Parameters in bold in Figure 4.3 vary during the simulation to reflect real changes in the system at different times.

The aggregate model was developed using MATLAB/Simulink and it can be used for different analysis and studies. First, the methods for analysing the case of a contingency is illustrated. The model can be applied in small insulated and large power system. The knowledge of the actual system parameters is preferable, especially for the system operation, otherwise the model can be used with different assumptions, for example in the case of very large power systems or for long-term planning. Afterwards, how the aggregate model can be used to study the normal frequency oscillations is showed.

The aggregate model's parameters and variables are described in Table 4.2.

Table 4.2. Description of parameters and variables of the aggregate model and for resource k.

Parameter		Description	Unit
System Inertia	$\frac{f_0}{2H_{sys}S_{tot}}$	f_0 is the nominal frequency H_{sys} is the aggregated system inertia S_{tot} is the total rated power of the generators	[Hz/MWs]
Permanent Regulating Energy	$E_{p_k} = -\frac{P_{n_k}}{f_0 \sigma_{p_k}}$	σ_{p_k} equivalent power plant droop P_{n_k} nominal active power	[MW/Hz]
Load Regulating Energy	$E_c = DP_L$	D change of load under percentage in frequency S_l total load of the system	[MW/Hz]
Zero Time Constant	T_{z_k}	Dynamic of thermal, hydro, gas, HVDC	[s]
Pole Time Constant	T_{p_k}	Dynamic of thermal, hydro, gas, HVDC	[s]
Mechanical power variation	ΔP_{m_k}	Variation in mechanical power due to the variation in frequency	[MW]
Imbalance	ΔP_L	Active power imbalance in the system	[MW]
Reference frequency	Δf_{rif}	Reference signal for frequency	[Hz]
Variation in frequency	Δf	Variation of frequency due to the imbalance	[Hz]
Secondary/FRR control	$k_p + \frac{1}{k_T s}$	k_p proportional term k_T integral term	[p.u.] [s]
Participation factor	ρ	$\rho_{PRI} = E_{p_k}/E_{p_{TOT}}$ for primary/FCP $\rho_{SEC} = P_{n_k}/P_{n_{TOT}}$ for secondary/FRP $\rho_{TER} = \rho_{SEC}$ for tertiary/RRP	[p.u.]

4.3.1 Inertia calculations

When all the generators' inertia constant and nominal power are known, it is possible to derive the total system inertia and kinetic energy using Equation (3.14) and (3.15). However, when such detail is not available, as in academia or for future and very large power system, it is possible to use typical values per generating units.

Beside the knowledge of the parameters, it is necessary to have the details of which are the online power plants to correctly reconstruct a scenario. While this information can be available for system operation, in the planning phase the output is often given by aggregating generation units per type. In this case, assumptions are needed to know which is the number of online generation units.

The inertia is changing over the time, hour by hours, based on the dispatched generator for that hour and hence the rated power for each generator running is

needed on an hourly basis; market studies do not provide such detailed information since the forecast is just by generation typology; typical constant of inertia are assumed for different power plants fired by different fuels and in different countries. This level of accuracy is deemed sufficient to assess an approximation of the inertia of the SA from market study data at each hour of a simulated year. In [28] an overview of these assumptions and values is reported.

Generally, in the power system planning process, data are requested from all the TSOs for different studies, while future scenarios data include installed capacities, demand, and cross border capacities. For each scenario, a market simulation is performed. The requested data for frequency studies are the typical values of inertia $H_{g,i}$ provided by TSOs per fuel type g and the nominal capacity $P_{gn,i}$ of the generator i for all the N synchronous plants in the country. This information is organized into subcategories based on technologies type, from which the average inertia constant H_g and the reference average capacity P_{gn} for each type of synchronous units is established per country:

$$H_g = \frac{\sum_{i=1}^{N} H_{g,i} P_{gn,i}}{\sum_{i=1}^{n} P_{gn,i}} \tag{4.13}$$

$$P_{gn} = \frac{\sum_{i=1}^{N} P_{gn,i}}{N} \tag{4.14}$$

The market modelling simulation gives the total generated power in [MW] for each hour h and fuel type per country $P_g(h)$. The number of units n running for each technology can be estimated by using the reference average capacity of a unit:

$$n_g(h) = \frac{P_g(h)}{P_{gn} \cdot l_g} \tag{4.15}$$

where l_g is the loading factor per country and for the generator technology type g. The loading factor is the ratio between the generated energy in a year divided by the energy the plant would have produced if generating at the maximum power. Generally, high loading factors characterize nuclear and conventional power plants, while lower values for renewable energy sources. The number of units is rounded up for having an integer value and to be precautionary.

In this way it is possible to calculate the inertia for one specific hour h in a specific zone z using the number of dispatched units multiplied by the average capacity and the inertia constant of the unit type:

$$H_z(h) = \frac{E_{k,z}}{P_{tot,z}} = \frac{\sum_{g=1}^{G} H_{g,z} P_{gn,z} n_{g,z}}{\sum_{g=1}^{G} P_{gn,z}} \tag{4.16}$$

where $E_{k,z}$ is the kinetic energy and $P_{tot,z}$ the total running capacity of the zone z at hour h.

In this way, the estimated inertia is calculated based on online generator's capacity, neglecting the contribution from the demand and RES is considered not contributing to the inertia.

From the point of view of the system inertia, it is important to distinguish between the *installed inertia (or kinetic energy)*, linked to the installed conventional generation, determined and constant for a certain period, and the *dispatched inertia (or kinetic energy)*, related to the online conventional units in a certain timeframe, based on the markets and operation needs.

In the case future scenarios are not available, it possible to create reduced inertia scenarios solving a mixed-integer linear programming minimization problem. To keep the situation as real as possible, the desired percentage of reduced kinetic energy can be reached opening some thermal power plants and replacing their production with the variation on the HVDC links or the increase of RES generation. The minimization problem is formulated as follows:

$$\min\left\{a \cdot E_{k,sys} - \sum_{i=1}^{N} E_{k,i} \cdot x_i\right\} \quad (4.17)$$

$$\text{s.t. } x_i \in (0,1) \text{ for } i = 1, \ldots, N$$

where a [p.u.] is the share of inertia reduction (e.g., 0.1, 0.3 and 0.5), N is the total number of thermal power plants in the system, x_i is a binary variable containing the i-th thermal power plant status for i = 1, 2,… N, whose components are 0 if the plant is open or 1 if the plant is closed, $E_{k,sys}$ [MWs] is the amount of present situation kinetic energy and $E_{k,i}$ [MWs] contains the kinetic energy for the i-th thermal power plant. The scope is to minimize the difference between the desired kinetic energy reduction (expressed as the percentage a of the total kinetic energy) and the kinetic energy given by the actual power plants present in the system. For the new values of kinetic energy, the effects of the reference incident are evaluated and compared to the present situation.

4.3.2 Typical values of inertia per generating unit

Given the definition of inertia given in (3.6), inertia depends on the kinetic energy stored in the rotating masses and the nominal power of the machine. Nevertheless, it is not possible to find a unique relation between the inertia constant and the size of the machine, as it is confirmed by several authors from academia and industry. Figure 4.4 reports the inertia constants values for different size and type of generating units [169].

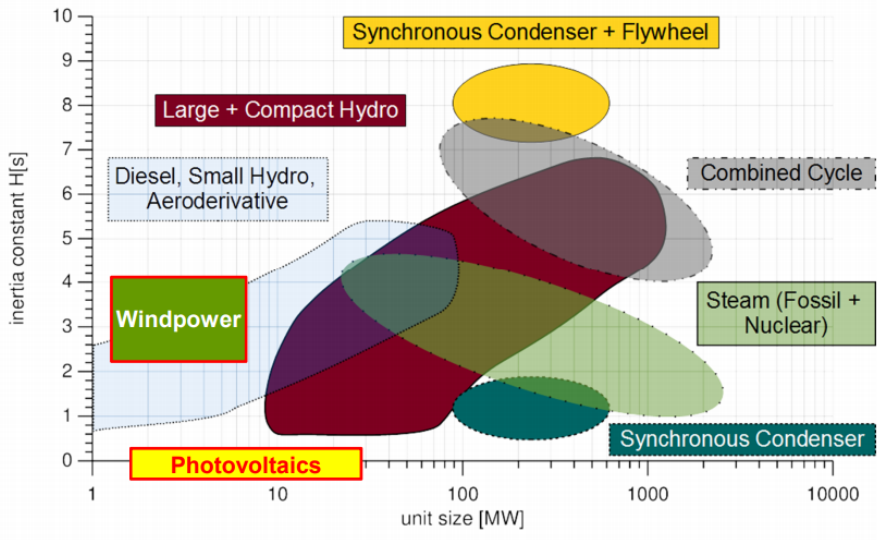

Figure 4.4: Inertia constants for different type of generating units [169].

The inertia constant varies across different technologies and different size of the same technology, while for some types it increases with the size, e.g., for hydro, the opposite happens for others, e.g., steam and combined cycle plants.

Gas generators tend to have higher inertia constants [170]. Traditional synchronous condensers have an inertia constant around 1.0-2.0 s, while it can increase up to 7.0-9.0 s if a flywheel is added to the rotor. However, the inertia constant varies unevenly among different generating units of the same technology. The Australian Energy Market Commission [171] reports range of 3.0-5.0 s for brown coal, 2.0-7.5 s for hydro, 2.5-7.5 s for black coal, 3.5-10 s for CCGT and 2.0-12.0 s for OCGT.

Table 4.3 provides the normal range for the inertia constant for different types of synchronous units and represent the combined inertia of the generator and the turbine [172], [40].

Table 4.3. Normal range of the inertia constant for different types of synchronous units.

Type of generating unit	H
Thermal	
3600 r/min (2-pole)	2.5 to 6.0
1800 r/min (4-pole)	4.0 to 10.0
Hydro	
Turbine/Pump	2.0 to 4.0
Run of River	1.0 to 2.0
Nuclear	6.0
Synchronous Condenser	
Traditional	1.0 to 2.0
With flywheels	7.0 to 9.0
Synchronous Motor with Load	1.0 to 5.0

RESs connected via power converters have zero mechanical inertia, except for the doubly fed induction generators which have small inertia because its stator is synchronously connected to the electrical network.

Figure 4.5 reports the values of inertia and kinetic energy with respect to the ratings for hydro, thermal and geothermal generators (>10 MW) of the Italian

power system. While there is no evident relation among inertia and rated power, the kinetic energy is almost directly proportional to the generators' rated power.

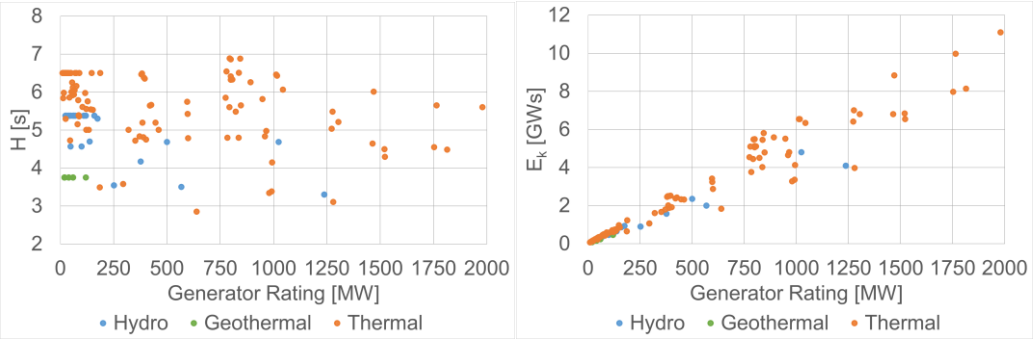

Figure 4.5: Levels of inertia and kinetic energy provided by different synchronous generating technologies in the Italian power system.

4.3.3 Analytical solution of the second order frequency model

It is possible to solve analytically the second order frequency response of a single machine equivalent system, linearizing Equation (3.11). Using the Laplace transform, considering the zero-pole transfer function for the governor and a damping coefficient for the load, it is possible to derive:

$$\frac{\Delta f}{\Delta P_L} = -\frac{1}{sM + E_C + G_f(s)} = \frac{1 + sT_p}{sM(1 + sT_p) + E_P(1 + sT_z)} \tag{4.18}$$

Equation (4.18) is a transfer function and the polynomial at the denominator is the characteristic polynomial. The zero at the numerator only affects the width of the component that depend on the initial condition. For $s \to 0$, E_P is obtained, with a steady-state value $\Delta f_\infty = -\Delta P_L / E_p$ while $s \to \infty$ yields $E_P T_z / T_p = E_T$. It is possible then to find the solutions λ of the associated characteristic equation, in the form $\lambda = \sigma + j\omega$:

$$s^2 + s\left(\frac{1}{T_p} + \frac{E_T}{M}\right) + \frac{E_P}{M\,T_p} = 0 \tag{4.19}$$

$$\lambda_{1,2} = -\frac{M + E_T Tp}{2MT_p} \pm \sqrt{\left(\frac{M + E_T T_p}{2MT_p}\right)^2 - \frac{E_p}{MT_p}} \tag{4.20}$$

where the damping ratio ξ, the natural frequency ω_n, the discriminant Δ and the time constant of the poles τ of the transfer function are:

$$\xi = \frac{\left(\frac{1}{T_p} + \frac{E_T}{M}\right)}{2\omega_n} = \cos\theta \tag{4.21}$$

$$\omega_n = \sqrt{\frac{E_P}{M\,T_p}}$$
$$\Delta = (\xi^2 - 1)\,\omega_n$$
$$\tau = \frac{1}{\xi\,\omega_n} = -\frac{1}{\sigma}$$
$$\omega = \omega_n\sqrt{1-\xi^2}$$

The geometric meaning of the parameters in Equation (4.21) is depicted in Figure 4.6 on the complex axis.

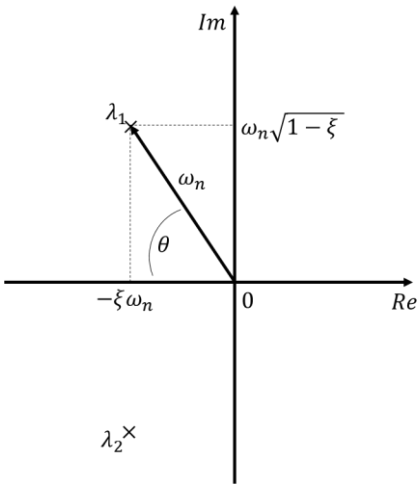

Figure 4.6: Representation of damping ratio, natural frequency and eigenvalues on the complex plan.

A solution for Equation (4.18) can be found distinguishing the case of complex conjugated poles ($0 \leq \xi < 1$):

$$\Delta f = A\,e^{-\frac{t}{\tau}}\sin(\omega t + \varphi) - \frac{\Delta P_L}{E_P} \tag{4.22}$$

where

$$\varphi = \operatorname{atan}\frac{M\tau\omega}{M - E_P\tau}$$
$$A = -\Delta P_L\sqrt{\left(\frac{\left(\frac{1}{E_P} - \frac{\tau}{M}\right)^2}{\omega\tau}\right) + \frac{1}{E_P^2}} \tag{4.23}$$

And the case of real poles ($\xi \geq 1$):

$$\Delta f = k_1 e^{-\frac{t}{\tau_1}} + k_2 e^{-\frac{t}{\tau_2}} - \frac{\Delta P_L}{E_P} \tag{4.24}$$

where

$$k_1 = \frac{\Delta P_L}{\tau_1 - \tau_2}\left(\frac{\tau_1}{E_P} - \frac{\tau_1\tau_2}{M}\right) \tag{4.25}$$

$$k_2 = \frac{\Delta P_L}{\tau_1 - \tau_2}\left(-\frac{\tau_2}{E_P} + \frac{\tau_1 \tau_2}{M}\right)$$

The frequency performance indicators T_{nadir} and f_{nadir} can be evaluated in an algebraic form for both cases of complex conjugated and real poles, obtaining the values in Table 4.4.

Table 4.4. Algebraic form of the frequency performance indicators for the cases of complex conjugated and real poles.

Complex conjugated poles	**Real poles**
$t_{nadir} = (\theta - \varphi)/\omega$	$t_{nadir} = \frac{\tau_1 \tau_2}{\tau_2 - \tau_1} \ln\left(-\frac{\tau_2 k_1}{\tau_1 k_2}\right)$
$f_{nadir} = A\, e^{-\frac{t_{nadir}}{\tau}} \sin(\omega t_{nadir} + \varphi) + \Delta f_\infty$	$f_{nadir} = k_1 e^{-\frac{t_{nadir}}{\tau_1}} + k_2 e^{-\frac{t_{nadir}}{\tau_2}} + \Delta f_\infty$

It is possible to understand the differences between the analytical solution of the second order frequency model and the aggregate model developed in MATLAB/Simulink. The test case is a system similar to the Italian power system at the 2030 horizon, considered as isolated from the CE. It is evident from Figure 4.7 that the analytical solution is not able to consider the saturations in the FCR as the aggregate model do. Consequently, the analytical solution provides a better frequency response, which is not the real system behaviour. The same response can be obtained from the aggregate model removing the saturations. The aggregate model has thus more capabilities than the analytical solution, as it can consider saturations and it also gives the possibility to add many governors. On the other side, the analytical solution is faster than the aggregate one. The analytical solution could be used to detect the worst hours in the year to analyse later in deep using the aggregated model.

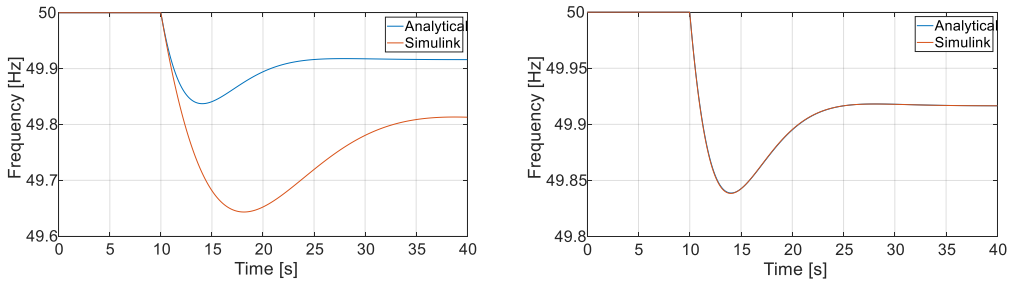

Figure 4.7. Comparison between the analytical and the aggregate model frequency response a) with saturation in the aggregate model, b) without saturation in the aggregate model.

4.3.4 Large contingencies studies

A typical contingency is applied to the forward model to analyze the correct LFC activation. The ΔP_L is 250 MW and it is simulated as a ramp of 1 second; the characteristics and parameters of the system are the ones used in the next Chapter's case study. In Figure 4.8 frequency and power reserves profiles after the contingency are shown, with a zoom over the first 100 s: after a first decay, the frequency is stabilized by the FCR and then returns to nominal value thanks to the FRR activation. RR activates when FRR signal level reach saturation (200 MW of FRR is used with a $TER_{up} = 85$).

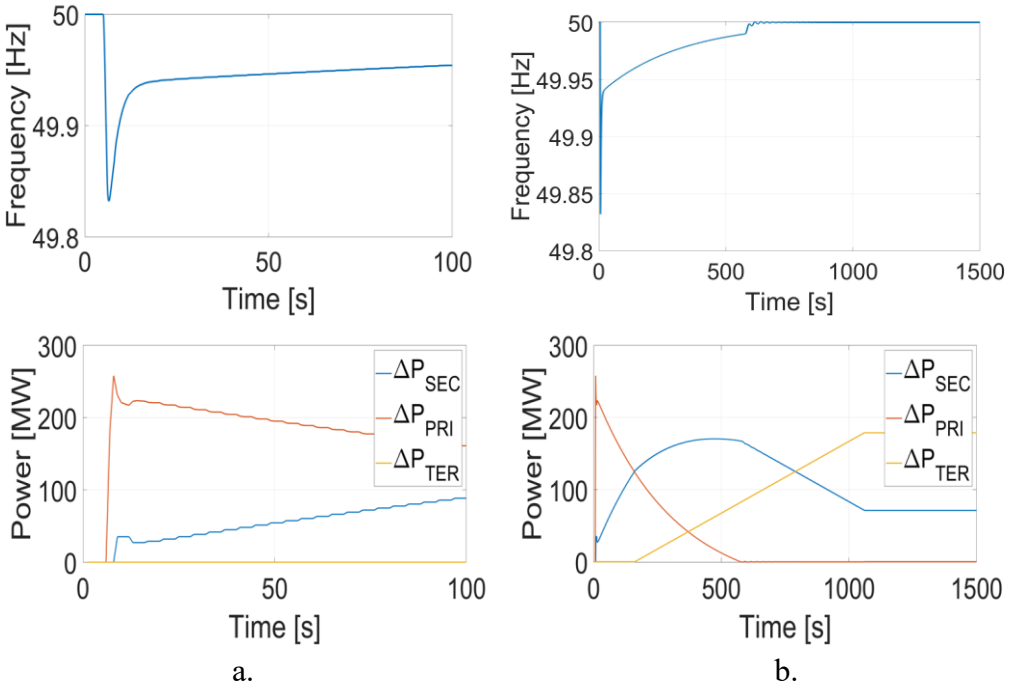

a. b.

Figure 4.8: Frequency and power reserve profiles during a contingency event: a. first 100 s; b. 1500 s [69].

4.3.4.1 Reference incident

The reference incident has been largely discussed in Chapter 3. To study its impact, the analysis can be limited to the first 30 seconds after the imbalance, where the highest stress for frequency stability is usually detected [173]. Therefore, it is possible to use only the primary control of the aggregate model, as the primary response shall be fully activated in less than 30 seconds [65].

Based on the considerations made in the previous Chapter, after a power imbalance up to the reference incident, a new equilibrium at a lower frequency than the nominal one can be reached, thanks to the primary regulation and, in minor measure, to the load regulating energy.

Nevertheless, if the imbalance is relevant, frequency can reach dangerous values, in a very limited time frame, with the intervention of under-frequency and

over-frequency protection devices. If the imbalance is higher than the primary reserve, frequency cannot be stabilized, and the system could collapse. To avoid dangerous frequency variations, it is necessary to undertake control actions, which constitute the emergency control [161] and consist in automatic load or generation shedding when frequency or its derivative reach determined values. It is distinguished between under frequency and over frequency actions. These actions tend to restabilize the load-generation imbalance, even if not at the nominal frequency, but avoiding larger blackouts and system collapse.

The adopted protection schemes and thresholds are based on the regulation established by the European Commission in [72], [174], [53] and translated in the defence plan by each TSO. Each TSO implement automatic Under and Over-Frequency Control Schemes (U/O-FCS) and in different steps with shedding shares of load and generation activated at a specific frequency and tripped on frequency and its derivative values. Each control scheme can be associated to a time delay. A summary of load shedding actions in CE is reported in [77].

For the Italian power system, the O-FCS comprises generation disconnection, with RES preferred to synchronous units (e.g., hydro shedding at 51 Hz). The U-FCS concerns pumping shedding from 49.6 to 48.9 Hz, interruptible loads shedding starting at 49.5 Hz and automatic load shedding (for extreme situations from 48.8 Hz) in a decreasing frequency values scale. Based on these considerations, the implemented U/O-FCS for smaller power system in this thesis is reported in Table 4.5. RES shedding starts from 50.6 Hz with a time delay of 0.2 s, pump shedding starts at 49.7 Hz, automatic load shedding is activated at 49 Hz or -0.3 Hz/s and the trip starts at 48.8 Hz.

Table 4.5: U/O-FCS example for load and RES shedding, with thresholds, steps and delays.

LOAD SHEDDING					**RES SHEDDING**		
Threshold	**Frequency activation [Hz]**	**ROCOF trip [Hz/s]**	**Frequency trip [Hz]**	**Percentage of Load Shed**	**Threshold**	**Frequency activation (Hz)**	**Delay (s)**
1	49.00	-0.3	48.80	9%	1	50.6	0.2
2	48.90	-0.6	48.70	7%	2	50.7	0.2
3	48.80	-0.9	48.60	7%	3	50.8	0.2
4	48.70	-1.2	48.50	8%	4	50.9	0.2
			48.40	10%			
			48.30	12%			
			48.20	10%			
			48.10	8%			

The aggregate model in Figure 4.3 is then reduced to the model in Figure 4.9 to study the impact of the reference incident, with the presence of protection schemes and possible resources to support the frequency response, such as ESS, whose model will be detailed in Section 4.6.

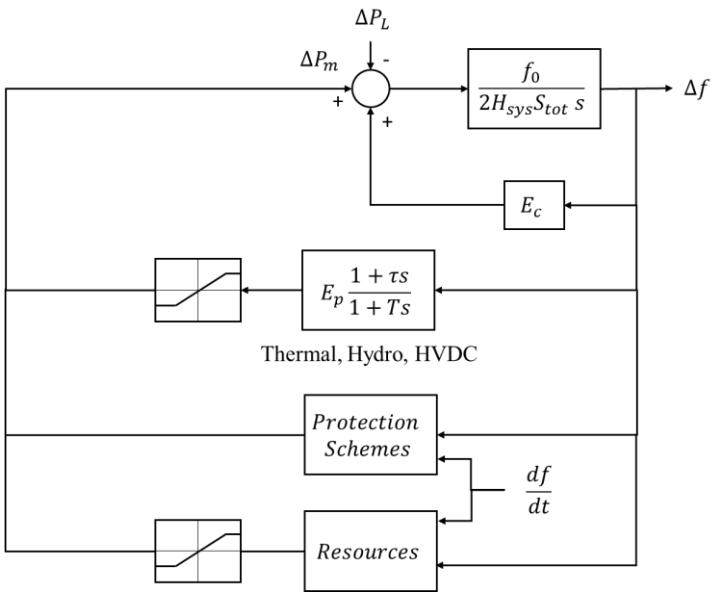

Figure 4.9: Aggregate dynamic model to study the impact of the reference incident, with protection schemes and additional resources [175].

The block protection schemes include protection setting which can be implemented in MATLAB/Simulink as in Figure 4.10.

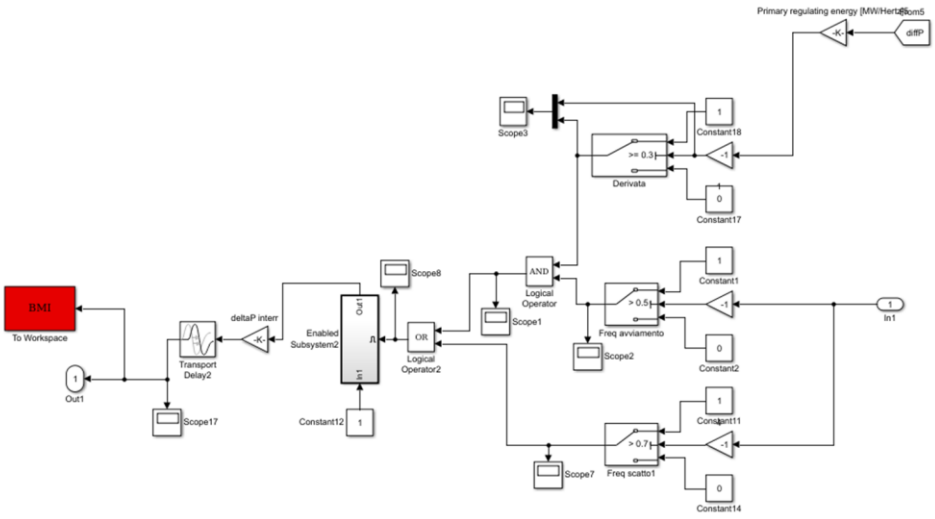

Figure 4.10: Example of implemented protection schemes in MATLAB/Simulink.

4.3.4.2 Technical benefits of network enhancement projects

Many network enhancement projects are planned for the EU interconnected grid with the main goal of improving network or markets adequacy. Those projects may also provide benefits in terms of network stability in low inertia scenarios. As an example, some of those projects presently under consideration in the TYNDP 2018 [25] are: ① RES in north of Portugal, which consists in introducing network reinforcements to allow the connection of new hydro ②

IFA2, a new HVDC VSC link between France and Great Britain, ③ NordLink, a new HVDC connection between Norway and Germany, ④ Swiss Ellipse I, which helps to accommodate new pump storage units, ⑤ Italian HVDC Tyrrhenian link between Continental Italy, Sicily and Sardinia.

The goal is also to set a framework to assess their potential benefits in terms of the improvement of the stability of the interconnected network. With reference to the EU context and the coordination of different possible interventions on the interconnected grid, it is crucial to be able to assess and compare the possible contribution of different alternatives with quantitative indicators. Some indices can be monetised while others are quantified in their typical physical units (such as tonnes or GWh) and maybe hard to be transformed in monetary units in such a way that the full range of costs and (monetary and non-monetary) benefits can be represented. That would allow for highlighting the characteristics of a network enhancement project and providing sufficient information to decision makers. If the benefits can be monetarized, they can be compared with the investment cost to implement a financial cost-benefit analysis. For system security and stability, the benefit analysis of investments may be translated into monetary unit, but this process requires several assumption and further studies. The indicators proposed in Section 4.2 are used to assess the technical impact of an investment in infrastructural assets (non-embedded HVDC, storage, synchronous units) for the frequency stability enhancement based on the aggregate model.

The overall workflow is depicted in Figure 4.11, where H_i is the inertia time constant, P_{ni} the rated capacity, l_i the loading factor and P_{Gi} the output active power from the market simulations of the generator technology type i.

Using the proposed model for frequency stability calculations, the following network enhancement projects can be evaluated:

1. Non-embedded HVDC, for both FCR and/or inertial support in the case of VSC technology.
2. Synchronous generation units (thermal, hydro, CCGT, SyCs).
3. Storage units (e.g., BESSs).

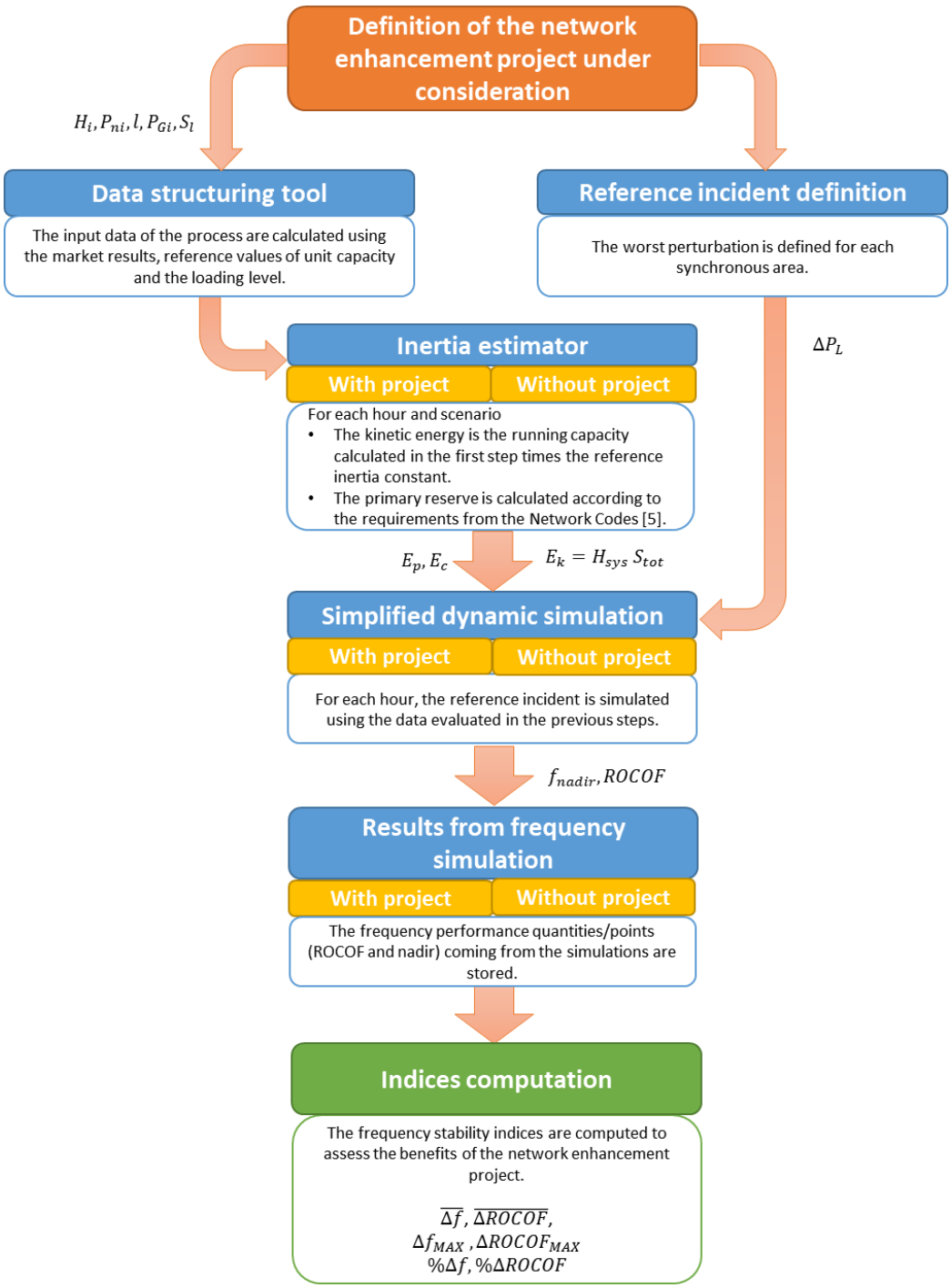

Figure 4.11. Workflow of the methodology to assess the technical benefits of a network enhancement project to support frequency control.

4.3.4.3 System split

Severe system disturbance can cause heavily loaded lines to be tripped, which may bring to cascade failures and result in the separation of the interconnected system into islands [176]. Currently, there are a few studies on the definition of a methodology for the identification of system splits. Some studies aimed at determining the splitting boundary to damp the system oscillations post-fault. A

method for searching those splitting boundaries is presented in [177] to minimize the load-generation imbalance in each island. An approach for systematic identification of critical system split topologies is described in [178], with the definition of relevant initial contingencies corroborate by time domain simulations to determine the actual cascading line failure leading to a system split.

Following the first studies conducted to determine the critical power unbalances and maximum admissible ROCOF, it is showed that the reference incident does not imply particular concerns for the overall frequency stability of the CE synchronous system [94]. However, past system splits outlined the possibility of imbalance higher than the reference incident and especially in smaller regions and with high penetration of PEIG. As discussed in Section 3.3.3, in case of multiple line outages, cascading line failures can occur separating the synchronously interconnected transmission grid into two or more asynchronous areas. In these cases, the frequency stability of the system is jeopardized, considering the increasing power exchange between various regions resulting in larger power imbalances and the decreasing system inertia leading to higher frequency gradients [77]. In sum, while small SAs would see rapid and large frequency excursions following a normal generation loss, large SAs would not see the same size of frequency excursions unless a significant disturbance occurs such as a system split.

The generalized approach adopted by ENTSO-E to handle ROCOF of 2 Hz/s aims at covering any system split scenario without conducting detailed analysis of the potential split topologies. However, under some conditions, it is reasonable to consider the existence of large initial ROCOFs exceeding 2 Hz/s.

In a system split event the SA splits into separate islands. The exports and imports between these islands, prior to the system split event, turn into power imbalances for the separate islands after the split. A system split is more prone to occur across congested transit corridors and thus interrupting these transits. Larger export or import before the split determine greater imbalance after the split and therefore major need for large and quick regulations in subsequently formed islands. The resulting imbalances are difficult to predict, but the frequency response is influenced also by the resulting system inertia, which will differ from island to island.

The **system split methodology** developed in this thesis focuses on identifying and characterizing the consequences of the theoretical system splits in large, interconnected power systems, with particular reference to the planning phase, where all the electrical characteristics are not full known.

The starting point is the definition of the market zones, i.e. the area within which market participants can exchange energy without capacity allocation. If the number of market zone is very large, it can be possible to wisely aggregate them for implementation reasons. The market zones can be considered as nodes of a graph which constitute the entire power systems. The separations of the market

zones in two or more parts are searched iteratively, from each node, extending with neighboring nodes and ensuring the cut creates only connected sets.

The **split line** is defined by a set of market zones and the power imbalance is evaluated through each split line.

Assuming that the system splits into two islands, one island will invariably have an excess of generation and the other a surplus of load, since the separation usually does not result in islands whose loads and generation are in equilibrium. This results in high frequency in one island and low frequency in the other due to the imbalance between load and generation in each of the islands. In the discussion that follows, it is assumed that **a system is split into two islands**, one with over-frequency and one with underfrequency and the effect on the frequency stability of each island are considered.

The European bulk power system is divided into different interconnected market zone, which are characterized by interchanged transfer capacities. The ENTSO-E has agreed common definitions for these exchanges [179]: Net Transfer Capacity (NTC), Available Transfer Capacity (ATC), Transmission Reliability Margin (TRM) and Already Allocated Capacity (AAC).

NTC and ATC are important basis for the market to anticipate and plan cross-border transactions and for the TSOs to manage the electricity exchanges. NTC calculations require that TSOs perform extensive studies of load flows in the interconnected European transmission system. The NTC is interpreted as the expected maximum volume of power that can be exchanged through the interface between two systems, which does not lead to network constraints in either systems, respecting some technical uncertainties on future network conditions. Future market simulation tools use the future NTC as constraint to calculate the AAC for each hour of the year. In this work the **Already Allocated Capacity** is used as the possible imbalance that could follow a system split.

The imbalance of an area is the sum of the AAC flows going out of the area area towards the rest of the SA (except if the link is purely HVDC). HVDC links within a synchronous area are ignored in the computation of splitting cuts. It is assumed that the HVDC link would remain in service after the split, which is confirmed from other past major blackouts [76]. When two separated areas within a SA are connected via a purely DC link, the flows are ignored in the imbalance: the HVDC is replaced by two loads.

The initial ROCOF and the magnitude of the frequency deviation depend on the imbalance between generation and demand compared to the total kinetic energy and the frequency dependency of the load, based on the swing equation. A set of zones constitutes a subsystem of the interconnected power network. The ROCOF df/dt can be computed by subsystem s and by hour h:

$$\left.\frac{df(h)}{dt}\right|_{s} = \frac{f_0 \, \Delta P(h)}{2 \, E_{k,s}} \tag{4.26}$$

where E_k is the kinetic energy of the subsystem, f_0 is the nominal frequency and ΔP_h an imbalance can occur in the subsystem at hour h.

High values of ROCOF imply faster balancing actions, leading to more unit disconnected and implications on the system security. The focus is on ROCOF as it describes the instantaneous response of the system. What happens next depends on the load sensitivity to frequency, the generators primary control time response, the primary reserve, the generating units protection design and settings, the defence plan design and settings, based on the regulation coming from the network codes.

The **System Split Indicator** (SSI) is evaluated as frequency performance indicator to rank the split lines:

$$SSI = \frac{\frac{df(h)}{dt}_s}{\left|\frac{df(h)}{dt}_s\right|_{max}} \tag{4.27}$$

where $\left|\frac{df(h)}{dt}_s\right|_{max}$ is the maximum absolute ROCOF obtained from the computation in one scenario or more for comparison reasons. The SSI indicator is positive in case of over-frequency and negative in case of under-frequency phenomena.

The market modelling outputs are given with an hourly granularity and show the hourly dispatch for each unit's type and for the countries in the interconnected areas. Knowing the imbalance and the sets of market zone, the inertia and running capacity in each set can be evaluated as discussed in Section 4.3.1 and the frequency performance indicators can be computed. The overall process is depicted in Figure 4.12.

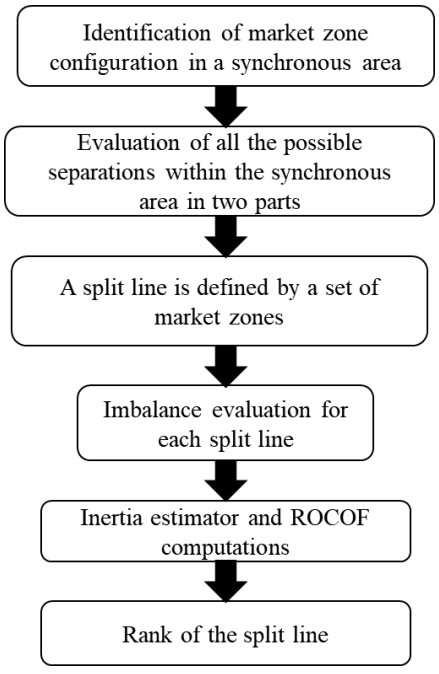

Figure 4.12: Split identification methodology.

4.3.5 Normal operation

The aggregate model is basically a transfer function, which can be inverted obtaining the "reverse" model. The "reverse" model can estimate the generation-load imbalance ΔP_{mis} based on two inputs: the frequency signal Δf_{REAL} and its numerical derivative. All the blocks and parameters are equal to the forward model. If the computed load imbalance ΔP_{mis} is fed from the reverse model in the forward model, the original frequency signal $\Delta f_{SIM_{real}}$ can be reproduced. Then, it is possible to add new resources (e.g., BESSs) or to modify model parameters (e.g., reduced inertia). Computing the new frequency signal $\Delta f_{SIM_{new}}$ the direct impact of such modifications in the grid can be quantified. Figure 4.13 reports a schematic view of the proposed methodology.

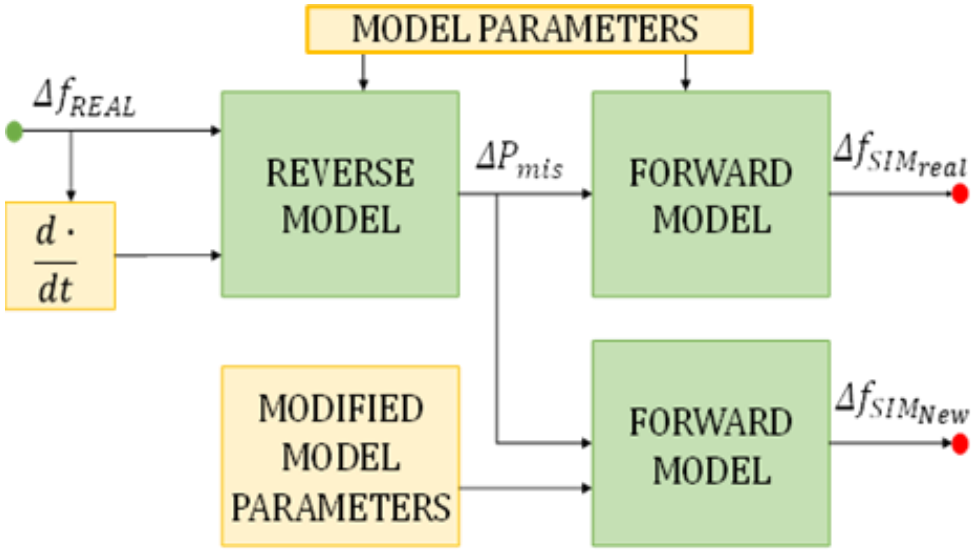

Figure 4.13: Flowchart of the proposed approach to study the frequency dynamic in the normal operation [69].

Using the evaluated frequency and the reverse model is then possible to reconstruct the ΔP_{mis} as shown in Figure 4.14 and compare it with the original ramp: the two trajectories are equal except for very small differences around the cuspid points at 5 and 6 seconds due to small imprecisions of the numerical methods of the solvers.

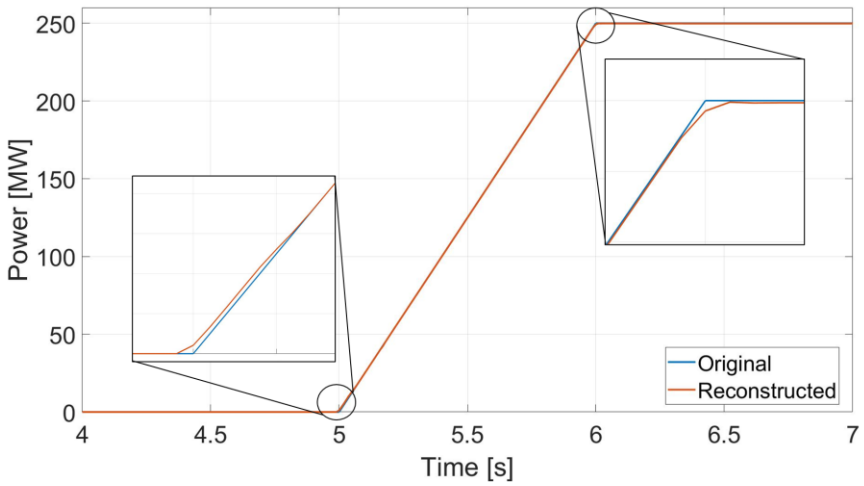

Figure 4.14: Original ΔP_L and reconstructed ΔP_{mis} profiles with zooms on cuspid points [69].

4.4 Technical and Economic Impact on Unit Commitment

A potential solution to mitigate frequency stability issues can be implementing inertia and frequency stability constraints directly in the power plant unit commitment already in the market phase. In [180], [181] FCR is incorporated in the market designs, considering the provision of inertia and the RES uncertainty. The identification of the minimum allowable level of synchronous generation is the main challenge [182]. This limit has important implications, as it can imply RES curtailment or more costs to keep the conventional generation. Unit commitment and economic dispatch-based strategies are investigated in [183] using constraints and operational metric related to the initial ROCOF following an imbalance and the level of wind curtailment. Novel mixed integer linear dispatch models are presented describing frequency performance requirements as a function of both system inertia and the maximum contingency size, to reduce operational costs and RES curtailment [184], to optimize generation and the inertial and primary frequency response allocation, as well as FFR, against the largest plant outage [185], to apply stochastic unit commitment to schedule multiple frequency services [102], or to quantify the economic value of inertia [186]. In [187] more conventional generation is introduced to update the unit commitment when worst values for the frequency nadir follow the worst contingency. The environmental-economic generation dispatch while considering frequency stability in the optimization problem has been considered in [188], leaving in any case the final decision to the TSO. Various methods are proposed to solve problems with conflicting objectives to find the best compromise, as in the case of environmental, economic or security targets [189]. The multi-objective can be converted into a single-objective optimization problem by weighted aggregation method. Nevertheless, multi-

objective evolutionary algorithms have shown the ability of finding effective optimal solutions [190]. Other works implemented the constraints by linearizing the inertia constraint [191] [192] [193], even if the real behaviour is strictly non-linear. However, ensuing very conservative results that would lead to costs overestimation make these approaches not easy to be exploited for real planning studies by the TSO. Furthermore, a practical methodology to select the best compromise solution in the inertia-dependent unit commitment is still needed.

This Section investigates the impact of different frequency control constraints on the unit commitment, proposing a methodology to apply in the economic dispatch algorithm currently used by the power system utilities. A systematic market analysis is carried out through consecutive steps considering different significant inertia thresholds: the outputs are compared in terms of overall system costs and frequency security performance, using dynamic simulations. A methodology to find the best compromise in a technical-economic view is outlined, using a multiple criteria decision analysis methodology. The approach is tested on the small insular power system of the Sardinia Island using the results of market simulations in the DG 2030 scenario, characterized by the most relevant RES penetration [26]. The main contribution is the implementation of frequency security constraints in the TSO's economic dispatch model, with the possibility to select different constraints to optimize the unit dispatching. In the second stage, the Technique for Order Performance by Similarity to Ideal Solution (TOPSIS) method is applied to help the decision maker in extracting the best compromise solution in terms of frequency performance and economic costs.

4.4.1 Unit commitment problem formulation

The minimum cost unit commitment is increasingly relevant in modern planning studies, due to possible constraints imposed to the conventional generation to balance the high and not-uniformly distributed RES penetration.

Generally, the unit commitment problem has to be solved finding the set of powers generated by the thermal units, minimizing the overall fuel cost and respecting the upper and lower capacity bounds of both thermal units and interconnection lines [194]. Several factors should be considered, such as interchange constraints between contiguous areas, depending on the capacity of each individual interconnection and on contractual agreements.

The market simulator used by the Italian TSO is Promed Grid. It performs the optimization of the generation emulating a coordinated hydro-thermal scheduling over a year with hourly details [195]. The aim is the minimization of the overall generation cost to maximize the market surplus, defined as the sum of the producer surplus, consumer surplus and congestion rents. This allows the TSO to assess the economic social welfare gain related to the development actions in planning scenarios, consistently with the basic approaches indicated by ENTSO-E

[196]. The simulations are based on the market zones equivalent network model, with the entire European interconnected system as the study's perimeter. The merit order of the offers is created based on the generation variable costs, the bidding strategies of the units, the main constraints of thermal units such as flexibility, technology, and provision of reserve, and the optimization of the usage of water reservoir of the hydro power plants and renewable generation. The simulation of the market behaviour is obtained by calculating the optimal medium-term operation schedule of the power system. A large quadratic programming optimization problem is performed to determine the market outcomes, minimizing the overall cost borne in one year by the energy buyers, based on the assumptions of the bidding behaviour at different operation points. This approach is rigorous and fast, as well as robust and conceptually simple, as shown in [197]. An equivalent network model of the interconnected European power system is used. The European market zones are represented as single nodes equipped with detailed generation and load information and interconnected by means of single branches of transmission capacity equal to the real one (the hourly power transfer capacity in each direction is detailed to adequately model real daily and seasonal differences). Electricity price forecasting is performed through two computational steps: Unit Commitment, where the hourly on/off state of each thermal unit based on a merit order of the offers and fulfilling the constraints is determined, and Dispatching, where the hourly generation scheduling of each thermal unit is determined in coordination with the hydro dispatching, compliant with the constraints.

Considering a multi-area system with A areas interconnected by J lines, for each area $a = 1, \ldots, A$, the hourly cost curve $f_a(P_a)$ of the equivalent thermal unit is defined in function of the power P_a to be supplied. The multi-area thermal dispatching problem is formulated with the objective to find the power P_a that minimizes the overall fuel cost F subject to the minimum T_{jm} and the maximum T_{jM} transfer capacity constraints of each interconnecting line $j = 1, \ldots, J$. Denoting with s_{jn} the sensitivity matrix coefficients of the DC load-flow, the power transfer on the line j is expressed as:

$$T_j = \sum_{a=1}^{A} s_{ja} P_a \tag{4.28}$$

The optimal multi-area thermal dispatching is expressed as:

$$\min F = \sum_{a=1}^{A} f_a(P_a) \tag{4.29}$$

subject to:

$$\sum_{a=1}^{A} P_a = 0 \tag{4.30}$$

$$T_j - T_{jm} \geq 0\,; \;\; T_{jM} - T_j \geq 0 \quad \text{for } j = 1, \ldots, J$$

The market simulator solves the hydro-thermal dispatching optimization problem considering flexibility constraints (duration of permanence in the same ON/OFF state) for thermal generation units and zonal reserve margin constraints.

4.4.2 Inertia constraints

Three metrics are considered to address the frequency stability in the unit commitment which have different impacts on the system inertia: C1) Minimum kinetic energy, C2) Minimum available synchronous capacity, C3) Maximum level of System Non-Synchronous Penetration.

4.4.2.1 Minimum kinetic energy

The minimum kinetic energy $E_{k,\min}$ needed for a defined admissible value of the *ROCOF* in the system is introduced under the condition:

$$\sum_{i=1}^{N} x_{i,t}\, H_i\, S_{\mathrm{n}i} \geq E_{k,\min} \tag{4.31}$$

where $x_{i,t}$ is a binary variable that represents the i-th generator status (0 = offline, 1 = online) at time *t* for i = 1, 2, …, *N*.

The characteristics of an entire SA must be considered to define the *ROCOF* withstand capability correctly, based on the analysis of a reference incident for the concerned grid, as discussed in Chapter 3. The reference incident could be a system split in a large SA with a significant change of inertia and power imbalance in the resulting subsystems, or the loss of the largest power generating module or HVDC link in the case of smaller SAs. The *ROCOF* withstand capability should ideally be provided as a change in frequency over a defined time period, which filters short-term transients and therefore reflects the actual change in the synchronous grid frequency [198]. The minimum kinetic energy that should be present in the system is given by Equation (3.21) :

$$E_{k,min} \geq \frac{f_0\, \Delta P_{L_{max}}}{2\left(\frac{df}{dt}\right)_{max}} \tag{4.32}$$

In this work, the admissible ROCOF is 2 Hz/s and a sensitivity analysis on the imbalance is performed, depending on the size of the system. ROCOF values higher than 2 Hz/s indicate critical events that, in some cases, can start a chain reaction of adverse events and drive the system to unpredictable system states.

4.4.2.2 Minimum available synchronous capacity

The minimum available synchronous capacity $S_{t,\min}$ to feed a percentage of the total demand capacity is considered as second constraint. $S_{t,\min}$ is defined as a fraction ψ of the demand capacity $S_{t,\text{load}}$ (the total load apparent power at hour *t*):

$$S_{t,\min} \geq \psi \, S_{t,\text{load}} \tag{4.33}$$

Such that

$$\sum_{i=1}^{N} x_{i,t} \, S_i \geq S_{t,\min} \tag{4.34}$$

A sensitivity analysis with different values of the fraction ψ is considered. The synchronous capacity is directly linked to the system inertia, improving the frequency stability but affecting the costs for the system.

4.4.2.3 Maximum level of System Non-Synchronous Penetration

The System Non-Synchronous Penetration (*SNSP*) ratio ξ_{SNSP} is a dimensionless indicator based on [199] and recently adopted by the Irish TSO [200], defined in [201] as:

$$\xi_{SNSP}(t) = \frac{P_{PEIG}(t) + P_{import}(t)}{P_{demand}(t) + P_{export}(t)} \tag{4.35}$$

where $P_{\text{PEIG}}(t)$ is the power generation by PEIG [MW] at time t, $P_{\text{import}}(t)$ is the imported power through HVDC [MW] at time t, $P_{\text{demand}}(t)$ is the power demand [MW] at time t, and P_{export} represents the exported power through HVDC [MW] at time t.

The *SNSP* index has been selected from a specific set of feasible indicators assessing flexibility requirements for the power system [202] as the most representative of PEIG integration. Recent studies conducted by the Italian TSO have evaluated the average value of the *SNSP* index for the whole Italian power system [203] and for a specific critical section of the Italian power system [204].

This indicator is limited by the maximum value $\xi_{\max}$:

$$\xi_{SNSP} \leq \xi_{\max} \tag{4.36}$$

The value considered for Ireland was $\xi_{\max}$ = 0.5 in [205]. The conclusions of the Irish TSO recommend a restriction on "inertia-less penetration" to about 50%, which has been recently extended to 65%, and it is expected to arrive at 75% in the next future [206]. For this purpose, in this thesis a sensitivity analysis is considered with $\xi_{\max}$ = [0.5, 0.65, 0.75]. These values are considered suitable for small power systems, as values 0.5 and 0.65 have been currently handled in the Irish system and a level of 0.75 has been set as a threshold for a secure operation [207].

4.4.3 Methodology for the selection of the technical-economic compromise

The base case has no inertia constraints implemented. The three constraints described in the previous Section are implemented in the market optimization tool, which gives different results in terms of hourly power plants unit commitment to respect the imposed constraints. Starting from the hourly market simulations results in the considered scenario, the online thermal capacity needed is identified based on fixed and variable costs and the minimum stable power of the generating units. If the available thermal capacity does not satisfy the maximum admissible constraint, consecutive iterations are carried out comparing the remaining available thermal units in terms of economic efficiency (merit order) and technical characteristics (minimum stable power). Once the hourly annual thermal production profiles are defined, input data are modified, and market simulations are repeated. Figure 4.15 shows the flowchart of the constraints' implementation in the market unit commitment.

The results are then compared in a technical-economic perspective, considering the frequency stability performance of the system and the associated costs. The frequency stability of the system is assessed for each hour, with dynamic simulations performed with the aggregate model described in Section 4.3, considering the hourly worst-case under frequency contingency.

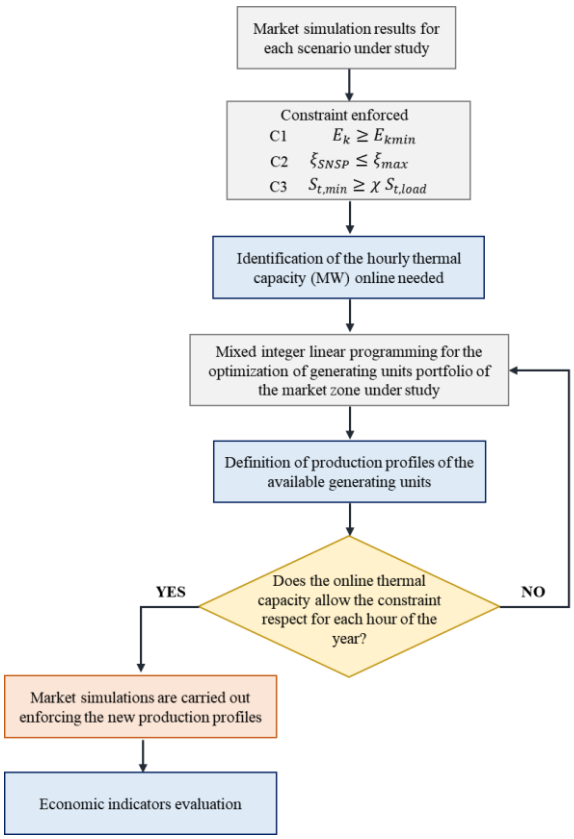

Figure 4.15: Flowchart of the proposed approach with details on how to set the frequency stability constraints [208].

The performance of the frequency response is assessed selecting the following indicators from Section 4.2:

i. initial *ROCOF*, and
ii. maximum transient frequency deviation with respect to the rated frequency, denoted as $\Delta f_{max.}$

The economic outcomes from the market simulations are evaluated in terms of the following indicators, defined in [196]:

a. Socio-Economic Welfare (*SEW*),
b. cost of CO_2 emissions, and
c. cost of fuel.

A decision maker must take one single solution between the different alternatives proposed and can do this by experience. Nevertheless, when dealing with a large set of suitable solutions, a method to rank the alternatives can be very useful, falling in the context of **Multiple-Criteria Decision Analysis** (MCDA).

Multi-Criteria Decision Analysis (MCDA) or Multi-Criteria Decision (MCDM) is a set of tools used to deal with decision-making problems with a wide array parameters and conflicts of interest. In this thesis, MCDA is used to identify the best trade-off which better reflects the priorities of the decision-maker, comparing technical and economic targets. MCDA is used in many situations and different fields, such as economics, finance, mathematics, health care, environmental protection, etc. In the energy sector, MCDA can express its full potential by including knowledge about economic, social and ecological issues.

Therefore, the results are compared and analysed to find non-dominance between the different alternatives, using the Pareto theory. In practice, for a multi-objective optimization problem, a solution u_1 is said to dominate a solution u_2 if both the next conditions are true:

a) The solution u_1 is not worse than u_2 in all objectives.
b) The solution u_1 is strictly better than u_2 in at least one objective.

After obtaining the Pareto front of the optimization problem, the decision maker needs to select one solution, which will satisfy the different goals to some extent. Such a solution is called best compromise solution.

The selection of the best compromise in terms of technical and economic values is made using a MCDA tool.

The MCDA methods can be generally divided into three main categories: elementary methods, compensatory methods and outranking methods [209]. The **elementary methods** include simple tools that can quickly define the best choice, such as the weighted sum method, in which the preferred option is the highest scoring option, calculated as the sum of each criteria multiplied by its weight. In the **compensatory methods**, the different perspectives of the problems contribute to identify a single function to be optimized. Examples of this category include:

Analytical Hierarchy Process (AHP) method, which is weighted sum method for criteria ordered hierarchically; TOPSIS, in which the main principle is that the ideal alternative has the best level for all criteria and the selected best option is the closest to the ideal alternative; MCDA combined fuzzy logic, which involves fuzzy set theory to better describe human judgment and qualitative criteria. Finally, the last category is represented by **outranking methods**, such as Elimination et choice translating reality (ELECTRE) or Preference ranking organization method for enrichment evaluation (PROMETHEE). These algorithms use outranking relations between alternatives to obtain the final ranking of all options. Outranking relations are binary relations defined on a set of alternatives. For any pair of alternatives, there are sufficient arguments to say that one alternative is at least as good as another one, and at the same time there is any strong reason to say the opposite. Outranking methods are complex to apply, less versatile and require high computation efforts compared to elementary and compensatory methods [210].

In MCDA, each criterion is associated to a weight that reflects its relative importance to the decision. The selection of the weights can be judgmental, reflecting the subjective assessment of experts [211]. The literature offers some tools to assist the decision-making process, with different ways to reduce the impact of the personal judgment of the decision maker. The simple weighted sum is exposed to the uncertainties of the opinions of the decision makers. The AHP uses the 9-point scale defined by Saaty [212] to express the relative preferences between pairs of criteria and applies a consistency criterion to ensure that the preferences have been expressed in a consistent way. The Ordered Weighted Averaging [213] orders the weights based on their relative importance and uses a transformation function to modify the weighted values of the criteria and obtain a multi-criteria combination procedure guided by a single parameter. The TOPSIS method evaluates the criteria based on their distance to reference (ideal) points [214], [215]. Other methods that compare pairs of weights are ELECTRE [216] and PROMETHEE [217]. The selection of the weights is a crucial point for any multi-criteria assessment. For example, the weighting of criteria to be assessed in extreme situations, such as blackouts, together with other objectives assessed in normal situations, would be a critical issue, because of the excessive difference between these situations.

However, this is not the case of the criteria considered in this work.

The role and impact of uncertainties can be relevant. Although fuzzy-based MCDM solves a major issue of uncertainty or fuzziness in a decision-making problem, there are many drawbacks based on the literature. There is no standard solution technique to solve, mathematical model to represent a problem, increased complexity, and ambiguity. It is not possible to incorporate any quantitative factor, and the determined solution is very difficult to be analysed. Given that, it

has been decided to not consider the uncertainty as a first step in the methodology developed in this thesis.

Despite the development of many multicriteria decision methods, none can be considered as the most appropriate for all decision-making situations [218]. It is suggested to study different MCDA methods and to characterize their application domains. The authors in [219] reviewed the application and use of decision-making approaches regarding energy management problems (196 published papers, from 1995 to 2015 in 72 important journals related to energy management). They categorised MCDA as a particularly useful method in this context, thanks to its capability to deal with criteria of different fields, different nature and different objectives. AHP and TOPSIS were ranked among the most used for renewable energy-based papers. The aim of [220] is to provide a systematic review of the literature to identify which research subjects have been prioritized in the fields of energy and sustainability in recent years. Researchers tend to rely on fuzzy reasoning to deal with uncertainty across different MCDA methods, dominated by AHP and TOPSIS.

[221] presents a comparative analysis of AHP and TOPSIS in the context of supplier selection decision making. The results have shown that both methods are suitable for the problem of supplier selection, particularly to support group decision making and modelling of uncertainty. The comparison was made based on the factors: adequacy to changes of alternatives or criteria; agility in the decision process; computational complexity; adequacy to support group decision making; the number of alternative suppliers and criteria; and modelling of uncertainty. However, the comparative analysis has shown that the TOPSIS method is better suited to the problem of supplier selection regarding changes of alternatives and criteria, agility and number of criteria and alternative suppliers. Furthermore, another advantage of TOPSIS is to overcome the problem of interdependency between objective and alternatives of the AHP. Overall, TOPSIS presents almost all the qualities considered necessary for this work and it is selected for this application.

The criteria are compared among them based on their relative closeness to the ideal solution, thus introducing a quantitative reference that reduces the impact of subjective judgement.

Five criteria to be minimized are considered for the MCDA:

$a)$ $ROCOF_{95\%}$, the value of *ROCOF* occurring in 95% of the cases with violations compared to a predefined system *ROCOF* threshold.

b) $\Delta f_{\text{nadir95\%}} = f_0 - f_{\text{nadir95\%}}$, the difference between the nominal frequency and the value of frequency nadir occurring in 95% of the cases with violations compared to a predefined system frequency nadir threshold.

c) χ_{SEW}, the ratio between the *SEW* calculated in the constrained alternative and in the base case.

d) χ_{CO_2}, the ratio between the cost of CO_2 calculated in the constrained alternative and in the base case.

and) χ_{fuel}, the ratio between the cost of fuel calculated in the constrained alternative and in the base case.

The violations have the following alarm thresholds: a) 0.5 Hz/s for the *ROCOF*; b) 49.2 Hz for the frequency nadir. Values higher than 0.5 Hz/s and 49.2 Hz are based on studies performed and published by ENTSO-E [30] as standard for protection settings and as a first alarm threshold for relevant imbalances in the power system.

The overall methodology follows the workflow depicted in Figure 4.16.

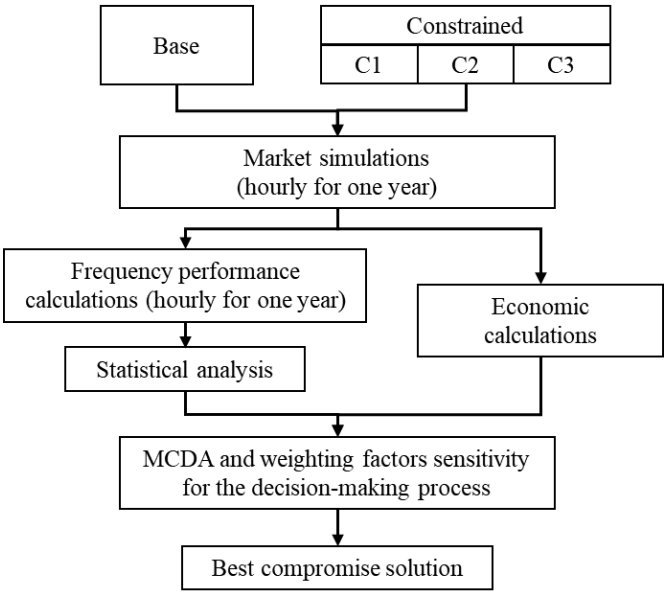

Figure 4.16: Flowchart of the proposed methodology to implement and evaluate the technical and economic performance of the frequency stability constraints in the market simulations [208].

4.4.4 The TOPSIS method

TOPSIS is a ranking method which re-order several alternatives based on the concept that the ideal alternative has the best level for all criteria, whereas the negative ideal is the one with all the worst criteria values. The selected best alternative should have the shortest distance from the positive ideal solution in geometrical sense while it has the longest distance from the negative solution. This method has a wide application area ranging from microgrid/energy planning, energy management, supply chain and logistics, water and waste resource management, manufacturing and design engineering, business and industrial management, etc. [222]. In [223] TOPSIS method is employed to help the decision maker to extract the best compromise solution in an environmental/economic dispatch problem with competing objectives of fuel cost, emission and real power loss. In [224] a coordination assessment system is established to coordinate power plants planning and power network planning in

the electricity market environment. the TOPSIS method is adopted to implement multiple attribute decision making. In [225] an approach to deal with the multi-objective economic dispatch problem in smart grids as a multi-criteria decision making is presented, considering four objectives (emissions, energy cost, distance of supply and load balancing) and using TOPSIS to automatically select the most suitable power output configuration.

The TOPSIS method, based on the concept that the chosen alternative should have the shortest distance from the positive ideal solution and the farthest distance from the negative ideal solution, can identify the best alternative from a finite set of alternatives quickly. The application of TOPSIS [226] is expressed as follows:

1. Construct the normalized decision matrix.

The normalized decision matrix $\mathbf{R} = \{r_{mz}\}$ is constructed starting from the matrix $\mathbf{D} = \{d_{mz}\}$ of $m = 1, \dots, M$ alternatives and $z = 1, \dots, Z$ criteria; for each column $z = 1, \dots, Z$:

$$r_{mz} = \frac{d_{mz}}{\sqrt{(d_{1z}^2 + \cdots + d_{Mz}^2)}} \tag{4.37}$$

2. Construct the weighted normalized decision matrix

In the MCDA, the decision maker's weighting factors need to be defined for each criterion, to consider the importance the decision makers can give to different criteria. The weighted normalized decision matrix is constructed using the decision maker's weighting factors λ_z applied to the criteria $z = 1, \dots, Z$ and the information entropy given by Δ_z:

$$\Delta_z = -k \sum_{m=1}^{M} \frac{d_{mz}}{(d_{1z} + \cdots + d_{Mz})} \ln\left(\frac{d_{mz}}{(d_{1z} + \cdots + d_{Mz})}\right) \tag{4.38}$$

where $0 \leq \Delta_z \leq 1$ using $k = \frac{1}{\ln M}$. The aggregated weight w_z is computed as:

$$w_z = \frac{\lambda_z \frac{1 - \Delta_z}{\sum_{j=1}^{Z}(1 - \Delta_j)}}{\sum_{v=1}^{Z} \lambda_v \frac{1 - \Delta_v}{\sum_{j=1}^{Z}(1 - \Delta_j)}} \tag{4.39}$$

The weighted normalised decision matrix is given by:

$$\mathbf{V} = \mathbf{R} \cdot \mathbf{W}_{Z \times Z} \tag{4.40}$$

where $\mathbf{W}_{Z \times Z}$ is the diagonal matrix with the elements w_z on the diagonal.

Given *M* independent events (i.e., the *M* alternatives) with probability p_m for *m* = 1, …, *M*, the Shannon entropy is expressed as $\mathcal{E} = -\sum_{m=1}^{M} p_m \ln(p_m)$ and corresponds to the average amount of information received per event. The maximum Shannon entropy $\mathcal{E}_{\max} = \ln(M)$ is obtained when all events have equal probability, that is, $p_m = \frac{1}{M}$. The information entropy measure used in (17) is the normalised Shannon entropy calculated by considering the *M* alternatives as independent events for the criterion *z* under analysis.

3. Identify the positive and negative ideal solutions

The positive and negative ideal solutions of the alternatives are taken from the best and worst elements of the matrix **V**, respectively:

$$\boldsymbol{a}^{+} = \{v_1^{+}, \dots, v_Z^{+}\};\ \boldsymbol{a}^{-} = \{v_1^{-}, \dots, v_Z^{-}\} \tag{4.41}$$

4. Distance of the alternatives from the ideal solutions

The distances of each alternative from the positive and negative ideal solutions are given by:

$$\delta_m^{+} = \sqrt{\sum_{z=1}^{Z}(v_{mz} - v_z^{+})^2};\ \delta_m^{-} = \sqrt{\sum_{z=1}^{Z}(v_{mz} - v_z^{-})^2} \tag{4.42}$$

5. Calculate the relative closeness to the ideal solution

The relative closeness coefficient c_m of each alternative is:

$$c_m = \frac{\delta_m^{-}}{\delta_m^{-} + \delta_m^{+}} \tag{4.43}$$

6. Rank the preference order

The alternatives are ranked in descending order of c_m. The best solution has the maximum value of c_m.

4.4.4.1 Decision maker's weighting factors

To give a broader view on the choice of the weighting factors in the decision-making process, a sensitivity analysis is implemented. At first, the criteria are divided into two groups, namely, frequency stability performance criteria (with cardinality σ_f) and cost-based performance criteria (with cardinality σ_c). Then, equal weights are established for the frequency stability performance criteria ($\lambda_{f,1} = \lambda_{f,2} = \cdots = \lambda_{f,\sigma_f} = 1/\sigma_f$) and for the cost-based performance criteria ($\lambda_{c,1} = \lambda_{c,2} = \cdots = \lambda_{c,\sigma_c} = 1/\sigma_c$).

The parametric analysis is executed by assuming a coefficient of variation α for the two groups of performance criteria, such that the outcome of the parametric analysis depends only on the coefficient α that satisfies the relation:

$$\alpha \sum_{v=1}^{\sigma_f} \lambda_{f,v} + (1-\alpha) \sum_{q=1}^{\sigma_c} \lambda_{c,q} = 1 \tag{4.44}$$

For $\alpha = 0$ only the cost-based performance criteria are considered, while for $\alpha = 1$ only the frequency stability performance criteria are considered.

4.5 Assessing the distributional impact of PEIG

Following the main concepts outlined in Chapter 3, the term **distributed inertia** is introduced here to identify different areas of an interconnected power system with different levels of inertia-equipped resources, due to an uneven distribution of conventional synchronous generators and non-conventional RES.

In this Section, some metrics are defined to evaluate the inertia distribution. The analysis of the inertia distribution can be made punctually, considering the spatial localization of the units and their connection to the power system, or considering the subdivision of the system in zones, e.g., the market zones, which are defined with economic and electrical criteria. First, for each zone a mapping of the conventional and non-conventional generation and the related inertia and kinetic energy is needed. Later, a set of buses to monitor and to which apply the reference contingency is selected. The monitoring bus is the one where the metrics are computed, while the contingency bus is the bus where the reference contingency is applied.

The metrics to evaluate the impact on stability are the **inertia intensity** of the zone, the **mesh degree** of the zone and the **electrical distance** from the contingency and monitoring bus.

The inertia intensity χ is defined as the ratio between the total kinetic energy and the sum of conventional P_C and non-conventional generation P_{NC}:

$$\chi = \frac{E_k}{P_C + P_{NC}} \tag{4.45}$$

This indicator highlights how many MWs of kinetic energy are present in the system for each MW of conventional and non-conventional generation (installed or dispatched). The index decreases if the non-conventional generation grows or with conventional generator of similar power but very different inertia constants. Inertia intensity tries to capture the penetration of non-conventional generation over the kinetic energy.

The mesh degree is considered using two different indices:

- **Short-circuit power** S_{cc}, which is a consolidated indicator of the system strength, defined as

$$S_{cc} = \sqrt{3}\, I_{cc} V_n \tag{4.46}$$

  where I_{cc} is the short-circuit current and V_n the nominal voltage.

- **Number of incident lines** on a bus, which is calculated summing the row of the incidence matrix of the system. For a zone, the number of incident lines is given by the sum of the incident lines on the bus of the zone. This index is used to consider the short-circuit power influence of the generators and not only by the meshing of the connections.

The distance from the contingency point is evaluated in terms of electrical distance using the impedance matrix of the system. Considering a bus g and a second bus d, the electrical distance Δ_{gd} between the two buses is given by the equivalent impedance:

$$\Delta_{gd} = \left|\left(\boldsymbol{Z}_{gg} - \boldsymbol{Z}_{gd}\right) - \left(\boldsymbol{Z}_{gd} - \boldsymbol{Z}_{dd}\right)\right| \tag{4.47}$$

where $\boldsymbol{Z}_{gg}$ is the g-row, g-column of the impedance matrix, $\boldsymbol{Z}_{gd}$ is the g-row, d-column of the impedance matrix and $\boldsymbol{Z}_{dd}$ is the d-row, d-column of the impedance matrix. If two buses are directly connected, the electrical distance is given by only $\left|\boldsymbol{Z}_{gd}\right|$.

4.6 Modelling technologies to support frequency control

The selected technologies to support frequency control in this thesis are ESS (focusing on BESS), SyC, and HVDC.

The **Energy Storage Systems** (ESS) allow to control in an independent and fast way the active and reactive power produced, contributing to the power system stability and to damp the grid oscillations. A ESS consist of an energy source (that supply or store the energy) connected to the grid with a DC/AC converter (Figure 4.17).

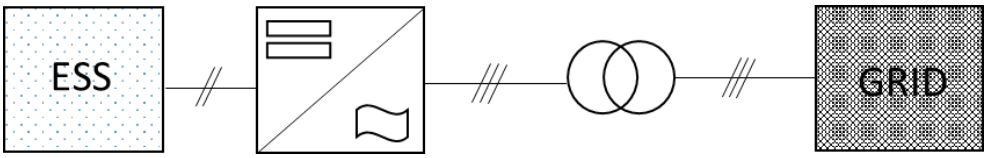

Figure 4.17. Main components and scheme of an ESS.

BESS are characterized by a primary source of electrochemical type. The main parameters for a BESS are:

- **V_{oc}** is the open-circuit voltage of the battery, that is function of the State of Charge [V]
- **I_{es}** is the generated/adsorbed current [A]
- **Q** is the capacity of the battery [Ah]
- **T_c** is the operation temperature [°C]
- **SoC** is the State of Charge of the battery [p.u.], given by:

$$\frac{dSOC}{dt} = -\frac{I_{es}}{Q} \tag{4.48}$$

An electric equivalent model for a BESS is depicted in Figure 4.18. It comprises electrical parameters to model the voltage drop due to the connections

and battery internal losses, the series resistance R_s and internal resistance R_p and the capacitive effects C_p. Generally, these parameters are functions of the SoC and aging of the BESS.

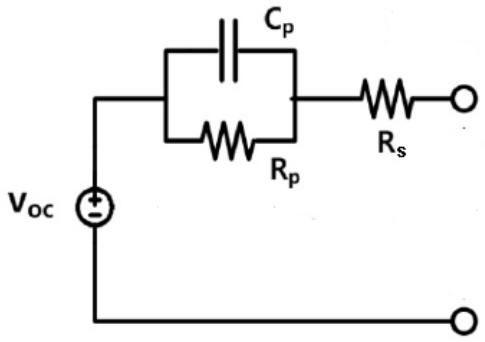

Figure 4.18. Electric equivalent circuit of a BESS [227].

The dynamic model for the BESS is shown in Figure 4.19. The ESS model derives from [166], with the difference that the contribution due to the derivative of frequency is instantaneous, to emulate the inertial synchronous response.

The component related to Δf is the primary frequency control level, whereas the component related to df/dt aims to simulate the virtual inertia. The battery primary control is modelled as a first order transfer function [228], which is suited for power system stability studies.

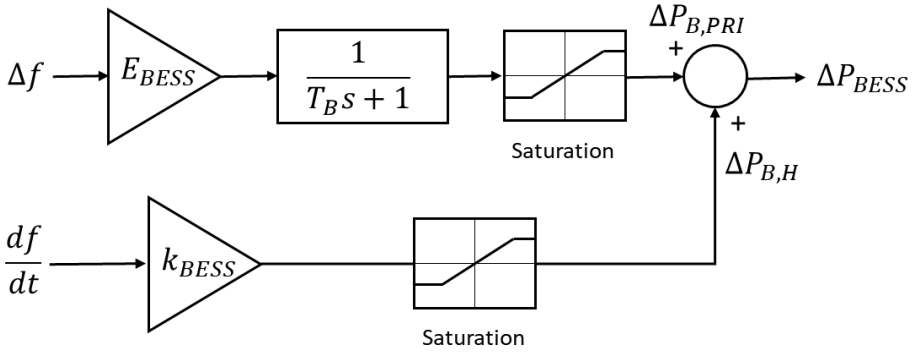

Figure 4.19: Dynamic model of a BESS [175].

The dynamic model is composed by the following block parameters:

- Virtual regulating energy of the BESS, defined as:

$$E_{BESS} = -\frac{P_B}{f_0 \sigma_B} \tag{4.49}$$

  where σ_B is the equivalent BESS droop and P_B is the BESS nominal active power.
- Equivalent BESS's pole time constant T_B.
- BESS's virtual inertia response factor, defined as:

$$k_{BESS} = \frac{2\,H_{BESS}P_B}{f_0} \tag{4.50}$$

where H_{BESS} is the virtual inertia constant.

- BESS's power injection for regulation ΔP_{BESS} which can be divided in the inertial contribution $\Delta P_{B,H}$ and primary contribution $\Delta P_{B,PRI}$.

A **Fixed Droop** strategy is considered as control strategy of the BESS. Therefore, in the primary frequency control a low droop can be used, much more performing with respect to the usual value of the traditional generation [229]. In the case of conventional plants, the band reserved for FCR is a share of the maximum power (e.g., in Sardinia $\Delta P_{MAX}/P_n = 10\%$), whereas a BESS can use 100% of its band. Consequently, a new equivalent value for the droop can be computed, imposing the BESS's reserve saturation at the same frequency deviation of a conventional unit but with $(\Delta P_{MAX}/P_n)_B = 1$. The frequency at which the reserve is saturated is computed as:

$$\Delta f_{MAX} = \frac{\Delta P_{MAX}}{P_n}\, f_0 \sigma_p \tag{4.51}$$

$$\sigma_B = \frac{\Delta f_{MAX}}{f_0}\left(\frac{P_n}{\Delta P_{MAX}}\right)_{BESS} = 0.005 \tag{4.52}$$

which is equal to 0.005 if $\Delta P_{MAX}/P_n = 10\%$.

An **Equivalent Saturation Logic** (ESL) is used to calculate the virtual inertia contribute H_{BESS} of the BESS, using the hypothesis of the saturation for an extreme ROCOF of 1 Hz/s [230]. The idea is to replicate the inertial behaviour of the synchronous generators, which produces an instantaneous active power variation for every value of ROCOF in the system. In the case of the BESS, a conventional extreme ROCOF is decided and the active power variation is imposed as the maximum available. Therefore, it is possible to calculate the virtual inertia contribution H_{BESS}

$$H_{BESS} = \frac{f_0\,\chi_B}{2\left|{df}/{dt}\right|_{MAX}} \tag{4.53}$$

where χ_B is the **inertial control share** participation of the BESS over the total power, whereas 1-χ_B represents the share of participation in the primary control.

The primary contribution is calculated as:

$$\Delta P_{B,PRI} = \frac{P_B(1-\chi_B)}{\sigma_B f_0} \tag{4.54}$$

Four different strategies for BESS simulation are used in this thesis, based on active power band devoted to inertial or primary control:

1. 50% of active power used for inertial and primary control $\chi_B = 0.5$, with two different pole time constant.
    i. $T_B = 0.1$ s.
    ii. $T_B = 0.3$ s.
2. Only inertial control $\chi_B = 1$.
3. Only primary control $\chi_B = 0$ with $T_B = 0.3$ s.

The BESS's **secondary contribution** is also investigated during the normal operation. An additional share $\Delta P_{B,SEC}$ of P_B can be used for the secondary control, through the participation factor $\rho_{SEC_B} = \frac{\Delta P_{B,SEC}}{FRR_{tot}}$, where FRR_{tot} is the total FRR.

A simple model to compute the SoC of the BESS is represented in Figure 4.20, where a constant charge/discharge efficiency ϵ is considered. Integrating Equation (4.48) and considering SOC_0, i.e., the initial SoC, the SOC is given by:

$$\Delta SOC = SOC_0 - \frac{\int_0^t I_{es} dt}{Q} \tag{4.55}$$

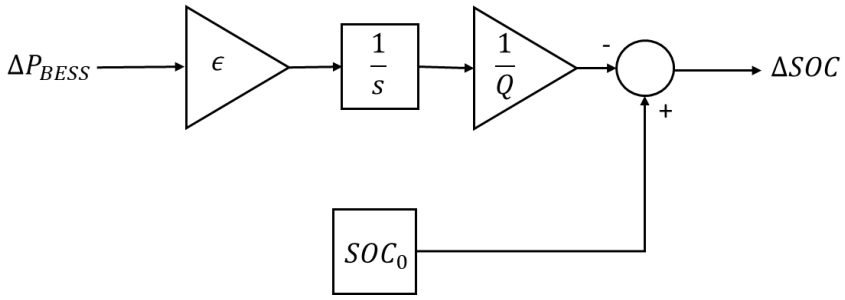

Figure 4.20. SoC computation model.

In the next Chapter, the SoC computation will be neglected, as the focus is on the power system effects assuming the BESS ready to provide services to the grid.

Synchronous compensators are added in the aggregate model and they contribute to increase the kinetic energy through the parameters H_{sys} and S_{tot}. While BESSs are able of providing both synthetic inertia and primary frequency control, SyCs can provide only physical inertia. In this work, each SyC is characterised by an inertia constant of 2 s and an apparent power of 250 MVA.

Non-embedded **HVDC** can transmit different balancing power, but only the FCR exchange between two asynchronous areas is considered in this thesis: the frequency is measured at both sides of HVDC converters and the need for FCR exchange can be derived as difference between frequency deviations. The exchanged power is obtained by multiplication of the frequency deviation difference for a droop factor. Other feasible ways of interventions are: Frequency

Restoration Reserve (FRR) and Replacement Reserve (RR), but they are not considered in our models. The aim is to investigate the effects of the HVDC in contributing to the system frequency stability, particularly in the shorter timeframe.

HVDC links can modify the active power exchange ΔP depending on the frequency variations Δf. The primary frequency regulation can be described by the following equation:

$$\Delta P(s) = \frac{1}{\sigma_p f_n} \cdot \frac{1 + sT_1}{(1 + sT_2)(1 + sT_3)} \cdot P_{reg} \cdot \Delta f \tag{4.56}$$

where σ_p is the droop [p.u.], T_1 the zero-time constant [s], T_2 the pole time constant, T_3 the filter time constant [s] and P_{reg} the regulating power [MW].

One of the main aspects in modelling the HVDC contribution to the frequency support is the correct computation of the primary reserve. In case of regulated/agreed contract (as the HVDC connection between France and GB), the reserve is fixed value, in both upward and downward directions.

In the case of small, islanded power systems in the same control area of one TSO (as Sardinia), it may happen that the reserve depends on the operating conditions and it varies if the link is in import or export, according to the maximum and minimum operative point. Up-band means increase production in the area, so if HVDC is in export it means to reduce the export, if HVDC is in import it means to increase the import. Down-band means decrease production in the area, so if HVDC is in export it means to increase the export, if HVDC is in import it means to decrease the import.

Considering an LCC-HVDC with n_{pol} poles of 500 MW capacity and 50 MW minimum each, the up-band and down-band reserves are calculated as in Table 4.6, considering an actual flow of 400 MW in export/import.

Table 4.6. Calculation of the power reserve for a HVDC connecting two asynchronous areas in the same control zone exporting and importing from the smaller one.

	Max	**Min**	**Power Flow [MW]**	**Up-band**	**Down-band**
HVDC export	500*n_{pol}	50*n_{pol}	400 (export)	400-50*n_{pol}	500*n_{pol} -400
HVDC import	500*n_{pol}	50*n_{pol}	-400 (import)	500*n_{pol} -400	400-50*n_{pol}

While both LCC and VSC can modulate active power based on frequency deviations, VSC-HVDC can provide a contribution in terms of inertia at the AC side of the converter, by regulating the DC voltage and controlling the energy delivered by the DC capacitors on the DC side. When the ROCOF during large frequency disturbances is critically affected by a sudden imbalance and there is a DC voltage variation on the capacitor, the VSC active power output is changed proportional to the DC capacitance. It is possible to derive the relationship

between the emulated VSC inertia time constant and DC voltage variations, as explained in [231]:

$$H_{VSC} = \frac{\frac{NCV_{dc0}^2}{2S_{VSC}}\left(\left(\frac{\Delta V_{dc}}{V_{dc0}}+1\right)^2-1\right)}{2\Delta f/f_0} \tag{4.57}$$

where N is the total number of capacitors in HVDC or MTDC systems, S_{VSC} is the VA rating of the VSC, C the converter terminal capacitance, V_{dc0} the nominal DC voltage. The inertia emulation control proposed in [231] uses the stored energy in the DC capacitors of the HVDC to provide an inertial response, varying the DC voltage according to the frequency changes in the system. The DC voltage variation can be limited within the ±15% of nominal voltage, although the exact limits depend on the rating and functionalities of the converter and insulations. In this thesis, a limit of ±10% is considered to be more restrictive. The VSC-HVDC has therefore the potential to emulate a wide range of inertia time constants, accordingly to the allowed variation of the DC voltage, the value of the DC link capacitors and the active power limit of the converter. The assumptions are a rated DC voltage for the MTDC of 500 kV and two values of capacitance, 5 mF and 15 mF [232]. In Figure 4.21 the range of inertia constants that can be provided by the HVDC with the allowed variation in the DC voltage and the specific frequency changes is shown. For the maximum frequency deviation, emulated inertia time constants in the range of 1 s to 2 and 5 s are feasible respectively for a capacitance of 5 mF and 15 mF. Using relatively large capacitors, larger inertia constants can be feasible for a specific frequency deviation. The inertia emulation control system for the VSC-HVDC is considered in the single-bus model as an additional control loop.

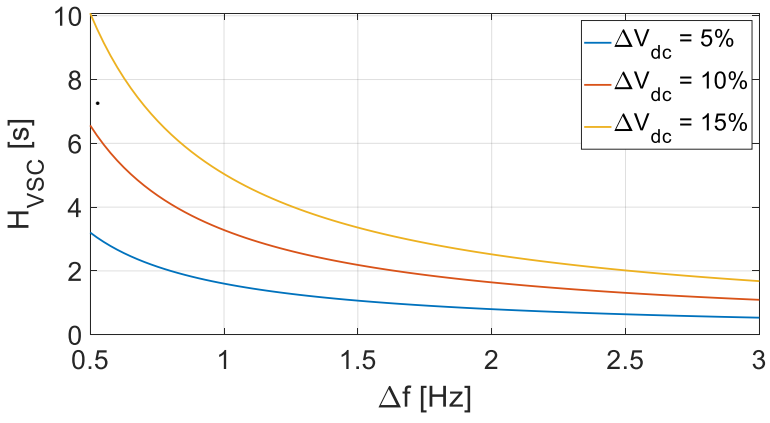

a.

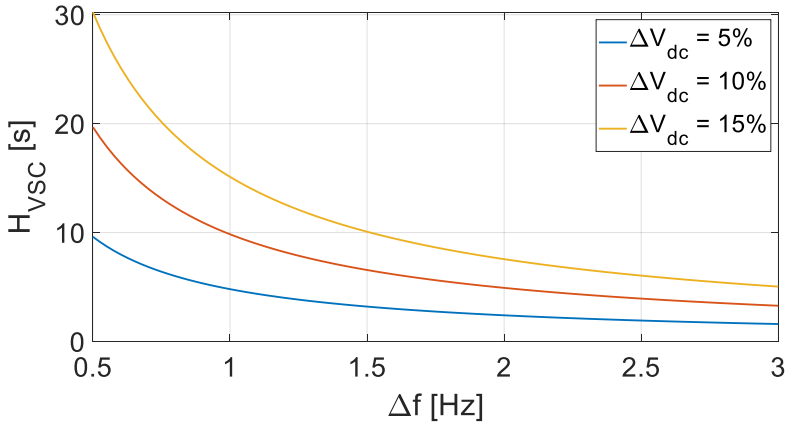

b.

Figure 4.21: Emulated inertia constants based on the considered frequency deviation with different allowable DC voltage deviations (a: C=5 mF, b: C=15 mF).

Chapter 5

5 Stability Assessment of European and Italian Scenarios

5.1 The Sardinian Case Study

The Sardinia region in Italy is an especially interesting real case because it is an islanded power system, asynchronous, with a high share of RES and presence of HVDC links and BESS [233].[5]

The Sardinian high voltage network is characterized by four voltage levels: 380 kV, 220 kV, 150 kV and 70 kV. The transmission grid is composed by 28 substations (9 substations at 380 kV, 12 substations at 220 kV, 7 substations at voltage minor than 150 kV), 181 lines (9 lines at 380 kV, 22 lines at 220 kV, 150 lines at voltage minor than 150 kV), 37 transformers (13 at 380/220 kV, 15 at 220/150 kV, 9 at 150 kV). The system is mainly constituted by overhead lines with north-south extension. The total length of 380 kV lines is 314 km while for 220 kV is 552 km.

The total installed capacity connected to the high voltage network is around 3380 MW composed by thermal (1800 MW), hydro (370 MW), wind (around 970 MW) and photovoltaic (70 MW). Other minor plants are connected to the high voltage network with a total of 170 MW. The installed capacity in medium and low voltage is around 660 MW. The thermal generation is mainly coal (964 MW), while 600 MW are syngas, 80 MW oil and 180 MW diesel fuel.

The demand is characterized by a large diffusion of distributed loads. Only a few loads are connected directly to the high voltage network. The demand's trend present minimum at night around 600-800 MW and evening peaks around 1300-1600 MW. In 2019 the peak load was 1.6 GW (8th July at 13:45h), while the

[5] Parts of this chapter were also published in [175], [239], [241], [69], [208].

minimum was 0.63 GW (11th February at 03:00h). The demand trend and demand duration curve in 2019 are depicted in Figure 5.1.

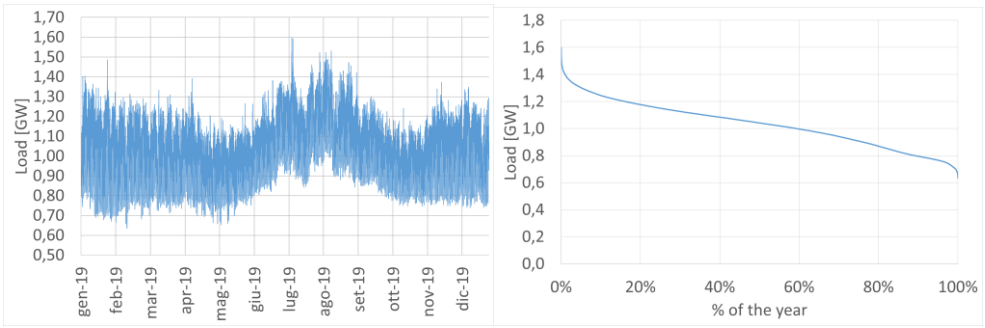

Figure 5.1. Demand trend and demand duration curve in 2019.

An overview of the Sardinian grid is reported in Figure 5.2.

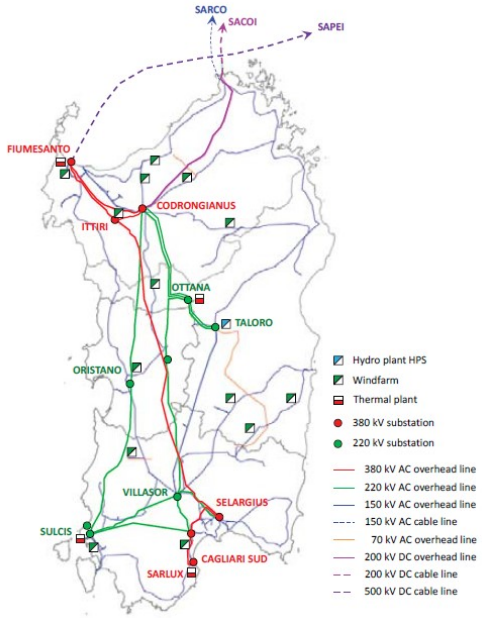

Figure 5.2. Schematic view of the Sardinian power system [233].

Sardinia is connected to the continental grid through two HVDC systems, named SACOI (Sardinia-Corsica-Italy) and SAPEI (Sardinia-Italian Peninsula).

The SACOI link was commissioned in 1966 and it is currently still in operation. It is a monopolar LCC-HVDC with sea return and a capacity of 300 MW among two converter substations, respectively located in Codrongianos (Sardinia island) and Suvereto (Italian mainland), with one 50 MW tap station in Lucciana (Corsica island).

Until 1987 the SACOI had only two terminals, used to transmit power from Sardinia to Italy using Corsica has physical bridge. Later, a new terminal has been added to withdrawal energy in Corsica. SACOI has been the first three-terminal HVDC in the world, assuming the name SACOI1. In 1992 new converter stations has been realized, with modern technologies and adding the frequency power regulation (SACOI2). The refurbishment of the link is planned, through the

substitution and strengthening of the cables and stations, with an increased transmitted power up to 400 MW (SACOI3) and an increased withdrawal in Corsica up to 100 MW. Sardinia and Corsica are also synchronously interconnected via the 150 kV HVAC submarine cable SARCO: therefore, the SACOI. can be considered as a partially embedded DC (Direct Current) link [234].

In 2011, SACOI was joined by the SAPEI, another HVDC that directly connects Sardinia and Italy. SAPEI is a bipolar LCC-HVDC composed by two cables of 500 MW each.

Both HVDC links can modify active power exchanges depending on the frequency variations of the Sardinia grid, providing frequency power regulation to support the system for both primary and secondary.

The physical exchanges in 2019 among Sardinia and the Centre-South and Centre-North Italian market zones are reported in Figure 5.3 as duration curves.

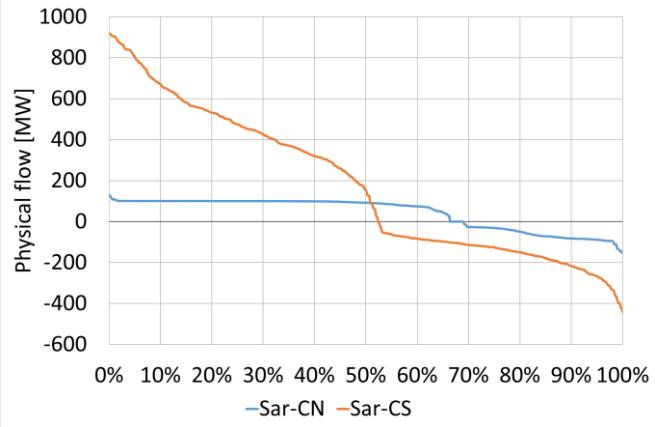

Figure 5.3. Physical exchanges in 2019 among Sardinia and the Centre-South and Centre-North Italian market zones.

The decarbonisation targets are imposing a change in the Sardinian generation mix, characterized by coal thermal generation. To increase the transmission capacity with the continent and to guarantee adequacy and a major exploitation of renewable sources, the planned solution is the realization of two HVDC links between Sardinia and Sicily, the Continental Italian Peninsula and Sicily, named the Tyrrhenian link [36]. This future link is planned for 2027 with a capacity of 1000 MW and an estimated length of 843 km. The possible additional support by the Tyrrhenian Link to frequency stability providing inertial and primary regulation will be investigated and discussed in this Chapter. Table 5.1 shows the main features of the current and future planned links.

Table 5.1: Main data of Sardinian HVDC links.

Name	Nominal Power	Nominal Voltage	Year	Technology
SAPEI	2 x 500 MW	500 kV	2011	HVDC-LCC
SACOI	300 MW	200 kV	1965/1992	3 terminals HVDC-LCC
SARCO	135 MW	150 kV	2006	50 Hz cable
Tyr Link	2 x 500 MW	500 kV	In planning	HVDC-LCC or VSC

Situations of low demand and high RES generation are nowadays the most complicated for a secure operation [235], [236] and they will be used as reference to assess the frequency stability in this thesis. Sardinia power system is generally managed using traditional synchronous units to cover most of the demand with, while the excessive wind generation is exported to the continent through the two HVDCs. The HVDCs typically represent the highest contribution in the regulating energy of the island.

The aggregate model is fed using the parameters showed in Table 5.2 to set the dynamics of thermal, hydro, HVDC, FRP (proportional and integral gains) and RRP, using values found from literature and grid codes [51], [40], [63]. The 10% power band is coming from the Italian grid code requirements (10% of the maximum power for Sardinia). The HVDC reserve depends on the operating conditions, and it varies if the link is importing or exporting, according to the maximum and minimum operation point. For HVDC no dead band is considered, as dead band is imposed to traditional units for mechanical reasons which are not needed by power electronics devices without rotating masses. The FCP of thermal, hydro and HVDC units is modelled using time constants values based on the technologies. Sardinia is a single area system, thus there is no tie-line power mismatch ΔP_s (see Equation (4.10)) to be controlled, and the FRP restores only the nominal system frequency.

Table 5.2. Dynamic data for FCP, FRP and RRP [69].

FCP		**Zero-time constant τ [s]**	**Pole time constant T [s]**	**Droop d [%]**
	Thermal	3	10	5%
	Hydro	-1	6	4%
	HVDC	3.3	10	5%
FRP	k_p		k_T	
	0.05		300	
RRP	TER_{up}	TER_{dw}	TER_{time}	
	85	15	10 min	

5.1.1 Reference incident assessment

The aggregate model is calibrated using real events happened on the Sardinian grid. Figure 5.4 illustrates the comparison between the simulated and actual frequency response for two disturbance: a) HVDC failure in 2018 and b) thermal unit failure in 2019. The HVDC was exporting and its trip originated an over-frequency event, while the under-frequency is related to the thermal unit trip.

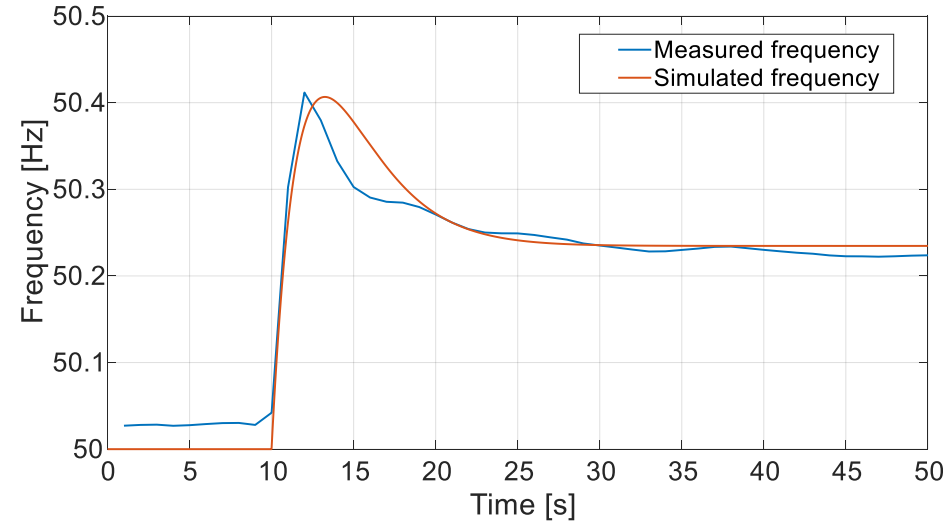

a. Over-frequency event

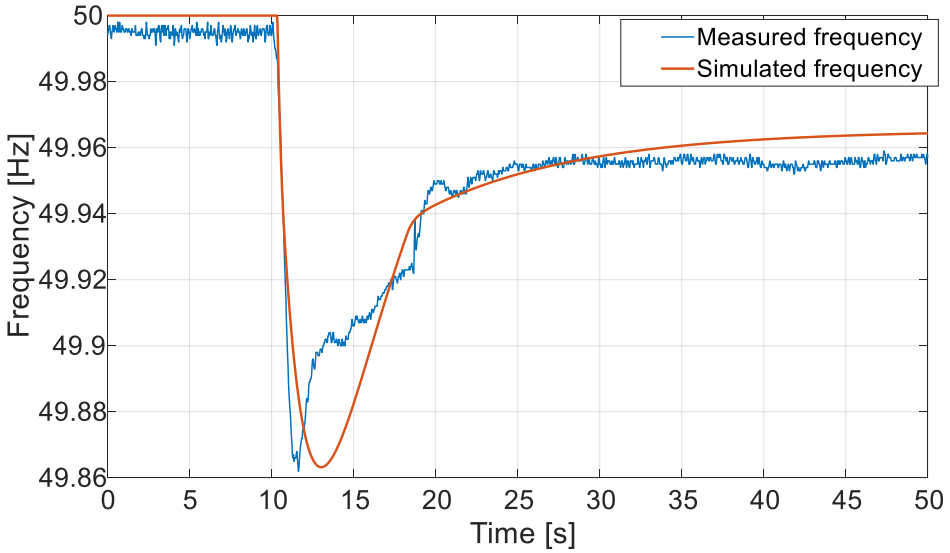

b. Under-frequency event

Figure 5.4: Model validation for an actual disturbance [175].

Table 5.3 compares the main frequency performance indicators obtained by the aggregate model and the measured ones. The ROCOF is evaluated as the maximum difference between the measured frequency values, sampled in 1 second.

Table 5.3. Frequency performance indicators results from the model calibration [175].

a. Over-frequency event	**Measured**	**Simulated**
Zenith [Hz]	50.41	50.41
ROCOF [Hz/s]	0.36	0.37
T_{zenith} [s]	2	3.26
f_{reg} [Hz]	50.22	50.23
b. Under-frequency event	**Measured**	**Simulated**
Nadir [Hz]	49.86	49.86
ROCOF [Hz/s]	0.76	0.80
T_{nadir} [s]	1.63	3.03
f_{reg} [Hz]	49.96	49.96

After having calibrated the aggregate model, frequency stability analysis is performed considering under and over-frequency disturbances in several scenarios.

The winter peak on January 17th, 2018 at hour 10:30 is chosen as the base case scenario. The SACOI was out of service while the SAPEI was exporting 430.4 MW in monopolar operation. The missing of the SACOI made the situation already critical. Thermal generation was around 980 MW, hydro generation around 1.3 MW for a total demand of 1131 MW (of which 81.4 MW of hydro-pumping). Wind generation was 630 MW, while PV around 50 MW. In this starting situation, the over-frequency reference incident is the one-pole failure of the SAPEI (215.2 MW), as it was exporting and in bipolar operation. The other pole can still regulate frequency-power. The under-frequency reference incident is the thermal unit trip producing around 210 MW. The frequency performance indicators simulating these reference incidents are listed in Table 5.4.

Table 5.4: Frequency performance indicators for the current situations in the case of under- and over-frequency reference incident.

	ROCOF [Hz/s]	**Δf_{MAX} [Hz]**	**$f_{nadir/zenith}$ [Hz]**	**$T_{nadir/zenith}$ [s]**	**t_{reg} [s]**	**f_{reg} [Hz]**
Under-freq	0.5464	0.2293	49.7707	1.74	8.11	49.9518
Over-freq	0.4235	0.0814	50.0814	0.71	8.2	50.029

The same reference incidents are kept for the future scenarios. Future scenarios with lower inertia are created by reducing of 10%, 30% and 50% the inertia in the winter peak starting situation, replacing the thermal generation with the same increase of wind production using the minimization problem formulated in Section 4.3. For each scenario, the addition of SyCs and BESSs is analysed. For the BESS, a sensitivity analysis is performed on the quantity of provided primary and inertial response. The performance of the frequency regulation is assessed using the indicators given in Section 4.2. The frequency performance indicators worse with reduced inertia scenarios: the maximum frequency deviation, ROCOF, time of zenith/nadir and time of steady-state frequency deviation increase, whereas the steady-state frequency deviation decreases, because the system has less regulating energy to maintain its condition after an event. The protection schemes are not activated for this study.

Figure 5.5 details the frequency behaviour following the under-frequency and over-frequency reference incident in the initial situation (starting point) and the considered scenarios.

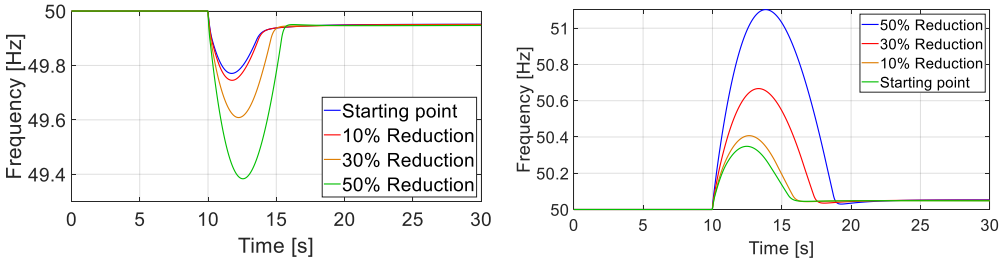

Figure 5.5: Comparison of the impact of the under-frequency reference incident for the scenarios and the actual situation [175].

To improve the situation, the case of 6 and 10 SyCs (in the initial situation only 2 compensators are present) and two systems of 50 MW and 100 MW BESSs are analysed. For the BESSs, a sensitivity analysis is carried out with different values of inertial control shares χ_B and of dynamic pole constant T_B (0.1 and 0.3 s). The 8 situations considering BESS addition are summarised in Table 5.5. Situation #1 is the base case, with 2 SyCs and without BESSs.

Table 5.5: Situations with BESS addition [175].

10 – 30 – 50% Reduced Inertia			
n	**MW**	T_B	χ_B
1	0	0	-
2	50	0.3	0.5
3	50	0.1	0.5
4	50	0.3	1
5	50	0.3	0
6	100	0.3	0.5
7	100	0.1	0.5
8	100	0.3	1
9	100	0.3	0

5.1.1.1 Under-frequency reference incident

In the 10% reduced inertia scenario, the frequency nadir is 49.75 Hz, within the intervention of pump shedding protections, while the ROCOF is 0.60 Hz/s. Thus, the 10% reduced inertia case is already a feasible situation. In the 30% reduced inertia scenario, the frequency nadir is 49.61 Hz, while the ROCOF is 0.78 Hz/s. The frequency nadir reaches 49.38 Hz in the 50% reduced inertia scenario. This value of frequency would have caused activation of the protection schemes, with pump shedding at 49.5 Hz threshold. The frequency response considering the activation of protection schemes is plotted in Figure 5.6.

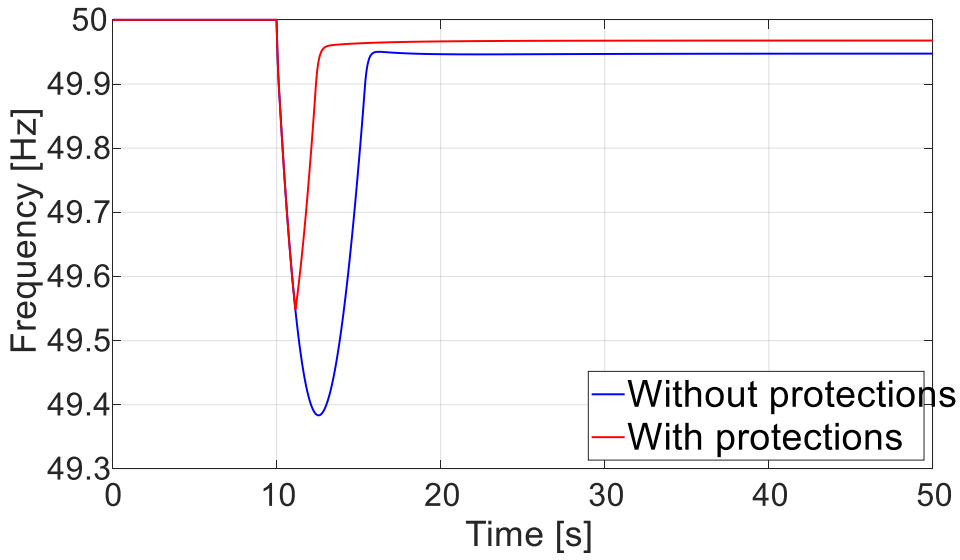

Figure 5.6: Comparison of the impact of the worst-case under-frequency contingency for 50% reduced inertia scenario with and without the implementation of actual protection schemes [175].

In the following only the scenarios with 50% inertia reduction are considered, as the most critical one. The ROCOF value passes from 0.55 Hz/s in the initial situation to 1.07 Hz/s in the 50% reduced inertia scenario, making the situation dramatically worse. The addition of SyCs increases the inertia of the power system affecting both frequency nadir and ROCOF. It is evident that the steady state frequency does not change, connected to the missing regulating energy capacity of the SyCs. With 10 synchronous compensators, the frequency nadir improves by 0.4% with respect to the initial value (passing from 49.38 to 49.57 Hz), while the ROCOF improves by 41.5% (passing from 1.07 to 0.62 Hz/s). The addition of SyCs improves the performance more on the ROCOF than in the maximum frequency deviation, as they do not add primary reserve in the system.

When adding BESS, the results vary based on the 8 situations listed in Table 5.5. The frequency performance generally improves with a higher BESS capacity. Using the two selected pole-time constants for the BESS, slightly changes the results, as it can be seen comparing situations #2 and #3, #6 and #7. This suggests that the time pole constant does not have relevant effect on the situation. The inertial control share χ_B is instead fundamental for a wise operation of the BESS. Using only inertial control (n = 4) leads to the best situation for ROCOF (which changes from 1.066 Hz/s to 0.850 Hz/s) but the lowest improvement of the nadir frequency (which changes from 49.38 Hz to 49.49 Hz). On the contrary, using only primary control (n = 5) gives the best situation for the frequency excursion (from 49.38 Hz to 49.71 Hz) but the ROCOF does not basically change from the initial situation (around 1.07 Hz/s). A compromise is reached with the same share of inertial and primary control (n = 2), having a new value for frequency nadir of 49.63 Hz and for ROCOF of 0.95 Hz/s. The best improvements in frequency nadir reach 0.82% in the case of only primary regulation for the BESS, and 41.5% for

the ROCOF in the case of 10 SyCs added. The entire set of results for the 50% reduced inertia scenarios is reported in Table 5.6.

Table 5.6: Results of the under-frequency scenario with 50% reduced inertia [175]

Starting situation					
n	**Nadir [Hz]**	**ROCOF [Hz/s]**	T_{nadir} **[s]**	T_{reg} **[s]**	f_{reg} **[Hz]**
1	49.3835	1.066	2.57	5.78	49.9474
Addition of Synchronous Compensators					
n	**Nadir [Hz]**	**ROCOF [Hz/s]**	T_{nadir} **[s]**	T_{reg} **[s]**	f_{reg} **[Hz]**
6	49.5167	0.7866	2.57	5.78	49.9474
10	49.5969	0.6232	2.72	6.11	49.9474
Addition of BESS					
n	**Nadir [Hz]**	**ROCOF [Hz/s]**	T_{nadir} **[s]**	T_{reg} **[s]**	f_{reg} **[Hz]**
2	49.6288	0.946	1.85	9.07	49.9487
3	49.6437	0.9459	1.85	9.02	49.9487
4	49.4863	0.8503	2.63	5.9	49.9474
5	49.7144	1.0659	1.11	9.8	49.9499
6	49.7413	0.8502	1.23	9.73	49.9499
7	49.7638	0.8501	1.26	9.66	49.9499
8	49.5558	0.7071	2.68	6.02	49.9474
9	49.792	1.0659	0.72	9.97	49.9522

Figure 5.7 contains the values of frequency nadir and ROCOF with respect to the different shares of reduced inertia, starting from the situation without adding BESS (n = 1) and the other cases listed in Table 5.5. The addition of BESS significantly improves the performance of the system, obtaining results near and beyond the initial situation (represented by the dashed line).

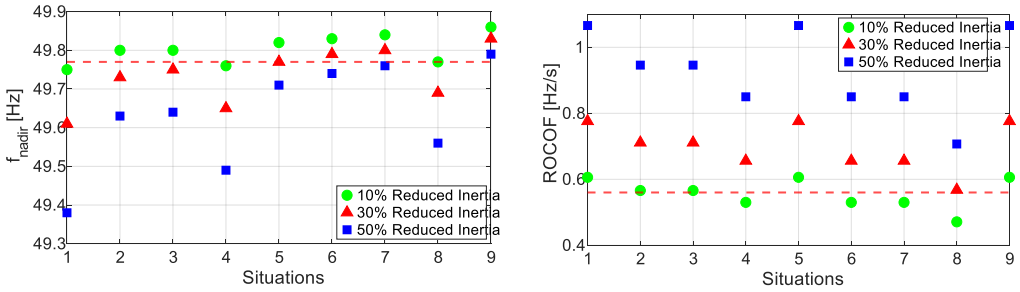

Figure 5.7: Comparisons of the impacts of the under-frequency reference incident for the scenarios and the initial situation, considering the 9 different situations listed in Table 5.5. The dashed line is the initial situation [175].

5.1.1.2 Over-frequency reference incident

Only the most critical 50% reduced inertia scenario is reported for the over-frequency reference incident. The results for the different scenarios are reported in Table 5.7. Similar considerations to the under-frequency case can be made. The highest improvement in the frequency zenith is 1.61% for the case n = 9, whereas the improvement in the ROCOF is 41.51%, with 10 SyCs added.

Table 5.7. Results of the over-frequency scenario with 50% reduced inertia [175]

Starting situation					
n	**Zenith [Hz]**	**ROCOF [Hz/s]**	**T_{zenith} [s]**	**T_{reg} [s]**	**f_{reg} [Hz]**
1	51.1025	1.0913	3.85	12.46	50.0523
Addition of Synchronous Compensators					
n	**Zenith [Hz]**	**ROCOF [Hz/s]**	**T_{zenith} [s]**	**T_{reg} [s]**	**f_{reg} [Hz]**
6	50.8575	0.8055	4.01	12.93	50.0523
10	50.7074	0.6383	4.12	9.34	50.0523
Addition of BESS					
n	**Zenith [Hz]**	**ROCOF [Hz/s]**	**T_{zenith} [s]**	**T_{reg} [s]**	**f_{reg} [Hz]**
2	50.6777	0.9685	2.99	6.89	50.0510
3	50.6653	0.9685	3.00	6.94	50.0510
4	50.9146	0.8706	3.97	9.09	50.0523
5	50.4888	1.0913	2.1	9.8	50.0499
6	50.4185	0.8706	2.15	9.63	50.0499
7	50.3945	0.8705	2.16	9.46	50.0499
8	50.7852	0.7242	4.06	9.25	50.0523
9	50.2784	1.0912	0.81	10.43	50.0476

However, when protection schemes are activated, the wind shedding mitigate the frequency zenith from 51.10 Hz to 50.67 Hz, as shown in Figure 5.8. Wind shedding helps to support frequency stability, but the TSO must pay for the wind power curtailment (197.1 MW of curtailment in this simulation).

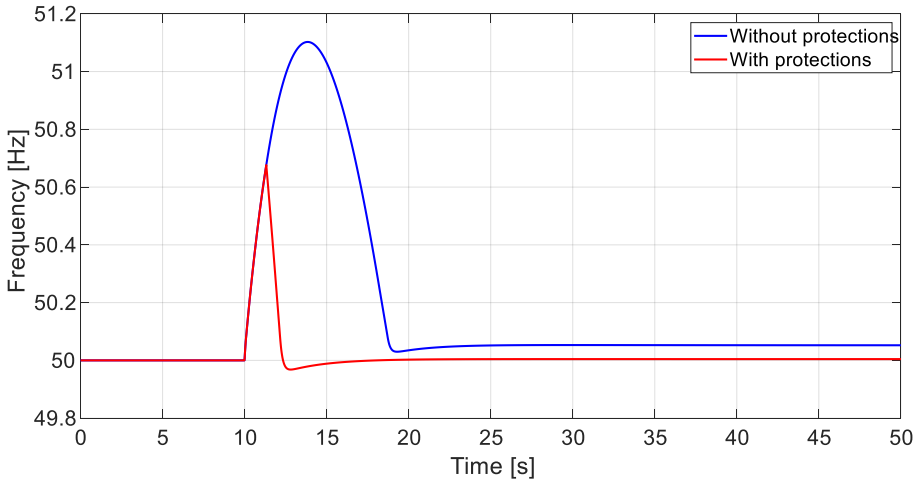

Figure 5.8: Comparisons of the impacts of the worst-case over-frequency contingency for 50% reduced inertia scenario with and without the implementation of actual protection schemes [175].

5.1.1.3 Equivalent Saturation Logic benefits

It is common to use different values for the BESS's parameters H_{BESS} and E_{BESS} depending on the control logic. For example, in [237] H_{BESS} varies in the range 0.01 to 500. Some simulations have been performed starting from case #6 over-frequency event scenario to easily compare the ESL with other settings. In particular, the parameters have been changed using ten times lower and higher values. Figure 5.9 reports the inertial and primary shares of the BESS delivered power in the ESL case (1, 2), lower (3, 4) and higher (5, 6) values cases.

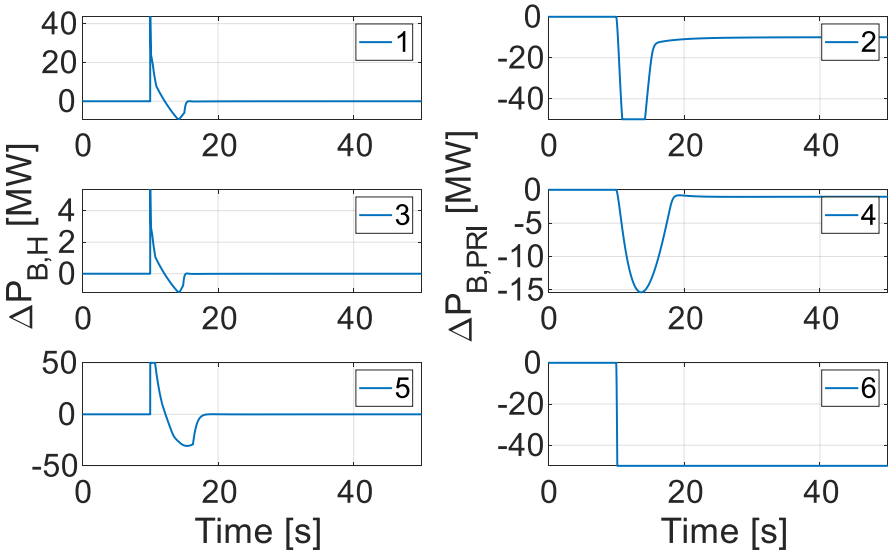

Figure 5.9: Comparisons of the inertial and primary BESS delivered power with the ESL case (1, 2), with lower parameter values (3, 4) and with higher parameter values (5, 6) [175].

With lower values, the BESS support is not exploited enough, whereas with higher values the saturation of the BESS is reached with possible concerns for the BESS stress, degradation, and grid stability (especially in the case of ROCOF saturation, when inertia contribution goes to zero). It is evident that the ESL shows the best compromise in terms of BESS saturation and performance.

5.1.1.4 HVDC support to frequency control

Future scenarios of the Sardinian power system are used to investigate and evaluate the HVDC support on the frequency stability. The tests are made considering the future Tyrrhenian link.

The examined scenarios are the Sustainable Transition (ST) and the Distributed Generation (DG) referred to 2030-year horizon and based on the ENTSO-E data. Both scenarios are evaluated in terms of hourly market dispatch during the year with and without the Tyrrhenian link and compared with the situation in 2017. Four different scenarios are analyzed: 2030 DG in absence of the Tyrrhenian link; 2030 DG TRI in presence of the Tyrrhenian link; 2030 ST in absence of the Tyrrhenian link; 2030 ST TRI in presence of the Tyrrhenian link.

The main characteristics of these scenarios in terms of energy produced by typology of power plant and load absorbed are reported in Table 5.8 and compared to the 2017 [238].

Table 5.8: Energy balance in 2017 and future scenarios.

Scenario	Thermal [GWh]	Hydro [GWh]	RES [GWh]	Load [GWh]
2017	9480,5	323,6	2638,8	9096,5
2030 DG	1159,7	608,1	6096,3	9780,3
2030 DG - TRI	672,9	607,3	6096,3	9780,3
2030 ST	193,9	391,4	5351,2	9409,5
2030 ST - TRI	0	391,4	5351,2	9409,5

The future scenarios for 2030 foresee high de-carbonization, with the reduction of the energy produced by thermal plants even totally in the scenario ST2030.

For each scenario, a use case represents one hour of the year. All the use cases of the investigated scenarios are shown in Figures Figure 5.10, Figure 5.11, Figure 5.12 classified by the share of PEIG and conventional generation.

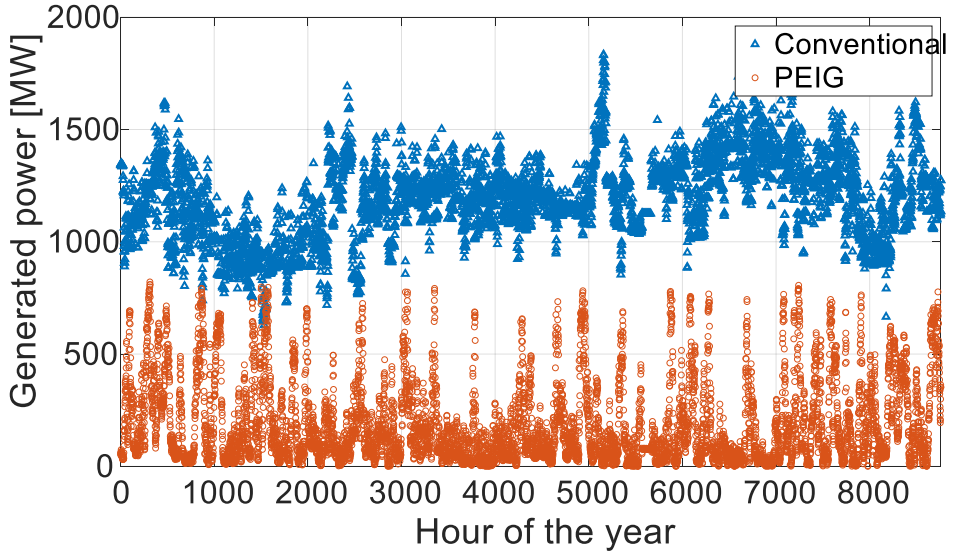

Figure 5.10: Conventional and PEIG generation in each use case – 2017 [239].

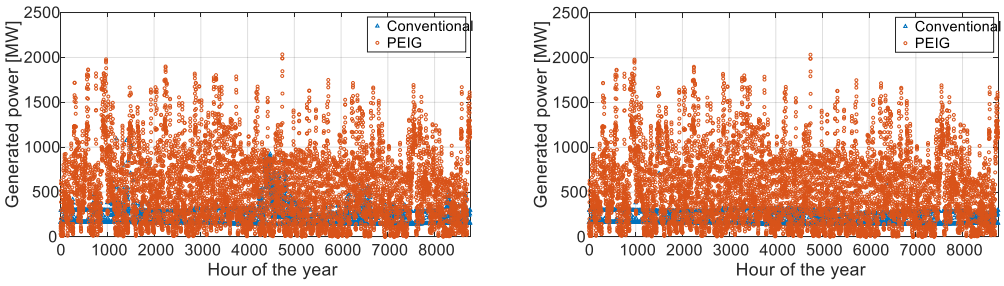

a. b.

Figure 5.11: Conventional and PEIG in each use case, 2030 ST, a) with the new HVDC, b) without the new HVDC [239].

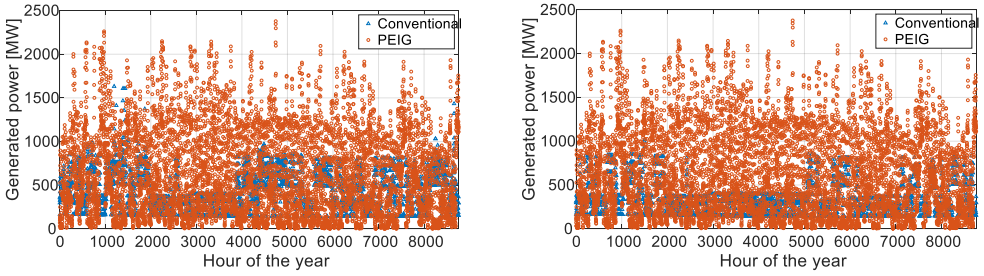

a. b.

Figure 5.12: Conventional and PEIG in each use case, 2030 DG, a) with the new HVDC, b) without the new HVDC [239].

In the 2017, the conventional generation is higher and the PEIG generation lower compared to the 2030. The planned Tyrrhenian link allows a smaller number of dispatched conventional units, as evident between the 2030 simulated scenarios with and without the new HVDC.

Figure 5.13 indicates the trend of the system kinetic energy and FCR during the explored scenarios. The maximum kinetic energy in 2017 was around 13 GWs, while the minimum around 6 GWs. In 2030 the maximum values drop from 10 GWs in 2030 DG to 6.4 GWs in 2030 ST TRI, while the minimum values drop around 3 GWs in all 2030 scenarios.

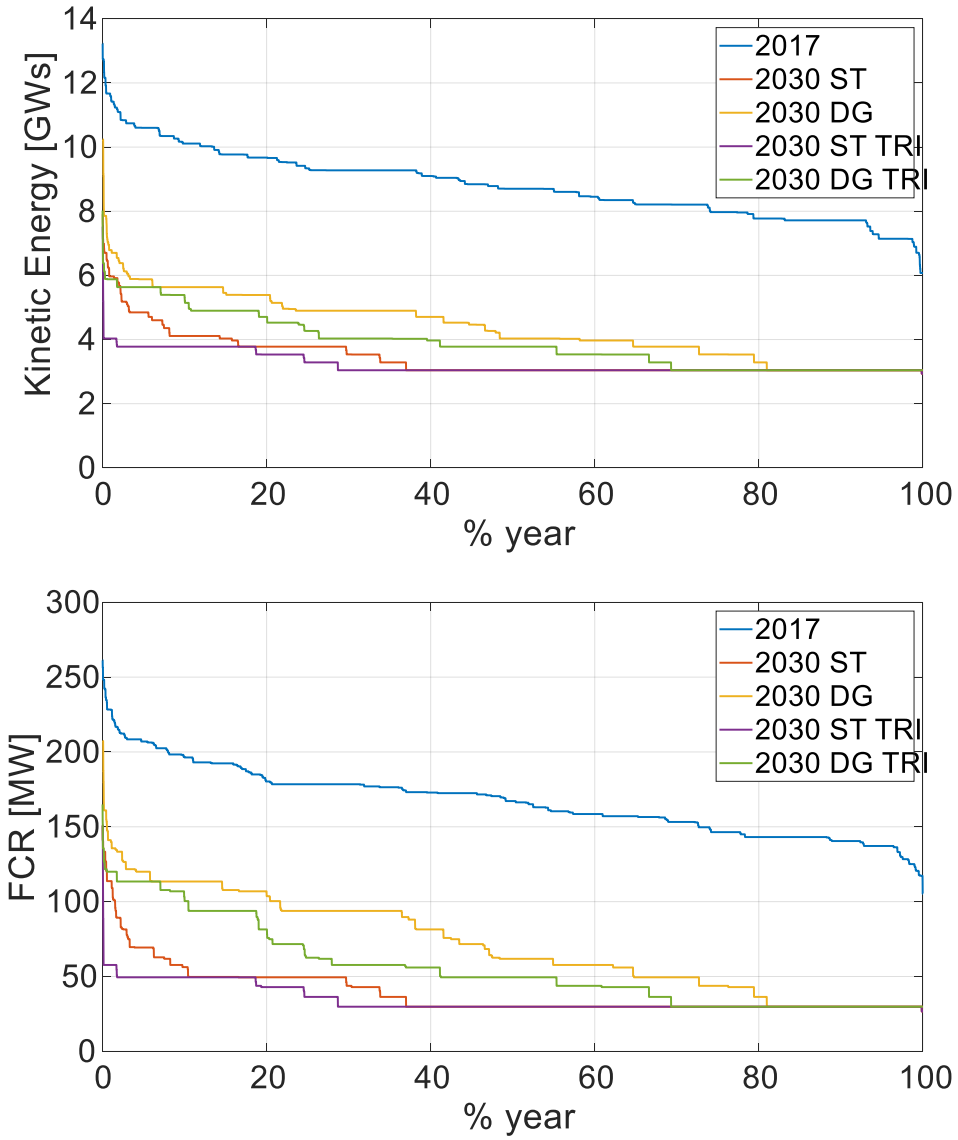

Figure 5.13: Kinetic energy and FCR duration curves – 2017, DG2030, ST2030 (with and without the new HVDC) [239].

The under-frequency reference incident changes in each use case according to the different dispatch. It is then simulated to assess the frequency stability. When the SAPEI and Tyrrhenian link are operated in bipolar mode, the worst contingency is the failure of one pole, while the other one can still regulate.

As the technology that will be used for the Tyrrhenian link is not still known, it was decided to consider both technologies, LCC or VSC, and for VSC the case with inertia emulation control.

In the future scenarios, with the forecasted coal phase-out, only few conventional generators are dispatched in the system and the situation is worse for the frequency performance. The Tyrrhenian link can enhance the frequency performance, as the system experiences improved levels of frequency nadir and ROCOF. The improvements in frequency nadir and ROCOF are evaluated comparing the correspondent use cases with and without Tyrrhenian link and plotted as duration curves in Figure 5.14. In the 2030 ST, improvements in frequency nadir are seen for the 84% of the use cases, whereas for the 61% in the 2030 DG. However, it is noticeable that in some use cases the situation can worse due to the different dispatch that impact the worst-case contingency. Furthermore, the addition of a new link would increase the dimensions of the contingency set in the system, both in terms of the addition of new contingencies or the increase of the possible imbalance, depending on the different power dispatched or transmitted by the links.

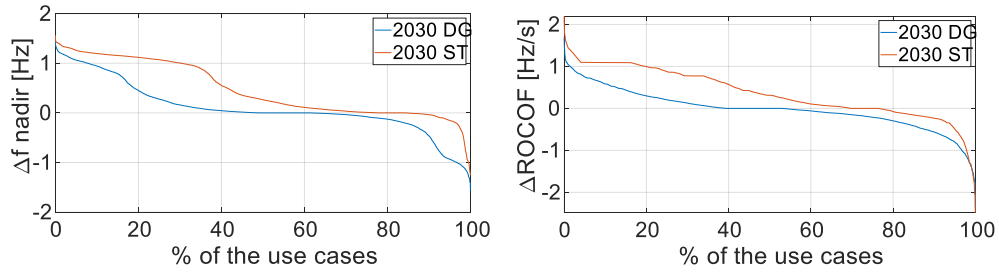

Figure 5.14: Duration curve of the improvements in frequency nadir and ROCOF with and without the Tyrrhenian link for the considered use case – worst-case under-frequency contingency – ST2030, DG2030 [239].

The inertial support is simulated in the case of a possible VSC-HVDC technology. A value of $H_{VSC} = 3\ s$ is considered for the calculations, based on the considerations in Section 4.6. The improvements in frequency nadir and ROCOF during the operation of the multi-terminal can be seen in Figure 5.15. The ROCOF improves almost in all use cases, as the inertial support acts on the initial derivative of the frequency. Differently, the improvements are lower for the frequency nadir.

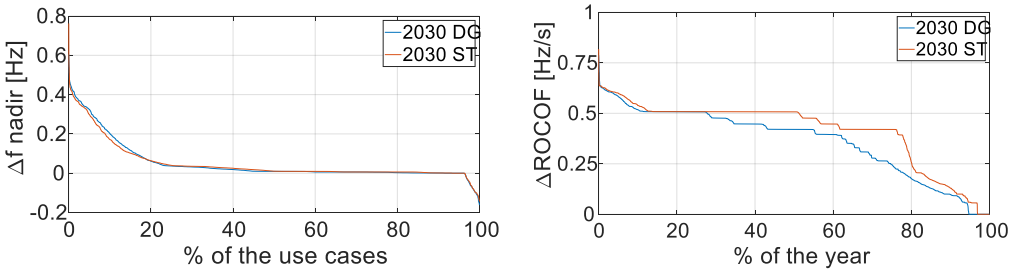

Figure 5.15: Duration curve of the improvements in nadir and ROCOF with the MTDC emulating inertia (the use cases considered are only the one with the MTDC online).

Table 5.9 illustrates the average nadir and ROCOF improvements in the scenarios and the percentage of the cases in which the situation is improved.

Table 5.9: Average improvements and percentage of use cases with improved situation.

	Scenario	Average Nadir [Hz]	% use cases	Average ROCOF [Hz/s]	% use cases
No inertial	DG2030	0.10	61%	0.02	53%
	ST2030	0.47	84%	0.37	76%
Inertial	DG2030	0.05	49%	0.36	95%
	ST2030	0.05	78%	0.42	97%

5.1.2 Normal operation assessment

The frequency and demand data used to investigate the normal operation comes from the Italian TSO. The time step of the data is 15 minutes for generation and demand, and 1 second for frequency data.

A base case scenario is constructed to reproduce a whole day of frequency signal. The signal was recorded on the Sardinian grid on the January 18th, 2018 (winter peak) with average equal to 50.0021 Hz and standard deviation equal to 0.0067 Hz. The inertia and frequency reserves vary during the day with the actual dispatch of regulating generators, as displayed in Figure 5.16. The Sardinian system presented a kinetic energy with a mean value of 9.6 GWs, ranging from a minimum of 9.3 GWs to a maximum of 10.3 GWs. The number of online synchronous units was changing from 18 to 22. To test the proposed model capabilities, two reconstructions are proposed: 1) simulation with only FCP; 2) simulation with FCP, FRP and RRP.

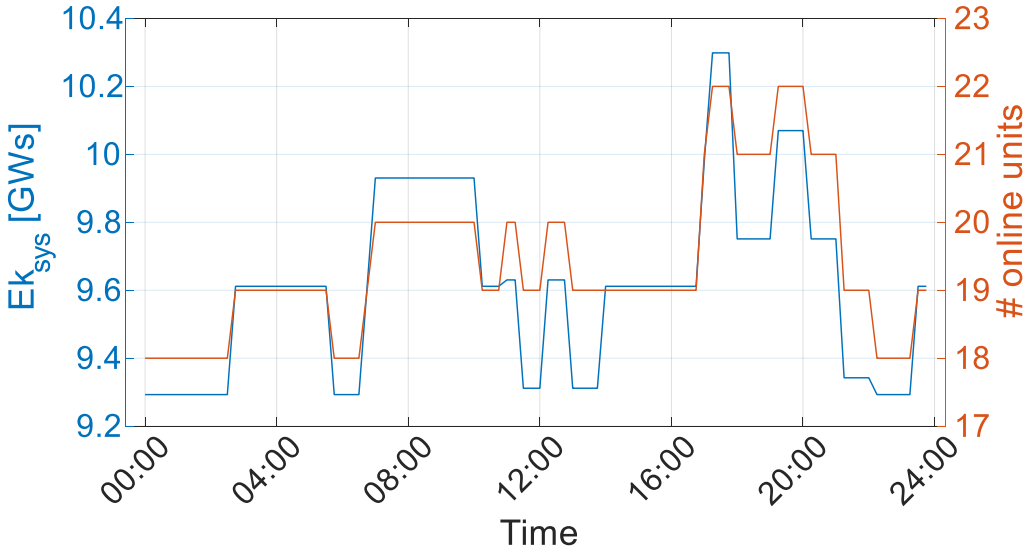

Figure 5.16: Kinetic energy and number of online synchronous units in Sardinia on January 18th, 2018 [69].

In Figure 5.17 the resulting ΔP_{mis} computed by the reverse model in case #1 is shown together with the frequency signal. The power mismatch between generation and consumption is specular to the frequency signal as only the FCP is present to counterbalance the oscillations.

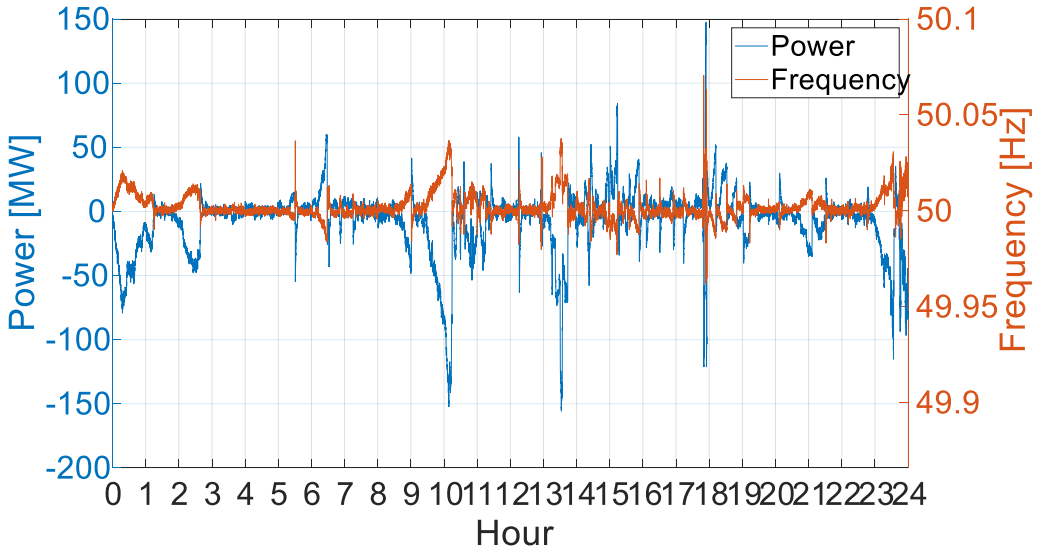

Figure 5.17: Comparison between the frequency signal and the reconstructed power imbalance with only FCP [69].

The ΔP_{mis} is fed into the forward model to calculate the frequency signal. Figure 5.18 reports the histogram of the error between the real and simulated frequency in the case of only FCP. The standard deviation of the error between the simulated and the real frequency is $2.03 \cdot 10^{-4}$ Hz, which is negligible, being much smaller than the typical dead band value of the governors (0.01 Hz). This error is mainly due to the non-linearity present in the models such as dead bands and saturations and it can also be further reduced by decreasing the maximum allowed time step of the simulations.

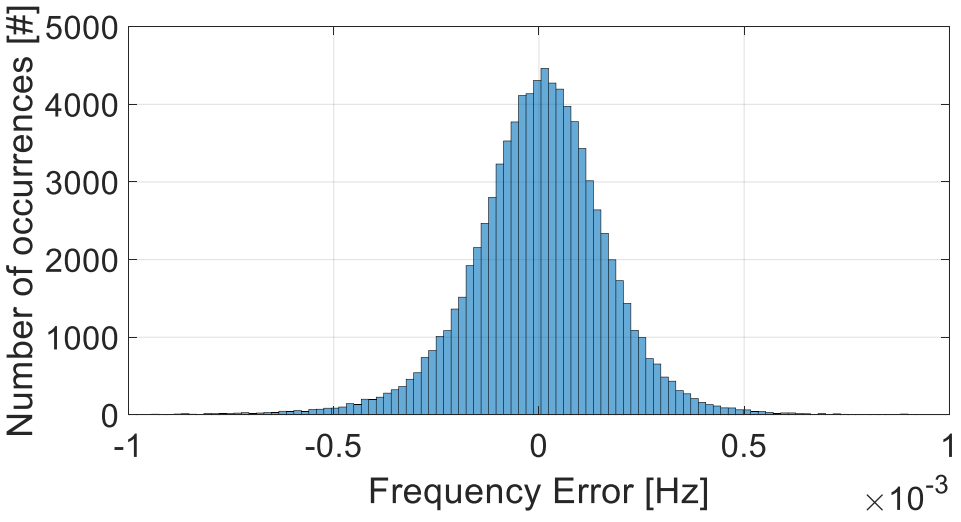

Figure 5.18. Histogram of the error between the real and simulated frequency in the case of only FCP.

In case #2 the results are obtained considering the presence of the FRP and RRP in the CE-based framework with the Sardinia frequency signal. The simulated FRR is 120 MW. This example was made to show the model capabilities, without representing the reality of the Sardinian frequency control. Sardinia island presents different FRP and RRP schemes with respect to the CE ones, in terms of actions and parameters.

The frequency error is similar in magnitude to the previous case with a standard deviation slightly higher than before, equal to $2.4 \cdot 10^{-4}$ Hz. Figure 5.19 contains the three simulated frequency reserves' profiles (FCR, FRR and RR). The ΔP_{TER} is continuously decreasing during the day since the frequency of the examined day is on average around 50.0021 Hz, higher than 50 Hz, and the FRR is therefore continuously decreasing.

It is possible to see the FCR, which is activated when the frequency overcome the dead band, the FRR is activated to bring the frequency value to the nominal value, while the RR is called during the day to restore the FRR.

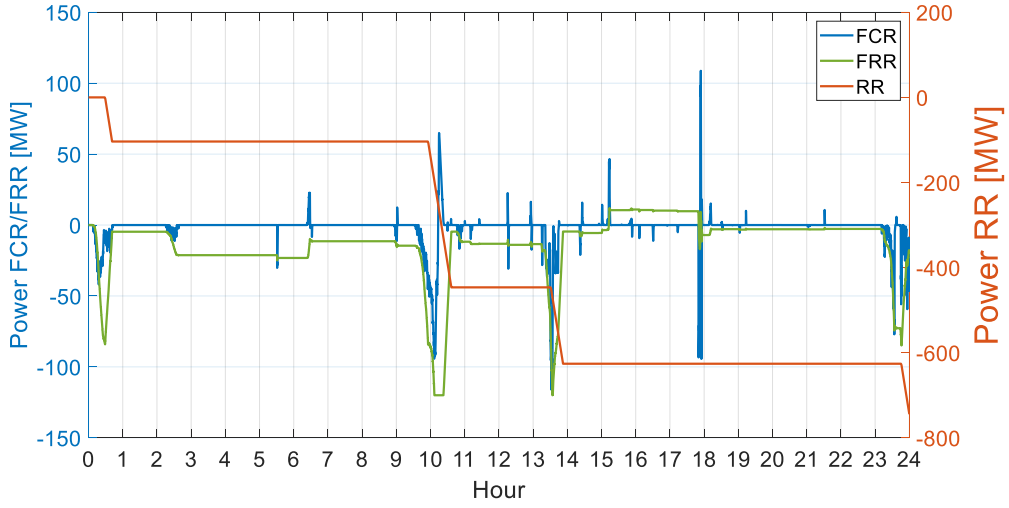

Figure 5.19: FCR, FRR and RR simulated profiles based on the frequency signal of January 18th, 2018.

Case #1 has been considered as the reference case to test the BESS addition. The technical impact of a BESS in fixed droop and with FCP and FRP operation mode is evaluated. The FCR of the BESS is divided in inertial and primary response. The performance of frequency control is assessed using the indicators introduced in Chapter 4: the mean value f_m and the standard deviation σ of the frequency.

5.1.2.1 BESS support to frequency control

A sensitivity analysis is performed on the capacity, droop and the share of inertial and primary response provided by the BESS. Two systems of 50 MW and 250 MW BESSs are analysed, with a pole time constant $T_B = 0.3\ s$. For the 250 MW case, two different droops σ_B of 0.005 and 0.004 are considered. The

frequency response of the BESS is compared using different shares of inertial and primary response, i.e., 50% of inertial and primary control, 100% inertial control and 100% of primary control. Figure 5.20 shows the frequency trend with the addition of a BESS of 250 MW in the FCP and only primary response $\chi_B = 0$, compared with the case without BESSs.

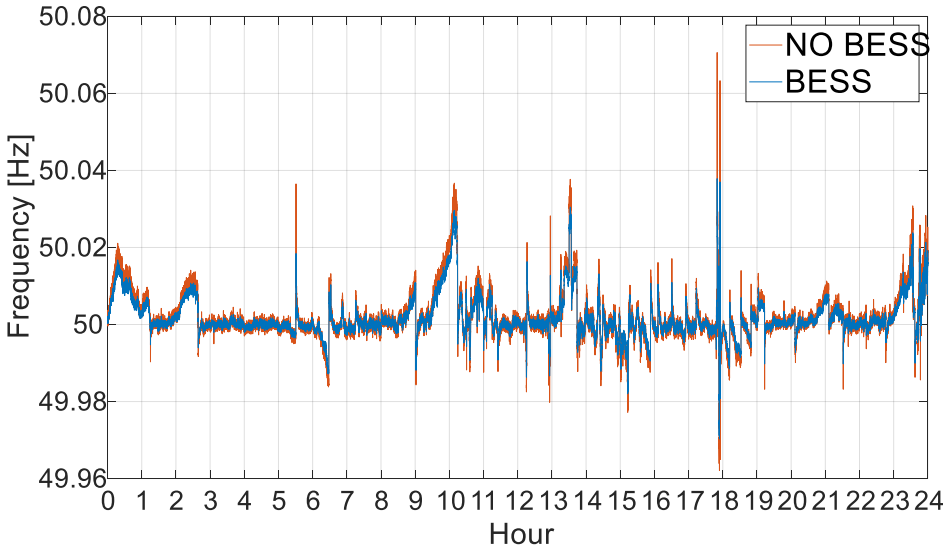

Figure 5.20. Comparison between the frequency signals with and without BESSs participating in the FCP [69].

In the second case, the BESS has been used only for the FRP (Figure 5.21).

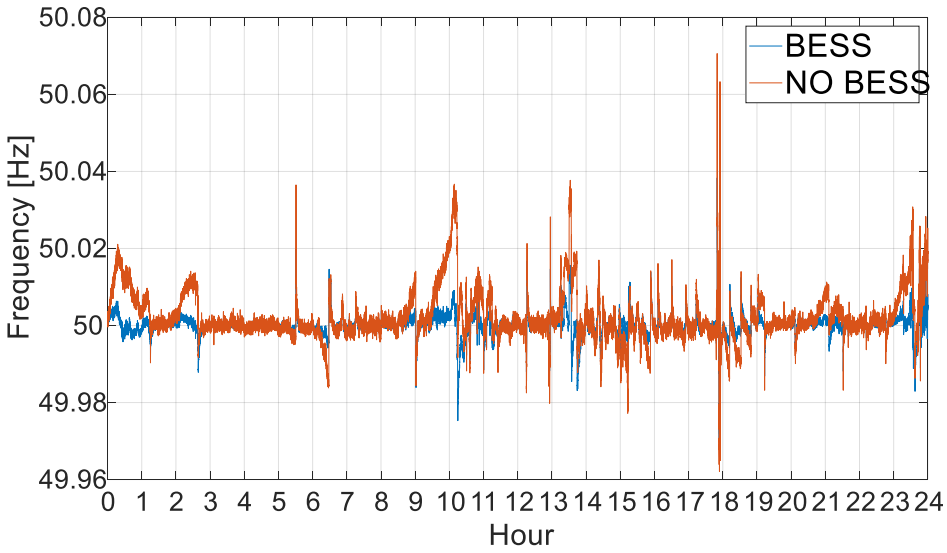

Figure 5.21. Comparison between the frequency signals with and without BESSs with FR control [69].

The impact in the case of normal operation is higher with respect to the FCP due to the integral part in the FRP. In fact, a purely proportional action, as in the FCP, is higher when the frequency deviation is higher. The proportional action is fast and reduce the error, without compensating it. In the FRP the action is proportional to the integral of the frequency deviation and keep memory of the

past deviation errors. It is higher in the case of a frequency signal unbalanced from the set-point, which is the case under examination. Table 5.10 reports the results of the two cases analyzed, with participation of the BESS in the FCP and the FRP.

Table 5.10. Results of the frequency control with participation of the BESS in the FCP and FRP [69].

	f_m [Hz]	sd_f [Hz]	σ_B	χ_B	FRP
Base	50.0021	0.0067	-	-	No
50	50.0020	0.0064	0.005	0	No
50	50.0021	0.0067	0.005	1	No
50	50.0020	0.0065	0.005	0.5	No
50	50.0000	0.0037	0.005	-	Yes
250	50.0017	0.0054	0.005	0	No
250	50.0021	0.0067	0.005	1	No
250	50.0019	0.0059	0.005	0.5	No
250	50.0018	0.0058	0.004	0.5	No
250	50.0016	0.0051	0.004	0	No
250	50.0021	0.0067	0.004	1	No
250	50.0000	0.0029	0.005	-	Yes

The best performance in terms of mean frequency and standard deviation are with the participation in the FRP only, with a mean frequency reported to the nominal value from the initial 50.0021 Hz and a standard deviation improved of 45% in the case of the BESS of 50 MW (from the initial value of 0.0067 to 0.0037) and of 57% in the case of the BESS of 250 MW (from 0.0067 to 0.0029). In the case of participation in the FCP only, the best improvements can be seen in the case with the BESS of 250 MW, lower droop $\sigma_B = 0.004$ and only primary control $\chi_B = 0$, with a mean frequency equal to 50.0016 Hz and a standard deviation improved of 24% (from 0.0067 to 0.0051).

5.1.3 Unit Commitment under inertia constraints

The Sardinian power system is taken as a real case of interest for testing the methodology proposed in Section 4.4 with market simulations including the inertia constraints. For the DG scenario in the 2030 horizon (characterized by the highest shares of new distributed energy sources, 1.7 GW of PV, 1.4 GW of wind, compared to the current 0.8 GW in PV, 1 GW in wind in 2018), the methodology described in Section 4.4 has been applied, obtaining a total of 7 use cases analysed, as listed in Table 5.11. In particular:

- the base case has no inertia constraints implemented;
- the minimum kinetic energy constraint is calculated using an admissible *ROCOF* of 2 Hz/s and an imbalance of 500 MW (the size of the possible reference incident in Sardinia);
- the minimum available synchronous capacity is calculated using the fractions ψ = [0.1, 0.3, 0.5];
- the maximum level of *SNSP* is determined with ξ_{max} = [0.5, 0.65, 0.75].

Table 5.11: Alternatives analysed with values to evaluate the constraints [208]

Alternative number	Alternative	Feature	Value
1	Base	No constraints	
2	C1 – Min E_k	Imbalance	500
3	C2 – Min Cap	ψ	0.1
4		ψ	0.3
5		ψ	0.5
6	C3 – *SNSP*	*SNSP*	0.5
7		*SNSP*	0.65
8		*SNSP*	0.75

5.1.3.1 Technical-economic results and MCDA

The market simulations provide the different dispatching results when different constraints are set up, and the hourly kinetic energy is computed. The kinetic energy is assessed considering the number of online synchronous generation units, dispatched each hour of the year by market results. The trend of kinetic energy for the alternatives in Table 5.11 are reported in Figure 5.22, as duration curves expressed in percentage of the year. The highest values of kinetic energy are in the alternative #5, where this constraint gives the high number of online synchronous generating units.

The hourly market results are used to feed the aggregated dynamic model described in Chapter 4 to evaluate the frequency performance indicators. Dynamic simulations are performed for each hour of the year, selecting the worst-case under-frequency contingency as reference incident (it can be either the largest thermal power plant or the HVDC connection, depending on the operating conditions). The cost-based performance indicators are obtained directly from the market simulator. The values of *ROCOF* and frequency nadir are statistically analysed, to find the performance indicators $ROCOF_{95\%}$ and $f_{nadir95\%}$, occurring in the 95% of the cases with violations, as input for the MCDA, jointly with the economic parameters.

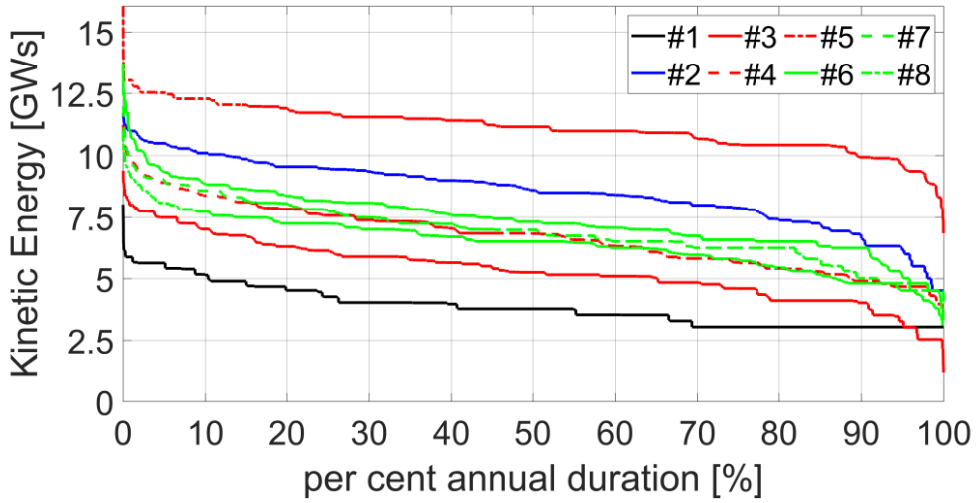

Figure 5.22: Kinetic energy duration curves for the analysed alternatives [208].

The empirical cumulative distribution functions of the violations and the values taken for 95% probability are depicted in Figure 5.23, for the alternative #2. *ROCOF* and $f_0 - f_{nadir}$ violations observed at least in 95% of the cases are considered as suitable estimates for the MCDA. Table 5.12 shows the values of each criterion for each alternative. Overall, taking the alternatives as solution points, all the indicated points correspond to non-dominated solutions and belong to the Pareto front, as any solution of this set represents a balance between objectives.

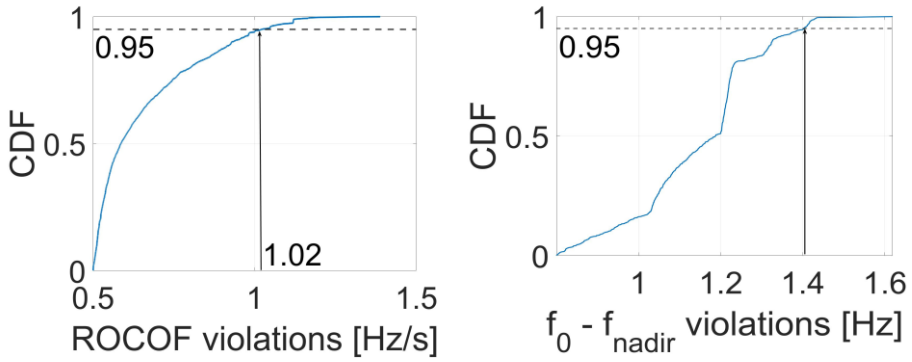

Figure 5.23: Empirical cumulative distribution functions for the *ROCOF* and $f_0 - f_{nadir}$ violations and values observed at least in 95% of the cases [208].

Table 5.12: Values of each criterion for each alternative.

Alternative number	$ROCOF_{95\%}$	$\Delta f_{nadir95\%}$	χ_{SEW}	χ_{CO_2}	χ_{fuel}
1	1.948	1.429	1.000	1.000	1.000
2	1.020	1.403	1.277	6.530	12.643
3	1.371	1.432	1.137	2.682	5.737
4	1.067	1.325	1.218	6.843	8.811
5	0.808	1.221	1.454	11.987	20.913
6	1.023	1.357	1.306	4.054	13.371
7	1.003	1.391	1.281	3.124	12.699
8	1.159	1.407	1.250	2.633	9.885

It can be observed that the five criteria correspond to conflicting objectives, as having good frequency performance implies high inertia and a high number of dispatched synchronous generators, and consequently higher costs for the system. After obtaining the Pareto front of the problem, the decision maker is interested in selecting the best compromise solution. To decide which solution could be more effective, the TOPSIS method has been applied by using the following entries: $\lambda_1 = \lambda_2 = \frac{1}{2}$, $\lambda_3 = \lambda_4 = \lambda_5 = \frac{1}{3}$, and $\alpha = 0.5$. The normalized decision matrix **N** is shown in Table 5.13.

Table 5.13: Normalized decision matrix.

Alternative number	$ROCOF_{95\%}$	$\Delta f_{nadir95\%}$	χ_{SEW}	χ_{CO_2}	χ_{fuel}
1	0.5647	0.3682	0.2836	0.0604	0.0295
2	0.2958	0.3615	0.3622	0.3942	0.3734
3	0.3973	0.3689	0.3226	0.1619	0.1694
4	0.3093	0.3415	0.3455	0.4130	0.2602
5	0.2340	0.3146	0.4123	0.7235	0.6176
6	0.2964	0.3496	0.3704	0.2447	0.3949
7	0.2908	0.3584	0.3633	0.1886	0.3750
8	0.3361	0.3625	0.3546	0.1589	0.2919

The best compromise solution is given in Table 5.14, with the complete ranking of all options.

Table 5.14: Closeness coefficients and ranking of all the alternatives.

Alternative number	1	2	3	4	5	6	7	8
c_m	0.91	0.48	0.81	0.51	0.09	0.61	0.66	0.74
Rank	1st	7th	2nd	6th	8th	5th	4th	3rd

The higher variation in cost savings compared with the changes in the frequency performance criteria leads the best solution to the alternative #1 (base case), with a value of $c_m = 0.91$. The base case is the solution currently planned by the Italian TSO. It is important to observe that in the analysed scenario at 2030 horizon, the base case presents already some synchronous generators online (for around 2000 hours out of the year) even without frequency constraints, and this analysis demonstrates that they are enough to guarantee the frequency stability in a technical economic view. The base case is directly followed by the alternatives #3 and #8, with c_m respectively equal to 0.81 and 0.74. It is noticeable that the alternatives #3 and #8 correspond to lower values of thermal generation dispatched. Nevertheless, giving more relevance to the frequency stability criterion, the best solution moves away from the base case, as shown in the next paragraph.

5.1.3.2 Parametric analysis with different importance given to the performance criteria

To highlight the importance of the decision maker's weighting factors λ_z in the MCDA, as their variation can change the best solution, a sensitivity analysis has been implemented with α varying between 0 and 1 with step 0.01.

Figure 5.24a shows the best alternative selected for each value of α. It is evident that the cost-based performance criteria are dominant until α = 0.73, after which the best alternatives are respectively alternative #3, #8, #7 and #5. This means that in the analysed scenario in 2030, the system is planned in a secure way even without frequency constraints, as only high values of α can outline the importance of the frequency stability performance criteria over the costs. If the base case is removed (Figure 5.24b), e.g., in the case in which the regulator asks

only for inertia constrained alternatives, the best compromise solution is the alternative #3, which corresponds to the lower costs for the system, until α=0.78, after which different alternatives become the best compromise solutions. On these bases, the proposed methodology will be very important and necessary to understand frequency stability in future scenarios at 2050 (which are currently not available, as the long-term development plan covers 10 years) where it is foreseen the complete phase out of coal plants.

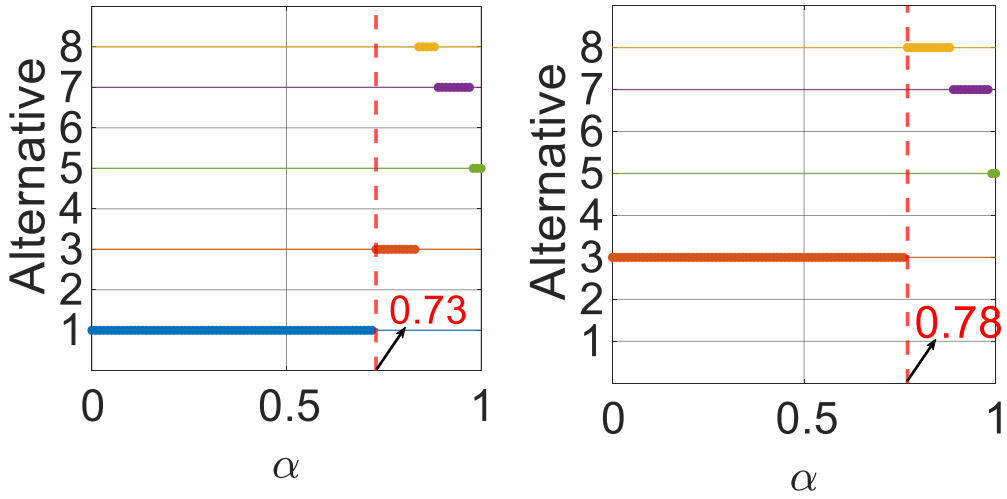

a. with all alternatives

b. without the base case

Figure 5.24: Best alternative for each value for α varying in [0,1] with step 0.01 [208].

5.2 The Italian Case Study

Two different analysis are performed using the Italian power system as a case study. In the first study, the frequency stability of the Italian power system separated by the CE is assessed in the scenarios DG 2030 and ST 2030 coming from the TYNDP 2018 of ENTSO-E, while in the second study the inertia distribution of the Italian power system is evaluated using the scenarios BAU, DEC and PNIEC coming from the Terna's National Development Plan 2020. A first assessment of the distributional impact of inertia is investigated using DIgSILENT PowerFactory on a dynamic model of the Italian power system in 2017.

5.2.1 Reference incident assessment

The installed and dispatched kinetic energy of the Italian power system is evaluated for the TYNDP 2018 scenarios coming from ENTSO-E. In Table 5.15, the values of capacity, loading factor and inertia constant of the base unit is reported, together with the total installed capacity and kinetic energy installed per type and per the scenarios BE 2025, DG 2030, ST 2030, DG 2040, and ST 2040.

Table 5.15: Values of capacity, loading factor and inertia constant of the base unit, total installed capacity, and kinetic energy per type and per scenario.

					SCENARIO									
		BASE UNIT			BE 2025		DG 2030		ST 2030		DG 2040		ST 2040	
Type		Capacity [MW]	Loading factor	Inertia [s]	Total installed capacity [GW]	Total installed E_k [GWs]	Total installed capacity [GW]	Total installed E_k [GWs]	Total installed capacity [GW]	Total installed E_k [GWs]	Total installed capacity [GW]	Total installed E_k [GWs]	Total installed capacity [GW]	Total installed E_k [GWs]
Conventional	Gas	168	0,95	4,46	34	162	33	154	33	154	31	144	31	145
	Coal	361	0,95	4,21	5	24	2	9	4	20	2	12	2	9
	Oil	763	0,95	4,37	0	3	0	3	0	3	0	0	0	3
	Other non-RES	104	0,95	3,7	6	23	5	20	5	20	5	20	5	20
	Total				46	212	40	186	42	197	38	176	38	177
Conventional RES	Hydro Pump	454	0,95	3,24	6	19	6	19	6	19	6	19	6	19
	Hydro RoR	59	0,95	2,7	5	16	6	16	6	16	6	16	6	16
	Hydro Turbine	383	0,95	3,93	16	68	16	68	16	68	16	68	16	68
	Other RES	68	0,95	3,7	5	20	5	20	5	20	5	20	5	20
	Total				32	123	32	123	32	123	32	123	32	123
	Total Conventional				78	335	72	309	75	320	70	299	70	300
Non-conventional RES	Solar Thermal	1	1,00	0,00	0	0	0	0	0	0	0	0	0	0
	Solar PV	1	1,00	0,00	22	0	45	0	24	0	114	0	55	0
	On-shore wind	1	1,00	0,00	12	0	14	0	14	0	16	0	16	0
	Off-shore wind	1	1,00	0,00	0	0	1	0	1	0	1	0	1	0
	Total				35	0	60	0	39	0	132	0	73	0
	Total				113	335	132	309	114	320	202	299	144	300
	% conventional				69%		55%		66%		35%		45%	
	% installed E_k compared to 2025					0%		-8%		-5%		-11%		-10%

The generation is divided between conventional non-RES, conventional RES, due mainly to hydro, and non-conventional PEIG (mainly wind and PV). Besides, the total value of generation with inertia is reported for each scenario compared to the inertia of BE 2025 scenario. It is evident the inertia reduction from 335 GWs in 2025 to 300 GWs in 2040.

A first analysis on the PEIG impact on the frequency stability was conducted considering the case of the Italian power system in a hypothetically permanent regime separated from CE. In this hypothesis, the frequency stability relies only on the Italian kinetic energy. The national reference incident is set to 800 MW (largest CCGT plant trip) and a warning threshold of 0.5 Hz/s for ROCOF.

The kinetic energy and FCR duration curve for the analysed scenarios are given in Figure 5.25. The ST 2030 scenario present a more conservative nature of compared to the DG 2030 scenario, with higher values of kinetic energy during the hours of the year. The maximum kinetic energy is 237 GWs and 232 GWs in DG 2030 and ST 2030 scenarios respectively, while the minimum is 39 GWs and 38 GWs. This minimum value would be compatible to keep the ROCOF below 0.5 Hz/s, also considering the effect of the governors which is not included in the previous calculation of minimum kinetic energy. The FCR values oscillate between 140 and 730 MW for most of the year. The maximum FCR is 734 MW and 725 MW in DG 2030 and ST 2030 scenarios respectively, while the minimum is 148 MW and 143 MW.

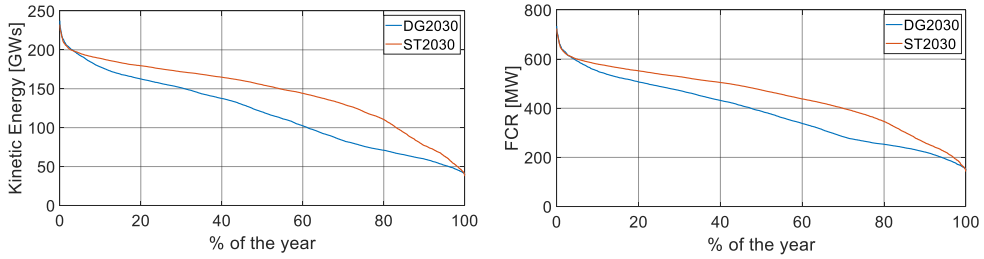

Figure 5.25. Kinetic energy and FCR duration curves for Italy in scenarios DG 2030 and ST 2030.

The aggregate model with only FCR and without protection schemes is used to simulate the reference incident in each hour of the year. The frequency performance parameters are reported as duration curves in Figure 5.26.

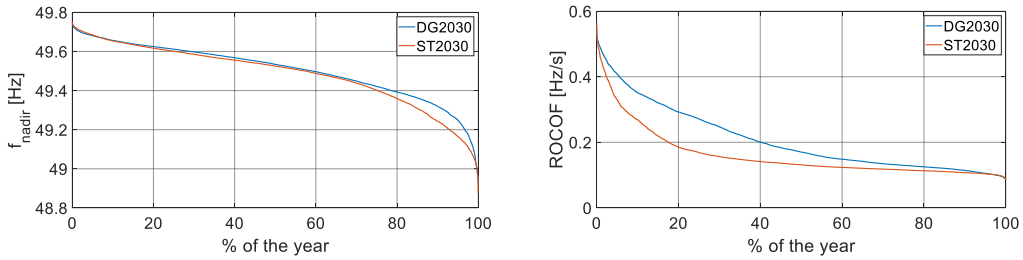

Figure 5.26. Frequency nadir and ROCOF duration curves for Italy in scenarios DG 2030 and ST 2030.

The worst frequency performance indicators are 48.94 Hz (at hour 5359) and 0.55 Hz/s (at hour 2370) for DG 2030 scenario and 48.88 Hz (at hour 2334) and 0.56 Hz/s (at hour 2334) for ST 2030 scenario. The frequency nadir values would have caused load shedding. However, these results should be reflected only for the remote possibility of isolated operation for the Italian system. These studies do not consider transient and voltage stability or the dynamic problems that may occur at the local level.

In recent years, Terna is installing SyCs in some areas of the national system to improve the stability of the system. To have an idea of the contribution in kinetic energy, considering the standard size of synchronous compensators (250 MVA) and their typical constant of inertia (around 2 s), a compensator provides a kinetic energy of 500 MWs. Therefore, in the case of the ST2030 scenario under examination, for example, to reach the minimum value of 40 GWs, 2000 MWs

would be required, which could be supplied by at least 4 synchronous compensators in parallel. The compensators that Terna currently plans to adopt can have inertia constants up to 7 s and therefore 2 synchronous compensators are sufficient.

5.2.2 PEIG distribution

The largest share of installed kinetic energy is in the regions with the largest conventional generators, and therefore in the North, Lazio, and Puglia. While the distribution of PV is quite homogeneous throughout the country, the distribution of wind power is prevalent in the South, with little installed power in the North.

Among the various scenarios by 2030, the lowest values of non-conventional generation are seen in the BAU scenario, with a total of 43.6 GW installed, compared to the 67.5 GW of the PNIEC and 68.2 GW of the DEC. While PV growth is homogeneous across the country, wind continues to grow mainly in the South, going from about 9 GW installed in 2018 to just over 17 GW for the DEC scenario. Table 5.16 represents the generation park, with reference to the installed power and the available inertia, by region and market area with reference to 2018 and to the 2030 scenarios.

Table 5.16. Installed capacity by type of conventional and non-conventional plant and installed inertia by region and market area of the national system - 2018, 2030

Zone di mercato	Regioni	Idro [GW]				Termo [GW]				FV [GW]				Eolico [GW]				Inerzia installata [GWs]	
		2018	PNIEC	BAU	DEC	2018	PNIEC	BAU	DEC	2018	PNIEC	BAU	DEC	2018	PNIEC	BAU	DEC	2018	2030
NORD	PIEMONTE	3,8	3,8	3,8	3,8	4,9	4,6	4,7	4,7	1,6	4,2	2,3	4,2	0,0	0,0	0,1	0,0	44,3	41,3
	VALLE D'AOSTA	1,0	1,0	1,0	1,0	0,0	0,0	0,0	0,0	0,0	0,1	0,0	0,1	0,0	0,0	0,0	0,0	3,9	3,9
	LOMBARDIA	6,2	6,2	6,2	6,2	11,5	11,1	10,9	11,2	2,4	6,1	3,2	6,0	0,0	0,0	0,0	0,0	86,6	69,7
	TRENTINO ALTO ADIGE	3,4	3,4	3,4	3,4	0,3	0,3	0,3	0,3	0,4	1,2	0,6	1,1	0,0	0,0	0,0	0,0	14,7	14,2
	VENETO	1,2	1,2	1,2	1,2	3,3	3,1	2,4	2,4	2,0	5,0	2,7	5,0	0,0	0,0	0,0	0,0	17,4	13,8
	FRIULI VENEZIA GIULIA	0,5	0,5	0,5	0,5	1,7	1,5	1,2	1,2	0,5	1,5	0,7	1,4	0,0	0,0	0,0	0,0	13,2	8,9
	LIGURIA	0,1	0,1	0,1	0,1	1,5	1,5	1,5	1,5	0,1	0,3	0,2	0,3	0,1	0,0	0,1	0,0	14,8	8,1
	EMILIA ROMAGNA	0,7	0,7	0,7	0,7	6,5	5,9	6,0	6,0	2,1	5,3	2,9	5,3	0,0	0,0	0,1	0,0	37,9	32,3
	TOTALE	*16,9*	*16,9*	*16,9*	*16,9*	*29,7*	*28,0*	*27,1*	*27,2*	*9,1*	*23,7*	*12,6*	*23,3*	*0,1*	*0,1*	*0,3*	*0,1*	*232,8*	*192,2*
CENTRO NORD	TOSCANA	0,4	0,4	0,4	0,4	3,2	3,0	2,8	2,8	0,8	2,2	1,2	2,1	0,1	0,2	0,2	0,2	18,1	9,0
	MARCHE	0,3	0,3	0,3	0,3	0,6	0,3	0,3	0,3	0,5	1,3	0,7	1,3	0,0	0,0	0,0	0,0	3,8	0,4
	TOTALE	*0,7*	*0,7*	*0,7*	*0,7*	*3,8*	*3,2*	*3,1*	*3,0*	*1,3*	*3,5*	*2,0*	*3,4*	*0,1*	*0,2*	*0,2*	*0,2*	*21,9*	*9,4*
CENTRO SUD	UMBRIA	0,5	0,5	0,5	0,5	0,7	0,9	0,9	0,9	1,1	2,8	1,6	2,8	0,0	0,1	0,0	0,0	2,0	3,8
	LAZIO	0,4	0,4	0,4	0,4	5,9	3,8	4,5	3,0	1,4	3,2	2,1	3,3	0,1	0,1	0,1	0,1	36,2	26,6
	ABRUZZO	1,0	1,0	1,0	1,0	1,5	1,5	1,2	1,2	0,7	1,8	1,2	1,8	0,2	0,5	0,5	0,5	8,2	8,1
	CAMPANIA	1,3	1,3	1,3	1,3	2,4	0,8	0,8	0,8	0,2	0,4	0,3	0,3	0,4	0,6	0,5	0,6	4,8	14,7
	TOTALE	*3,2*	*3,2*	*3,2*	*3,2*	*10,5*	*7,0*	*7,4*	*5,9*	*3,4*	*8,3*	*5,2*	*8,2*	*0,7*	*1,2*	*1,1*	*1,3*	*51,2*	*53,2*
SUD	MOLISE	0,1	0,1	0,1	0,1	1,1	2,1	2,5	3,3	0,8	2,0	1,3	1,9	1,5	2,9	2,7	3,0	15,3	4,8
	PUGLIA	0,0	0,0	0,0	0,0	7,8	5,7	4,3	4,2	2,7	5,1	4,3	5,1	2,5	4,1	3,1	4,3	30,9	29,5
	BASILICATA	0,1	0,1	0,1	0,1	0,2	0,2	0,2	0,2	0,4	0,7	0,6	0,7	1,2	1,8	1,6	2,2	0,5	0,0
	TOTALE	*0,2*	*0,2*	*0,2*	*0,2*	*9,1*	*7,9*	*7,0*	*7,7*	*3,9*	*7,8*	*6,1*	*7,7*	*5,2*	*8,8*	*7,5*	*9,5*	*46,7*	*34,3*
CALABRIA		0,8	0,8	0,8	0,8	3,7	3,6	4,1	4,0	0,5	1,1	0,8	1,0	1,1	1,8	1,3	1,8	24,7	18,7
SICILIA		0,7	0,7	0,7	0,7	5,3	4,4	4,8	5,2	1,4	3,5	2,4	3,5	1,8	3,4	2,1	3,7	20,6	16,6
SARDEGNA		0,5	0,5	0,5	0,5	2,4	0,7	2,1	2,5	0,8	2,2	1,4	2,2	1,0	2,1	1,1	2,2	11,4	8,0
TOTALE		*22,9*	*23,0*	*23,0*	*23,0*	*64,5*	*54,9*	*55,6*	*55,6*	*20,4*	*50,0*	*30,5*	*49,3*	*10,1*	*17,5*	*13,6*	*18,9*	*409,4*	*332,4*

The inertia intensity is calculated per market zone in the winter peak and compared for 2018 and PNIEC 2030 and displayed in Figure 5.27. A reduction in the intensity of inertia is observed in the analysed situation of the winter load peak, with the lowest percentage variation for the North area (30%) and the greatest percentage variation (91%) compared to 2018 for the Sardinia area, with an index that goes from 3.7 to 0.3. This is due both to the decommissioning of coal plants and to the results of the market which favour the dispatching of non-conventional generation.

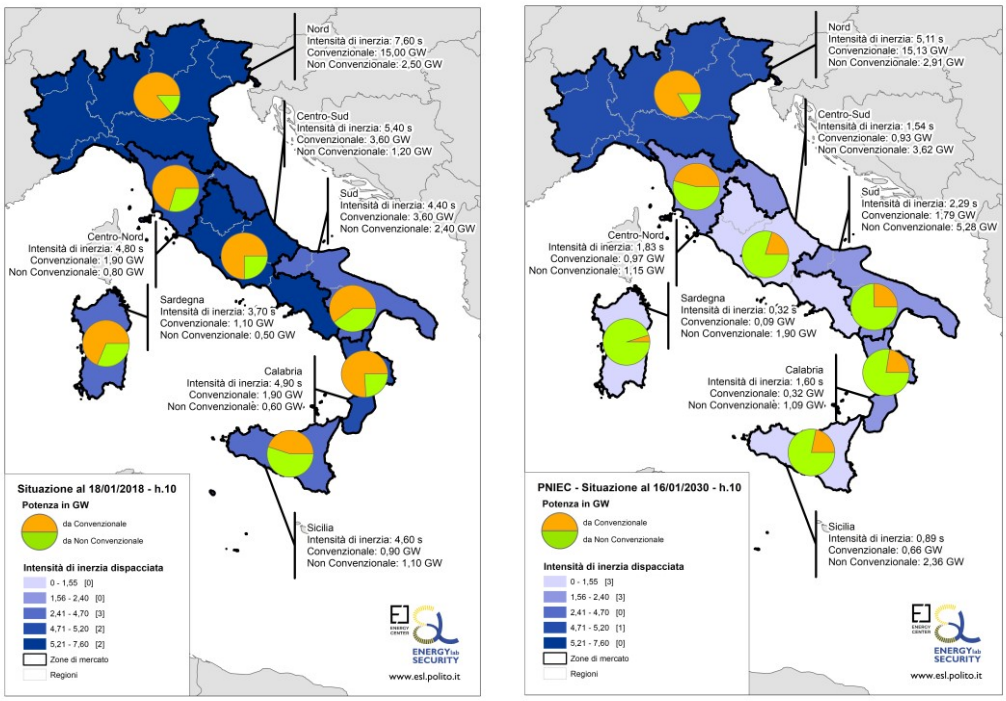

Figure 5.27. Inertia intensity per market zone in 2018 and PNIEC 2030.

Table 5.17 lists the inertia intensity and conventional/non-conventional generation per market zone in 2018 and 2030.

Table 5.17. Inertia intensity, conventional and non-conventional generation for the winter peak in 2018 and PNIEC 2030 by market zone.

	Inertia intensity [s]		Conventional [GW]		Non-Conventional [GW]	
	18/01/18 h10:00	16/01/2030 h10:00	18/01/18 h10:00	16/01/2030 h10:00	18/01/18 h10:00	16/01/2030 h10:00
NORD	7,6	5,1	15	15,1	2,5	2,9
CENTRO NORD	4,8	1,8	1,9	1,0	0,8	1,1
CENTRO SUD	5,4	1,5	3,6	0,9	1,2	3,6
SUD	4,4	2,3	3,6	1,8	2,4	5,3
SICILIA	4,6	0,9	0,9	0,7	1,1	2,4
SARDEGNA	3,7	0,3	1,1	0,1	0,5	1,9
CALABRIA	4,9	1,6	1,9	0,3	0,6	1,1

The values of lower intensity are generally found in the South, with values about half compared to the North, both in 2018 (4.4 s against 7.6 s) and in 2030 (2.3 s against 4.7 s). In the same two peak situations, the substantial increase in production from non-conventional generation is denoted in 2030, which involves

a reduction in the intensity of inertia compared to 2018, despite some stable value in conventional generation, as in the North.

Since the dispatched inertia varies during the year based on market outcomes and plant availability, Figure 5.28 shows the duration curves of the intensity of inertia by market area with reference to the total number of hours per year, according to the PNIEC 2030 scenario. It is observed that the inertia intensity values remain lower for the South and the islands throughout the year.

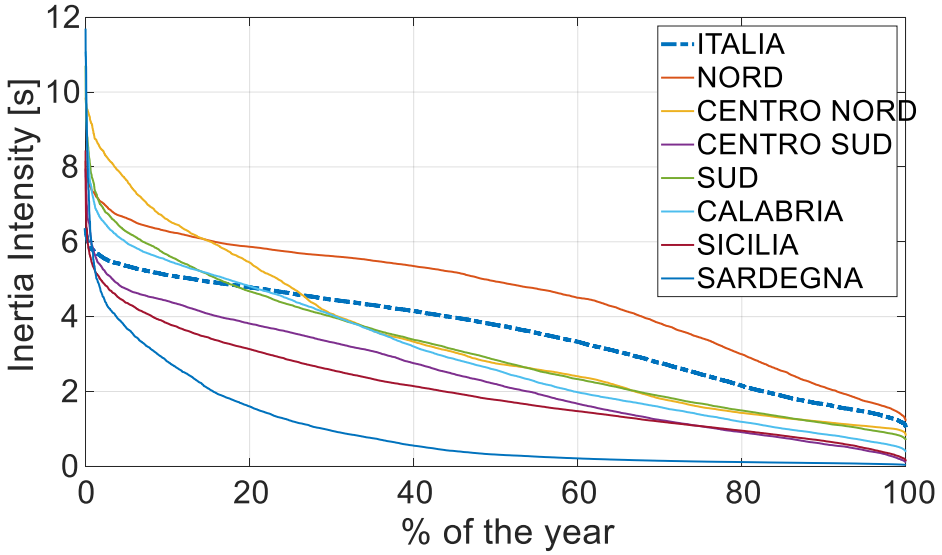

Figure 5.28. Inertia intensity duration curve by market zone with reference to the total number of hours per year, PNIEC 2030 scenario.

The current situation of the Italian distribution of conventional and non-conventional generation leads to a not uniformly distributed inertia between the North and South of the peninsula. In 2018, the North zone shows a theoretical availability of kinetic energy almost double compared to the Central South and South zones together (233 GWs against 123 GWs). However, given this availability, what matters is the dispatch inertia, which depends on the effects of the market, the dispatching priority of RES and the phasing-out of conventional generation. The dispatched inertia analysis in correspondence of the winter peak shows a significant reduction of the inertia intensity in the 2030 PNIEC scenario, passing from a total kinetic energy of 213 GWs (North 133 GWs and Centre South-South 52 GWs) in 2018 to 124 GWs (North 92 GWs and Centre South-South 7 GWs). The significant decrease in available kinetic energy indicates an increase in production from non-conventional generation, which lays the foundations for in-depth analysis of stability, also with a view to a non-uniform distribution of inertia, given the significant variability between the North and South areas of the territory national.

A first assessment of the distributional impact of inertia was investigated using the indicators developed in Chapter 4. The simulations were performed using DIgSILENT PowerFactory on a dynamic model of the Italian power system in 2017. The model has 1659 buses (1167 in Italy), 1501 lines (891 in Italy), 1080

transformers (795 in Italy), 611 synchronous generators (434 in Italy) and 2063 loads (1787 in Italy). The foreign grid is modelled as an equivalent. The analysis is started selecting the contingency buses and a monitoring bus for each Italian political region. The selected buses are at the 380 kV voltage level. The same contingency of 600 MW is applied in the North (Lombardy at bus 615) and in Sicily (at bus 855). The sparsity of the Italian admittance matrix is reported in Figure 5.29, with a total of 5833 elements.

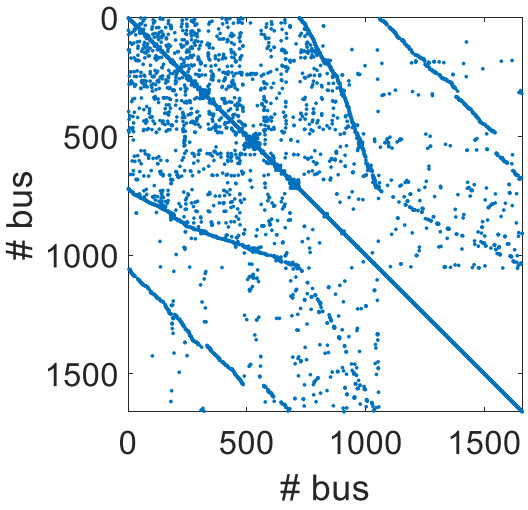

Figure 5.29. Sparsity of the Italian power system admittance matrix.

The monitored buses are listed in Table 5.18, with the short-circuit power at the bus, the region's number of incident lines and inertia intensity.

Table 5.18. Monitoring bus, incident lines. short circuit power and inertia intensity for each region.

	Region	Monitored bus	Incident Lines	P_{CC} [GVA]	Inertia Intensity [s]
1	Piedmont	419	306	21,33	6,39
2	Aosta Valley	664	41	5,54	1,88
3	Lombardy	1004	619	19,78	8,11
4	Trentino-Alto Adige/Südtirol	293	193	1,82	1,68
5	Veneto	804	291	11,32	6,02
6	Friuli-Venezia Giulia	260	97	9,23	9,21
7	Liguria	1026	89	9,04	6,79
8	Emilia-Romagna	400	152	16,81	3,33
9	Tuscany	940	142	7,95	3,57
10	Umbria	661	36	8,23	1,07
11	Marche	1131	40	6,24	0,00
12	Lazio	737	227	11,36	3,50
13	Abruzzo	457	81	6,98	2,43
14	Molise	589	16	7,95	9,18
15	Campania	955	267	11,09	4,61
16	Apulia	59	196	10,52	6,42
17	Basilicata	278	37	10,00	0,00
18	Calabria	421	85	8,64	11,76
19	Sicily	219	258	5,23	2,04

Figure 5.30 (a) shows the results of the contingency simulation in Lombardy, while Figure 5.30 (b) in Sicily. The maximum frequency deviation and the ROCOF are plotted for each region and compared to the inertia intensity, short circuit power and electrical distance from the contingency bus. When the

contingency is in Lombardy, the worst values for the maximum frequency deviation is in Sicily, meaning that the disturbance location has less impact on the frequency trajectory after the disturbance. On the contrary, the worst ROCOF is in Lombardy, i.e., near the contingency. Sicily is an island, radially connected to Italy, and it oscillates more than the mainland after the contingency. When the fault is in Sicily, both the worst values for the frequency deviation and ROCOF are in the nearest bus to the contingency. The inertia intensity has major impact on the local ROCOF, while no significant relations are found with the short-circuit power.

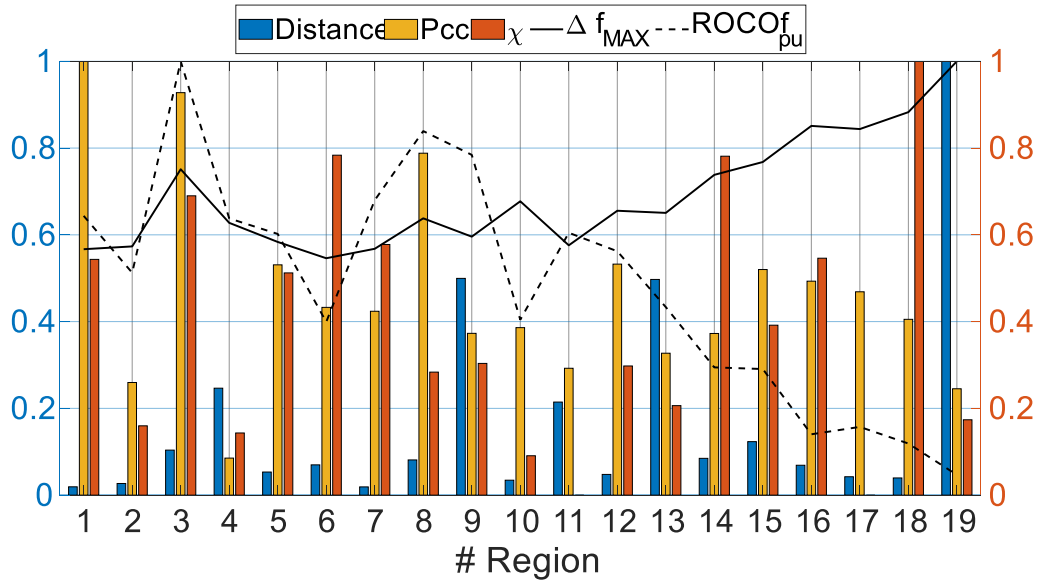

a.

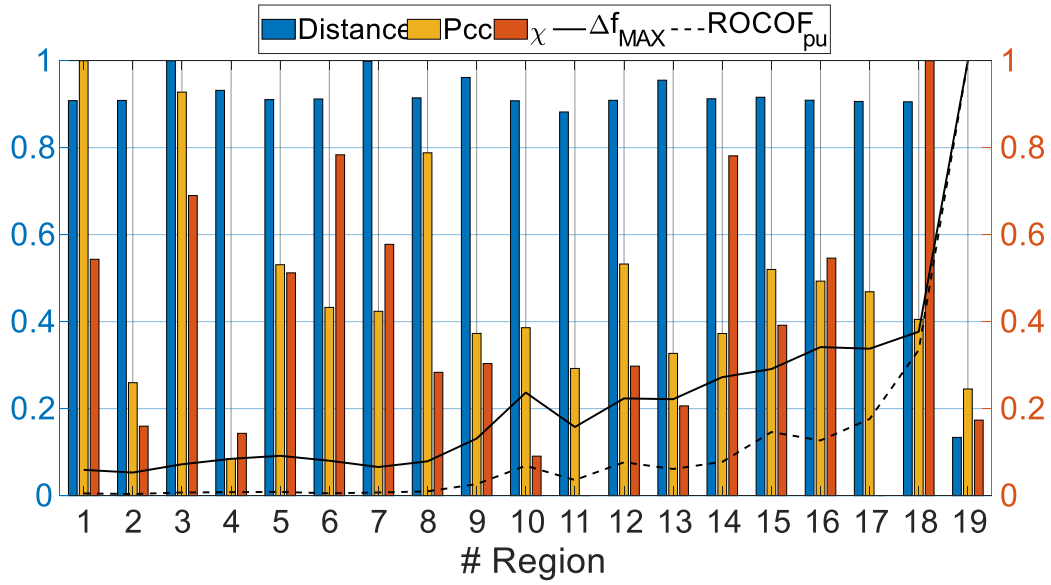

b.

Figure 5.30. Electrical distance from the contingency bus, inertia intensity of the region, short-circuit power, maximum frequency deviation and ROCOF in the monitored bus. a) contingency bus in Lombardy b) contingency bus in Sicily.

The maximum frequency deviation highly depends on the interconnection with the rest of the system, while additional grid meshing cannot decrease the initial ROCOF, as it depends on available on-line inertia and fault location.

These findings represent a first step in assessing the impact of PEIG distribution on the frequency stability of a large power system. It is important to further investigate the indicators, assessing eventual correlations among them and defining new ones (e.g., spinning reserve, FCR allocation, etc.). More scenarios, e.g., adding lines or new components, varying contingency and monitoring buses and simulations should be conducted to validate the indicators. After the validation, future developments could deal with the definition of a risk index per region and the possible selection of the critical ones, by using multiple criteria decision analysis.

All results are listed in Table 5.19.

Table 5.19. Monitored buses, electrical distance, and frequency performance parameters for a contingency in Lombardy and in Sicily by region.

			Contingency Lombardy			Contingency Sicily		
	Region	**Monitored bus**	Δf_{pu}	$ROCOF_{pu}$	**Electrical distance**	Δf_{pu}	$ROCOF_{pu}$	**Electrical distance**
1	Piedmont	419	0.567	0.644	0.019	0.059	0.005	0.908
2	Aosta Valley	664	0.573	0.513	0.027	0.053	0.004	0.909
3	Lombardy	1004	0.751	1.000	0.104	0.072	0.007	1.000
4	Trentino-Alto Adige/Südtirol	293	0.628	0.638	0.247	0.085	0.008	0.932
5	Veneto	804	0.584	0.602	0.053	0.092	0.009	0.911
6	Friuli-Venezia Giulia	260	0.546	0.399	0.070	0.080	0.005	0.912
7	Liguria	482	0.568	0.680	0.903	0.066	0.007	0.999
8	Emilia-Romagna	400	0.638	0.839	0.081	0.079	0.010	0.915
9	Tuscany	940	0.596	0.784	0.500	0.131	0.027	0.961
10	Umbria	661	0.677	0.404	0.034	0.237	0.069	0.908
11	Marche	1131	0.576	0.605	0.215	0.158	0.036	0.882
12	Lazio	737	0.656	0.562	0.048	0.224	0.077	0.909
13	Abruzzo	457	0.651	0.433	0.497	0.222	0.061	0.955
14	Molise	589	0.738	0.294	0.085	0.272	0.078	0.912
15	Campania	955	0.768	0.291	0.123	0.291	0.146	0.916
16	Apulia	59	0.851	0.140	0.069	0.342	0.127	0.909
17	Basilicata	278	0.844	0.157	0.042	0.338	0.176	0.906
18	Calabria	421	0.883	0.119	0.040	0.377	0.335	0.905
19	Sicily	219	1.000	0.047	1.000	1.000	1.000	0.134

5.3 The European Case Study

A frequency stability study was conducted using the aggregate model on the interconnected CE power system in the scenarios DG 2030 and ST 2030. The reference incident is set to 3000 MW and a warning threshold of 0.5 Hz/s is set for ROCOF. The inertia studies are performed on eleven types of units: Nuclear, Lignite, Coal, Gas, Oil, Hydro, Wind, Solar, Other Renewable, Bio. These units are further divided into 44 sub-units based on technology type. Each subcategory has its own parameters for inertia constant and average capacity. The inertia study is a post process of the market modelling output, which uses the inertia parameters collected by ENTSO-E.

The kinetic energy and FCR duration curve for the analysed scenarios are given in Figure 5.31. The maximum kinetic energy is 1047 GWs and 1149 GWs in DG 2030 and ST 2030 scenarios respectively, while the minimum is 135 GWs and 179 GWs. This last minimum would be compatible to keep the ROCOF below 0.5 Hz/s, also considering the effect of the governors which is not included in the previous calculation of minimum kinetic energy. The FCR values oscillate between 1900 and 6100 MW for most of the year. The maximum FCR is 6057 MW and 6183 MW in DG 2030 and ST 2030 scenarios respectively, while the minimum is 1992 MW and 1943 MW.

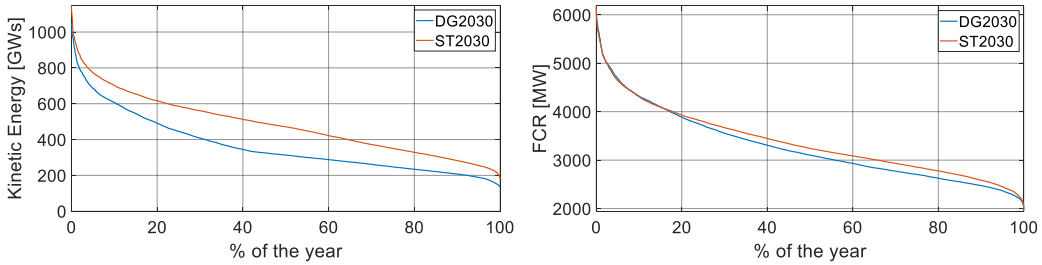

Figure 5.31. Kinetic energy and FCR duration curves for CE in scenarios DG 2030 and ST 2030.

The aggregate model with only FCR and without protection schemes is used to simulate the reference incident in each hour of the year. The frequency performance parameters are reported as duration curves in Figure 5.32.

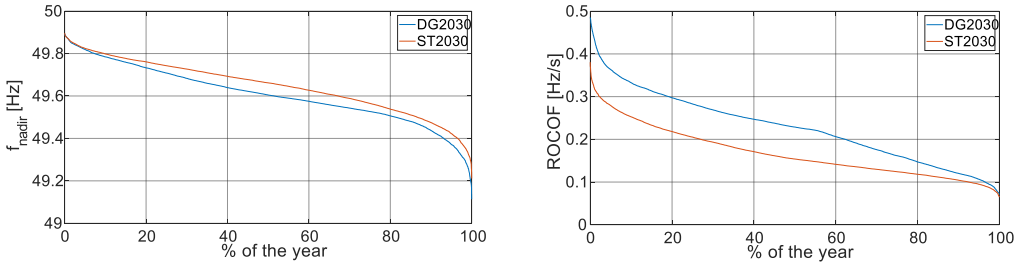

Figure 5.32. Frequency nadir and ROCOF duration curves for CE in scenarios DG 2030 and ST 2030

The worst frequency performance indicators are 49.11 Hz (at hour 5527) and 0.49 Hz/s (at hour 5885) for DG 2030 scenario and 49.21 Hz (at hour 5863) and 0.38 Hz/s (at hour 7718) for ST 2030 scenario. These indicators confirm the reference incident does not imply concerns for the overall frequency stability of the CE synchronous system, at least at the 2030 horizon.

5.3.1 Technical benefits of network enhancement projects

The methodology proposed in Chapter 4 is tested on two possible network enhancement projects:

a. The construction of a new HVDC link between two asynchronous areas, considering only primary frequency control.
b. The installation of a BESS considering both inertial and primary frequency control.

The computation of the indices is undertaken on an hourly basis over a timeframe of one year. The analysis is referred, at the planning level, to future systems scenarios foreseen in terms of hourly power generation by technology type and loads per European country.

The HVDC can provide primary frequency support to one SA, using the kinetic energy and reserve from the other SA. In this case the impact of an HVDC of 1000 MW on a larger power system are evaluated. The HVDC is considered providing half band in primary frequency regulation. The frequency performance is evaluated in each hour of the year. Figure 5.33 shows the frequency performance indicators with and without the HVDC project, considered as duration curves.

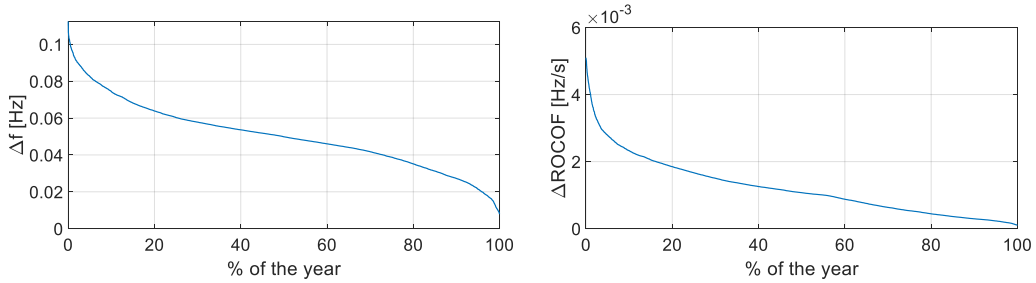

Figure 5.33. Frequency performance indicators duration curves, comparison with and without a HVDC project, under-frequency reference incident, DG 2030.

The frequency performance adding a BESS are evaluated in each hour of the year and plotted as a duration curve for a BESS of 100 MW with a half contribution in inertial and primary control. Figure 5.34 shows the frequency performance indicators with and without the BESS project, considered as duration curves.

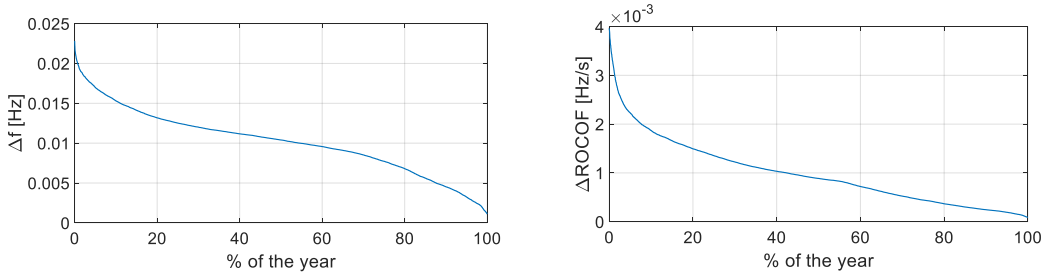

Figure 5.34. Frequency performance indicators duration curves, comparison with and without a BESS project, under-frequency reference incident, DG 2030.

Table 5.20 lists the computed frequency performance indicators for both network enhancement projects.

Table 5.20. Frequency performance indicators for both network enhancement projects

Project	**Scenario**	$\overline{\Delta f}$ **[Hz]**	$\overline{\Delta R}$ **[Hz/s]**	Δf_{MAX} **[Hz]**	ΔR_{MAX} **[Hz/s]**	%Δf **[%]**	%ΔR **[%]**
HVDC	DG2030	0.0503	0.0012	0.1125	0.005	0.049	0.002
BESS	DG2030	0.0102	0.001	0.0228	0.004	0.01	0.001

5.3.2 System splits assessment

The system split methodology proposed in Section 4.3.4.3 has been applied to the Continental Europe SA in 2030 and 2040 scenarios coming from the TYNDP 2018. The considered scenarios are Sustainable Transition (ST) 2030 simulated by Plexos and Global Climate Action (GCA) 2040 simulated by Promed Grid both for climatic year 2007 [240]. The market simulations are performed considering the European market zones used for the TYNDP 2018, which are reported in Figure 5.35.

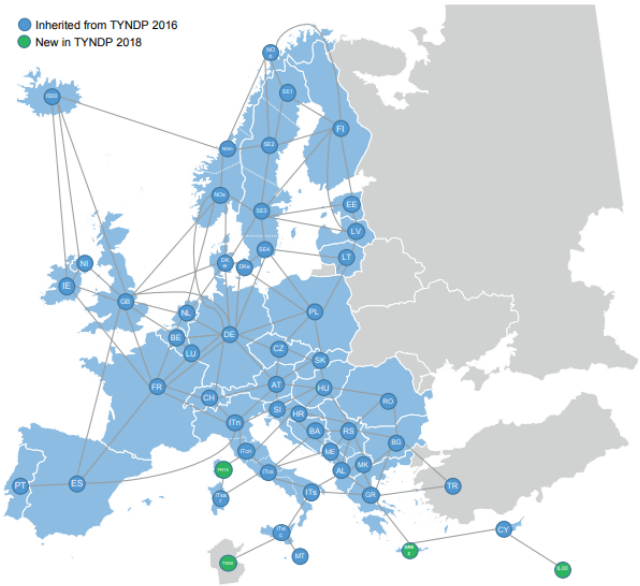

Figure 5.35: European market zones used in the TYNDP18.

The market model considers the 32 market zones composing the CE grid, which are reduced to 20 nodes for computational reasons and showed in Figure 5.36 using the graph framework.

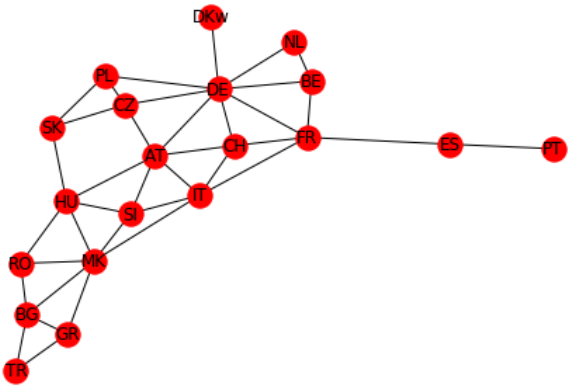

Figure 5.36: Graph of the considered market zones composing the CE grid [241].

The merged market zones are reported in Table 5.21. Smaller market zones have been aggregated (Balkan countries), small structural antennas have been aggregated to bigger nodes (Luxembourg) and the Italian market zones in a unique one.

Table 5.21: Merged market zones for computational reasons [241].

Node	SA	Market zones
BE	CE	['BE', 'LUb‘,'LUg',]
DE	CE	['DE', 'LUv', 'LUg']
FR	CE	['FR', 'LUf']
IT	CE	['IT', 'ITcn', 'ITCO', 'ITcs', 'ITN', 'ITS', 'ITsar', 'ITsic', 'MT']
MK	CE	['AL', 'BA', 'HR', 'ME', 'MK', 'RS']

All the theoretical bisections are found using the process described in Section 4.3.4.3. Considering 20 market zones, 730 valid partitions of CE are obtained. An example of two split areas is reported in Figure 5.37. For each split line, the imbalance is calculated summing the AAC flows.

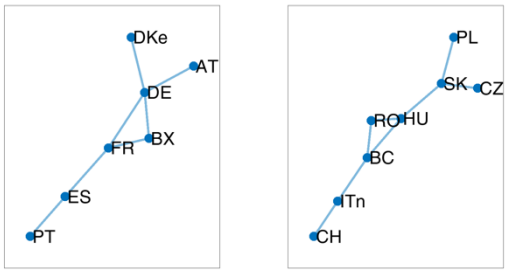

Figure 5.37: Example of separated asynchronous areas [241].

The values of the SSI are calculated for all the possible subsystems and for each hour of the year. First, the case for only one subsystem is reported (the Italian area separated from CE), followed by the values for all subsystems, filtered by the area's size.

All the computed SSI values for Italy separated from CE are plotted in Figure 5.38 with respect to the subsystem total load. Separated situations are identified for over-frequency and under-frequency using different colours (orange for over-frequency and blue for under-frequency). To compare the two scenarios, the SSI values for the Italian subsystem separated from the rest of Europe are referred to the maximum absolute ROCOF in both the ST 2030 and GCA 2040. In the ST 2030 scenario, the worst under-frequency situation is at hour 1680 ($SSI = -0.20$) with an imbalance around 13 GW and a total load around 31 GW. The worst over-frequency situation is at hour 8555 with $SSI = 0.04$, due to an imbalance around 7 GW and a total load around 32 GW. In the GCA 2040 scenario, the worst under-frequency situation is at hour 2670 ($SSI = -1$) with an imbalance around 14 GW and a total load around 28 GW. The worst over-frequency situation is at hour 8571 with $SSI = 0.19$, due to an imbalance around 8 GW and a total load around 26 GW. It is possible to see from Figure 5.38 a slight trend towards higher values of SSI with low load situations.

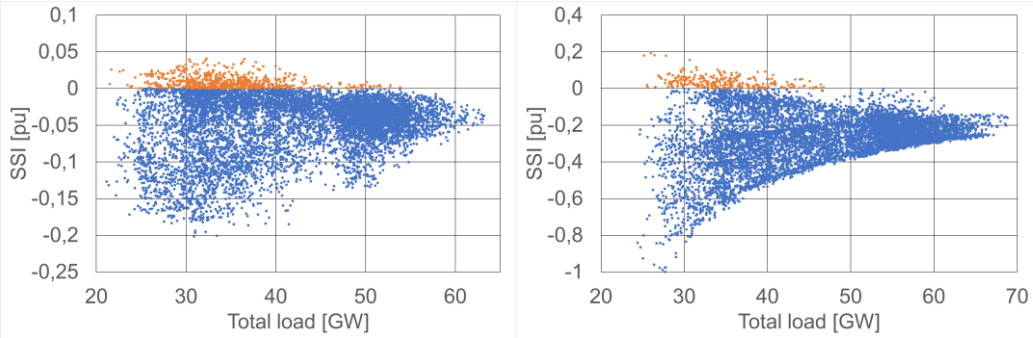

a. b.

Figure 5.38: SSI values vs total load for all hours for the Italian subsystem separated from CE (a. ST 2030, b. GCA 2040) [241].

The results are plotted in Figure 5.39 as duration curves for all the hours of the year for the Italian subsystem separated from the rest of Europe, for the two scenarios ST 2030 and GCA 2040. As Italy is importing for most of the hours of the year, the worst situation is for under-frequency phenomena, with negative SSI values for 8472 and 7986 hours, respectively, in the ST 2030 and GCA 2040.

Figure 5.39: SSI duration curve for all hours for the Italian subsystem separated from CE (ST 2030, GCA 2040) [241].

The situation is increasingly worsening moving towards 2040. The maximum absolute value of ROCOF is for the scenario GCA 2040 in under-frequency. The worst under-frequency SSI for ST 2030 is -0.2, around 20% of the worst SSI for the GCA 2040. The worst over-frequency SSI is 0.04 for ST 2030 and 0.19 for GCA 2040.

All the cases with a subsystem load higher than 15 GW are filtered out. 15 GW is considered here as suitable to identify large power system areas possibly affected by dangerous splits. Figure 5.40 shows the values of the SSI for the two analysed scenarios, plotted with respect to the total subsystem load. The SSI is calculated using the maximum absolute ROCOF for all considered subsystems and scenarios.

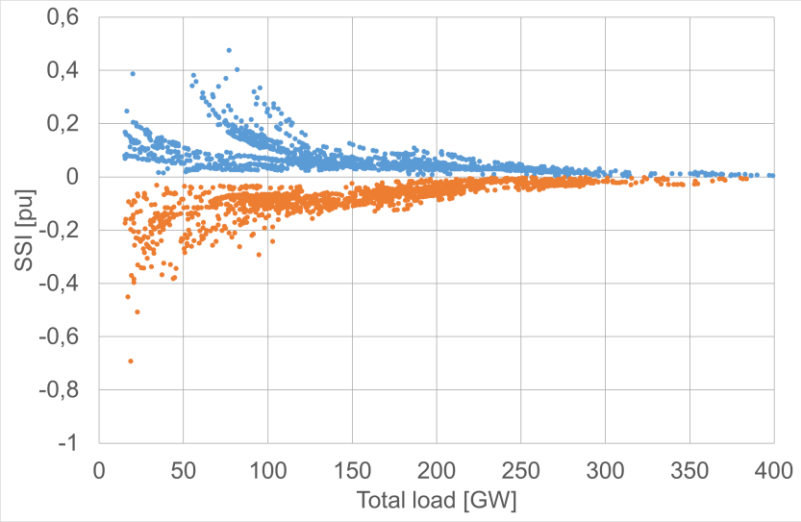

a.

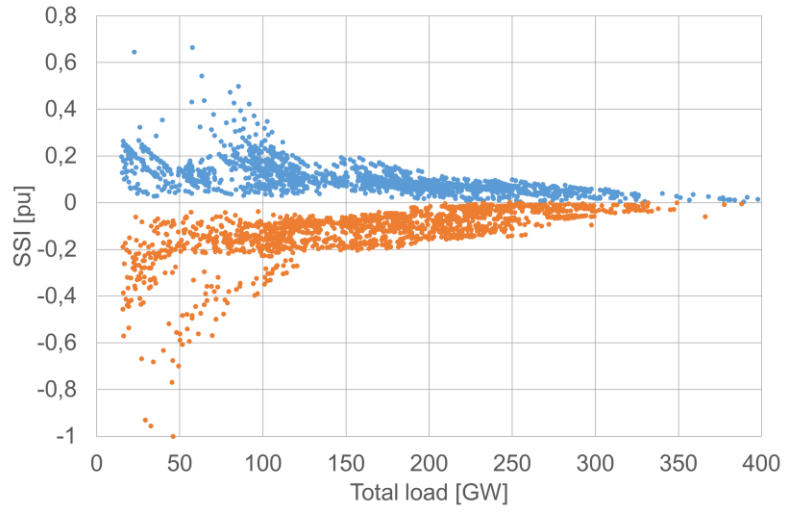

b.

Figure 5.40: SSI values for subsystems with total load higher than 15 GW with respect to the total load (a. ST 2030, b. GCA 2040) [241].

In ST 2030 2864 points are found, while in GCA 2040 2863 points and 593 splits over 730 splits. The worst under-frequency case is the separation of Austria-Switzerland-Slovenia at hour 358, with a SSI of -0.69, due to an imbalance around 11 GW and a total load of 18.6 GW in the scenario ST 2030, while the separation of Austria-Italy appears at hour 7, with a SSI of -1 Hz/s, due to an imbalance around 20 GW and a total load of 46 GW in the scenario GCA 2040. The worst over-frequency case is the separation of Germany-Denmark at hour 4258, with a SSI of 0.47 Hz/(GWs), due to an imbalance around 24 GW and a total load of 77 GW in the scenario ST 2030. In the scenario GCA 2040, the worst over-frequency case is the same separation of Germany-Denmark at hour 4530, with a system split indicator of 0.66, due to an imbalance around 26 GW and a total load around 58 GW. Table 5.22 reports the ranking of the worst ten split lines for the cases of under- and over-frequency per scenario.

Table 5.22. Ranking of the worst split lines in the scenario ST 2030 and GCA 2040 [241].

	ST 2030		**GCA 2040**	
	Under-frequency			
	Split line	***SSI* [pu]**	**Split line**	***SSI* [pu]**
1	AT_CH_SI	-0.69	AT_IT	-1
2	BE_NL	-0.51	CH_IT	-0.96
3	AT_HU	-0.45	IT_SI	-0.93
4	AT_CH_HU	-0.40	AT_IT_SI	-0.77
5	AT_CZ	-0.38	AT_CH_IT	-0.70
6	AT_CH_IT	-0.38	CH_IT_SI	-0.68
7	AT_IT	-0.38	GR_IT_MK	-0.68
8	AT_HU_SI	-0.37	BE_NL	-0.67
9	CH_IT	-0.37	IT_MK	-0.63
10	AT_CH_IT_SI	-0.34	AT_CH_IT_SI	-0.61
	Over-frequency			
1	DE_DKw	0.48	DE_DKw	0.66
2	DE_DKw_NL	0.40	BE_NL	0.64
3	BE_NL	0.39	CH_DE_DKw	0.54
4	AT_DE_DKw	0.38	DE_DKw_NL	0.50
5	CH_DE_DKw	0.37	AT_DE_DKw	0.47
6	AT_DE_DKw_SI	0.36	CZ_DE_DKw	0.44
7	CZ_DE_DKw	0.34	BE_DE_DKw_NL	0.43
8	BE_DE_DKw_NL	0.34	AT_DE_DKw_SI	0.43
9	CH_DE_DKw_NL	0.33	CH_DE_DKw_NL	0.42
10	AT_DE_DKw_NL	0.32	AT_CH_DE_DKw	0.39

In sum, fast frequency response including fast control reserves or frequency related defence measures e.g., LFSM-O or LFDD will be needed to face system splits. According to the system defence operation guidelines, system split will result in an emergency state, because of out-of-range contingency. TSOs will not act preventively to mitigate the impact of out-of-range contingency but will react by activating their defence plan. Defence plans are designed to help during those severe disturbances but cannot stabilise all system split scenarios with extreme imbalances. Potentially needed restoration plans will employ adequate resources to stabilize the islands and later to re-synchronise the system.

Chapter 6

6 COVID-19 pandemic: an experiment of high RES penetration and low inertia

6.1 Introduction

The worldwide spread of the COVID-19 pandemic in 2020 forced most countries to intervene with policies and actions, including lockdowns, social-distancing and smart-working measures, aimed to mitigate risks for the health system. The electricity sector was also impacted, with performances largely reflecting the changes in the industrial and commercial sectors operations and in the social behaviour patterns. The most immediate consequences concerned the power demand profiles, the generation mix composition and the electricity price trends. In some countries, the electricity sector experienced a foretaste of the future, with higher RES penetration and concerns for the security of supply. This Chapter presents a systemic approach towards assessing the impacts of the COVID-19 pandemic on the power sector, to quantify and track the short-term effects[6]. Various metrics are defined in different areas - system operation, security, and electricity markets - to quantify those impacts. The methodology is applied with major details to the Italian power system and then to the main European countries, to produce a comparative assessment of the main effects in different contexts. The covered period is from the beginning of March 2020 until June 2020, with focus on April 2020, as the month most affected by the restrictions.

[6] Parts of this chapter were also published in [256], [247], [248], [265].

6.2 Analysing the effect of pandemic on electricity systems

The World Health Organisation (WHO) first reported a cluster of unknown origin cases of pneumonia on December 31, 2019 in Wuhan, China. The new coronavirus disease was named 2019-nCoV, and commonly referred to as COVID-19 as from February 11, 2020. The first case of novel coronavirus outside China was confirmed in Thailand on January 13, 2020 and in the USA on January 20, 2020, from that time on spreading rapidly through Japan, South Korea, Iran, Europe, and Australia. The novel coronavirus started to spike for the first time in Europe with cases in Italy on February 21, 2020 and a week later in Spain, on March 3, 2020. COVID-19 was declared a worldwide pandemic on March 11, 2020, given the concerns both about the alarming levels of spread and severity, and about the inaction in some countries [242]. Quarantines and restrictions were imposed by several countries to prevent further spread of the pandemic and to avoid the collapse of their health system, under pressure due to the increasing number of people admitted in intensive care. China was the first to deploy such measures, quarantining Wuhan and the rest of Hubei province starting from January 23, 2020, involving more than 760 million people. Italy declared nationwide lockdown on March 9, 2020, followed by Spain, France, UK (March 23). On March 25, 2020 nearly one third of the world population was on lockdown, reaching later 4.2 billion people as of April 28th.

The international emergency due to the spread of COVID-19 and the implemented procedures for its containment had an important impact on the whole economy, sociality, habits, and activities [243]. Millions of people were quarantined in their homes, a great majority working remotely, and students followed their classes online. Traditionally, changes in the productive and social behaviours have direct effects on the electrical power system performance [244]. Inevitably the COVID-19 pandemic and the relative adopted restraining measures, affecting behaviours and activities, influenced the power system in many respects [245]. Several studies and analyses started exploring the COVID-19 impact on the power sector, both in the shorter and longer terms, nonetheless capturing the overall systemic consequences requires accurate data and an adequate assessment framework [246]. For example, the quarterly analysis released by ENEA showed the dramatic energy demand reduction in Italy, around -7% in the first three months of 2020 compared to the same period of 2019, altogether for oil, gas, and electricity. The impact on CO_2 emissions, market prices and transport sector were also investigated [247]. The ENEA analysis was extended to April 2020 and reported in [248]. The International Energy Agency provided several insights on the energy sector impact, dealing with oil, gas, electricity and the prospects for renewables deployment and investments implementation [249]. The Industry Technical Support Leadership Committee of the IEEE Power and Energy Society published a report on the first response of the power industry on the pandemic [250], in which health, technical and business impacts were analysed, as well as

the approaches followed by utilities and system operators to manage the new scenarios due to the COVID-19 pandemic. The change in social habits resulted in demand power profile modifications, and the decrease of industrial production lowered the electricity consumption [251], [252]. A direct impact was observable in the alteration of demand in terms of both absolute values and temporal arrangement, affecting both energy consumption and power profiles as the increase in the residential consumption could not compensate the drastic reductions in industrial, commercial, and tertiary activities. The demand drop depended on the measures adopted, their severity and duration. According to the International Energy Agency, the reduction in the demand will affect the whole 2020, with 5% and 10% yearly reductions in different regions [249].

Besides this direct impact, indirect effects were related to the market prices and the generation mix [253], [254], [255]. One example was the increase in the share of RES, which has led to market price reduction and increased concerns in terms of system security [256], [257], [258]. The impacts were different for each country, based on the electricity system's structure (generation mix, share of distributed energy sources…) and the social and economic context.

The changes in social habit are translated in load profile adaptation, with different peaks in time and magnitude. Some countries observed a shift of morning peaks to later hours, while others, such as the CAISO system, have experienced a reduction in demand in the daylight hours and the worsening of the duck curve effect impacted by solar photovoltaic (PV) generation [250]. The presence in the energy mix of a predominant share of RES has some consequences on the secure operation of the power system, in terms of voltage and frequency management. With less electricity needed, but large amounts of solar PV and wind energy coming onto the system, the grid needs to work harder to provide energy when the sun stop to shine, and the wind stop to blow. This can lead to significant curtailment of RES because the system cannot handle it all from a stability perspective [259]. In this sense, the pandemic is providing a glimpse into the challenges of the energy use and it shows what it can be expected in the future in terms of higher penetration of RES, bigger duck curve and voltage management issues.

Other studies highlighted also non-technical factors. For instance, EPRI carried out an extensive analysis of EU, USA, and China, focusing mainly on the human resource management by the electric utilities under the pandemic [260]. Many analyses have not investigated weather variations, which could significantly contribute to load variations given the correlation with the power profiles [261]. Such effects should be examined before assessing the impact of COVID-19 on demand changes, granting that the shock on the power sector is undeniable. Weather effects are usually modelled by expressing the load as a linear regression of meteorological factors such as temperature, wind speed, humidity, etc. Although the extremely wide variety of required weather variables, studies have

shown that a few basic meteorological factors usually account for the weather-dependent load and temperature [262]. Some institutions created websites to track the COVID-19 lockdown effects. In [263] an electricity tracker was implemented to compare differences in electricity consumption between 2020 and 2019, with an overview of what is occurring across Europe, with data updated daily as new information emerges.

6.2.1 Direct impact on demand

The direct and measurable impacts of the pandemic on electricity systems are displayed in the evolution of the electricity demand. The demand variation can be measured both in terms of power profile and energy consumption. This variation is evaluated comparing power profiles with corresponding past periods without pandemics using a set of metrics able to quantitatively capture the variation.

Different metrics are defined to evaluate the impact on power demand and profile under pandemic. First, the demand trend is analysed considering the time lag of the pandemic among different countries. The energy demand variation (D_{var}) in the year y_N of pandemic with the previous year y_{N-1} is reported in percentage as:

$$D_{var} = \frac{D_{yN} - D_{yN-1}}{D_{yN-1}} \cdot 100 \tag{6.1}$$

where D_{yN} and D_{yN-1} are the total demand in the examined timeframe of the year y_N and y_{N-1}. The demand is plotted with calendar adjustment between the years y_N and y_{N-1}. The ratio $D_{yN}(h)/D_{yN-1}(h)$ is computed per each calendar-adjusted time step h and plotted as a duration curve. The maximum (P_{max}), minimum (P_{min}) and average (P_{ave}) power demanded and the load factor (ζ), defined as the ratio between P_{ave} and P_{max}, are evaluated and compared among the year y_N of pandemic with the previous year y_{N-1} in the examined timeframe.

The temperature effect on the demand variation is analysed for a selected number of countries. The temperature of air at 2 metres above the surface of land, sea, or inland waters, is taken from Copernicus Land Monitoring Service 2020, by the European Environment Agency [264]. Figure 6.1 shows a typical correlation between the values of temperature and energy demand. It is possible to see the demand increase in full winter and summer, where lower and higher temperatures impose the need for more electricity, respectively for heating and cooling. In the mid-season instead, a variation of 1°C of temperature affects less the demand.

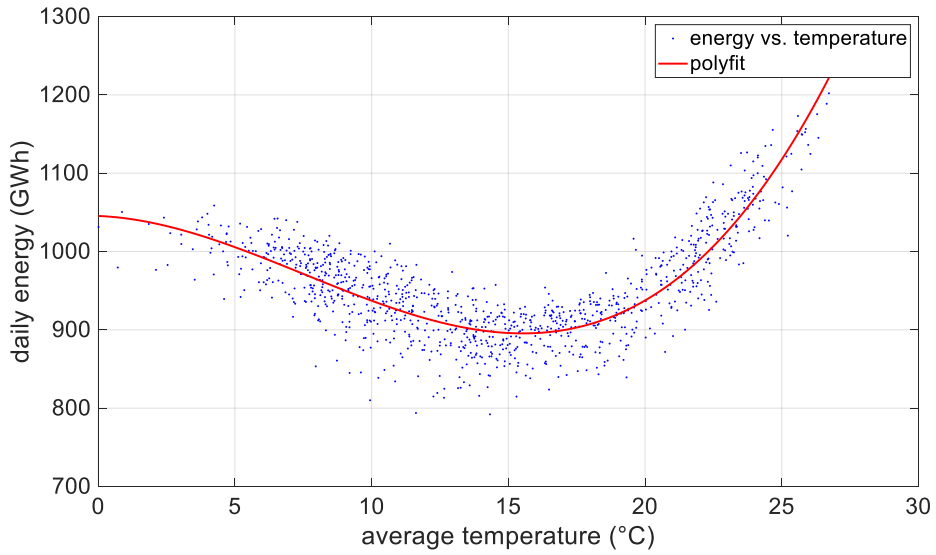

Figure 6.1: Typical correlation between temperature and energy demand [265].

Given the demand temperature dependency in the form

$$E(T) = a\,T^3 + b\,T^2 + c\,T + d \tag{6.2}$$

the weather effect can be evaluated using the following equations:

$$\Delta E = \frac{dE}{dT}(T_{20}) \cdot (T_{20} - T_{19}) \tag{6.3}$$

$$\Delta E_{w\%} = \frac{(E_{20} - \Delta E - E_{19})}{E_{19}} \cdot 100 \tag{6.4}$$

where T_{19} and T_{20} are the temperature in 2019 and 2020, E_{19} and E_{20} are the energy demand in 2019 and 2020 respectively, ΔE and ΔE_w are the demand variation without and with weather correction.

The load shape in function of time gives information on the effect of the measures applied to contain the pandemic. Energy consumption gradually changes over short (seasonally) and long (years, tens of years) timeframes. However, sudden changes in the social and productive habits can yield to unexpected demand shape variations. It is important then to identify some useful parameters for a comprehensive load shape analysis. Traditionally, load shapes can be characterized by their maximum, minimum and average values, which vary considering working days and holidays. The typical load shape has two main peaks, one in the morning and the second in the evening. During holidays, the evening peak is usually more pronounced than the morning peak, while the opposite occurs during working days. The difference of magnitude between the two peaks follows the same pattern. The morning and evening ramps have usually higher slope in working days than in holidays. In this thesis, the working day (WD) and holiday (HD) Average Daily Load Profile (ADLP) are evaluated. The ADLP is the defined as the mean load for each step during the days in a selected

timeframe. The metrics deployed to identify the difference between the load profiles during the pandemic and the same period of last year are:

- Maximum ($ADLP_{max}$), minimum ($ADLP_{min}$) and mean ($ADLP_{ave}$).
- Peak Value (PV), defined as the maximum value of the ADLP, which could be a Morning Peak (MP), defined as the maximum value of the ADLP between 6h and 15h, or an Evening Peak (EP), defined as the maximum value of the ADLP between 18h and 0h.
- Peak Time, defined as the hour at which the PV occurs.
- Peak difference ($\Delta Peaks$), defined as the difference between MP and EP.
- Morning Ramp (MR), defined as:

$$MR = \frac{MP - MB}{T_{MP} - T_{MB}} \tag{6.5}$$

where MB is the Morning Base, i.e., the minimum value of the ADLP between 0h and the time at which the MP occurs.

- Evening Ramp (ER), defined as:

$$ER = \frac{EP - EB}{T_{EP} - T_{EB}} \tag{6.6}$$

where EB is the Evening Base, i.e., the minimum value of the ADLP between 15h and the time at which the EP occurs.

A graphic representation of the metrics is depicted in Figure 6.2.

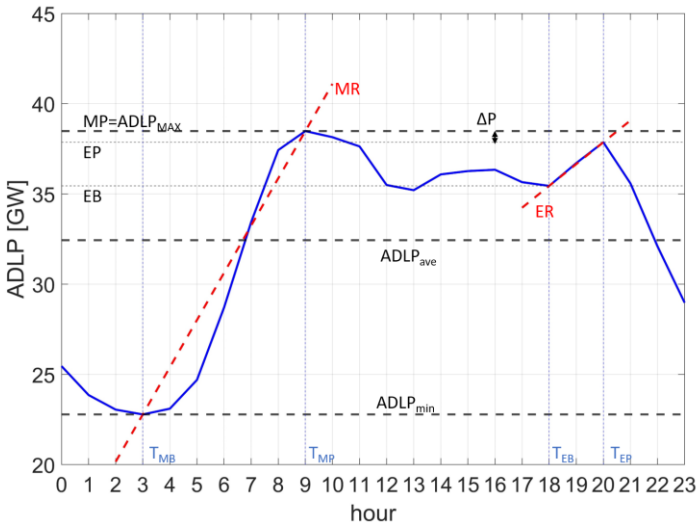

Figure 6.2. Average daily load profile (ADLP) characterization [265].

6.2.2 Indirect impact: system operation

Modern societies are fully dependent on electricity and maintaining security of supply is crucial for COVID-19 response and recovery. In the context of generation from renewable sources, comprising geothermal, hydroelectric,

photovoltaic, wind and biomass, photovoltaic and wind are referred to as non-conventional generation, opposed to thermoelectric and hydroelectric conventional generation. The non-conventional generation poses some challenges to system security, as it is characterized by uncertainty in the generated power, making difficult both its control and forecasting. In addition to not contributing to the system inertia, the unconventional generation also implicates a reduction of the short-circuit power and of the frequency and voltage regulation capabilities. An assessment of the possible effects on the operation and security of the measures following the spread of COVID-19 pandemic can be carried out using the following indicators:

- Electricity generation from RES (TWh) and its share over the total demand.
- Electricity generation from fossil (TWh) sources and its share over the total demand.
- Electricity generation from conventional/non-conventional units (TWh).
- Non-conventional penetration index σ, defined as the share of non-conventional generation compared to the total generation (sum of conventional and non-conventional). The difference between σ and the RES penetration lies in the presence of the conventional generation, basically hydro. In terms of security, the instantaneous penetration of non-conventional generation σ is preeminent, as it indicates the share of non-predictable and non-programmable sources.

In addition, the power interchanges among the Member States were affected due to the need to keep each national system feasible and secure with a minimum number of traditional generators.

6.2.3 Indirect impact: electricity markets

The immediate impact of the COVID-19 pandemic on electricity markets is analysed in terms of price drop in the Day-Ahead Market (DAM). A set of metrics is defined to evaluate the impact on volumes and prices in the DAM. The first indicator is the load-weighted weekly moving average of the hourly wholesale price in each bidding zone $\overline{(DAMp_h)}$, defined as:

$$\overline{DAMp_h} = \frac{\sum_{i=1}^{N_C} DAMp_{h_i} \cdot DF_{h_i}}{\sum_{i=1}^{N_C} DF_{h_i}} \tag{6.7}$$

where $DAMp_{h_i}$ is the DAM price for the bidding zone i, DF_{h_i} is the demand forecasted and N_C is the number of considered countries.

This indicator is used to single out the effect of the pandemic on wholesale prices (€/MWh) trend per bidding zone for a number of years before the year y_N

of pandemic to establish a baseline for comparison. Other metrics used to investigate the dynamics of the electricity market include:

- the variation of the load weighted weekly moving average of DAM prices in each bidding zone $DAMp_{var}$ [€/MWh] in the year y_N of pandemic with the previous year y_{N-1} in percentage as:

$$DAMp_{var} = \frac{DAMp_{yN} - DAMp_{yN-1}}{DAMp_{yN-1}} \cdot 100 \quad (6.8)$$

- The minimum DAM price $DAMp_{min}$ [€/MWh], defined as the minimum price reached in the DAM in the selected timeframe.
- The number of hours with negative prices (where they are allowed) Nh_{neg}.
- The DAM volumes in [GWh], defined as the total load for all the bidding zones for the year 2020 w.r.t the previous years.
- Time series decomposition of zonal time series of prices. The goal is to capture the different components of the average DAM price time series; each series is processed using a simple decomposition method for showing three components: the trend (weekly moving average), the seasonal component repeating weekly, and the random component. Adding the three components up, the time series of DAM prices in each zone is obtained.

In this context, the term "seasonal" carries a different meaning than in previous Section: in the statistical decomposition of the zonal DAM prices the term indicates the part of the zonal prices trend that repeats over each week, and that should be subtracted from the observations to identify the real trend.

For Italy, the examined markets were the Day Ahead Market (MGP), the Intra-Day Market (MI), the Dispatching Services Market (MSD) and the Balancing Market (MB), using the following metrics:

- PUN (Prezzo Unico Nazionale), P_{MI}, P_{MSD}, P_{MB}, defined as the monthly average price respectively in the MGP, MI, MSD and MB;
- ΔPUN, ΔP_{MI}, ΔP_{MSD}, ΔP_{MB}, defined as the variation of prices in percentage between the same month of the previous year respectively in the MGP, MI, MSD and MB;
- Q_{MGP}, Q_{MI}, Q_{MSD}, Q_{MB} defined as the total volumes moved respectively in the MGP, MI, MSD and MB;
- ΔQ_{MGP}, ΔQ_{MI}, ΔQ_{MSD}, ΔQ_{MB}, defined as the variation of volumes in percentage between the same month of the previous year respectively in the MGP, MI, MSD, and MB.

For the MSD ex-ante and MB, the total of purchases and sales was considered as volume and the weighted average between purchases and sales as price.

6.3 Immediate impacts on Italy

Italy was the first country in Europe hit by the pandemic. The restrictions have been of different magnitude, starting from February 23, 2020 for some towns in Lombardy and Veneto regions, with the successive extension throughout the whole country after March 8, 2020 (Phase 1 - lockdown). On March 11, 2020, the closure of all commercial activities was ordered, except for grocery stores, basic needs, pharmacies. On March 22, 2020, the government imposed the lockdown of all face-to-face activities related to production chains concerning non-essential goods. These measures implicated a considerable reduction in the electrical demand with consequent impacts on both electrical markets and operation strategies of the Transmission System Operator (TSO). The measures have been extended until May 3, 2020, although with partial reopening starting from April 14, 2020 (stationery stores, bookstores, clothing stores for children and babies, forestry, and the wood industry). On April 26, 2020, the so-called "phase two" started, in force from May 4, 2020 and for the following two weeks, with the reopening of manufacturing, construction and brokerage activities real estate and wholesale. Due to the low demand, compared to usual load conditions, fewer conventional power plants were dispatched in the DAM; therefore, a decrease in the price of energy occurred, as well as an increment of the renewable penetration. At the same time, conventional power plants played a key role in the Ancillary Services Market to ensure the safe operation of the transmission system. In this Section, the reduction of the electrical demand and its impacts on both electrical markets and network operation strategies are analysed and discussed for the Italian power system.

6.3.1 Power profiles and demand

The impact of COVID-19 on the Italian electricity demand is analysed in terms of energy and requested power, also observing the subdivision in the six zones which compose the Italian electricity market. The electricity data are taken from the transparency platform of Terna, the Italian TSO [266]. Figure 6.3 shows the load profile in the period between the first Monday of March and the last Sunday of May 2020 and compares it with 2019, together with the polynomial trend lines of the second order (dashed lines). The drop in demand is evident during all the examined period, except for August, where all the containment measurements were loosened.

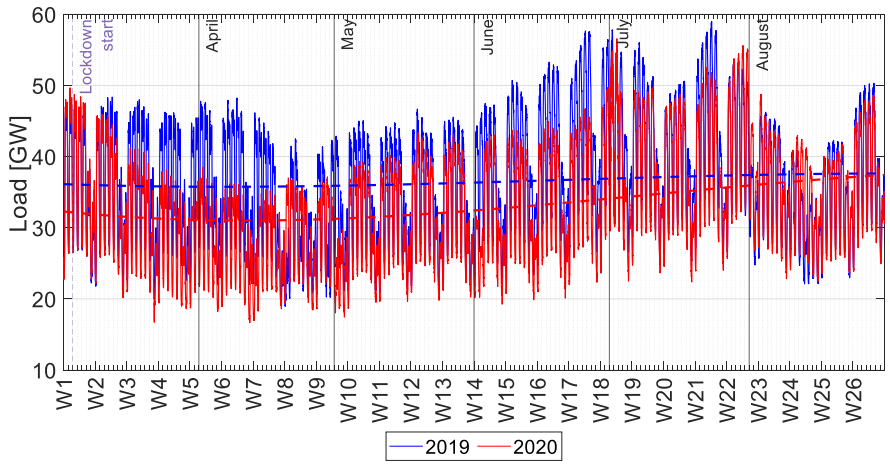

Figure 6.3. Hourly Italian load pattern between the first Monday of March and the last Sunday of August: comparison 2019-2020.

Table 6.1 reports the behaviour in terms of electricity consumption by market zone for the months of January, February, March, April, and May, compared between 2019 and 2020. The zones which compose the Italian market zone (IT) are: North (N), Centre-North (CN), Centre-South (CS), South (S), Sicily (Sic) and Sardinia (Sar). Externalities as weather effect or calendar have not been considered in the demand variation analysis.

Table 6.1. National and market zones electricity demand (January-May 2019/2020).

Electricity demand [TWh]		N	CN	CS	S	Sic	Sar	IT
JAN	'19	15,92	3,11	4,41	2,68	1,75	0,74	28,60
	20	15,48	2,83	4,16	2,53	1,62	0,80	27,43
	Δ	-2,7%	-9,0%	-5,6%	-5,4%	-7,1%	7,9%	-4,1%
FEB	19	14,62	2,70	3,85	2,29	1,47	0,67	25,60
	20	14,79	2,69	3,81	2,33	1,47	0,66	25,75
	Δ	1,2%	-0,5%	-0,9%	1,5%	0,2%	-2,0%	0,6%
MAR	19	15,15	2,89	3,88	2,35	1,50	0,67	26,43
	20	13,16	2,52	3,61	2,30	1,52	0,60	23,70
	Δ	-13,2%	-12,7%	-7,0%	-2,3%	1,7%	-9,8%	-10,3%
APR	19	13,55	2,66	3,62	2,20	1,38	0,63	24,05
	20	10,82	2,08	3,09	2,04	1,31	0,57	19,92
	Δ	-20,1%	-21,8%	-14,7%	-7,3%	-5,2%	-9,5%	-17,2%
MAY	19	14,39	2,73	3,78	2,27	1,39	0,70	25,26
	20	12,73	2,35	3,40	2,21	1,39	0,60	22,67
	Δ	-11.5%	-13.9%	-10.1%	-2.6%	0%	-14.3%	-10.3%

While in January and February the demand has not changed significantly (-4% and 0.6% respectively at national level), in March and April the variations were more pronounced. In March 2020, electricity consumption decreased by 10% compared to the same month of 2019, passing from 26.4 TWh to 23.7 TWh. The largest reduction in percentage occurred in the North and Centre North areas (with values around -13%), even if in absolute terms the largest difference was in the North with -2 TWh. The South and Islands areas were less affected by the load

reduction (with values between -2% and -10%), with a maximum absolute value of -0.27 TWh in the Centre-South area. In April 2020, the electricity demand decreased by 17% compared to the same month last year, from 24.1 TWh to 19.9 TWh. The temperature correction brings this value to -18.2%. In this case, the reduction affected all market areas in a more marked way, with higher values in percentage in the North and Central North areas (around -20% compared to April 2019) and a reduction in absolute value in the North equal to -2.7 TWh. In the South and Islands areas the maximum reduction in absolute terms (-0.53 TWh) and percentages (-14.7%) was in the Centre-South zone.

In May 2020, the national electricity demand was 22.7 TWh, with a slight increase compared to April 2020 (+12%), but still in decline compared to May 2019 (-10.3%). In particular, starting from the week of 18-24 May, a slow and gradual recovery in the electricity demand is seen, following the reopening of several productions and activities [267]. The average weekly power went from a maximum of 36 GW in the week 02-08 March 2020 (+ 2% compared to the same week in March 2019) to a minimum value of 26.4 GW in the week 13-19 April 2020 (-26 % compared to the similar week of April 2019, which had been in correspondence of the Easter holidays). The week of 6-12 April 2020 was the second week with the lowest average power value (27.4 GW). The average weekly power grew in the following weeks of May, after the partial reopening of 4 May, passing to 30.1 GW in the week 4-10 May 2020 (-13% compared to 33.9 GW in the similar week of May 2019) and 30.7 GW in the week 11-17 May 2020 (-10% compared to 33.9 GW of the similar week of May 2019).

Table 6.2 highlights the impact of the pandemic on the national power profile and it compares the evolution of the electrical situation of the different market areas, in terms of the monthly maximum power, average power and load factor (defined as the ratio between average and maximum power) for the weekdays of April 2019 and 2020, as the most influenced month by the full lockdown. While there is a slight reduction in the load factor for the Centre-South, South, Sicily, and Sardinia areas, meaning a power profile fairly aligned between April 2019 and 2020, for the North and Centre-North areas it has slightly increased, meaning a maximum power value that decreases more than the average power.

Table 6.2. Maximum power, average power, and load factor for the weekdays of April 2019 and 2020 by market zone.

	[GW]	N	CN	CS	S	Sic	Sar
apr-19	Pmax	24,97	4,78	6,49	3,98	2,55	1,13
	Pmed	20,32	3,90	5,22	3,13	1,96	0,91
	u	0,81	0,82	0,80	0,79	0,77	0,81
apr-20	Pmax	19,21	3,53	5,70	3,72	2,48	1,02
	Pmed	16,11	3,02	4,42	2,88	1,85	0,81
	u	0,84	0,85	0,77	0,77	0,75	0,80

The maximum power decreases respectively by 23% and 26% for the North and Central North areas, while by 12, 7, 3 and 9% for the Central South, South, Sicily, and Sardinia areas. The average power decreased by 21% and 23% for the

North and Central North areas respectively, while by 15, 8, 6 and 11% for the Central South, South, Sicily, and Sardinia areas.

The ADLP is evaluated for April 2019 and 2020. Figure 6.4 depicts the ADLP for the North and South zones.

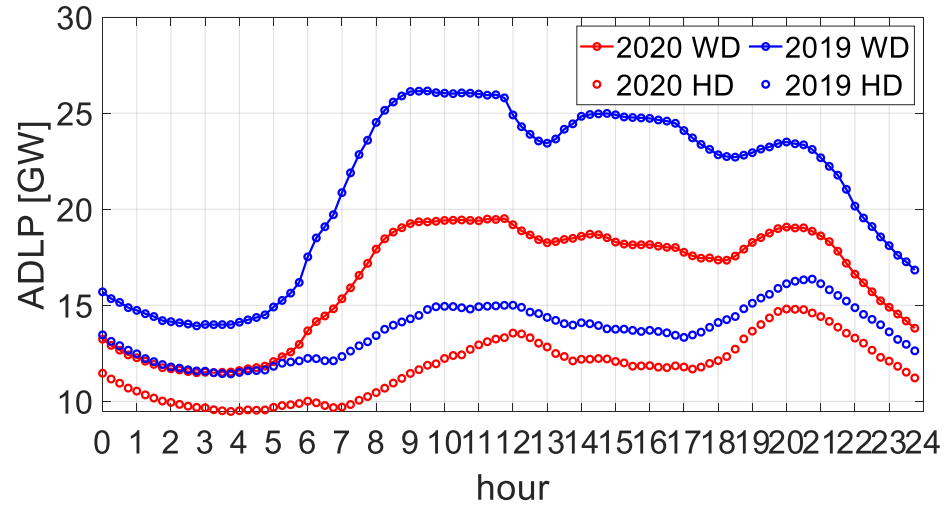

a. North

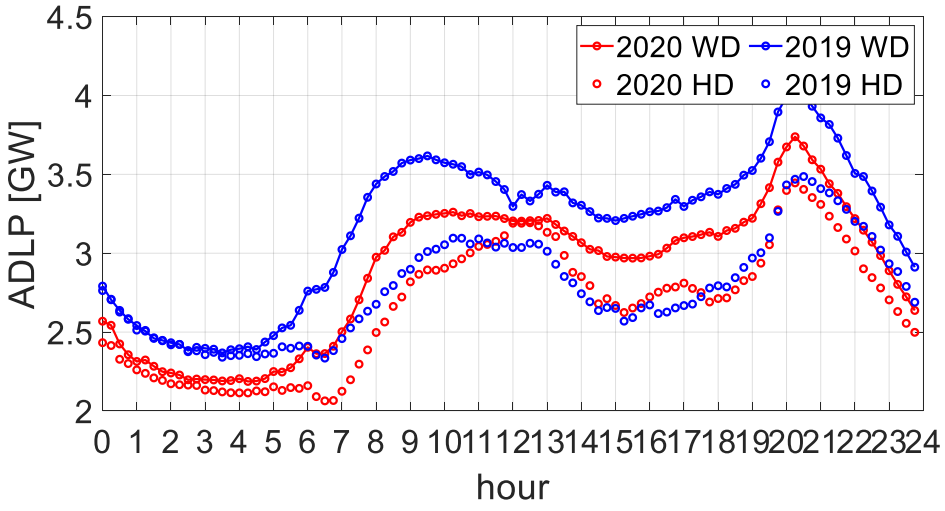

b. South

Figure 6.4. ADLP for North (a) and South (b) zone in April 2019, 2020 [256].

Generally, morning and evening ramps are less steep on holidays compared to working days, due to the distributed timing of the demand over longer periods during holidays (few people getting up at the same time for going to work). In the North, the working days have maintained a certain distance from holidays, both in 2019 and 2020. MR and ER slightly reduced in working days comparing 2019 and 2020. A large demand reduction is noticed in both holidays and working days. In the South, the profiles in 2020 showed a greater similarity approaching the holidays profile in 2019. In this case, there are not evident differences in the morning and evening ramps between 2019 and 2020 and working days and holidays.

The demand reduction is larger for the North, in both weekdays (from 21 to 16 GW) and holidays (from 14 to 12 GW). While in the North the peak load was in the morning for the weekdays of 2019, in April 2020 the distance between the morning and evening peaks weakened, approaching the behaviour of the holidays, which remained aligned between 2019 and 2020. The weekdays morning peak shifted in time from 9 a.m. to 11.45 a.m. and from 26 GW to 20 GW, while the evening peak kept the same time (20 p.m.) but reduced from 23.5 to 19 GW. The difference between the morning and evening peak reduced of -1.5% (2.5 GW vs 1 GW) in April 2020. These variations are lower for South, where the average load changed from 3 to 2.9 GW during weekdays, and from 2.8 to 2.7 GW during holidays. This is mainly due to the different consequences of the lockdown on the productivity of the zones: North is historically more electricity intensive than South, and the stop impacted more those regions.

The load profile metrics are reported in Table 6.3.

Table 6.3. Load profile metrics for North and South market zones of Italy, April 2019-2020.

			Peak Time	$\boldsymbol{ADLP_{MAX}}$	$\boldsymbol{\Delta Peaks}$	$\boldsymbol{ADLP_{ave}}$	**MR**	**ER**
North	WD	2019	9:30	26.16	2.66	21.09	0.45	0.13
		2020	11:45	19.51	0.44	16.35	0.22	0.25
	HD	2019	20:45	16.36	1.36	13.68	0.11	0.21
		2020	20:00	14.81	1.25	11.73	0.12	0.34
South	WD	2019	20:15	4.03	0.42	3.17	0.05	0.07
		2020	20:15	3.74	0.48	2.89	0.04	0.07
	HD	2019	20:30	3.49	0.39	2.78	0.05	0.08
		2020	20:15	3.45	0.25	2.67	0.05	0.08

6.3.2 Impact on the generation mix

The national generation mix is analysed comparing April 2020 and 2019, as the most influenced month by the full lockdown. The monthly thermal generation decreased from around 13 TWh to 9 TWh, with a 53% share in April 2019 and 46% in April 2020. Hydro increased from 3.2 TWh to 3.6 TWh, with a share of 13% in April 2019 and 17% in April 2020. Wind and PV production increased slightly, from 3.2 TWh in April 2019 to 3.5 TWh in 2020. It is interesting to observe the reduction of about 70% in net foreign exchanges, with 2.5 TWh in April 2019 compared to 0.8 TW in the same month of 2020. Figure 6.5 compares the coverage of national needs by source for the month of April 2019 and 2020, with evident reduction in demand, net foreign exchanges, and the increase in the share of PV and wind power in April 2020 compared to 2019. In particular, the monthly demand in April 2020 was covered for the 47% by RES, with +7.5% compared to April 2019. The maximum hourly coverage of demand by RES in April 2019 was 67% (April 27, 2019 at 1 pm), while 76% in April 2020 (April 25, 2020 h13), with a total generation from RES equal respectively to 19.6 GWh and 19.2 GWh, distinguished between geothermal (0.7 GWh), hydroelectric (4.8 and

4.1 GWh), PV (10.2 and 11.1 GWh), and wind power (2.5 and 2 GWh) on a total demand of 29.4 and 25.2 GWh. In both cases, thermoelectric production is attested at around 9.5 GWh.

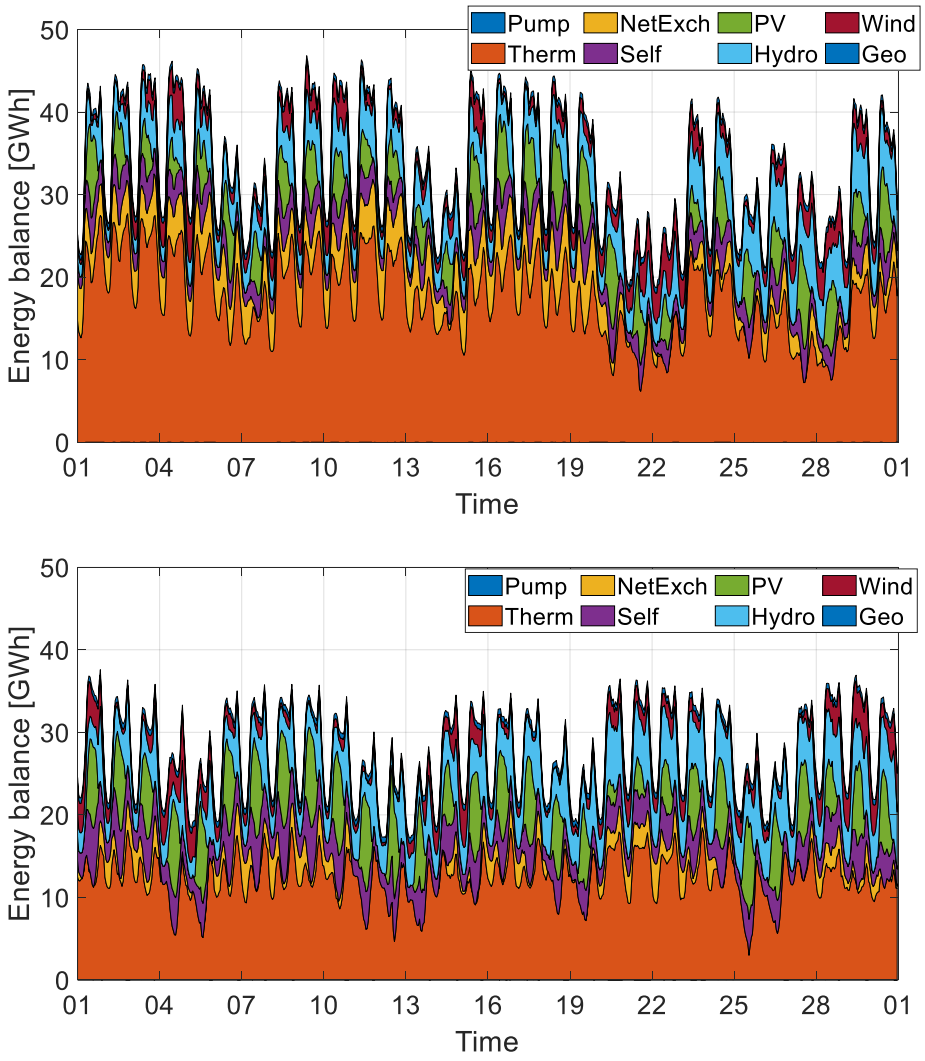

Figure 6.5. National generation mix (April 2019 and 2020) [256].

In May 2020, the electricity demand was covered for the 51% by RES (+11.9% compared to May 2019). The demand reduction during the lockdown and the growing non-conventional generation led to a drastic drop in energy imports across the foreign border. Reducing import is necessary to keep thermal generation on to balance and secure the system. On the north border, in April 2020 there was an average hourly physical exchange in imports of 1541 MWh, a decrease compared to 3962 MWh in the same month of 2019. The decrease regards all foreign trade, particularly with Switzerland (-1373 MWh, from 1688 to 315 MWh), with France (-332 MWh, from 1394 to 1062 MWh) and Slovenia (-665 MWh, from 714 to 49 MWh). Considering the total of foreign exchanges, Figure 6.6 shows an inversion of flows from Italy to abroad for about 30% of the hours of April 2020. The reduction of imported energy was 70% (equal to about 1.7 TWh) in April 2020 compared to last year, while in March 2020 there was a

slight increase in total imported energy, from 3.8 TWh in 2019 to 3.9 TWh in 2020, due largely to higher imports in the first half of March 2020.

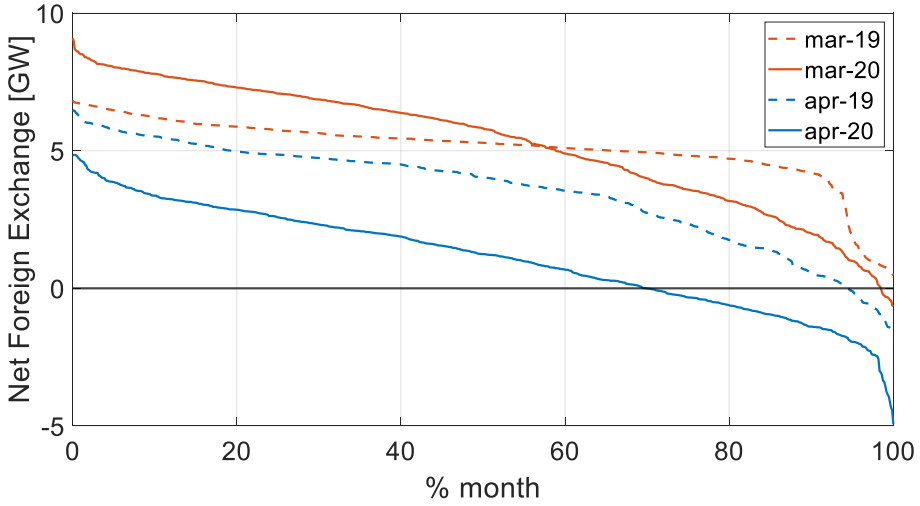

Figure 6.6. Duration curve of the total exchanged power in March and April 2019 and 2020 [256].

The non-conventional penetration index γ was calculated hourly for the months of March and April in 2019 and 2020 and reported in Figure 6.7 as a duration curve. While in March 2019 and 2020 comparison there is no noticeable difference in the maximum values, but a decrease in the minimum values in 2020, an increase in the non-conventional penetration is visible in April 2020 compared to the same month of the last year. In particular, the maximum value grows from 0.47 to 0.52, with more than 60% of the month higher than in 2019.

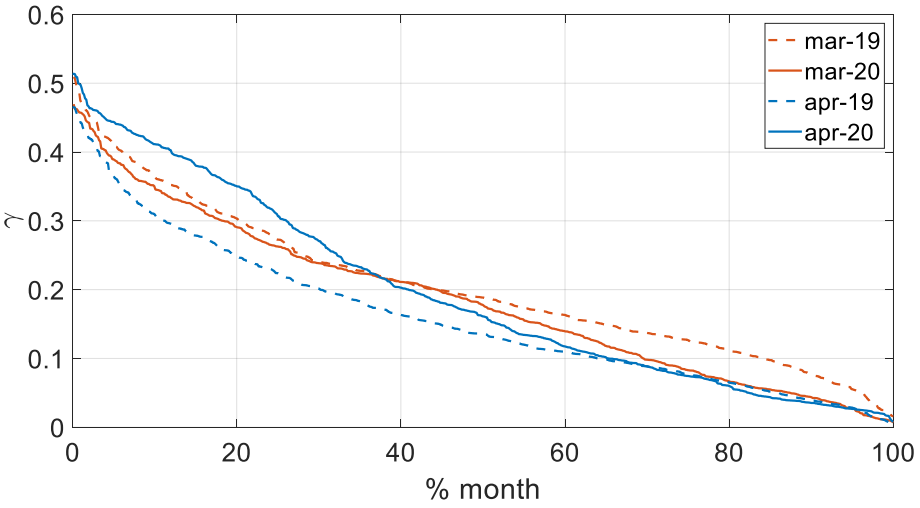

Figure 6.7: Hourly duration curve of the non-conventional penetration index for March and April 2019 and 2020 [256].

6.3.3 Impact on the electricity markets

The performance of different electricity markets in terms of prices and quantities was analysed globally for the months of January, March, and April 2018, 2019 and 2020.

The data are taken from the Italian Market Operator (GME) transparency platform [268]. All electricity markets (MGP, MI, MB MSD) were affected by the reduction in volumes, from a maximum of 23% for MI to a minimum of 18% for MGP, except for the MSD which saw a 77% increase in volumes treated. In general, all markets have seen price cuts from 54 to 23%.

The demand reduction has effects mainly on the market, having a direct consequence in the reduction in thermal generation due to its higher positioning in the order of economic merit than renewable, with a reduction in energy prices in the Day Ahead Market. The health emergency therefore accentuated the typical seasonal market dynamics of the months of March and April, characterized by annual minimums in terms of quantity and prices.

In the DAM the PUN (National Single Price) had a strong reduction in 2020 compared to 2019. In April 2020 there was a 53% reduction compared to the same month last year, down by 7.2 €/MWh on the previous value of March 2020 and reaching the lowest level ever recorded since the start of the electricity exchange, equal to 24.81 €/MWh [269]. The quantities treated in the MGP also decreased progressively in the months of March and April 2020 compared to the same months of 2019, with reductions of 10% respectively (24.57 TWh in March 2019, 22.09 TWh in March 2020) and 18% (22.39 TWh in April 2019, 18.42 TWh in April 2020). Figure 6.8 shows the prices and volumes in the MGP comparing the years 2019 and 2020 from January to April.

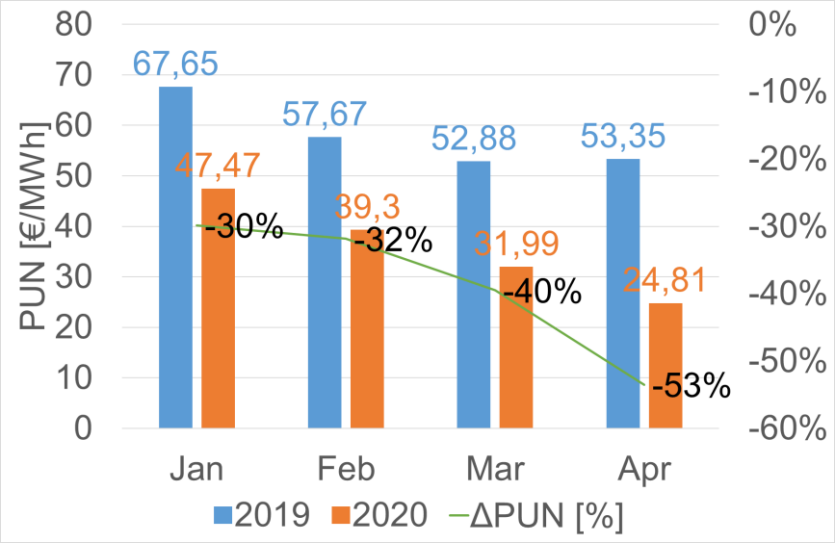

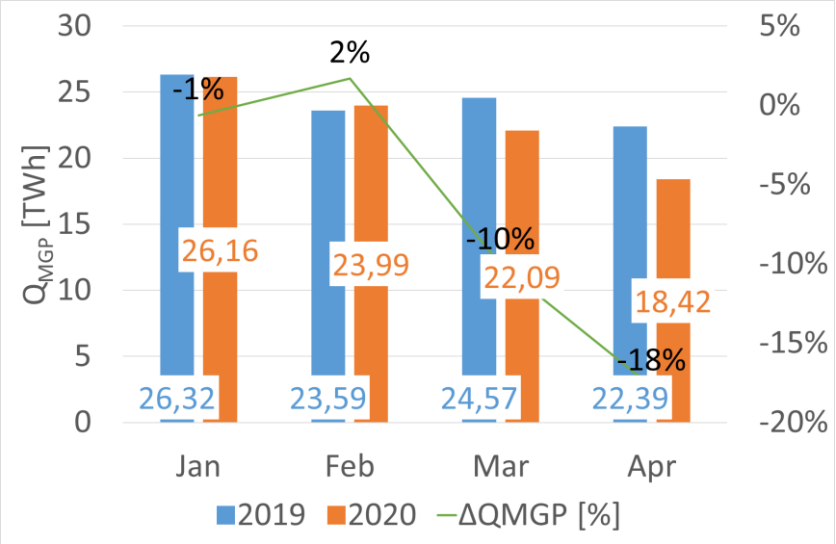

Figure 6.8. PUN and overall volumes on the Day Ahead Market (January-April 2019, 2020) [256].

The price reduction also affected the main neighbouring markets, also at historic lows and characterized by negative values in some hours of the month (on Easter Monday the daily price stood at -6.5 €/MWh in France and -13 €/MWh in Germany). In the context of demand contraction, the consequent reduction in the inter-zonal congestions led to decreasing differentials between the prices of the national market areas in March and April 2020, compared to the same months of last year, with a standard deviation going from 4.2 €/MWh to 0.75 €/MWh between March 2019 and 2020 and from 4.8 €/MWh to 0.56 €/MWh between April 2019 and 2020 (Figure 6.9).

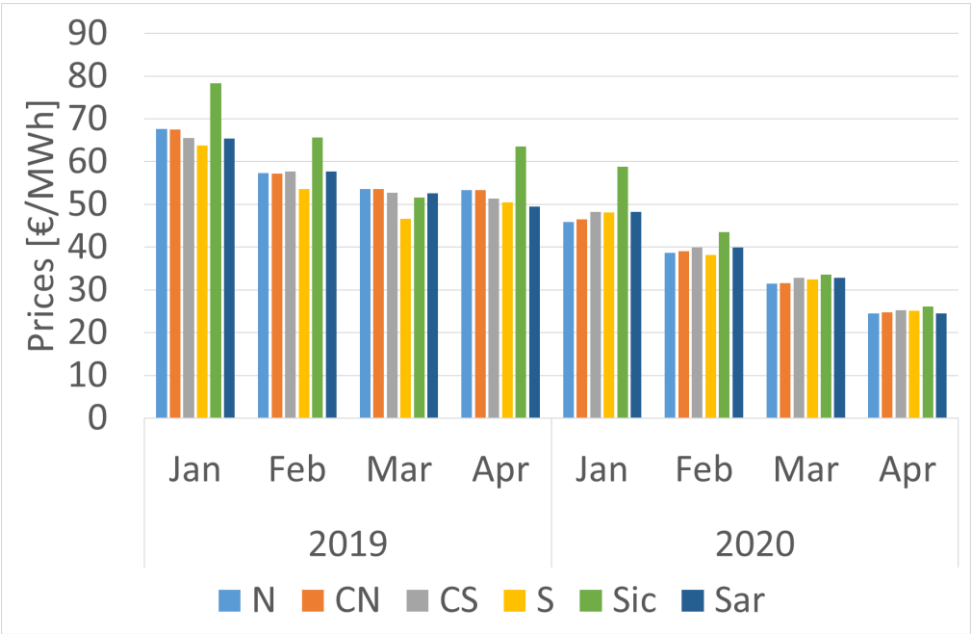

Figure 6.9. Italian zonal market prices for the Day Ahead Market (January-April 2019, 2020) [256].

The maximum price differential was 14 €/MWh in April 2019 and dropped to 1.6 €/MWh in April 2020. It is noticeable the proximity of prices between South

and Sicily, the latter generally characterized by the highest selling prices, which occurred both in March and April 2020, compared to March 2019 alone. In particular, the South-Sicily transit was congested only in 6% of the monthly hours in April 2020, compared to 35% of the hours of April 2019.

The historical minimums for the average purchase price were also reached in the seven sessions of the Intra-day Market in April 2020, equal to 24.9 €/MWh, with an inflection of 53.7% compared to the same month last year, and a reduction of 22% compared to 32.0 €/MWh in March 2020 [269].

In the examined context, there is an increase in the volumes purchased and sold in the ex-ante Dispatching Services Market (MSD), with values among the highest for over a decade. Figure 6.10 shows the total quantities in MSD for the months of January, March, and April, divided between purchases and sales, for the years 2018, 2019 and 2020. It is observed that typically the spring months are confirmed as those with the greatest movement in volumes, also being the months where the largest share of generation from non-programmable renewable sources is concentrated. In particular, the further uncertainty due to the prolongation of the COVID-19 pandemic, and the consequent needs in terms of security, have increased volumes in 2020. In detail, in April the total purchases were equal to 1.2 TWh (+118% compared to April 2019), and sales stood at 1.6 TWh (+52% in April 2019), while in March total purchases were equal to 1.1 TWh (+109 % compared to March 2019), and sales stood at 1.3 TWh (+43% in March 2019).

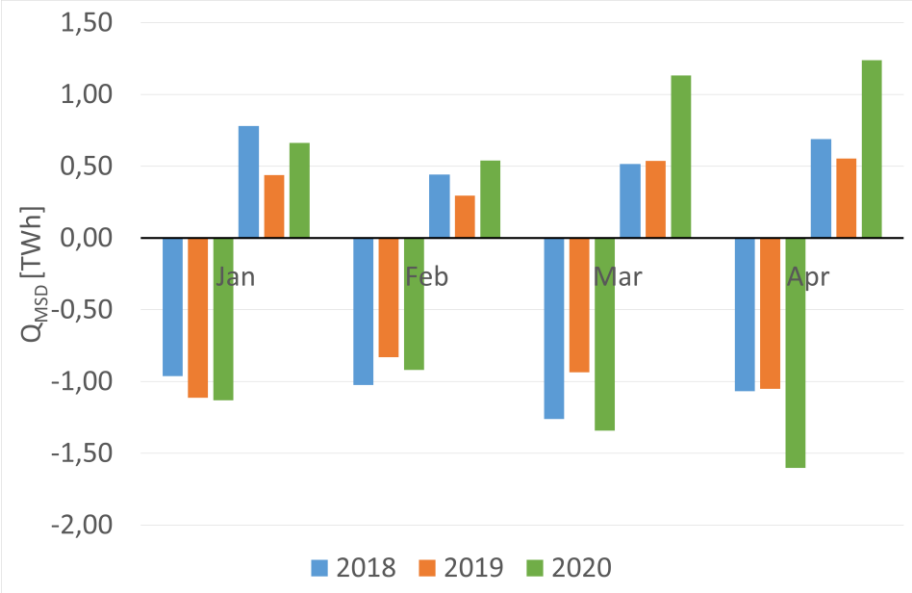

Figure 6.10. Purchased and sold volumes in the MSD for the month from January to April 2018, 2019 and 2020 [256].

The greater movement in volumes leads to a decrease in prices in €/MWh also in MSD. However, total costs increased both in March and April 2020 compared to the same months of last year, going from 99.7 million euros to 109.6 million euros between March 2019 and 2020 (+9.9%), and from 203.1 million euros to 254.9 million euros between April 2019 and 2020 (+25.5%).

6.4 Pan-European Impacts

A comparative analysis is conducted at the European level considering a selected number of countries, namely France, Spain, Germany, and Sweden. The load data of the EU countries are taken from the ENTSO-E Transparency Platform [270].

6.4.1 Power profiles and demand under pandemic

In April 2020, the consumption for EU countries was 181 TWh, compared to 207 TWh in April 2019; therefore, the power consumption in the EU dropped of around 26 TWh, around -12.6%. Largest demand reduction happened in France (-18.9%), Spain (-16.9%), UK (-15.2%), Belgium (-13.3%), The Netherlands (-12.0%) among the countries with monthly energy demand higher than 5 TWh. On the other side, a light reduction or even an increase in the demand was noticed in countries which did not imposed very strict lockdowns and where the industrial production was kept on. This is the case of the Nordic countries, Norway (+5.3%), Sweden (-0.3%), Finland (-0.9%), and Switzerland (+0.3). In Figure 6.11 the calendar-adjusted load profile for a selected number of countries is depicted, starting from the first Monday of March to the last Sunday of May of 2020, and comparing it with the analogous days of 2019.

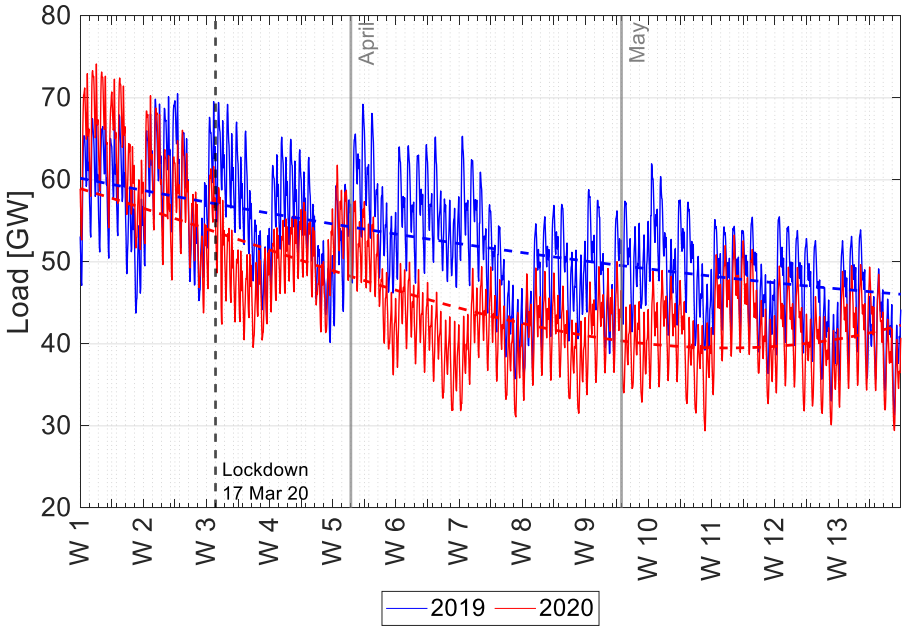

a. France

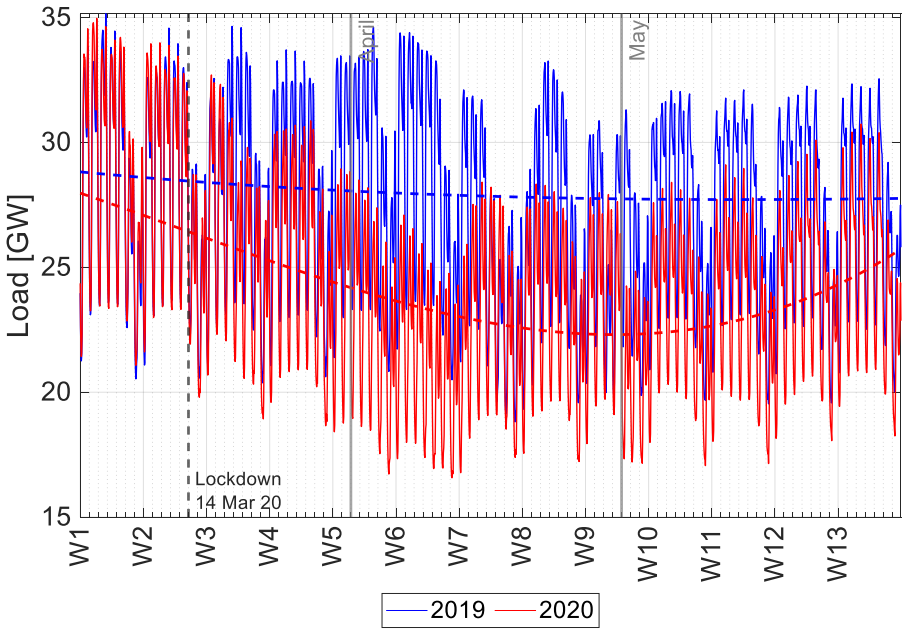

b. Spain

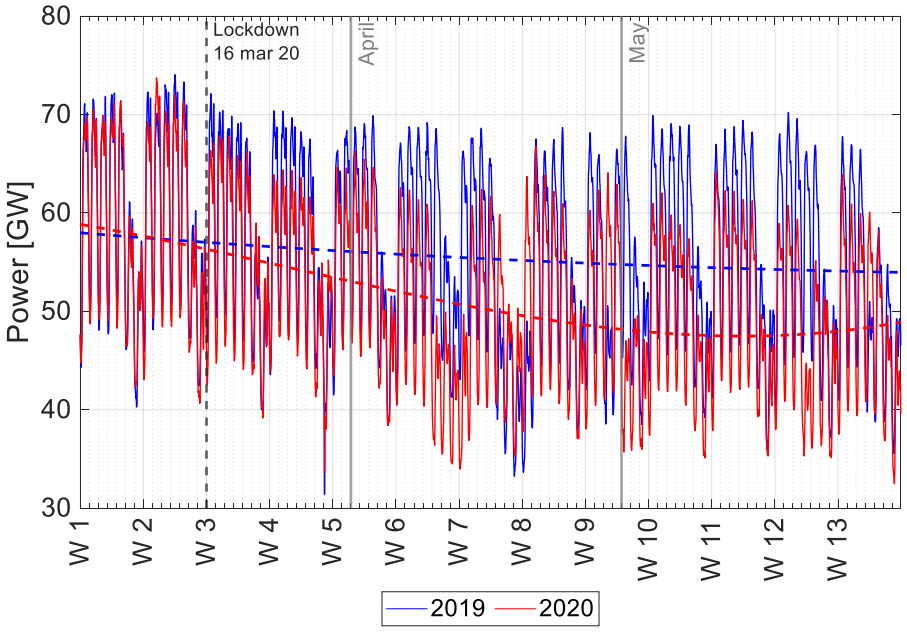

c. Germany

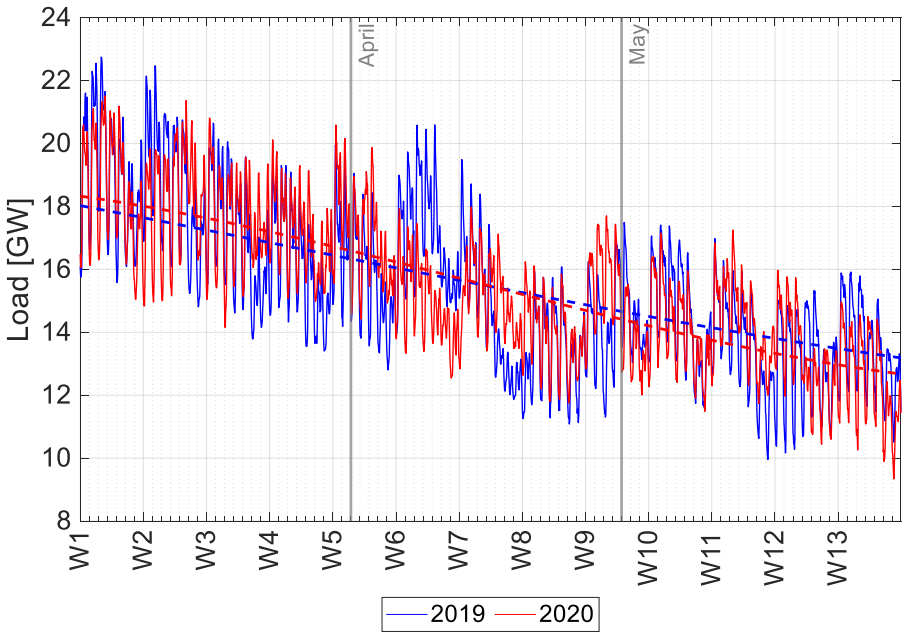

d. Sweden

Figure 6.11. Weekly power profile during pandemic for selected countries [265].

For Spain, the temperature corrected demand reduction in April 2020 moves from 16.9% to -16.2% and for Germany from -8.3% to -8.0%, while for France changes from to -18.9% to -11.6%, due to the higher temperature variation (+2.5°C average in 2020 compared to 2019).

Figure 6.12 shows the ratio between the 2020 and 2019 electrical demands in the period from the first Monday of March to the last Sunday of May for a selected number of countries, plotted as a duration curve.

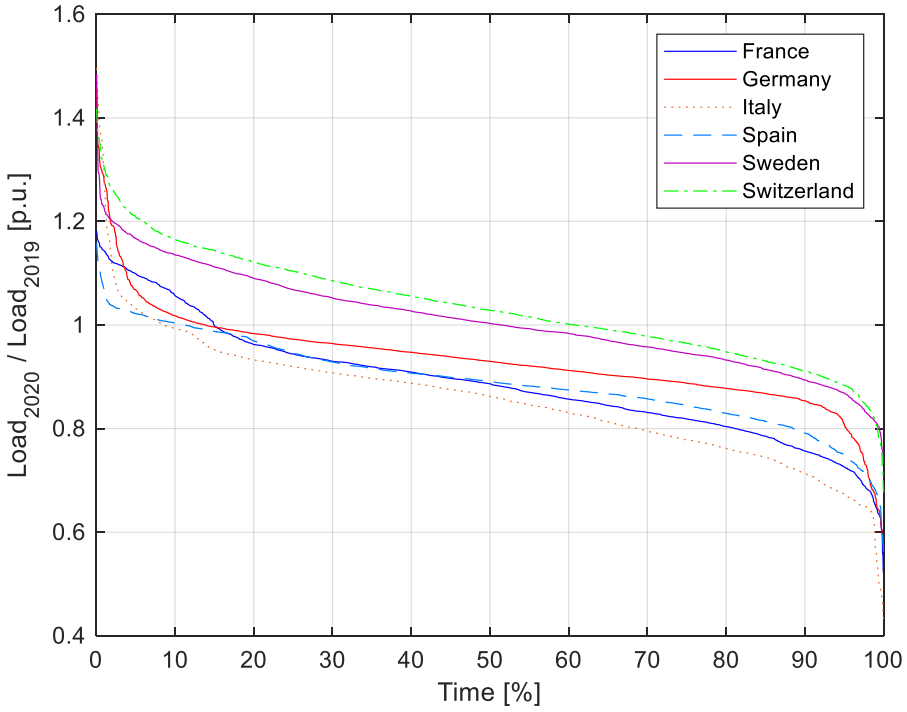

Figure 6.12. Duration curve of the ratio between the 2020 and 2019 power demand for a selected number of countries [265].

The curves represent the time-percentage in which the ratio D_{2020}/D_{2019} was equal or higher than the corresponding value on the y-axis. Italy was the country where the demand reduction was higher (the minimum value of the ratio is equal to 0.43 p.u.) and longer in time (for around 90% of time, the ratio is lower than 1). Vice-versa, Sweden and Switzerland had a ratio greater than 1 for more than 50% of the time due to the mild measures adopted to avoid the widespread of the virus.

For the EU countries most affected by the lockdown, the ADLP has been very different from usual. The gap between the morning and evening peak lifted in 2020 compared to 2019. The working days of 2020 are very similar to the weekends of 2019. The working day $ADLP_{max}$ shifted in time, from morning to evening for The Netherlands, Slovenia, Luxembourg, UK, and to lunch time for France, Austria, Belgium, Bosnia, Czech Republic, Slovakia, Lithuania, and Greece. For all the other countries, the peak time did not change. The working day $ADLP_{max}$ diminished for almost all the countries, with reductions higher than 15% for Luxembourg (-24%), France (-17%), Spain (-15%), Belgium (-15%) and Bosnia (-15%). This trend makes the working day ADLP quite similar to the holiday ADLP of April 2019, both in terms of timing, values and ramps. In the case of strict lockdown, the morning and evening ramps (MR, ER) are less steep on working days 2020, comparable to the holidays in 2019 (MR -48% for France in WD). The reason is probably that loads had been distributed over longer periods due to the smart working practices. During holidays in 2020, ADLP presents lower slopes compared to 2019. In the context of high production from PV, the evening ramps are noteworthy, as they are accentuated by the simultaneous increase in residential load. Nevertheless, some countries saw noticeable reduction in power values but not in ramps, as Germany (-7% in $ADLP_{max}$, -5% in MR), so they have similar shapes but reduced values. For countries without strict lockdown, the $ADLP_{max}$ lightly increased from April 2019 to 2020, as in the case of Switzerland (+2%), Montenegro (+3%) and Norway (+1%).

In summary, the behaviour of the ADLP in the case of strict lockdown exhibited working days in 2020 very similar to holidays in 2019, and holidays in 2020 with lower values and ramps compared to holidays in 2019. Figure 6.13 represents the ADLP for a selected number of countries. It is noticeable the drastic changes in the ADLP for Spain and France, in terms of timing, peak values and ramps. The changes are less evident for Germany and Sweden, which kept the same ADLP shape and in the latter case with similar values.

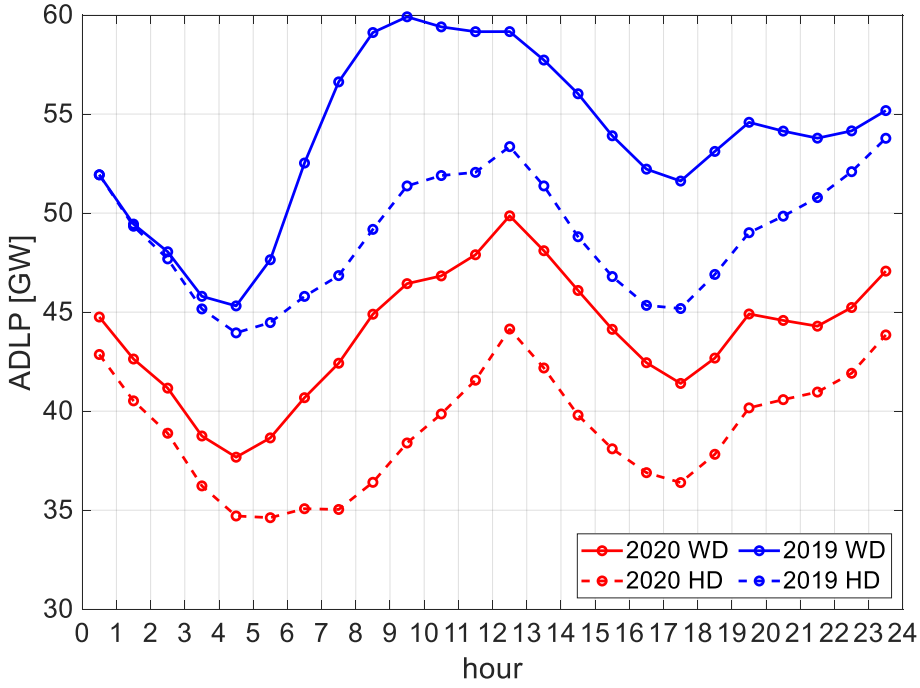

a. France

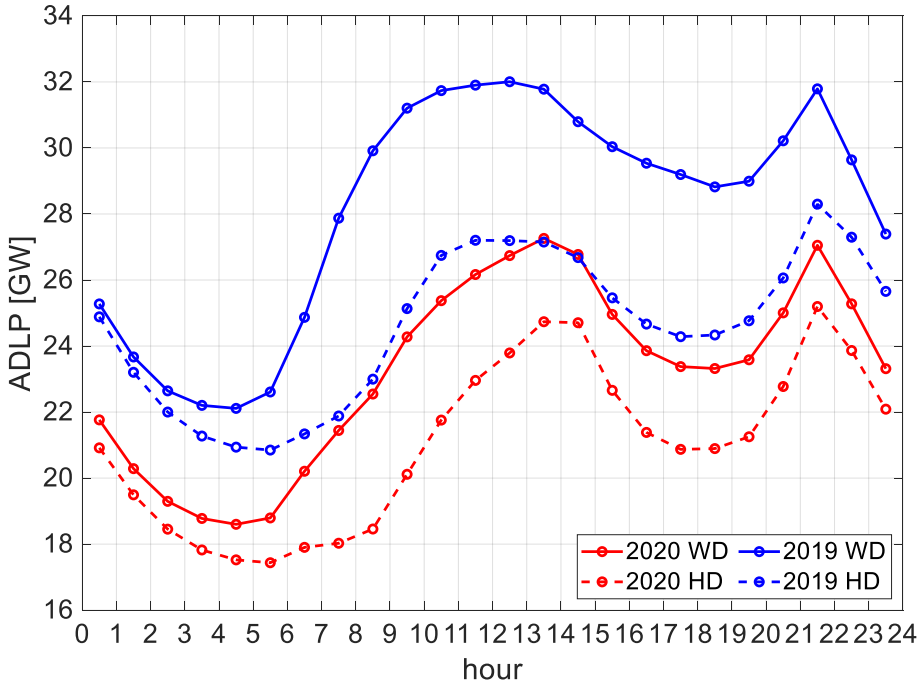

b. Spain

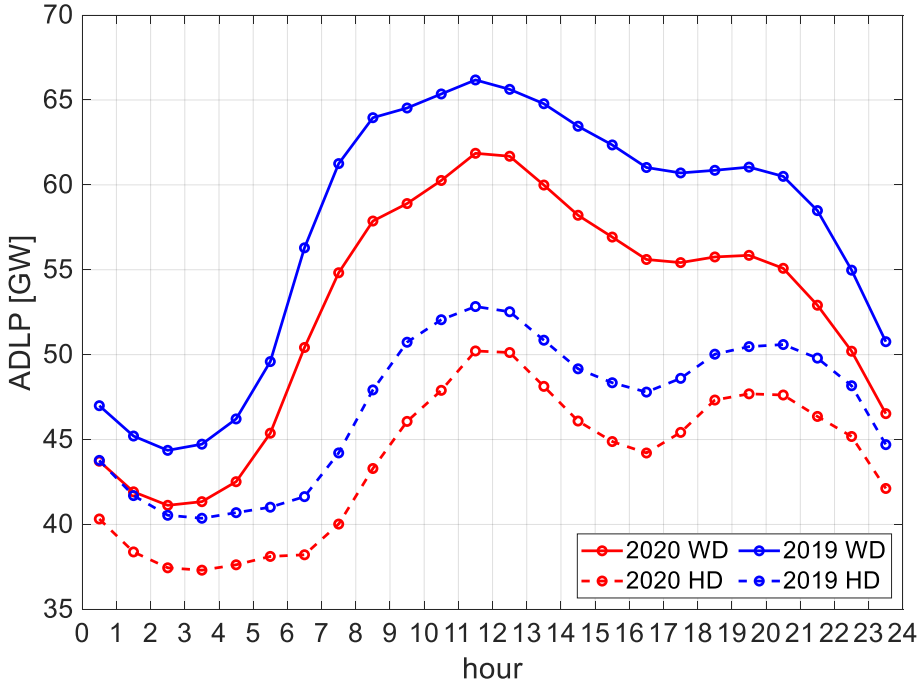

c. Germany

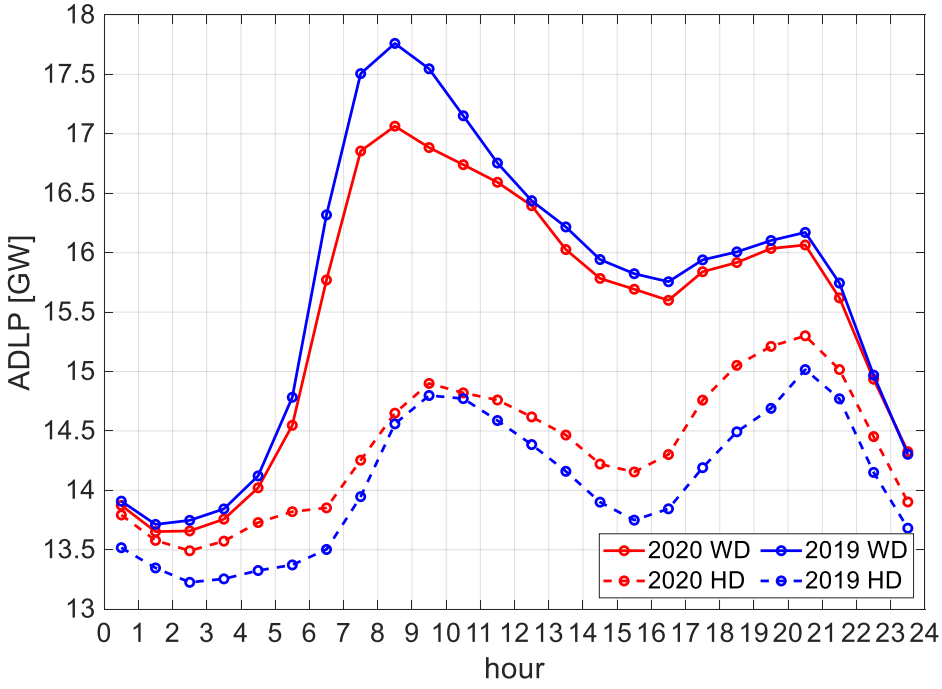

d. Sweden

Figure 6.13. ADLP for the selected countries [265].

6.4.2 Operational issues

Conventional generation decreased in all countries, except Bosnia, North Macedonia, Norway, and Finland. The greater fall was in Germany (-28.7%), UK (-25.4%), Italy (-18.3%), Belgium (-16.4%), France (-15.0%), Poland (-14.1%) and Spain (-10.7%) considering the countries with demand higher than 5 TWh.

Among such countries, only Norway (+24.8%) and Finland (+1.3%) saw an increase of conventional generation. This translated into a high share of non-conventional generation, except for Spain (-11.1%) and UK (-0.8%). Figure 6.14 compares the coverage of national electricity demand by source for the month of April 2019 and 2020 for Spain, where the fossil generation decreased from 5.8 TWh to 3.8 TWh (24% of the total share in April 2020) and Germany, where the fossil generation decreased from 16.4 TWh to 9.3 TWh (26% of the total share in April 2020).

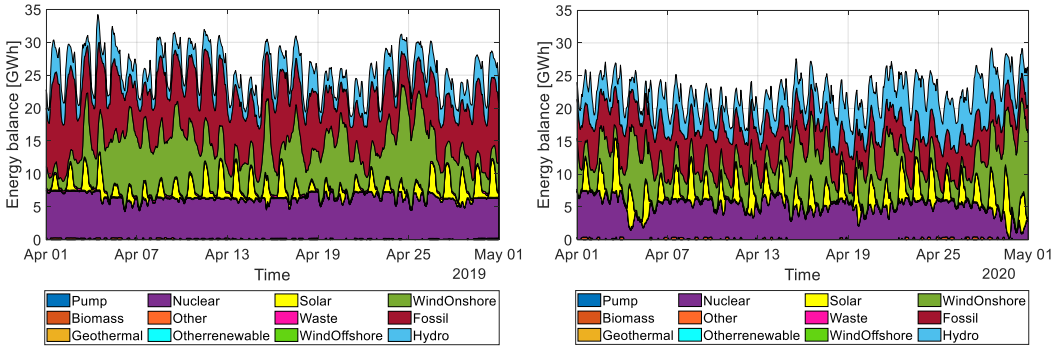

a. Spain

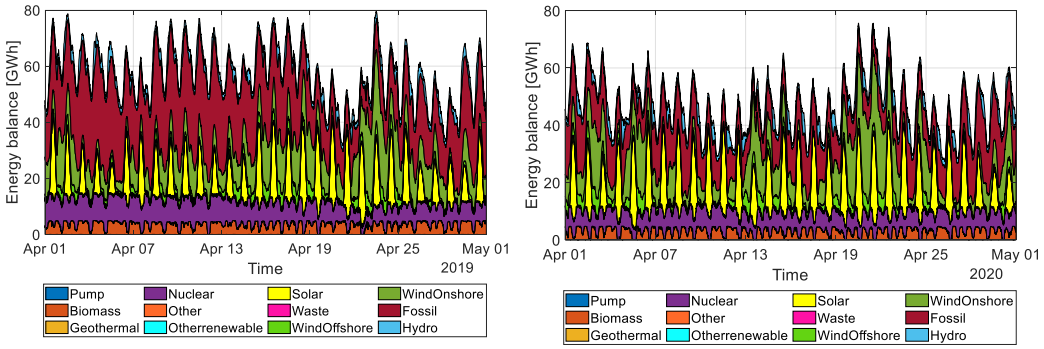

b. Germany

Figure 6.14. Load coverage by source for a) Spain, b) Germany [265].

The γ index is calculated hourly for the months of March and April in 2019 and 2020 and its duration curve is reported in Figure 6.15.

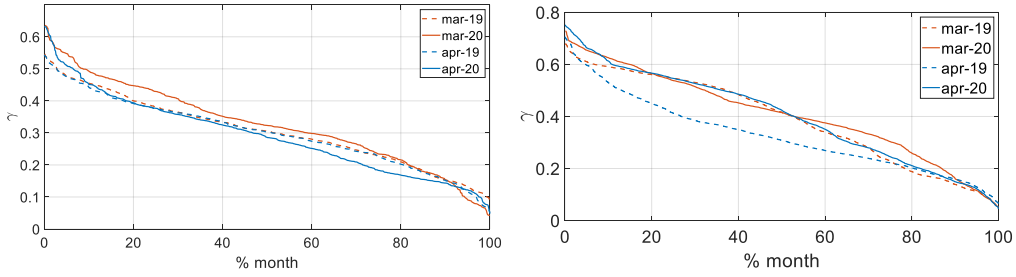

a. Spain b. Germany

Figure 6.15. Duration curves of non-conventional penetration index for a selected number of countries [265].

While in the March 2019 and 2020 comparison there is no noticeable difference in the maximum values for all the selected countries (expect for Switzerland), an increase in the non-conventional penetration index is visible in

April 2020 compared to the same month of the last year. The increase is not as dramatic as one would have expected from the situation post pandemic. For Italy, the maximum value grows from 0.47 to 0.52 in April, while for France from 0.26 to 0.30, for Germany from 0.71 to 0.75, for Spain from 0.54 to 0.63. However, all countries had higher values in April 2020 compared to 2019 for more than 60% of the month, except Spain.

6.4.3 Electricity markets

Historical time series of day-ahead spot prices are analysed for the first half of the year (from January 1st to June 30th) from year 2015 until 2020. The analysed time series start in 2015 as this year marks the launch of the EUPhemia combined market clearing at the European level and the entry into force the legislative basis for European cross-border electricity day-ahead market exchanges (the Regulation on Capacity Allocation and Congestion Management).

The metrics described in Section 6.2.3 to evaluate the immediate impact of the COVID-19 pandemic on the electricity markets are applied on the pan-European DAM. Data have been gathered thanks to the European Power Exchanges, provided directly or through Platts® database to the European Commission – Joint Research Centre. Data for the forecasted day-ahead load per bidding zone were collected through the ENTSO-E Transparency Platform when available, and in the few cases when the data were not available actual load per hour was used instead.

First, the effect of the pandemic on wholesale European prices (€/MWh) trend is single out for the last five years before the 2020 using the load-weighted weekly moving average $\overline{(DAMp_h)}$. Figure 6.16 shows that since mid-March the prices for 2020 decreased more than the previous years, even comparing with the 2016 characterized by lower oil price [271]. This finds a quite exact concurrence with the time (mid-March) when widespread lock-down measures have been adopted almost everywhere throughout Europe. Prices in the pan-European DAM started to recover only since the beginning of June 2020, with the almost total release of lock-down measures.

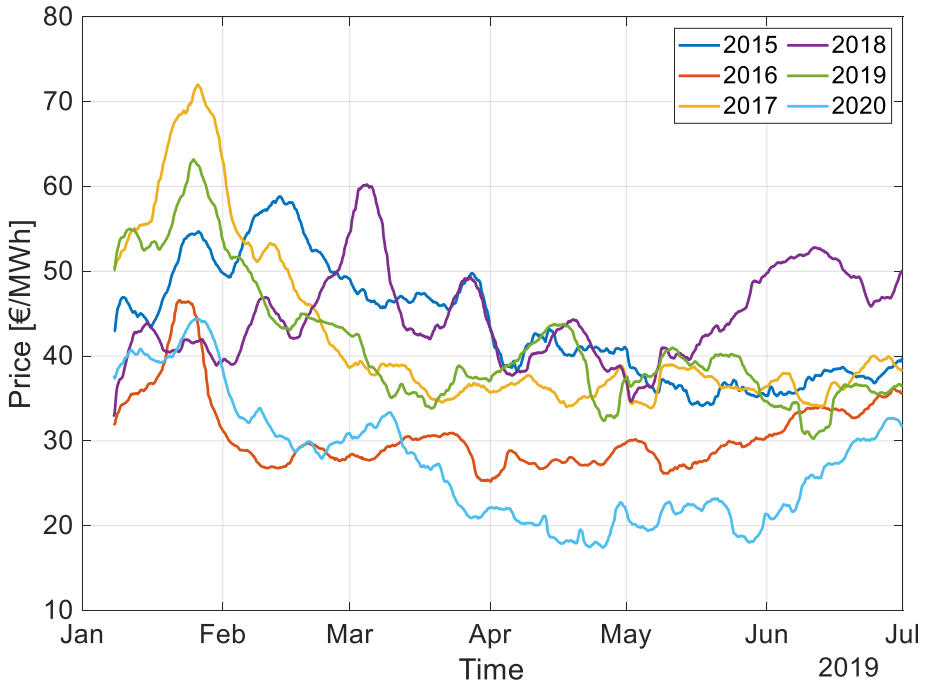

Figure 6.16. Pan-European load weighted moving average of all bidding zones [265].

The stark contrast of price dynamics in 2020 w.r.t previous years is even clearer looking at the box plots in Figure 6.17, which depicts the cumulated observations during each year. On each box, the central mark indicates the median, and the bottom and top edges of the box indicate the 25th and 75th percentiles, respectively. The whiskers extend to the most extreme data points not considered outliers, and the outliers are plotted individually.

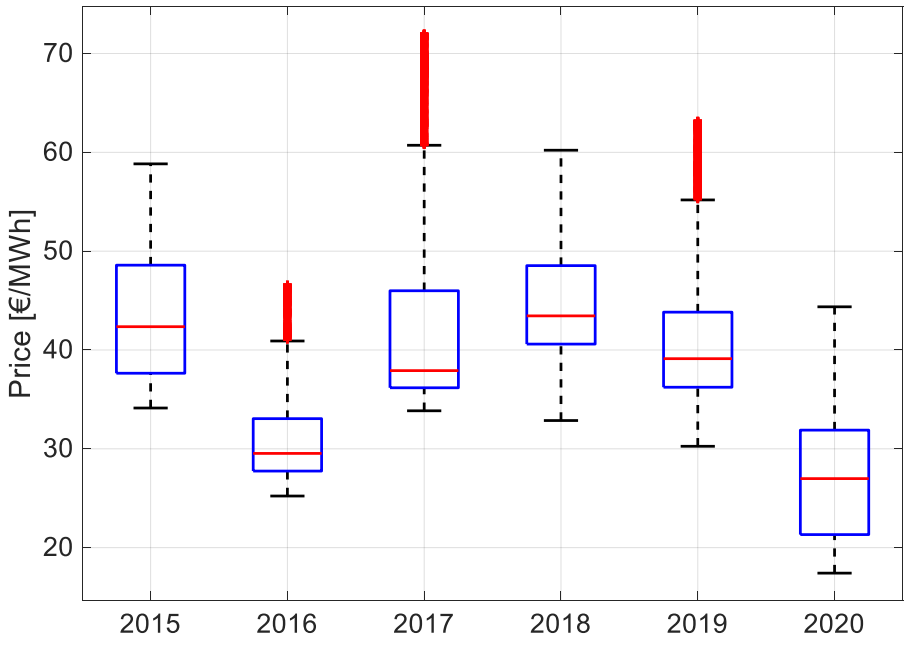

Figure 6.17. Load-weighted weekly moving pan-European averages of the DAM prices across the selected years [265].

From Figure 6.17, it is possible to infer how deeply the pandemic hit electricity markets in Europe: prices have plummeted in the first 6 months of the year 2020 w.r.t previous years, pointing to the fact that the sharp decrease in demand has been directly translated into lower market prices in the DAM.

In general, there have been big reductions in the DAM prices for all analysed countries and for the considered months in 2020 compared to the same months in 2019. Starting from the end of February, the day-ahead price decreased in many of the analysed countries. The minimum value of the respective trends for many of the represented countries occurred around mid-April. Another minimum happened about mid-May, after a recrudescence of the pandemic swept again the country with two new peaks of cases on May 1st and May 7th.

In detail the average reduction in prices in March 2020 for all analysed countries has been -44% compared to the same month in 2019. In April 2020, the average prices have reduced even further by -60% compared to April 2019 and by -57% in May 2020 compared to May 2019. Surprisingly, the largest reductions in DAM prices were in the Nordic countries (Sweden and Norway) with Norwegian prices in April 2020 reduced by -89% compared to April 2019.

6.5 First assessment and lessons learnt

The COVID-19 spread and the associated consequent socio-economic and health related prevention and protection measures have impacted all the energy and electrical systems. The most immediate effects regarded the power consumption levels, the generation mix structure and the electricity market price. The European countries adopted different mitigation and protection strategies, some implemented more stringent containment measures (e.g., Italy, France, Germany) whereas others followed lighter approaches (e.g., Sweden). In the former group, due to the modification of social habits and the closure of factories, electrical energy consumption decreased by about 15% compared to the previous years and changes in the load profile could be observed. In the latter group, no significant changes in the consumption occurred.

In general, risks for the system are greater in the case of demand increase, a situation in which there may be a lack of redundancy in the generation and greater stress on the infrastructure. From the point of view of system operation, the decrease of the electricity demand resulted in a reduction of the conventional generation for countries where a severe lockdown was imposed. This led to an increment of RES generation over the total one. An increase of the non-conventional generation amplifies the operational challenges and the need for regulation capabilities in terms of keeping frequency stability and procuring resources for the voltage regulation. The impact on the electrical market is twofold: on one side, the load reduction eliminated the need for the most expensive conventional power to balance the demand in the day-ahead market, resulting into lower electricity market prices. On the other side, the transmission

system operators had to promptly dispatch conventional units, whose services are acquired from the ancillary service market, leading to an increase of the cost for ancillary services.

Future works will investigate in detail the impact on the ancillary services markets and the consequent implications on security, following the current evolution of the pandemic and the related containment measures. Nevertheless, with Europe willing to drastically reduce carbon emissions down to net-zero within 2050, power from RES will grow even further. The immediate impact of COVID-19 on the European Electricity Systems revealed already a foretaste of this future.

Chapter 7

7 Conclusions

PEIG brings a level of variability and uncertainty never seen before by the system operators. Their integration in unsuitable grids is representing the basis for the disruption of the electricity landscape, with the need to rethink to our system in a smarter and more flexible way. The objective is to transform this challenge into an unprecedented opportunity for research, institutions, and utilities to clean the electricity system keeping the traditional levels of quality, security, and stability. A first step is to develop methodological frameworks to assess the PEIG impact by exploring, applying, adapting, and combining the main methods, tools, and solutions.

This Ph.D. dissertation addressed different challenge in the field of frequency stability assessment in modern and future power systems with low inertia. While many approaches have been developed, an overall structured methodological framework is needed to correctly face such issue.

First, a set of tools to estimate and calculate the inertia and parameters to quantify the frequency performance was defined and implemented. A dynamic aggregate model was developed, including the system inertia, the equivalent power plant transfer function for synchronous generators, the load damping and primary, secondary and tertiary control models. The aggregate model was validated against real past events and adapted to assess several case studies with different size, timescale, and objectives, ranging from contingency analysis, normal operation and dynamic behavior in the market unit commitment.

The aggregate model can answer questions evaluating the main frequency performance indicators. It is fast enough to be implemented online for security contingency studies and to carry out extensive parametric studies for system planning purposes. Moreover, the model provides an understanding of the way in which important system parameters affect the frequency response. This

understanding is difficult to achieve from high-order models, where many system variables are influent for the system. The aggregate model is the basis in the frame of a novel methodology to reproduce frequency fluctuations and to study the normal operation in a two-step process (forward and reverse). The results are satisfactory and depend on the accuracy of dynamic parameters and behaviour of generators and loads, as well as on the system variable estimation, which in turn depends on the quality of the measurements coming from the system.

The impact of SyCs, HVDC and BESSs on the frequency performance was investigated simulating the reference contingency both in over and under frequency in low inertia scenarios. shows the importance of the reserves and the frequency-power dynamic of the HVDC was shown. The BESSs contribution was divided in primary and inertial control and its accurate dimensioning was ensured using an Equivalent Saturation Logic, which imitates the behaviour of synchronous generators. The results show that both SyCs, HVDC and BESSs can improve the frequency response. The importance of power reserve is emphasized to control the frequency deviation, while inertia is preeminently in containing the initial ROCOF. For the BESS, the division of half band for inertial and primary control emerges as the most promising solution. It is shown that the implementation of virtual inertia alone is not enough, and a fast-primary response is needed at the same time. The impact of BESSs was explored during the normal operation as well, and strictly depends on the characteristics of the services and of the frequency signal itself. In normal day oscillations, the virtual inertia control is not effective in containing the frequency oscillations, the participation of the BESS in the primary control improves lightly the frequency signal while the secondary is the most useful service. Typically, frequency dynamics are characterized by cyclical slow components, therefore it is expected that slower services such as the secondary are more effective in decreasing the oscillations, while in the case of fast changes, as sudden contingencies, virtual inertia, and the primary are more important.

In the context of large power systems, the reference incident does not imply concerns for the overall frequency stability of large synchronous system compared to the eventuality of system splits. This is the reason for the development of a methodology to identify large power system splits in subsystems and to evaluate their frequency stability using a system split indicator. The system is considered composed of market zones, and all the possible separations in two synchronous areas are found using a graph approach. Results show interesting findings to identify possible dangerous split lines to monitor already in the planning phase. It is shown that ROCOF values above 2 Hz/s could be verified across the spectrum of system split cases and in subsystem areas with load size larger than 20 GW.

Multiple frequency stability security constraints were implemented in the power plant unit commitment and evaluated in a techno-economic view, analyzing costs and dynamic performance, with a total of eight different alternatives that can be easily implemented and interpreted for practical scopes. A MCDA process has been outlined to select the best compromise solution, with a

parametric analysis on the choice of the decision maker's weighting factors. This method can be easily managed by a decision maker, giving the possibility to use different weights for security and cost importance.

Finally, the COVID-19 pandemic is highlighting the importance of the energy sector analyses to assess the immediate impacts of the restrictive measures following the spread of the pandemic. Energy consumption and economic development have always been linked to each other, and these analyses will also be able to determine if and when it will be possible to recover from the current economic crisis.

All the case studies provided numerical evidence to results and offered a background to assist system operators, researchers, and decision-makers in managing and planning future power systems. In sum, it is indeed possible from the thesis to derive insights to assess several case studies with different size, timescale, and objectives, ranging from contingency and system split analysis, normal operation, dynamic behavior in the market unit commitment. The thesis provides the theoretical understanding to recognize which methods better fit a specific operational or planning goal.

Many works still could be done. It could be possible to enhance the aggregate model in multiple area systems, e.g., considering one model for each market zone. The challenge is to find the coherent generators and to correctly model the interconnections. More simulations can be performed to better investigate the consequences of the frequency support services on HVDC and on the BESS's SoC and degradation and to quantify their benefit in terms of cost-benefit analysis. Using the HVDC capacity for security reasons than for market coupling can have relevant economic implications. Other challenges are related to the investigation of the admissible limits for the inertia constraints in the market unit commitment, their possible interdependencies, and the different weights to represent the importance of security and costs.

The identification of possible splits depends on several factors as aftermath of cascading outages, including the failure or misbehavior of protections and depending on the power transfers. These aspects could be considered in future developments, e.g., considering the probabilities of separation and the analysis of the worst situations in detailed dynamic simulations.

It is important to push future research to consider the distributional impact of inertia and PEIG allocation. The proposed indicators in this thesis need to be further validated and the methodology extended in the zones' selection. The outputs could be analysed using MCDA to rank the most dangerous zones, where possible solution to mitigate instability impact can be needed.

References

[1] K. Halsnæs and A. Garg, "Assessing the role of energy in development and climate policies—conceptual approach and key indicators," *World Development,* vol. 39, no. 6, pp. 987-100, 2011.

[2] F. Milano, F. Dörfler, G. Hug, D. J. Hill and G. Verbič, "Foundations and challenges of low-inertia systems," *2018 Power Systems Computation Conference (PSCC),* pp. 1-25, 2018.

[3] U. Tamrakar, D. Shrestha, M. Maharjan, B. P. Bhattarai, T. M. Hansen and R. Tonkoski, "Virtual inertia: Current trends and future directions," *Applied Sciences,* vol. 7, n. 7, p. 654, 2017.

[4] United Nations Sustainable Development, "AGENDA 21," in *United Nations Conference on Environment & Development*, Rio de Janerio, Brazil, 1992.

[5] United Nations Sustainable Development, "Kyoto Protocol to the United Nations Framework Convention on Climate Change," in *United Nations Framework Convention on Climate Change*, Kyoto, Japan, 1997.

[6] United Nations, "Paris Agreement," in *United Nations Framework Convention on Climate Change*, Paris, France, 2015.

[7] IEA, "Data and statistics," 2020. [Online].

[8] United States Environmental Protection Agency, "Overview of Greenhouse Gases," 2020. [Online]. Available: https://www.epa.gov/ghgemissions/.

[9] IEA, "Electricity generation by source," 2020. [Online]. Available: https://www.iea.org/.

[10] China National Renewable Energy Centre, "China Renewable Energy Outlook," Beijing, China, 2018.

[11] U.S. Energy Information Agency, "What is U.S. electricity generation by energy source?," 2020. [Online]. Available:

https://www.eia.gov/.

[12] EIA, “Annual Energy Outlook 2019,” Washington, USA, 2019.

[13] EC, “EU Climate Action Progress Report 2019,” Brussels, Belgium, 2019.

[14] Eurostat, “Renewable energy statistics,” Brussels, Belgium, 2020.

[15] S. Nies, “An introductory overview on institutional change: who determines energy policy at European level and how?,” in *The European Energy Transition: Agenda for the Twenties*, Deventer, The Netherlands, Claeys & Casteels Law Publishers, 2020, pp. 153-168.

[16] EC, “Clean energy for all Europeans package,” Brussels, Belgium, 2019.

[17] EC, “The European Green Deal,” Brussels, Belgium, 2019.

[18] EC, “EU Emissions Trading System (EU ETS),” Brussels, Belgium, 2005.

[19] Eurostat, “Electricity production, consumption and market overview,” 2020. [Online].

[20] S. Hagspiel and J. Paquel, “A forest of scenarios – the long-term evolution of the European energy system,” in *The European Energy Transition: Agenda for the Twenties*, Deventer, The Netherlands, Claeys & Casteels Law Publishers, 2020, pp. 553-571.

[21] IEA, “World Energy Outlook,” 2020. [Online]. Available: https://www.iea.org/topics/world-energy-outlook.

[22] EC, “EU Reference Scenario,” Brussels, Belgium, 2016.

[23] EC, “Technical report on Member State results of the EUCO policy scenarios,” Brussels, Belgium, 2016.

[24] European Parliament, “REGULATION (EU) 2019/943 OF THE EUROPEAN PARLIAMENT AND OF THE COUNCIL of 5 June 2019 on the internal market for electricity,” *Official Journal of the European Union,* 2019.

[25] ENTSO-E, “TYNDP 2018 Executive Summary,” Brussels,

Belgium, 2018.

[26] ENTSO-E, ENTSO-G, "TYNDP 2018. Scenario Report," Brussels, Belgium, 2018.

[27] ENTSO-E, ENTSO-G , "TYNDP 2020, Scenario Report," Brussels, Belgium, 2020.

[28] ENTSO-E, "Methodology: Frequency Stability Studies," Brussels, Belgium, 2019.

[29] ENTSO-E., "European Power System 2040 Completing the map," Brussels, Belgium, 2019.

[30] ENTSO-E, "System dynamic and operational challenges," 2020.

[31] Med-TSO, "Guidelines for Coordinated Planning: Grid Planning Methodology," Rome, Italy, 2014.

[32] E. Arco, E. Bompard, C. Mosca and F. Profumo, "Electricity based energy corridors connecting North and South shores of the Mediterranean," in *MED & Italian Energy Report*, Naples, Italy, Giannini Editore, 2020, pp. 127-145.

[33] M. Ruszel, "Energy Relations in the Euro-Mediterranean: A Political Economy Perspective," *Journal of Common Market Studies,* vol. 56, n. 6, pp. 1487-1488, 2018.

[34] EC DG for Internal Policies, "EU energy strategy in the South Mediterranean," Brussels, Belgium, 2011.

[35] Italian Government, "Integrated National Energy and Climate Plan," Rome, Italy, 2019.

[36] Terna, "Network Development Plan," Rome, Italy, 2020.

[37] Terna and SNAM, "Documento di Descrizione degli Scenari," Rome, Italy, 2019.

[38] J. Machowski, J. Bialek, J. R. Bumby and J. Bumby, Power system dynamics and stability, Chichester, West Sussex, United Kingdom: John Wiley & Sons, 2008.

[39] P. Kundur and al., "Definition and classification of power system

stability IEEE/CIGRE joint task force on stability terms and definitions," *IEEE transactions on Power Systems,* vol. 19, no. 3, pp. 1387-1401, 2004.

[40] P. Kundur, Power System Stability and Control, New York: McGraw-Hill, 1994.

[41] F. Gonzalez-Longatt, J. L. Rueda and D. Bogdanov, "Assessment of the critical clearing time in low rotational inertia power systems," in *2018 20th International Symposium on Electrical Apparatus and Technologies (SIELA)*, Bourgas, Bulgaria, 2018.

[42] M. Li, L. Xiong, H. Chai, L. Xiu and J. Hao, "Mechanism of PV Generation System Damping Electromechanical Oscillations," *IEEE Access,* vol. 8, n. 135853-135865, 2020.

[43] M. Ndreko, C. Petino and W. Winter, "High Penetration of Inverter Based Generation in the Power System: A Discussion on Stability Challenges and a Roadmap for R&D," in *Proceedings of the 4th International Hybrid Power Systems Workshop*, Crete, Greece, 2019.

[44] Wang, "Harmonic Stability in Power Electronic-Based Power Systems: Concept, Modeling, and Analysis," 2019.

[45] C. Buchhagen, M. Greve, A. Menze and J. Jung, "Harmonic stability-practical experience of a TSO," in *Proc. Wind Integr. Workshop*, Vienna, Austria, 2016.

[46] A. Poullikkas, Fundamentals of Energy Regulation, Nicosia, Cyprus: Easy Conferences Ltd., 2016.

[47] B. Kroposki, B. Johnson, Y. Zhang, V. Gevorgian, P. Denholm and B. M. H. B. Hodge, "Achieving a 100% renewable grid: Operating electric power systems with extremely high levels of variable renewable energy," *IEEE Power and Energy Magazine,* pp. 61-73, 2017.

[48] D. Groß, S. Bolognani, B. K. Poolla and F. Dörfler, "Increasing the resilience of low-inertia power systems by virtual inertia and damping," in *Proc. of IREP 2017 Symposium*, Espinho, Portugal, 2017.

[49] Y. K. Wu, Y. H. Li and Y. Z. Wu, "Overview of power system flexibility in a high penetration of renewable energy system," in *2018 IEEE International Conference on Applied System Invention (ICASI)*,

Chiba, Japan, 2018.

[50] E. Bompard, A. Mazza and L. Toma, "Classical grid control: frequency and voltage stability," in *Converter-Based Dynamics and Control of Modern Power Systems*, London, UK, Academic Pres, 2020, pp. 31-64.

[51] G. Andersson, Dynamics and Control of Electric Power Systems, ETH Zurich, 2012.

[52] M. Scherer, "Frequency Control in the European Power System Considering the Organisational Structure and Division of Responsibilities," *Ph.D. Thesis,* 2016.

[53] EC, "COMMISSION REGULATION (EU) 2017/1485 of 2 August 2017 establishing a guideline on electricity transmission system operation," *Official Journal of the European Union,* 2017.

[54] ENTSO-E, "All TSOs' proposal for the determination of LFC blocks for the SA CE," 2018.

[55] Regional Group Continental Europe, "Annex 1: Policy on Load-Frequency Control and Reserves," 2019.

[56] ENTSO-E, "Explanatory note for the FCR dimensioning rules proposal," 2018.

[57] ENTSO-E Incident Classification Scale Subgroup, "Incident Classification Scale," 2018.

[58] National Grid, "GC022 - Frequency Response," 2013.

[59] ENTSO-E SG System Protection and Dynamics, "DSA Project," 2018.

[60] Nordic TSOs, "Nordic System Operation Agreement (SOA) – Annex Load-Frequency Control & Reserves (LFCR)," 2019.

[61] ENTSO-E, "Future System Inertia 2," 2017.

[62] ENTSO-E, "All CE TSOs proposal for the dimensioning rules for FCR," 2018.

[63] Terna, "Partecipazione alla regolazione di frequenza-potenza,"

Grid Code - Annex A15, 2008.

[64] ENTSO-E, “Explanatory note for the calculation of FRCE Target Parameter for LFC blocks of SA CE,” 2018.

[65] European Commission, “Commission Regulation (EU) 2017/1485 - Establishing a guideline on electricity transmission system operation,” 2017.

[66] ENTSO-E, “An overview of the European Balancing Market and Electricity Balancing Guideline,” *Electricity Balancing In Europe,* 2018.

[67] ENTSO-E, “All CE TSOs’ agreement on frequency restoration control error target parameters,” 2018.

[68] UCTE, “Appendix 1: Load Frequency Control and Performance,” 2004.

[69] F. Arrigo, C. Mosca, E. Bompard and P. Cuccia, “Frequency Models and Control in Normal Operation: the Sardinia Case Study,” in *2020 55th International Universities Power Engineering Conference (UPEC)*, Turin, Italy, 2020.

[70] EC, “COMMISSION REGULATION (EU) 2016/631 of 14 April 2016 establishing a network code on requirements for grid connection of generators,” *Official Journal of the European Union,* 2016.

[71] ENTSO-E, “Limited frequency sensitive mode,” 2017.

[72] EC, “COMMISSION REGULATION (EU) 2017/2196 of 24 November 2017 stablishing a network code on electricity emergency and restoration,” *Official Journal of the European Union,* 2017.

[73] A. Monti, F. Milano, E. Bompard and X. Guillaud, Converter-Based Dynamics and Control of Modern Power Systems, London, UK: Academic Press, 2020.

[74] Med-TSO, “Deliverable 2.1.A Proposal of Common Rules about the provision of system services: Mediterranean Grid Code chapter,” 2018.

[75] P. D. G. Andersson, R. Farmer et al., “Causes of the 2003 major grid blackouts in North America and Europe, and recommended means

to improve system dynamic performance," *IEEE Trans. Power Syst.,* vol. 20, n. 4, pp. 1922-1928, 2005.

[76] UCTE, "Final Report of the Investigation Committee on the 28 Septermber 2003 Blackout in Italy," Brussels, Belgium, 2004.

[77] UCTE, "Final Report System Disturbance on 4 November 2006," Brussels, Belgium, 2007.

[78] M. Sforna and M. Delfanti, "Overview of the events and causes of the 2003 Italian blackout," in *2006 IEEE PES Power Systems Conference and Exposition*, Atlanta, GA, USA, 2006.

[79] ENTSO-E, "Report on blackout in Turkey on 31st March 2015," Brussels, Belgium, 2015.

[80] S. Larsson and E. Ek, "The black-out in southern Sweden and eastern Denmark, September 23, 2003," in *IEEE Power Engineering Society General Meeting*, Denver, CO, USA, 2004.

[81] C. D. Vournas, V. C. Nikolaidis and A. A. Tassoulis, "Postmortem analysis and data validation in the wake of the 2004 Athens blackout," *IEEE Trans. Power Syst.,* vol. 21, n. 3, pp. 1331-1339, 2006.

[82] ENTSO-E, "CE Significant Frequency Deviations - January 2019," Brussels, Belgium, 2019.

[83] C. Cooke, "GB Grid 9 August 2019 power outage and grid inertia," in *ICESF20*, Hertfordshire, UK, 2020.

[84] National Grid, "Technical Report on the events of 9 August 2019," London, UK, 2019.

[85] A. Martins et al., "Lessons learned in restoration from recent blackout incidents in Brazilian power system," in *Proc. CIGRE Paris Conf.*, Paris, France, 2012.

[86] A. Atputharajah and T. K. Saha, "Power system blackouts-literature review," in *2009 International Conference on Industrial and Information Systems (ICIIS)*, Sri Lanka, Sri Lanka, 2009.

[87] V. Rampurkar, P. Pentayya, H. A. Mangalvedekar and F. Kazi, "Cascading failure analysis for Indian power grid," *IEEE Trans. Smart Grid,* vol. 7, n. 4, p. 1951–1960, 2016.

[88] R. Yan, T. K. Saha, F. Bai and H. Gu, "The anatomy of the 2016 South Australia blackout: a catastrophic event in a high renewable network," *IEEE Transactions on Power Systems,* vol. 33, n. 5, pp. 5374-5388, 2018.

[89] AEMO, "Final Report – Queensland and South Australia system separation on 25 August 2018," Melbourne, Australia, 2019.

[90] R. H. Lasseter, Z. Chen and D. Pattabiraman, "Grid-Forming Inverters: A Critical Asset for the Power Grid," *IEEE Journal of Emerging and Selected Topics in Power Electronics,* vol. 8, n. 2, pp. 925-935, 2019.

[91] W. Uijlings, "An indipendent anlysis on the ability of generators to ride through rate of change of frequency values up to 2 Hz/s," DNV KEMA Ltd Cathedral Street, and SE London, 2013.

[92] EirGrid and SONI, "DS3 Joint Grid Code Working Group Position Paper on RoCoF," 2012.

[93] ENTSO-E, "Future System Inertia," 2013.

[94] ENTSO-E, "Frequency Stability Evaluation Criteria for the Synchronous Zone of Continental Europe," 2016.

[95] EirGrid and SONI, "RoCoF Modification Proposal - TSOs' Recommendations," 2012.

[96] C. Roberts, "Review of international grid codes.," Lawrence Berkeley National Laboratory, Berkeley, CA, USA , 2018.

[97] G. A. Chown, J. G. Wright, R. P. Van Heerden and M. Coker, "System inertia and Rate of Change of Frequency (RoCoF) with increasing non-synchronous renewable energy penetration," in *Cigré 2017: 8th Southern Africa Regional Conference*, Cape Town, South Africa, 2017.

[98] AEMO, "Inertia Requirements Methodology," Sidney, Australia, 2018.

[99] ENTSO-E WG SPD, "Task Force Code – System Dynamic Issues for the synchronous zone of Continental Europe," Brussels, Belgium, 2017.

[100] RG-CE System Protection & Dynamics Sub Group, "Rate of change of frequency (RoCoF) withstand capability," ENTSO-E, Brussels, Belgium, 2018.

[101] A. Dyśko, D. Tzelepis and C. Booth, "Assessment of Risks Resulting from the Adjustment of ROCOF Based Loss of Mains Protection Settings-Phase II," University of Strathclyde, Glasgow, UK, 2013.

[102] L. Badesa, F. Teng and G. Strbac, "Simultaneous Scheduling of Multiple Frequency Services in Stochastic Unit Commitment," *IEEE Trans. Power Syst.,* vol. 34, n. 5, pp. 3858-3868, 2019.

[103] S. H. Lee and J. W. Park, "Optimal placement and sizing of multiple DGs in a practical distribution system by considering power loss," *IEEE Transactions on Industry Applications,* vol. 49, n. 5, pp. 2262-2270., 2013.

[104] N. S. Rau and Y. H. Wan, "Optimum location of resources in distributed planning," *IEEE Transactions on Power systems,* vol. 9, n. 4, pp. 2014-2020, 1994.

[105] C. Wang and M. H. Nehrir, "Analytical approaches for optimal placement of distributed generation sources in power systems," *IEEE Transactions on Power systems,* vol. 19, n. 4, pp. 2068-2076, 2004.

[106] G. Zareiegovar, R. R. Fesaghandis and M. J. Azad, "Optimal DG location and sizing in distribution system to minimize losses, improve voltage stability, and voltage profile," in *2012 Proceedings of 17th Conference on Electrical Power Distribution*, Tehran, Iran, 2012.

[107] M. R. Shaik and A. S. Reddy, "Optimal placement of STATCOM with ABC algorithm to improve voltage stability in power systems," in *2016 International Conference on Signal Processing, Communication, Power and Embedded System (SCOPES)* , Paralakhemundi, India, 2016.

[108] D. Doheny and M. Conlon, "Investigation into the local nature of rate of change of frequency in electrical power systems," in *2017 52nd International Universities Power Engineering Conference (UPEC)*, Heraklion, Greece, 2017.

[109] B. A. Osbouei, G. A. Taylor, O. Bronckart, J. Maricq and M. Bradley, "Impact of Inertia Distribution on Power System Stability and

Operation," in *2019 IEEE Milan PowerTech*, Milan, Italy, 2019.

[110] R. Rudenberg, Transient performance of electric power systems, New York: McGraw-Hill, 1950.

[111] B. K. Poolla, S. Bolognani and F. Dörfler, "Optimal placement of virtual inertia in power grids.," *IEEE Transactions on Automatic Control,* vol. 62, n. 12, pp. 6209-6220, 2017.

[112] B. K. Poolla, D. Groß and F. M Dörfler, "Placement and implementation of grid-forming and grid-following virtual inertia and fast frequency response," *IEEE Transactions on Power Systems,* vol. 34, n. 4, pp. 3035-3046, 2019.

[113] U. Markovic, V. Häberle, D. Shchetinin, G. Hug, D. Callaway and E. Vrettos, "Optimal Sizing and Tuning of Storage Capacity for Fast Frequency Control in Low-Inertia Systems," in *2019 International Conference on Smart Energy Systems and Technologies*, Porto, Portugal, 2019.

[114] J. Đaković, M. Krpan, P. Ilak, T. Baškarad and I. Kuzle, "Impact of wind capacity share, allocation of inertia and grid configuration on transient RoCoF: The case of the Croatian power system," *International Journal of Electrical Power & Energy Systems,* vol. 121, n. 106075, 2020.

[115] Y. Wang, H. Silva-Saravia and H. Pulgar-Painemal, "Estimating inertia distribution to enhance power system dynamics," in *2017 North American Power Symposium*, Morgantown, WV, USA, 2017.

[116] H. Pulgar-Painemal, Y. Wang and H. Silva-Saravia, "On inertia distribution, inter-area oscillations and location of electronically-interfaced resources," *IEEE Transactions on Power Systems,* vol. 33, n. 1, pp. 995-1003, 2017.

[117] L. Pagnier and P. Jacquod, "Optimal placement of inertia and primary control: a matrix perturbation theory approach," *IEEE Access,* vol. 7, pp. 145889-145900, 2019.

[118] M. Nedd, C. Booth and K. Bell, "Potential Solutions to the Challenges of Low Inertia Power Systems with a Case Study Concerning Synchronous Condensers," in *52nd International Universities Power Engineering Conference (UPEC)*, Heraklion,

Greece, 2017.

[119] H. Nguyen, G. Yang, A. Nielsen et al., "Frequency stability improvement of low inertia systems using synchronous condensers," in *IEEE International Conference on Smart Grid Communications*, Sydney, Australia, 2016.

[120] AEMO, "National Transmission Network Development Plan," Melbourne, Australia, 2018.

[121] National Grid, "Network Options Assessment," London, UK, 2020.

[122] N. Al-Masood, R. Yan, T. K. Saha and N. Modi, "Frequency response and its enhancement using synchronous condensers in presence of high wind penetration," in *IEEE Power & Energy Society General Meeting*, Denver, CO, USA, 2015.

[123] E. Marrazi, G. Yang and P. Weinreich-Jensen, "Allocation of synchronous condensers for restoration of system short-circuit power," *Journal of Modern Power Systems and Clean Energy,* vol. 6, n. 1, pp. 17-26, 2018.

[124] H. T. Nguyen, G. Yang, A. H. Nielsen and P. H. Jensen, "Combination of synchronous condenser and synthetic inertia for frequency stability enhancement in low-inertia systems.," *IEEE Transactions on Sustainable Energy,* vol. 10, n. 3, pp. 997-1005, 2018.

[125] Y. Liu, S. Yang, S. Zhang and et al., "Comparison of Synchronous Condenser and STATCOM for Inertial Response Support," in *IEEE Energy Conversion Congress and Exposition*, Pittsburgh, PA, USA, 2014.

[126] M. Singh, L. A. Lopes and N. A. Ninad, "Grid forming Battery Energy Storage System (BESS) for a highly unbalanced hybrid mini-grid," *Electric Power Systems Research,* vol. 127, pp. 126-133, 2015.

[127] National Grid, "National Grid frequency services," London, UK, 2019.

[128] AEMO, "Quaterly Energy Dynamics - Q1," Melbourne, Australia, 2019.

[129] J. Fleer and P. Stenzel, "Impact analysis of different operation

strategies for battery energy storage systems providing primary control reserve," *Journal of Energy Storage,* vol. 8, pp. 320-338, 2016.

[130] X. Luo, J. Wang, M. Dooner and J. Clarke, "Overview of current development in electrical energy storage technologies and the application potential in power system operation," *Applied energy,* vol. 137, pp. 511-536, 2015.

[131] P. Brogan, R. Best, D. Morrow, K. McKinley and M. Kubik, "Effect of BESS response on frequency and RoCof during underfrequency transients," *IEEE Trans. Power Syst.,* vol. 34, n. 1, pp. 575-583, 2019.

[132] U. Markovic, V. Häberle, D. Shcetinin, G. Hug., D. Callaway and E. Vrettos, "Optimal Sizing and Tuning of Storage Capacity for Fast Frequency Control in Low-Inertia Systems," in *2019 International Conference on Smart Energy Systems and Technologies (SEST)*, Porto, Portugal, 2019.

[133] ENTSO-E and EURELECTRIC, "Deterministic frequency deviations–root causes and proposals for potential solutions," Brussels, Belgium, 2011.

[134] J. Cao, W. Du, H. Wang and M. McCulloch, "Optimal sizing and control strategies for hybrid storage system as limited by grid frequency deviations," *IEEE Trans. Power Syst.,* vol. 33, n. 5, pp. 5486-5495, 2018.

[135] F. Mele, A. Ortega, R. Zarate-Minano and F. Milano, "Impact of variability, uncertainty and frequency regulation on power system frequency distribution," in *2016 Power Systems Computation Conference (PSCC)*, Genoa, Italy, 2016.

[136] F. Arrigo, E. Bompard, M. Merlo and F. Milano, "Assessment of primary frequency control through battery energy storage systems," *Electrical Power and Energy Systems,* vol. 115, p. 105428, 2020.

[137] R. Lee, S. Homan, N. Mac Dowell and S. Brown, "A closed-loop analysis of grid scale battery systems providing frequency response and reserve services in a variable inertia grid," *Applied Energy,* vol. 236, pp. 961-972, 2019.

[138] EC, "COMMISSION REGULATION (EU) 2016/1447 of 26 August 2016 establishing a network code on requirements for grid

connection of high voltage direct current systems and direct current-connected power park modules," *Official Journal of the European Union,* 2016.

[139] O. E. Oni, I. E. Davidson and K. N. Mbangula, "A review of LCC-HVDC and VSC-HVDC technologies and applications," in *IEEE 16th International Conference on Environment and Electrical Engineering (EEEIC)*, Florence, Italy, 2016.

[140] L. Zhang, L. Harnefors and P. Rey, "Power system reliability and transfer capability improvement by VSC-HVDC," in *CIGRE 2007 Conference on Security and Reliability of Electric Power Systems*, Paris, France, 2007.

[141] P. Rodriguez and K. Rouzbehi, "Multi-terminal DC grids: challenges and prospects," *Journal of Modern Power Systems and Clean Energy,* vol. 5, n. 4, pp. 515-523, 2017.

[142] P. Tielens, Operation and control of power systems with low synchronous inertia, Leuven, Belgium: Ph.D. Thesis, 2017.

[143] K. S. Ratnam, K. Palanisamy and G. Yang, "Future low-inertia power systems: Requirements, issues, and solutions-A review," *Renewable and Sustainable Energy Reviews,* vol. 124, n. 109773, 2020.

[144] P. M. Ashton, C. S. Saunders, G. A. Taylor, A. M. Carter and M. E. Bradley, "Inertia estimation of the GB power system using synchrophasor measurements," *IEEE Transactions on Power Systems,* vol. 30, n. 2, pp. 701-709, 2014.

[145] G. R. Moraes, A. Berizzi, V. Ilea and G. D'Antona, "Inertia estimation of equivalent areas by a pmu-based approach following perturbations," in *2018 IEEE International Conference on Environment and Electrical Engineering*, Palermo, Italy, 2018.

[146] B. Berry, "Inertia Estimation Methodologies vs Measurement Methodology: Impact on System Operations," in *CIGRE Symposium*, Aalborg, Denmark, 2019.

[147] R. Eriksson, N. Modig and K. Elkington, "Synthetic inertia versus fast frequency response: a definition," *IET Renewable Power Generation,* vol. 12, n. 5, pp. 507-514, 2017.

[148] ERCOT, "Future Ancillary Services in ERCOT," Austin, Texas,

2013.

[149] National Grid, “System needs and product strategy,” London, U.K., 2017.

[150] National Grid, “Future of Frequency Response - Industry update,” London, UK, 2019.

[151] AEMO, “Fast Frequency Response in the NEM – Working Paper,” Melbourne, Australia, 2017.

[152] Terna, “Fast Reserve Regulation,” Rome, Italy, 2019.

[153] F. Mandrile, E. Carpaneto and R. Bojoi, “Grid-Feeding Inverter with Simplified Virtual Synchronous Compensator Providing Grid Services and Grid Support,” *IEEE Transactions on Industry Applications,* 2020.

[154] H. Bevrani, T. Ise and Y. Miura, “Virtual synchronous generators: A survey and new perspectives,” *International Journal of Electrical Power & Energy Systems,* vol. 54, pp. 244-254, 2014.

[155] V. Trovato, S. H. Tindemans and G. Strbac, “Demand response contribution to effective inertia for system security in the GB 2020 gone green scenario,” in *IEEE PES ISGT Europe 2013*, Lyngby, Denmark, 2013.

[156] S. Burger, J. P. Chaves-Avila, C. Batlle and I. J. Pérez-Arriaga, “The value of aggregators in electricity systems,” MIT Center for Energy and Environment Policy Research, Cambridge, MA, USA, 2016.

[157] B. Zhou, W. Li, K. W. Chan, Y. Cao, Y. Kuang, X. Liu and X. Wang, “Smart home energy management systems: Concept, configurations, and scheduling strategies,” *Renewable and Sustainable Energy Reviews,* vol. 61, pp. 30-40, 2016.

[158] D. Pudjianto, C. Ramsay and G. Strbac, “Virtual power plant and system integration of distributed energy resources,” *IET Renewable power generation,* vol. 1, n. 1, pp. 10-16, 2007.

[159] A. Moeini and I. Kamwa, “Analytical concepts for reactive power based primary frequency control in power systems,” *IEEE Transactions on Power Systems,* vol. 31, no. 6, pp. 4217-4230, 2016.

[160] P. M. Anderson and A. A. Fouad, Power system stability and control, New York: IEEE Press Power Engineering Series, 2002.

[161] R. Marconato, Electric Power Systems, Milano: CEI, 2008.

[162] J. Palermo, "International review of frequency control adaptation," AEMO, 2016.

[163] P. M. Anderson and M. Mirheydar, "A Low-Order System Frequency Response Model," *IEEE Transactions on Power Systems,* vol. 5, no. 3, pp. 720-729, 1990.

[164] M. Chan, R. Dunlop and F. Schweppe, "Dynamic equivalents for average system frequency behaviour following major disturbances," *IEEE Trans. on Power Apparatus and Systems,* Vol. PAS-91, n. 4, pp. 1637-1642, 1972.

[165] Q. L. F. Shi and H. Cui, "Analytical method to aggregate multi-machine SFR model with applications in power system dynamic studies," *IEEE Transactions on Power Systems,* vol. 33, n. 6, pp. 6355-6367, 2018.

[166] L. Toma, M. Sanduleac, S. A. Baltac, F. Arrigo, A. Mazza, E. Bompard and A. Monti, "On the Virtual Inertia Provision by BESS in Low Inertia Power Systems," in *IEEE International Energy Conference (ENERGYCON)*, Limassol, Cyprus, 2018.

[167] M. Krpan and I. Kuzle, "Towards the new low-order system frequency response model of power systems with high penetration of variable-speed wind turbine generators," in *2018 IEEE Power & Energy Society General Meeting (PESGM)*, Portland, OR, USA, 2018.

[168] W. Zhang, X. Yan and H. Huang, "Performance Tuning for Power Electronic Interfaces Under VSG Control," *Applied Sciences,* vol. 10, no. 3, p. 953, 2020.

[169] J. Hell and M. Schmid, "Energy Research Centre of Lower Saxony," November 2014. [Online]. Available: https://www.efzn.de/uploads/media/Technik2_Hell_Aktive_Netzstabilisierung.pdf.

[170] AEMO, "International Review of Freqeuncy Control Adaptation," October 2016. [Online]. Available: https://preprod.aemo.com.au/-/media/Files/Electricity/NEM/Security_and_Reliability/Reports/2016/F

PSS---International-Review-of-Frequency-Control.pdf.

[171] Australian Energy Market Commission, “System Security Market Frameworks Review,” Sydney, Australia, 2016.

[172] J. J. Grainger and W. D. Stevenson, Power system analysis, Singapore, Republic of Singapore: McGraw-Hill, 2003.

[173] J. Jomaux, T. Mercier and E. De Jaeger, “A methodology for sizing primary frequency control in function of grid inertia,” in *IEEE International Energy Conference*, Leuven, Belgium, 2016.

[174] EC, “COMMISSION REGULATION (EU) 2016/631 of 14 April 2016 establishing a network code on requirements for grid connection of generators,” 2016.

[175] C. Mosca, F. Arrigo, A. Mazza, E. Bompard, E. Carpaneto, G. Chicco and P. Cuccia, “Mitigation of frequency stability issues in low inertia power systems using synchronous compensators and battery energy storage systems,” *IET Gener. Transm. Distrib.,* vol. 13, no. 17, pp. 3951-3959, 2019.

[176] P. M. Anderson, Power system protection, New York: John Wiley & Sons, 1999.

[177] C. Wang, B. Zhang, Z. Hao, J. Shu, P. Li and Z. Bo, “A Novel Real-Time Searching Method for Power System Splitting Boundary,” *IEEE Trans. Power Syst.,* vol. 25, n. 4, pp. 1902-1909, 2010.

[178] C. Cieslak, J. Massmann, C. Their and A. Schnettler, “Identification of System Split Topologies in Transmission Grids,” in *2018 53rd International Universities Power Engineering Conference (UPEC)*, Glasgow, UK, 2018.

[179] ENTSO-E, “Definitions of Transfer Capacities in liberalised Electricity Markets,” Brussels, Belgium, 2001.

[180] E. Ela, V. Gevorgian, A. Tuohy, B. Kirby, M. Milligan and M. O'Malley, “Market Designs for the Primary Frequency Response Ancillary Service—Part I: Motivation and Design,” *IEEE Trans. Power Syst.,* vol. 29, n. 1, pp. 421-431, 2014.

[181] T. Xu, W. Jang and T. Overbye, “Commitment of Fast-Responding Storage Devices to Mimic Inertia for the Enhancement of Primary

Frequency Response," *IEEE Trans. Power Syst.,* vol. 33, n. 2, p. 1219–1230, 2018.

[182] H. Gu, R. Yan and T. K. Saha, " "Minimum synchronous inertia requirement of renewable power systems",., vol. 33. no. 2, pp. , .," *IEEE Trans. Power Syst,* vol. 33, n. 2, pp. 1533-1543, 2018.

[183] P. Daly, D. Flynn and N. Cunniffe, "Inertia considerations within unit commitment and economic dispatch for systems with high non-synchronous penetrations," in *Proc. IEEE Eindhoven PowerTech*, Eindhoven, The Netherlands, 2015.

[184] S. Püschel-Løvengreen and P. Mancarella, "Frequency response constrained economic dispatch with consideration of generation contingency size," in *Proc. PSCC 2018*, Dublin, Ireland, 2018.

[185] V. Trovato, A. Bialecki and A. Dallagi, "Unit Commitment with Inertia-Dependent and Multispeed Allocation of Frequency Response Services," *IEEE Trans. Power Syst.,* vol. 34, n. 2, pp. 1537-1548, 2019.

[186] L. Badesa, F. Teng and G. Strbac, "Economic Value of Inertia in Low-Carbon Power Systems," in *Proc. 2017 IEEE PES Innovative Smart Grid Technologies Conference Europe (ISGT-Europe)*, Torino, Italy, 2017.

[187] M. Brito, E. Gil and I. Calle, "Unit Commitment with Primary Frequency Control Requirements for Low-Inertia Systems," in *2018 IEEE PES General Meeting (PESGM)*, Portland, OR, USA, 2018.

[188] N. Nguyen, V. Johnson and J. Mitra, "Environmental-economic dispatch of power system in the presence of wind generation," in *Proc. 2015 North American Power Symposium (NAPS)*, Charlotte, NC, USA, 2015.

[189] I. J. Raglend, S. Veeravalli, K. Sailaja et al., "Comparison of AI techniques to solve combined economic emission dispatch problem with line flow constraints," *Int. J. Elect. Power Energy Syst.,* vol. 32, n. 6, p. 592–598, 2010.

[190] C. M. Huang and Y. Huang, "A novel approach to real-time economic emission power dispatch," *IEEE Trans. Power Syst.,* vol. 18, n. 1, pp. 288-294, 2003.

[191] H. Ahmadi and H. Ghasemi, "Security-constrained unit

commitment with linearized system frequency limit constraints," *IEEE Trans. Power Syst.,* vol. 29, n. 4, pp. 1536-1545, 2014.

[192] F. Teng, V. Trovato and G. Strbac, "Stochastic Scheduling With Inertia-Dependent Fast Frequency Response Requirements," *IEEE Trans. Power Syst.,* vol. 31, n. 2, pp. 1557-1566, 2016.

[193] Y. Wen, W. Li, G. Huang and X. Liu, "Frequency Dynamics Constrained Unit Commitment With Battery Energy Storage," *IEEE Trans. Power Syst.,* vol. 31, n. 6, pp. 5115-5125, 2016.

[194] O. Bertoldi and A. Rivoiro, "Fast Multiarea economic dispatching for planning applications by accounting for interchange constraints and transmission losses," in *Proc. 12th PSCC*, Dresden, Germany, 1996.

[195] B. Cova, P. Capurso, E. Elia et al., "Market integration in Europe: a market simulator taking into account different market zones and the increasing penetration of RES generation," in *CIGRE General Session 2012*, Paris, France, 2012.

[196] ENTSO-E, "Guideline for Cost Benefit Analysis of Grid Development Process," Brussels, Belgium, 2018.

[197] E. Carlini, P. Pericolo, F. Vedovelli et al., "Impact of CO2 reduction targets on transmission capacity expansion dictated by the power market clearing: application to the Italian and French systems," in *Proc. CIGRE*, Paris, France, 2010.

[198] S. Temtem and K. Creighton, "Summary of studies on rate of change of frequency events on the all-island system," EirGrid & Soni, Dublin, Ireland, 2012.

[199] J. O'Sullivan, A. Rogers, D. Flynn et al., "Studying the maximum instantaneous non-synchronous generation in an island system—frequency stability challenges in Ireland," *IEEE Trans. Power Syst.,* vol. 29, n. 6, p. 2943–2951, 2014.

[200] EirGrid, "System Non-Synchronous Penetration. Definition and Formulation, Operational Policy," August 27 2018. [Online]. Available: http://www.eirgridgroup.com/site-files/library/EirGrid/SNSP-Formula-External-Publication.pdf.

[201] M. Poncela, A. Purvins and S. Chondrongiannis, "Pan-European Analysis on Power System Flexibility," *Energies,* vol. 11, n. 7, p. 1765,

2018.

[202] ENTSO-E, “Scenario Outlook and Adequacy Forecast,” Brussels, Belgium, 2015.

[203] L. Michi, M. Migliori, A. Bugliari et al., “Transmission network expansion planning: towards enhanced renewable integration,” in *2018 AEIT International Annual Conference*, Bari, Italy, 2018.

[204] L. Michi, G. Donnini, B. Aluisio et al., “The DC power planning for network flexibility in the multi-area power system,” in *2018 AEIT International Annual Conference*, Bari, Italy, 2018.

[205] K. Creighton, M. McClure, R. Skillen et al., “Increased wind generation in Ireland and Northern Ireland and the impact on rate of change of frequency,” in *Proc. 12th Wind Integration Workshop*, London, UK, 2013.

[206] EirGrid and SONI, “Operational constraints update,” Dublin, Ireland, 2019.

[207] EirGrid and SONI, “Delivering a Secure, Sustainable Electricity System (DS3),” Dublin, Ireland, 2014.

[208] C. Mosca, E. Bompard, G. Chicco, B. Aluisio, M. Migliori, C. Vergine and P. Cuccia, “Technical and Economic Impact of the Inertia Constraints on Power Plant Unit Commitment,” *IEEE Open Access Journal of Power and Energy,* vol. 7, pp. 441-452, 2020.

[209] J. J. Wang, Y. Y. Jing, C. F. Zhang and J. H. Zhao, “Review on multi-criteria decision analysis aid in sustainable energy decision-making,” *Renewable and sustainable energy reviews,* vol. 13, no. 9, pp. 2263-2278, 2009.

[210] M. Baumann, M. Weil, J. F. Peters, N. Chibeles-Martins and A. B. Moniz, “A review of multi-criteria decision making approaches for evaluating energy storage systems for grid applications,” *Renewable and Sustainable Energy Reviews,* vol. 107, pp. 516-534, 2019.

[211] M. Bazerman, Judgement in managerial decision making, Hoboken, NJ, USA: Wiley, 2006.

[212] T. Saaty, “How to make a decision: the analytic hierarchy process,” *European Journal of Operational Research,* vol. 48, p. 9–26, 1990.

[213] J. Malczewski, T. Chapman, C. Flegel et al., "GIS multicriteria evaluation with ordered weighted averaging (OWA): case study of developing watershed management strategies," *Environment and Planning A,* vol. 35, p. 1769–1784, 2003.

[214] C. Hwang and K. Yoon, Multiple attribute decision making. Methods and applications: a state-of-the-art survey, Berlin and New York: Springer-Verlag, 1981.

[215] A. Mazza and G. Chicco, "Application of TOPSIS in distribution systems multi-objective optimization," in *Proc. 9th World Energy System Conference*, Suceava, Romania, 2012.

[216] B. Roy, "Classement et choix en présence de points de vue multiples," *Revue française d'informatique et de recherche opérationnelle (in French),* vol. 2, n. V1, p. 57–75, 1968.

[217] J. Brans and B. Mareschal, "Promethee Methods," *Multiple Criteria Decision Analysis: State of the Art Surveys,* vol. 78, p. 163–195, 2005.

[218] A. Guitouni and J. M. Martel, "Tentative guidelines to help choosing an appropriate MCDA method," *European journal of operational research,* vol. 109, no. 2, pp. 501-521, 1998.

[219] A. Mardani, E. K. Zavadskas, Z. Khalifah, N. Zakuan, A. M Jusoh, K. M. Nor and M. Khoshnoudi, "A review of multi-criteria decision-making applications to solve energy management problems: Two decades from 1995 to 2015," *Renewable and Sustainable Energy Reviews,* vol. 71, pp. 216-256, 2017.

[220] M. Tavana, A. Shaabani, F. Javier Santos-Arteaga and I. Raeesi Vanani, "A Review of Uncertain Decision-Making Methods in Energy Management Using Text Mining and Data Analytics," *Energies,* vol. 13, no. 15, p. 3947, 2020.

[221] F. R. L. Junior, L. Osiro and L. C. R. Carpinetti, " A comparison between Fuzzy AHP and Fuzzy TOPSIS methods to supplier selection," *Applied Soft Computing,* vol. 21, pp. 194-209, 2014.

[222] M. Behzadian, S. K. Otaghsara, M. Yazdani and J. Ignatius, "A state-of the-art survey of TOPSIS applications," *Expert Systems with applications,* vol. 39, no. 17, pp. 13051-13069, 2012.

[223] W. Qiu, J. Zhang, X. Jin and X. Bai, "Using multi-objective differential evolution and TOPSIS technique for environmental/economic dispatch with security constraints," in *4th International Conference on Electric Utility Deregulation and Restructuring and Power Technologies (DRPT)*, Weihai, China, 2011.

[224] Y. L. Wang, J. A. Shang and Q. Xue, "Coordination assessment of power plants and power network based on entropy and TOPSIS in power system planning," in *International Conference on Electrical and Control Engineering*, Wuhan, China, 2010.

[225] B. Lazzerini and F. Pistolesi, "A linear programming-driven MCDM approach for multi-objective economic dispatch in smart grids," in *2015 SAI Intelligent Systems Conference (IntelliSys)*, London, UK, 2015.

[226] D. Olson, "Comparison of weights in TOPSIS models," *Math. Comput. Model.,* vol. 40, no. 7-8, p. 721–727, 2004.

[227] N. A. Michailidis, N. A. Bezas, G. S. Misyris, D. I. Doukas, D. P. Labridis and A. G. Marinopoulos, "Comparative analysis of online estimation algorithms for battery energy storage systems," in *2017 IEEE PES Innovative Smart Grid Technologies Conference Europe (ISGT-Europe)*, Torino, Italy, 2017.

[228] S. Chen, T. Zhang, H. B. Gooi, R. D. Masiello and W. Katzenstein, "Penetration rate and effectiveness studies of aggregated BESS for frequency regulation," *IEEE Transactions on Smart Grid,* vol. 7, no. 1, pp. 167-177, 2015.

[229] Y. Z. Zhang, "Battery energy storage operation with adaptive droop control," in *2017 IEEE Conference on Control Technology and Applications (CCTA)*, Mauna Lani, HI, USA, 2017.

[230] DNV GL, "RoCoF Alternative Solutions Technology Assessment," London, UK, 2015.

[231] J. Zhu, C. D. Booth, G. P. Adam et al., "Inertia Emulation Control Strategy for VSC-HVDC Transmission Systems," *IEEE Transactions on Power Systems,* vol. 28, no. 2, pp. 1277-1287, 2013.

[232] T. Nam, H. Kim, S. Kim et al., "Trade-off strategies in designing capacitor voltage balancing schemes for modular multilevel converter HVDC," *Journal of Electrical Engineering & Technology,* vol. 11, n.

4, pp. 829-838, 2016.

[233] E. Ghiani, S. Mocci, S. Celli et al., "Increasing the flexible use of hydro pumping storage for maximizing the exploitation of RES in Sardinia," in *Proc. 3rd Renewable Power Generation Conference*, Naples, Italy, 2014.

[234] A. Iaria, R. Calisti, A. L'Abbate and M. R. Rapizza, "Impact of SA. CO. I. refurbishment: flexibility analysis of the Sardinian system," in *2019 AEIT HVDC International Conference (AEIT HVDC)*, Firenze, Italy, 2019.

[235] D. R. Drew, P. J. Coker, H. C. Bloomfield et al., "Sunny windy sundays," *Renewable Energy,* vol. 138, pp. pp. 870-875, 2019.

[236] P. Ledesma, F. Arredondo and E. Castronuovo, "Optimal curtailment of non-synchronous renewable generation on the island of Tenerife considering steady state and transient stability constraints," *Energies,* vol. 10, no. 11, pp. pp. 1-15, 2017.

[237] S. Alhejaj and F. Gonzalez-Longatt, "Impact of Inertia Emulation Control of Grid-Scale BESS on Power System Frequency Response," in *International Conf. for Students on Applied Engineering*, Newcastle upon Tyne, UK, 2016.

[238] Terna, "Statistical data," Terna, Rome, Italy, 2017.

[239] C. Mosca, E. Bompard, B. Aluisio, M. Migliori, C. Vergine and P. Cuccia, "HVDC for frequency stability under RES penetration: the Sardinia island case," in *2019 AEIT HVDC International Conference (AEIT HVDC)*, Firenze, Italy, 2019.

[240] ENTSO-E, "TYNDP 2018. Scenario Report," Brussels, Belgium, 2018.

[241] C. Mosca, E. Bompard, G. Chicco, J. Moreira, V. Sermanson and D. Powell, "Frequency Stability of the European Interconnected Power System Under Grid Splitting in Market Zones," *Energy Systems Research,* vol. 3, no. 4, pp. 37-47, 2020.

[242] W. H. Organization, "Timeline of WHO's response to COVID-19," [Online]. Available: https://www.who.int/news/item/29-06-2020-covidtimeline. [Accessed 30 June 2020].

[243] M. Mofijur, I. R. Fattah, M. A. Alam, A. S. Islam, H. C. Ong, S. A. Rahman and T. M. I. Mahlia, "Impact of COVID-19 on the social, economic, environmental and energy domains: Lessons learnt from a global pandemic," *Sustainable production and consumption,* vol. 26, pp. 343-359, 2020.

[244] H. Zhong, Z. Tan, Y. He, L. Xie and C. Kang, "Implications of COVID-19 for the electricity industry: A comprehensive review," *CSEE Journal of Power and Energy Systems,* vol. 6, no. 3, pp. 489-495, 2020.

[245] Y. Lu, R. Zhou and J. Wang, "Analysis of Power Generation and Load Change Under the Influence of Lockdown Based on COVID-19 Epidemic," in *2020 AEIT International Annual Conference (AEIT)*, Catania, Italy, 2020.

[246] H. M. Alhajeri, A. Almutairi, A. Alenezi and F. Alshammari, "Energy demand in the state of Kuwait during the covid-19 pandemic: technical, economic, and environmental perspectives," *Energies,* vol. 13, no. 17, p. 4370, 2020.

[247] B. Baldissara, A. Zini, F. Gracceva, E. Bompard, S. Corgnati and C. Mosca, "Prime stime degli effetti dell'emergenza COVID-19 sul sistema energetico italiano," *Quarterly analysis of the Italian energy system,* no. 1, pp. 7-16, 2020.

[248] F. Gracceva, E. Bompard, B. Baldissara, S. Corgnati, C. Mosca and A. Zini, "COVID-19 e sistema energetico italiano: una prima valutazione," *Energia,* no. 2, 2020.

[249] IEA, "Global Energy Review," 2020. [Online]. Available: https://www.iea.org/reports/global-energy-review-2020 .

[250] IEEE PES, "Sharing Knowledge on Electrical Energy Industry's First Response to COVID-19," 2020. [Online]. Available: https://resourcecenter.ieee-pes.org/publications/white-papers/PES_TP_COVID19_050120.html.

[251] S. Snow, R. Bean, M. Glencross and N. Horrocks, " Drivers behind Residential Electricity Demand Fluctuations Due to COVID-19 Restrictions," *Energies,* vol. 13, no. 21, p. 5738, 2020.

[252] A. Abu-Rayash and I. Dincer, "Analysis of the electricity demand trends amidst the COVID-19 coronavirus pandemic," *Energy Research*

& Social Science, vol. 68, no. 101682, 2020.

[253] J. V. Andrade, R. S. Salles, M. N. Silva and B. D. Bonatto, "Falling Consumption and Demand for Electricity in South Africa-A Blessing and a Curse," in *2020 IEEE PES/IAS PowerAfrica*, Nairobi, Kenya, 2020.

[254] D. Carmon, A. Navon, R. Machlev, J. Belikov and Y. Levron, "Readiness of small energy markets and electric power grids to global health crises: lessons from the COVID-19 pandemic," *IEEE Access,* vol. 8, pp. 127234-127243, 2020.

[255] E. Ghiani, M. Galici, M. Mureddu and F. Pilo, "Impact on electricity consumption and market pricing of energy and ancillary services during pandemic of COVID-19 in Italy," *Energies,* vol. 13, no. 13, p. 3357, 2020.

[256] C. Mosca, P. Colella, E. Bompard and Z. Yan, "Techno-economic Impacts of COVID-19 Pandemic on the Italian Electricity System," in *2020 AEIT International Annual Conference (AEIT)*, Catania, Italy, 2020.

[257] A. Werth, P. Gravino and G. Prevedello, "Impact analysis of COVID-19 responses on energy grid dynamics in Europe," *Applied energy,* vol. 281, no. 116045, 2020.

[258] E. Clair, "Looking at COVID-19 crisis from the EU electricity wholesale market," *FSR Blogpost Electricity,* 2020.

[259] S. Casa, Z. E. and A. Marchisio, "Italia: nel sistema elettrico post-Covid più spazio per le rinnovabili," June 2020. [Online]. Available: https://rienergia.staffettaonline.com/.

[260] EPRI, "COVID-19 Bulk System Impacts," April 2020. [Online]. Available: https://www.epri.com/research/products/3002018602.

[261] CIGRE, "System Operations impact of COVID-19: European Perspective," June 2020. [Online]. Available: https://www.cigre.org/article/GB/system-operations-impact-of-covid-19-european-perspective.

[262] S. A. H. Soliman and A. M. Al-Kandari, Electrical load forecasting: modeling and model construction, Oxford, UK: Elsevier, 2010.

[263] B. McWilliams and G. Zachmann, “Bruegel electricity tracker of COVID-19 lockdown effects,” April 2020. [Online]. Available: https://www. bruegel. org/2020/03/covid-19-crisiselectricity-demand-as-a-real-time-indicator .

[264] EEA, “Copernicus Land Monitoring Service 2020,” 2020. [Online]. Available: https://land.copernicus.eu/.

[265] E. Bompard, C. Mosca, P. Colella, G. Antonopoulos, G. Fulli, M. Masera, M. Poncela-Blanco and S. Vitiello, “The Immediate Impacts of COVID-19 on European Electricity Systems: A First Assessment and Lessons Learned,” *Energies,* vol. 14, no. 1, p. 96, 2020.

[266] Terna, “Transparency Report,” 2020. [Online]. Available: https://www.terna.it/it/sistema-elettrico/transparency-report.

[267] Terna, “Monthly Report on the Electricity System, May,” Rome, Italy, 2020.

[268] GME, “Transparency Platform,” 2020. [Online]. Available: https://www.mercatoelettrico.org/it/Statistiche/ME/DatiSintesi.aspx.

[269] GME, “Monthly Report April,” Rome, Italy, 2020.

[270] ENTSO-E, “ENTSO-E Transparency Platform,” 2020. [Online]. Available: https://transparency.entsoe.eu/dashboard/show .

[271] ACER and CEER, “Annual Report on the Results of Monitoring the Internal Electricity and Gas Markets in 2016, Electricity Wholesale Markets Volume,” Ljubljana, Slovenia, 2016.

[272] R. H. Lasseter, Z. Chen and D. Pattabiraman, “Grid-Forming Inverters: A Critical Asset for the Power Grid,” *IEEE Journal of Emerging and Selected Topics in Power Electronics,* pp. 925-935, 2019.

[273] Elering, “Synchronization with Continental Europe,” 2020. [Online]. Available: https://elering.ee/en/synchronization-continental-europe.